THE UNIVERSITY
of EDINBURGH

Remodelling cutin by transacylases in the plant epidermis: dynamic processes during growth and response to environmental stress

Anzhou Xin

Doctor of Philosophy – Cell and Molecular Biology

University of Edinburgh

2019

I. Declaration

I declare that this thesis has been composed solely by myself and that it has not been submitted, in whole or in part, in any previous application for a degree. Except where states otherwise by reference or acknowledgment, the work presented is entirely my own.

Anzhou Xin, Edinburgh, 2019

II. Abstract

Based on the discovery of the only known cutin-related GDSL transacylase, cutin synthase (CD1), we hypothesized that cutin can also be re-modelled by transacylases in the same family as CD1 post-synthetically. Cutin was hypothesized to be transiently cut (acyl donor), and then re-form ester bonds with a neighbouring cutin (acyl acceptor) or a cell-wall polysaccharide (acyl acceptor) molecule, in order to allow cell expansion and reinforce cutin strength respectively. These proposed novel transacylase activities were first observed by *in-* and *ex-situ* radiochemical assays (i.e. endogenous cutin as the acyl donor; exogenous cutin fatty acid, 16-[^{3}H]hydroxyhexadecanoic acid and xyloglucan oligomer, [^{3}H]XXXGol were models for their polymers as the acyl acceptors) and verified by product analysis via thin-layer chromatography, size exclusion chromatography etc. Moreover, we concluded that these two reactions were catalysed by different transacylases based on their pH optima and responses to growth, as well as temperature change. To test whether CD1 was one of the enzymes involved, we heterologously expressed, purified and assayed it *in vitro*; however, it did not catalyse either reaction. Environmental stresses were tested for effects on the two transacylase activities: cutin-to-[^{3}H]XXXGol transacylase activity was increased in the first 4 days at 4°C and then decreased; but the cutin-to-[^{3}H]HHA transacylase activity was decreased from the first day. It may suggest that the cutin-to-[^{3}H]XXXGol transacylase activity was involved in resisting short-term cold. Light and humidity did not affect either of the transacylase activities. In conclusion, two novel transacylase activities

(renamed as cutin-to-HHA and cutin-to-XGO transacylase activities) were found and their biological significances were studied, providing a breakthrough in cutin biochemistry studies.

III. Lay Summary

The plant epidermis is proposed to restrain organ expansion to some extent. An epidermal component, cutin, is a polyester matrix made of hydroxy fatty acids and was hypothesized to be re-modelled to accommodate cell expansion.

The first proposed re-modelling mechanism is that (1) cutin can be transiently broken by a novel enzyme activity, but that after incremental cell expansion, the enzyme will reattach the broken cutin molecule to a nearby one, so that the matrix becomes intact again. The second proposed mechanism is similar: (2) the broken cutin is ‘stitched’ onto cell wall polysaccharides by a novel enzyme activity, to reinforce the epidermal structure. The third proposal is that (3) cutin can be degraded in order to loosen the epidermal cell wall when cutin is not necessary (e.g. on the surface of a flower’s stigma).

In this thesis, the first two hypothesised enzyme activities (1 and 2, termed transacylases) were first observed in radio-chemical assays on pea epicotyl, ice-plant leaf and tomato fruit as model plant organs. The reaction mechanisms were subsequently elucidated via analysing products chromatographically. By characterising the first two new cutin re-modelling transacylase activities (e.g. measuring their pH optima and their responses to stressful environmental conditions), we conclude that they are conferred by two separate enzymes, which were not identified in this thesis. The third hypothesized reaction (3) was not detected here.

The two (1 and 2) novel cutin re-modelling transacylase activities' physiological significance was investigated. For example, the cessation of cell expansion at organ maturity correlated with reductions in the enzymes' activities, supporting our hypothesis – that they are required during rapid growth, possibly involving in loosening cutin (1) and reinforcing the cuticle (i.e. composed of cutin, wax and cell wall polysaccharide) (2). Moreover, the second new enzyme activity was observed to increase during a short-term cold period, leading to a speculation that it can regulate cell wall pore sizes to prevent ice formation. This study provides a new insight into cutin biochemistry and knowledge of plant physiological changes during cell expansion.

IV. Acknowledgement

I would like to thank Prof. Stephen C. Fry, who initiated this exciting project, and selected me to carry it on. I obtained extremely precious PhD experience by working with Steve and learning his outstanding research skills.

I would like to thank Prof. Andrew Hudson and Prof. Justin Goodrich, who provided their very useful advice to my project, and supported me as a thesis committee member. I would also like to thank Dr. Attila Molnar, who kindly agreed to collaborate with me; and his team (Dr. Yue Fei, PhD Aron Ferenczi and Muriel Monteiro) was extremely patient, and never hesitated to help me.

I also would like to deeply thank my family, who warmly supported my PhD life financially and mentally with immense love. And I would like to take this chance to express my gratitude to Dr. Klaus Herburger, who helped and supported me as a professional colleague, and also a life partner I could ever dream of.

I would like to thank the dear experts, Dr. Lenka Franková, Dr. Martina Pičmanová and PhD Thurayya Al Hinai, who never conserved their knowledge and always provided it whenever I need.

I would like to thank the whole lab; people built up a nice work place by helping each other.

Finally yet importantly, I would like to thank my internal and external examiners, who will use their precious time to look into my research.

V. List of Abbreviations

[1-^{14}C]HA: [1-^{14}C]Hexadecanoic acid

[^{3}H]Ara$_{8}$-ol: [^{3}H]Arabino-octaitol

[^{3}H]GalA$_{8}$-ol: [^{3}H]Galacturono-octaitol

[^{3}H]HHA: 16-Hydroxy-[16-^{3}H]hexadecanoic acid

[^{3}H]Man$_{3}$-ol: [^{3}H]Mannotriito

[^{3}H]Xyl$_{5}$-ol: [^{3}H]Xylopentaitol

2-MAGs: 2-Monoacylglycerols

2-MHG: 2-mono(10,16-dihydroxyhexadecanoyl)glycerol

3-D: 3-Dimensional

A: Absorbance

ABC transporter: ATP-binding cassette transporters

AMPS: Ammonium persulfate

AOPP: Aryloxyphenoxypropionate

ATR-FTIR: Attenuated total reflection-Fourier transforming infra-red

BAW: Butan-1-ol/acetic acid/water

BMGY: Buffered complex glycerol medium

BMMY: Buffered complex MeOH medium

Bp: base pair

BPW: Butan-1-ol/pyridine/water

Bq: Becquerel

BR: Breaker tomato tomato fruit

CD1: Cutin deficient 1

CDTA: 2-[2-[Bis(carboxymethyl)amino]cyclohexyl]-(carboxymethyl)amino]acetic acid

CER4 / FAR3: Eceriferum 4 / Fatty acid reductase 3

CM: Chloroform/methanol

CMNaOH: chloroform/methanol/4M NaOH

CMW: Chloroform/methanol/water

DAA: Days after anthesis

DAS: Days after sowing

DEPC: Diethyl pyrocarbonate

DiHHA: 10,16-Dihydroxyhexadecanoic acid

DMSO: Dimethyl sulfoxide

DR: Deep red tomato fruit

DTT: Dithiothreitol

EDC: 1-Ethyl-3-(3-dimethylaminopropyl)-carbodiimide

EDTA: Ethylenediaminetetraacetic acid

EIMS: Electron ionization mass spectroscopy

ER: Endoplasmic reticulum

FGSC: Fungal Genetics Stock Center

G3P: Glycerol-3-phosphate

GPAT: G3P acyltransferases

H bond: hydrogen bond

HHA: 16-Hydroxyhexadecanoic acid

LACS: Long-chain acyl-CoA synthase

LB: Luria broth

LR: Light red tomato fruit

LTP: Glycosylphosphatidylinositol-anchored lipid transfer protein

MAH: Mid-chain alkane hydroxylase

MG: Mature Green tomato fruit

MFW: Methanol/formic acid/water

NHS: *N*-Hydroxysuccinimide

NMR: nuclear magnitude resonance

OA: Oleic acid

OD: Optical density

OHA: 16-Oxohexadecanoic acid

OR: Orange tomato fruit

PBS: Phosphate-buffered saline

PBST: PBS with TWEEN-20

PCR: Polymerase chain reaction

PME: Pectin methylesterase

PMSF: Phenylmethylsulfonyl fluoride

***p*-NP**: *p*-nitrophenol

***p*-NPP**: *p*-nitrophenyl palmitate

PVPP: Polyvinylpolypyrrolidone

qRT-PCR: Quantitative reverse transcription-polymerase chain reaction

R_F: = distance travelled by the compound/ distance moved by solvent

RG-I: Rhamnogalacturonan I

SDS-PAGE: Sodium dodecyl sulfate- polyacrylamide gel electrophoresis

SEM: Scanning electron microscope

TBE: Tris/Borate/EDTA

TEM: Transmission electron microscope

TEMED: Tetramethylethylenediamine

TFA: Trifluoroacetic acid

TLC: Thin-layer Chromatography

TR: Turner tomato fruit

UV: Ultra-violet

WT: Wild-type

XEG: Xyloglucan-specific endo-β-1,4-glucanase

XET: Xyloglucan endotransglucosylase

XGOs: Xyloglucan and its oligomers

YEP: Yeast extract, peptone

YPDS: Yeast extract, peptone, dextrose, sorbitol

VI. List of tables

VII. List of figures

Table of Contents

Chapter 1. Introduction

1.1 General introduction

The cuticle is a hydrophobic interface between the aerial-epidermal cells in all land plants and the environment (reviewed by Nawrath, 2002; Yeats *et al.*, 2012) (Fig. 1). It consists of cutin and wax: the former is a continuous polyester matrix observed microscopically (transmission electron and light microscopy) (Jeffree, 2006; Yeats *et al*., 2012) and its insolubility in neutral organic solvents (Kolattukudy, 1977) provides chemistry evidence for the polyester nature, whereas the wax is soluble in neutral organic solvents since it does not contain polymer (e.g. polyester), but dominated by very long aliphatic molecules (e.g. C_{29} *n*-alkanes in *Arabidopsis* stem cuticle), which are embedded in cutin and form crystalloids or a smooth film exterior (reviewed by Kunst and Samuels, 2003; Suh *et al*., 2005) (Fig. 1).

Cuticle is widely accepted to be essential for preventing desiccation and UV damage, since it was acquired by land plants during the process of adapting to land atmosphere (Edwards *et al*., 1982; reviewed by Jeffree, 2006). Cuticle is found from bryophytes (e.g. phylloid of + and thallus of *Marchantia paleacea*) (Schönherr and Ziegler, 1975; Buda *et al*., 2013) to angiosperms (e.g. tomato fruit and *Arabidopsis* shoot) (Franke *et al*., 2005; Girard *et al*., 2012). Consistent with the putative cuticle function, it cannot be found in algae (Cook and Graham, 1998), only an osmiophilic layer is plesiomorphic of cuticle in algae as seen under the scanning electron microscope (SEM), because of the high humidity and lack of UV in sea and soil. Traditionally, it

was widely agreed that there is no cuticle in roots of land plants (Baker *et al*., 1982), only suberin because soil protects plants from desiccation and UV. However, a very recent study reported that a layer of cell wall modification in *Arabidopsis* root cap was observed under TEM, and it was susceptible to cutinase; furthermore, this modification layer cannot be observed or largely reduced after the cutin precursor biosynthesis genes (*GPAT4* and *8*) were knocked out (Berhin *et al*., 2019). Thus, this study introduced a new concept: cutin is not only in aerial shoot, but also very likely in root cap.

Cutin precursors, 2-monoacylglycerols (2-MAGs), are synthesized within cells and then pumped out to the apoplast by ATP-binding-cassette (ABC) transporters (reviewed by Beisson and Ohlrogge, 2012) (Fig. 1). Cutin is located between wax (reviewed by Beisson and Ohlrogge, 2012) and wall polysaccharides (Fig. 1) and contributes 40–60% dry weight of the cuticle varies between species (Martin, 1964; Domínguez *et al.*, 2008; Takahashi *et al.*, 2012; Belge *et al*., 2014). TEM showed no clear interface between them (Jeffree 2006; reviewed by Fernández *et al.*, 2016), and interfacial interactions between these three epidermis components are still not well understood.

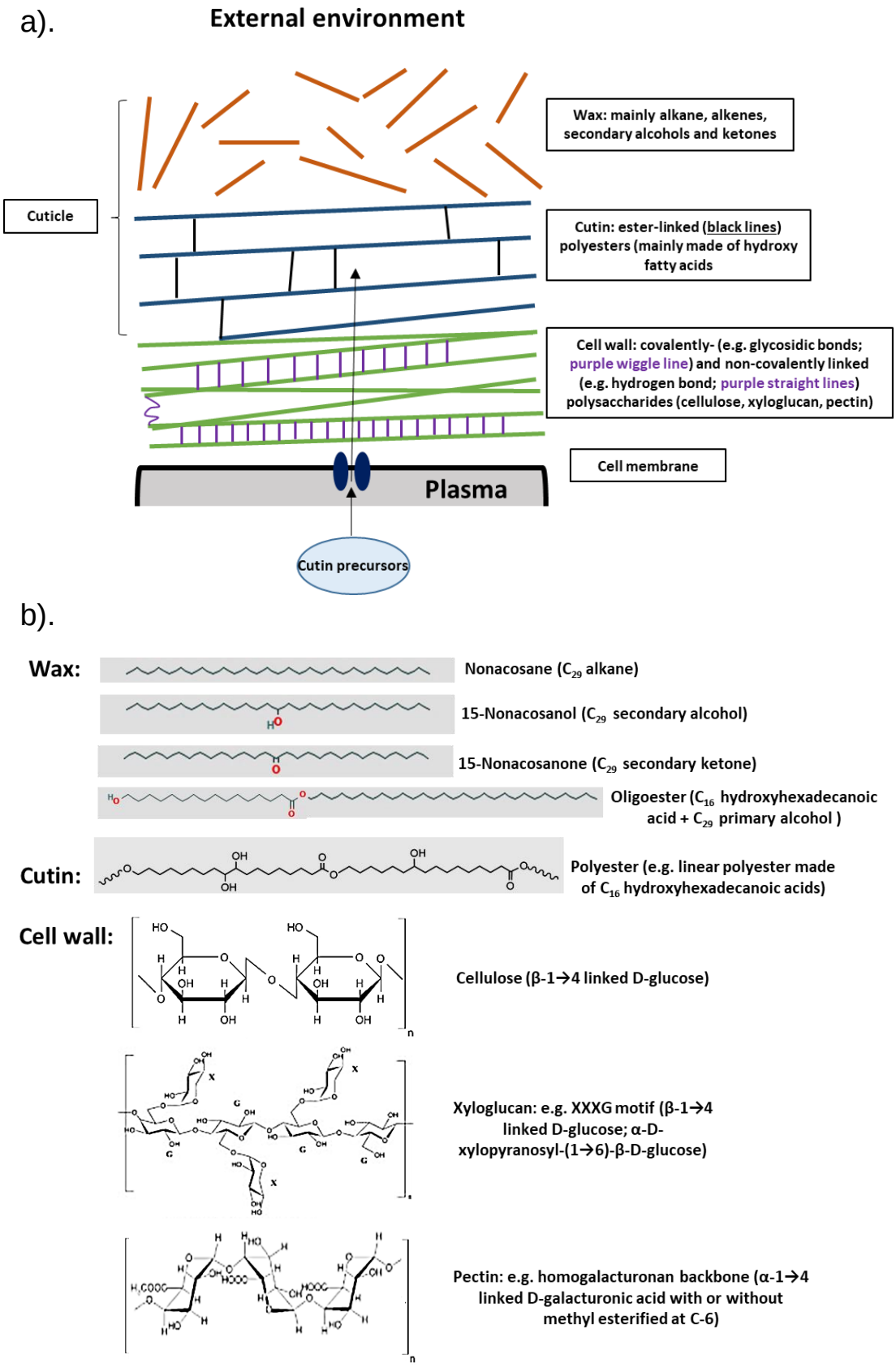

Figure 1. Localization of cutin in the cuticle (adapted from Beisson and Ohlrogge, 2012) and cuticle components. a) Cutin precursors are synthesized

intraprotoplasmically and then exported to apoplast (the black arrow indicates the cutin monomers' transport pathway). The main components and bond type in each epidermal layer were listed. Wax and cutin constitute cuticle. b) Chemistry structure of the main components of each epidermal compartment. A minor component of wax, oligoester, was also included.

Notably, besides the only known polyester, cutin, there are also oligo-esters found in wax, and they are the condensation products of primary alcohol and acyl groups (reviewed by Kunst and Samuels, 2003; Kunst and Samuels, 2009). For example, the major oligo-esters (C_{42-46}) in *Arabidopsis* stem wax are produced from C_{16} acyl-CoA and C_{26-30} primary alcohols in the endoplasmic reticulum (ER) (Lai *et al*., 2007; Li *et al*., 2008). These oligo-esters are also potential transacylation substrates for our proposed cutin transacylases (explained later), and should be carefully distinguished from cutin, which is a polyester. High-resolution nuclear magnitude resonance (NMR) studies of the intact cutin matrix also showed that free fatty acids are embedded in cutin (Deshmukh *et al*., 2003).

Cutin is an important trait for land plants (next section), and therefore, in this project, cutin will be investigated for its possible re-modelling mechanisms which help it to keep pace (i.e. no rupture) with cell expansion during healthy growth and in response to environmental stresses.

1.2 Cutin function

Cutin begins to be set up on the epidermal cell wall at early developmental stages, e.g. in grape berries (Casado and Heredia, 2008) and *Arabidopsis* embryos (Molina *et al.*, 2008), suggesting that cutin is an important trait.

Cutin defines organ boundaries during early embryo development (Sieber *et al.*, 2000), prevents water loss and nutrient leaching (with waxes) (Schreiber, 2005; Isaacson *et al.*, 2009) and protects plants from harmful chemicals (e.g. 2,4-dichlorophenoxyacetic acid) (Kirkwood, 1999; Schönherr and Baur, 1994), pathogens (Auyong *et al*., 2015), ultra-violet (UV) radiation (thanks to the phenolic constituents of the cuticle) (Rozema *et al.*, 2009) and physical abrasion.

However, cutin may also limit cell expansion (Hoffmann-Benning and Kende, 1994). For example, longitudinally-sliced rapidly growing internodes of *Oryza sativa* L. (deepwater rice) with epidermis on, showed an outward bending due to the expansion of epidermal cells and constraining of cutin, which was then reduced by treatment with cutinase (cutin hydrolase) from *Pseudomonas putida*, suggesting that cutin played a role in constraining epidermal cell growth (Hoffmann-Benning and Kende, 1994). Other studies about the role of cutin in controlling growth used sunflower hypocotyls because of their rapid expansion. The peeled sunflower hypocotyl elongated in water 400–600% faster than the intact sample, and shrank 75% faster after addition of an osmoticum, polyethylene glycol, leading to the speculation that epidermis might restrain plant growth (epidermal-growth-control theory) (Kutschera and Niklas, 2007), Nevertheless, there is no direct *in-vivo* evidence yet.

Based on the observations above, we proposed that cutin could be loosened transiently in response to growth promoters in this study. This hypothesis will be explained in '***cutin rearrangement in vivo***' section.

1.3 Cutin chemistry

Cutin is made of various ester-bonded monomers with an unknown polymerisation degree. The most common monomer in most vascular land plants is 10,16-dihydroxyhexadecanoic acid (diHHA) [e.g. forming 59%-84% in the cuticle of mature tomato fruits, *Solanum lycopersicum* (dicotyledon, vascular) (Kosma *et al.*, 2010; Nadakuduti *et al.*, 2010); and 69% in the cuticle of *Citrus aurantifolia* leaf (Baker and Holloway, 1970)], but only 28% in *Sphagnum palustre* (moss, non-vascular) cutin (Caldicott and Eglinton, 1976). Besides, 16-hydroxyhexadecanoic acid (HHA) and 18-hydroxy octadecanoic acid are usually the second or third most abundant monomers in tomato fruit cutin (Kosma *et al.*, 2010; Nadakuduti *et al.*, 2010). In the mostly used plant model, pea (*Pisum sativum*), the dominant cutin fatty acids are C_{18}, speculated from the precursor synthesis enzymes (Li *et al*., 2016).

Different from other vascular land plants, in the leaves and stems of *Arabidopsis*, the most dominant cutin fatty acid is octadecadien-1,18-dioic acid (Franke *et al*., 2005), which does not have a hydroxy group and but two unsaturated bonds. The *Arabidopsis*'s newly reported that root cap cuticle is also dominated by the same unsaturated fatty acid (Berhin *et al*., 2019).

To a minor extent, glycerol is also a cutin building block since it occurs in cutin precursors, 2-MAGs (Graça *et al.*, 2002; reviewed by Fich *et al.*, 2016). Moreover, at least in tomato fruit cutin, glycerol may be also involved in forming other types of esters, since the glycerol molecules with two terminal (1, 3) esterifications were also found (Philippe *et al*., 2016).

a).

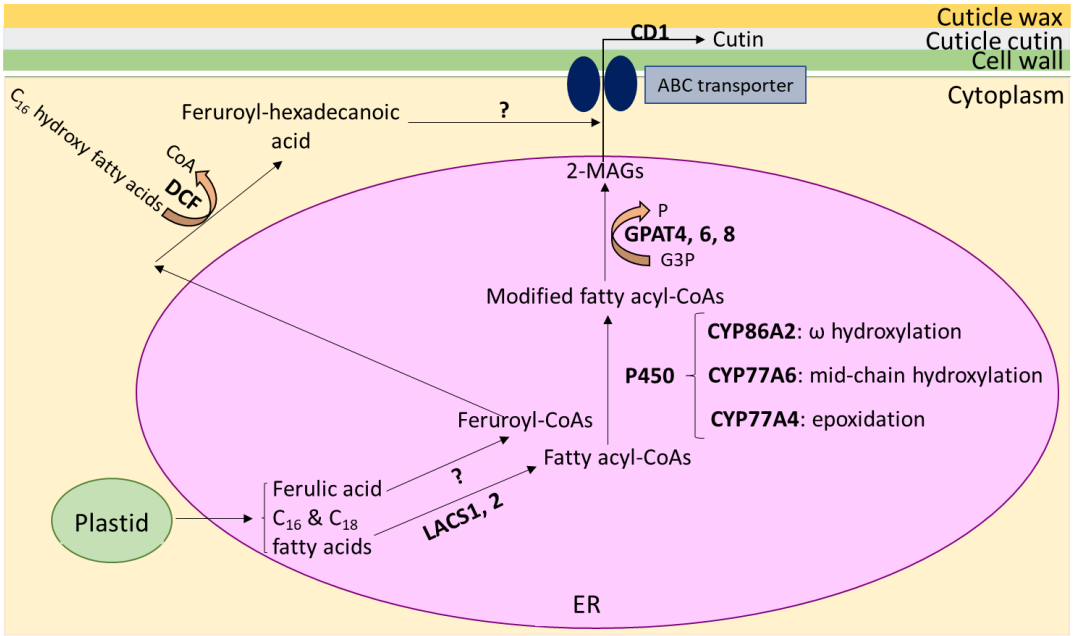
Cuticle wax
Cuticle cutin
Cell wall
Cytoplasm
CD1
Cutin
ABC transporter
Feruroyl-hexadecanoic acid
?
C16 hydroxy fatty acids
CoA
DCF
2-MAGs
P
GPAT4, 6, 8
G3P
Modified fatty acyl-CoAs
P450
CYP86A2: ω hydroxylation
CYP77A6: mid-chain hydroxylation
CYP77A4: epoxidation
Feruroyl-CoAs
Fatty acyl-CoAs
Ferulic acid
C16 & C18
fatty acids
?
LACS1, 2
Plastid
ER

b).

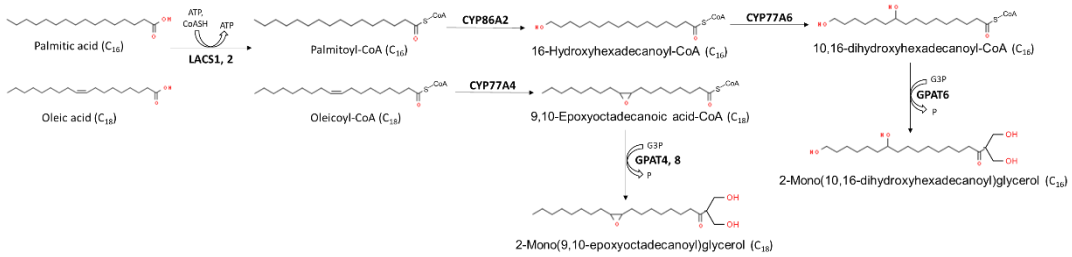
Palmitic acid (C16)
ATP, CoASH
ATP
LACS1, 2
Palmitoyl-CoA (C16)
CYP86A2
16-Hydroxyhexadecanoyl-CoA (C16)
CYP77A6
10,16-dihydroxyhexadecanoyl-CoA (C16)
Oleic acid (C18)
Oleicoyl-CoA (C18)
CYP77A4
9,10-Epoxyoctadecanoic acid-CoA (C18)
G3P
GPAT6
2-Mono(10,16-dihydroxyhexadecanoyl)glycerol (C16)
G3P
GPAT4, 8
2-Mono(9,10-epoxyoctadecanoyl)glycerol (C18)

c).

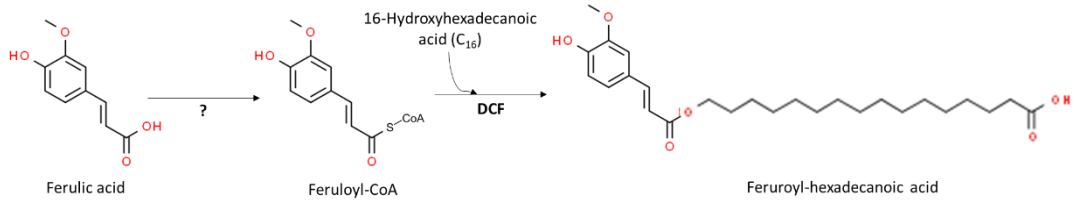
HO
OH
O
?
Ferulic acid
16-Hydroxyhexadecanoic acid (C16)
CoA
Feruloyl-CoA
DCF
Feruroyl-hexadecanoic acid

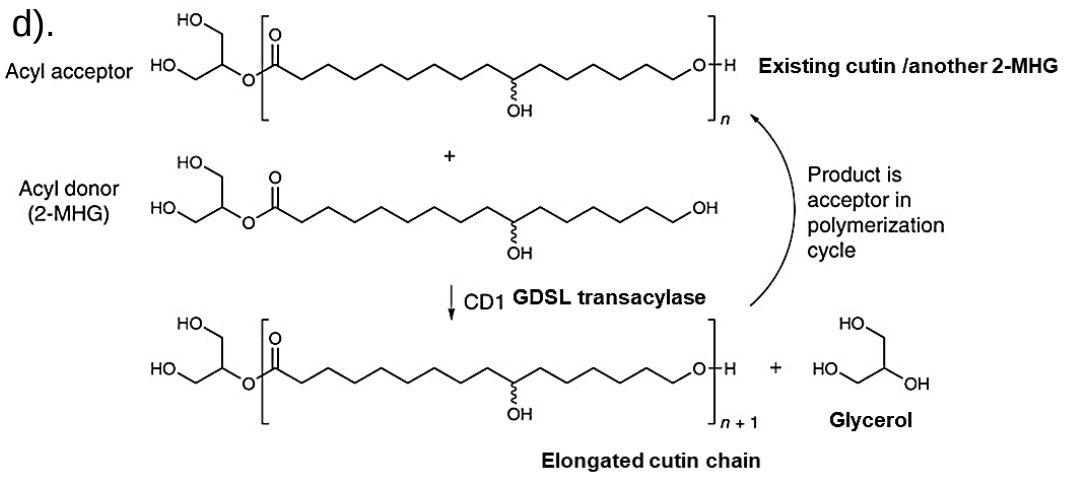

Figure 2. Cutin precursors's fate: intraprotoplasmic synthesis, transmembrane transport and extracellular polymerisation. a) A simplified summary of the putative mechanisms of cutin synthesis and transport pathways: common cutin monomer C_{16} and C_{18} fatty acids are synthesized *de novo* in the plastid (**green oval**), and then transported to cytoplasm, to be thio-esterified to CoA by LACS1 and 2 in ER (**pink oval**). Further modification of the fatty acids is catalysed by a group of P450 enzymes, followed by transfer of the acyl group by GPATs to G3P, resulting in formation of the cutin precursors, 2-MAGs in ER. These precursors are then transferred to apoplast via ABC transporters, and then polymerised to cutin by CD1. All the enzymes involved in are bold. ***** The size-ratio of plastid and ER does not refer to the real one. b) Biosynthetic reactions of 2-MAG species from C_{16} and C_{18} fatty acids. c) Biosynthetic reactions of cutin phenolics (e.g ferulic acid) precursor. d) Mechanism of cutin biosynthesis (Yeats *et al*., 2012).

Phenolics, such as *p*-coumaric acid and ferulic acid, in a minor amount were also reported in tomato fruit and *Arabidopsis* leaf cutin (Hunt and Baker, 1980; Rautengarten *et al*., 2012; reviewed by Fich *et al*., 2016), and since they were very difficult to be extracted from cutin by mild alkaline hydrolysis, covalent bonds might be formed between them and cutin (Riley and Kolattukudy, 1975). A more recent study provided more evidence for the existence of cutin–phenolics covalent bonds: a cytosolic protein discovered in *Arabidopsis* aerial organ epidermal cells, *deficient in cutin ferulate* (DCF) transfers feruloyl residues from feruloyl-CoA to the −OH group of 16-hydroxyhexadecanoic acid (HHA), resulting in ester bond formation (product:

16-feruroyl-hexadecanoic acid) *in vitro* (Rautengarten *et al*., 2012). Another acyl donor, *p*-coumaroyl-CoA was also found, but with a smaller activity (Rautengarten *et al*., 2012). The cellular localisation of DCF (cytosol) (Rautengarten *et al*., 2012) also suggested that the phenolic–fatty acid conjugate was formed before export to the apoplast.

By deleting a monooxygenase gene which involves in angiosperm's lignin biosynthesis, the cutin biosynthesis in *Physcomitrella patens* (moss) was impaired. Previous chemical analysis results suggest that cutin in moss is reminiscent of angiosperm's suberin (reviewed by Bession *et al.*, 2012), whereas functionally similar to lignin. These cross-talks between cutin, suberin and lignin may suggest that they share the same ancestral origin (Renault *et al.*, 2017).

Cutin components are also modified with evolution. For example, in non-vascular (e.g. mosses) and seedless vascular land plants (e.g. ferns), cutin monomers are usually dominated by HHA, instead of diHHA (Goñi and Hedges, 1990). Besides, the ratio of C_{14} fatty acid to C_{16} is much higher in early-diverging than later-diverging land plants (Goñi and Hedges, 1990). For example, there are no C_{14} fatty acid residues in tomato fruit cutin (Kosma *et al.*, 2010; Nadakuduti *et al.*, 2010), but 5-hydroxytetradecane dioic acid (C_{14}) is 130% of total C_{16} fatty acids in *P. patens* cutin (Buda *et al*., 2013). Moreover, the total C_{18} fatty acid amount is less in monocotyledon and gymnosperms generally (Hunneman and Eglinton, 1972; Goñi and Hedges, 1990). These data all suggest that the cutin fatty acid chain lengths increases with evolution.

In summary, cutin fatty acids might have elongated during evolution (i.e. from C_{14} to C_{18}), and more branching fatty acids were acquired by later-diverging land plants with unknown reason (reviewed by Fich *et al*., 2016).

1.4 Cutin precursor biosynthesis and the transport

1.4.1 Intraprotoplasmic biosynthesis and transport

It has been proposed that cutin's major building blocks, C_{16} and C_{18} fatty acids, are synthesized in plastids *de novo* via relying on acyl carrier protein etc. (reviewed by Li-Beisson *et al.*, 2010), and then released from the plastids and esterified to CoA to form acyl-CoAs (e.g. $C_{16:0}$ acyl-CoA), mainly by long-chain acyl-CoA synthetase 1 and (LACS 1 and 2) in the ER (Schnurr *et al.*, 2004; Lü *et al.*, 2009; reviewed by Fich *et al*., 2016), followed by hydroxylation or epoxidation by various cytochrome P_{450} enzymes, such as CYP86A2 catalysing ω-hydroxylation (Xiao *et al*., 2004), CYP77A6 catalysing midchain hydroxylation (Li-Beission *et al*., 2009) and CYP77A4 catalysing epoxidation (Sauveplane *et al*., 2008) (Fig. 2).

The products (e.g. $C_{16:0}$ dihydroxyhexadecanoyl-CoA) act as acyl donors because the CoA-attached acyl group was activated, and therefore the fatty acid part (with an activated acyl group) is then transferred to the *sn*-2 position (the middle −OH) of a glycerol-3-phosphate (G3P) molecule (acyl acceptor), catalysed by ER-localised G3P acyltransferases, GPAT4, 6, and 8 targeting different acyl-CoA species in *Arabidopsis* (Yang *et al.*, 2010; reviewed by Chen *et al.*, 2011 and Fich *et al.*, 2016).

These three GPATs are distinct from other members of the land plant GPAT superfamily, since they are bifunctional: first transferring acyl groups to glycerol molecules at *sn*-2; second removing the phosphorylation at *sn*-3 (Yang *et al.*, 2010; Yang *et al.*, 2012) (Fig. 2). The final products are 2-MAGs *in vitro* (Yang *et al.*, 2010), putative cutin precursors ready to be exported to apoplast. Another difference between these three GPATs and others is that only they were found in early non-vascular land plant (bryophyte), whereas other phosphatase-minus (only transacylation, no dephosphorylation activity) clades such as GPAT5 were only found in vascular land plants, providing another evidence that cutin, at least cuticle is essential for land atmosphere adaptation (Yang *et al.*, 2012). Consistent with the suggested physiological function (cutin precursor's synthesis) of these three GPATs, transcriptome studies showed that they are up-regulated in epidermal cells of *Arabidopsis* shoot (Suh *et al*., 2005).

In summary, cutin fatty acids were first synthesized in plastids, and then transferred to ER for modifications, which eventually form the cutin precursors, 2-MAGs (Fig. 2).

Physiological evidence of demonstrating that the three GPATs are essential for cutin formation came from the observations that double knockout *gpat4/gpat8 Arabidopsis* produced much less cutin in stems and leaves than wildtype (WT) (Li *et al.*, 2007), and that a *gpat6* knockout showed much less cutin in sepals and petals than WT (Li-Bession *et al.*, 2009). A substrate specificity study showed that GPAT4 and 8 prefers C_{18} acyl-CoAs over C_{16} ones *in vitro*, especially $C_{18:2}$ dicarboxylic acid-CoA (Yang *et al*., 2007), which

is the precursor for the dominant cutin fatty acid monomer in *Arabidopsis* stem and leaves (Franke *et al*., 2005). However, GPAT6 catalyses the transacylation reaction of 10,16-dihydroxyhexadecanoyl-CoA *in vitro*, which is the dominant precursor of cutin in *Arabidopsis* flower (Petit *et al*., 2016). In addition to the *in-vitro* activities, this correlation between the mutations and phenotypes provides another line of evidence that GPAT4, 6 and 8 produce the relevant cutin precursors, which are 2-MAGs.

2-MAGs were detected by electron ionization mass spectroscopy (EIMS) from various plant cutins (Graça *et al.*, 2002), but not in cuticular wax (Li *et al*., 2007), indicating that 2-MAGs are specific to cutin.

In summary, the cutin precursors, 2-MAGs, are synthesized from acyl-CoA and G3P intraprotoplasmically, catalysed by GPAT4, 6 or 8 depends upon the acyl-CoA species.

1.4.2 Transmembrane transport

ABC transporters have been widely suggested to play a role in transporting cutin precursors, based on biochemistry and plant physiology studies (Fig. 2). For example, cutin deposition in *Arabidopsis* flowers was reduced to half of the WT in a knockout of *abcg13* gene (expressing a half-sized ABC transporter) mutant, and sepal-to-sepal fusions were observed (Panikashvili *et al*., 2011, reviewed by Fich *et al.*, 2016). Similar morphology was also observed in *abcg11* (a mutant gene encoding another half-sized ABC transporter) knockout *Arabidopsis* mutant (Bird *et al*., 2007).

The transport mechanism of cutin precursor through cell wall is more mysterious than the one from cytoplasm to apoplast, because its hydrophobicity and cell wall's hydrophilicity repel each other naturally. Glycosylphosphatidylinositol-anchored lipid transfer proteins (LTPs) have been suggested to facilitate extra protoplasmic transport of cuticle lipids (Yeats and Rose, 2008). However, cutin chemistry analysis of *ltpg1* and *ltpg2* knockout *Arabidopsis* mutants showed no significant change in either cutin composition or quantity (Lee *et al*., 2009, Kim *et al*., 2012). More candidate extracellular proteins are required to be screened. Another question is how these precursors are polymerised to cutin chains; the mechanism will be introduced later in the '***cutin polymer biosynthesis***' section.

1.5 Cutin structure

Cutin structure is proposed to depend upon its monomers and physiological processes in the plant (e.g. rapid growth, ripening etc.) (reviewed by Fich *et al*., 2016).

In tomato fruit cutin (diHHA is the dominant cutin monomer), most of the primary hydroxy groups are involved in polymerization, whereas only about 40% of the secondary hydroxy groups are esterified (i.e. involved in branching), based on experiments distinguishing free hydroxy groups from esterified ones in intact cutin, via oxidizing free secondary −OH groups or mesylating all free −OH groups, coupled with depolymerisation and chemical analysis (Deas and Holloway, 1976; Kolattukudy, 1977).

An alternative method to study cutin structure is depolymerising cutin partially, via either enzymes (e.g. cutinase from *Fusarium solani*) or chemicals (e.g. low-temperature hydrofluoric acid); and surprisingly, the products from lime fruit cutin were mainly oligo-esters formed from diHHA molecules esterified at the mid-chain −OH groups (Fang *et al*., 2001). Similar results were also observed in tomato fruit cutin (Graça and Lamosa, 2010), contradicting to the results obtained by chemical marking methods above. This discrepancy might be because esters of secondary alcohols are more difficult to hydrolyse than primary (Fang *et al*., 2001; Deshmukh *et al*., 2003). As a comparison, there is no mid-chain ester found in *Hedera helix* leaf cutin, since no secondary −OH groups were found (Graça and Lamosa, 2010). In summary, these three findings suggested the existence of branched esters in cutin and the effect of cutin composition on its structure (Fang *et al*., 2001).

Arabidopsis cutin structure has not been studied yet, maybe because the cutin layer is very thin (Girard *et al*., 2012). As I have stated above, the abundant dicarboxylic acid (octadecadien-1,18-dioic acid, Franke *et al*., 2005) in *Arabidopsis* stem and leaves might act as a ‘bridge’, which forms ester bonds with hydroxy groups of two other hydroxy fatty acids, resulting in forming a cross-linking cutin matrix (Fig. 3).

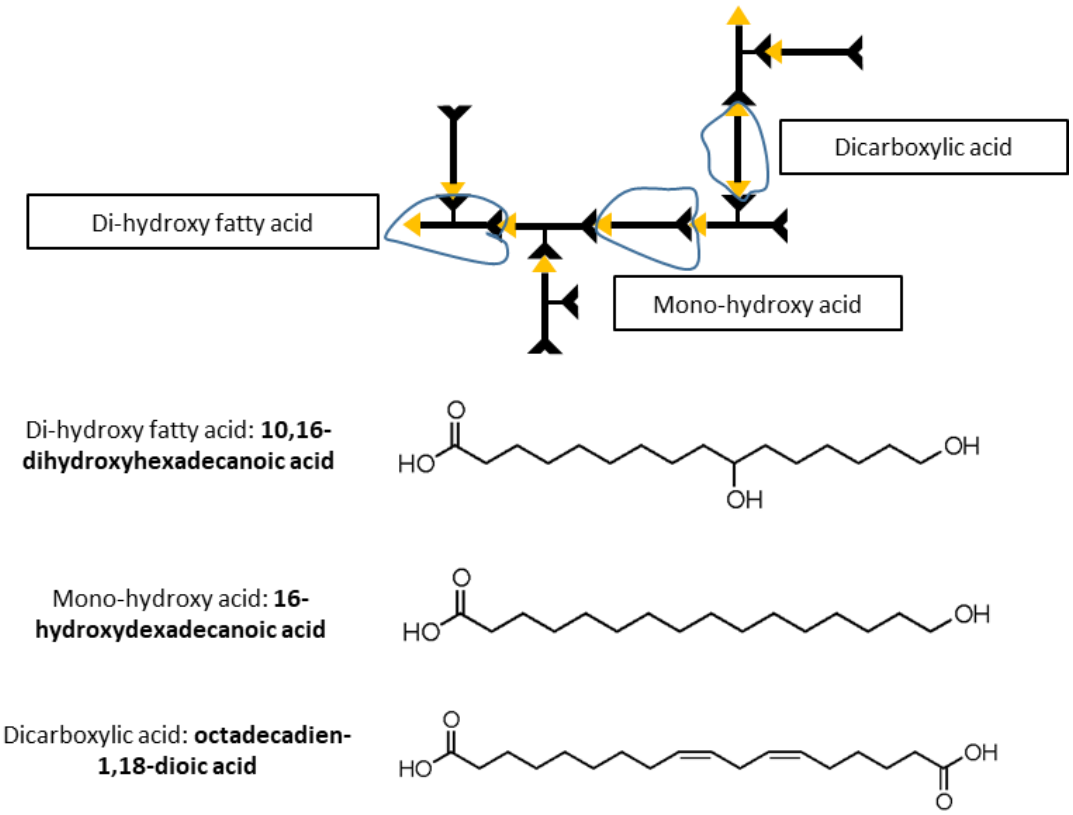

Figure 3. A proposed general cutin matrix pattern. Yellow triangle (▲) represents –COOH groups (free or engaged in ester bonds). Black half frame (⏷) represents –OH groups (free or in engaged in ester bonds). A thick black line (▬) represents C-C bonds. Di-hydroxy fatty acid [e.g. 10,16-dihydroxyhexadecanoic acid (di-HHA)] can be esterified via either the ω–OH group or the mid-chain –OH group; mono-hydroxy fatty acid [e.g. 16-hydroxyhexadecanoic acid (HHA)] can be esterified only via the ω–OH group. A dicarboxylic acid (e.g. octadecadien-1, 18-dioic acid) can potentially cross-link two neighbouring cutin molecules.

1.6 Cutin polymer biosynthesis

1.6.1 Cutin synthase, CD1 activity

An extracellular GDSL (a big family of enzymes containing a relatively conserved Gly-Asp-Ser-Leu consensus, the Leu can be substituted by Val for example) transacylase (40 kDa), exclusively located in cuticle layer of tomato fruit (immunolocalization), named cutin deficient 1 (CD1) (Yeats *et al*., 2012). It has been identified to be responsible for linearly polymerizing cutin via

transacylation of 2-mono(10,16- dihydroxyhexadecanoyl)glycerol (2-MHG) [a 2-MAG ester species] to another 2-MHG molecule or to a nascent cutin chain *in vitro* (*Eq.1*) (Yeats *et al.*, 2012; Yeats *et al.*, 2014). This reaction can be repeated to build up a (longer) cutin chain. This enzyme was identified in tomato (*S. lycopersicum*, cv. M82) fruit epidermis (Yeats *et al*., 2012), and more details will be introduced later.

CD1

acyl–glycerol + R–OH ↔ acyl–R + glycerol ***Eq. 1***

[acyl-glycerol: 2-MAG species, the acyl donor; R–OH: 2-MAG molecule or cutin chain, the acyl acceptor (R = e.g. 2-mono(hydroxy-C_{16} and/or C_{18})$_n$–glycerol)]

In-planta evidence showed that CD1 is also able to catalyse a transacylation reaction involving the secondary –OH group of diHHA in tomato fruit epidermis, as shown by attenuated total reflection–Fourier transforming infra-red (ATR-FTIR) microscopy to measure non-esterified –OH groups in wild-type and *cd1* knock-down tomato fruit, in which the *cd1* mutants showed significantly reduced secondary –OH esterification (Philippe *et al*., 2016). However, this research also showed that more primary –OH groups were esterified in mutants than in the WT, suggesting that another CD1-like transacylase compensated for the mutation, and CD1 predominantly catalyses the esterification of secondary –OH groups rather than primary ones, which was not observed *in vitro* (Yeats *et al.*, 2014). These two inconsistent results may indicate that CD1 functions differently according to environment hydrophobicity (more hydrophobic *in planta*).

Null *cd1* mutant mature (MG) green tomato fruit showed a >95% lower cutin load than the WT but recovered partially after re-introduction of a functional CD1-encoding sequence (Yeats *et al*., 2012). Girard *et al.* (2012) silenced the expression of *CD1* by RNAi, also resulting in cutin load reduction in developing tomato fruits (cv. Ailsa Craig). An accumulation of 2-MHG was detected by GC-MS in *cd1* mutants during the stage at which *CD1* was highly expressed, but not in the WT. The accumulation of substrate in the absence of the corresponding enzyme provides additional convincing evidence for the newly discovered CD1 activity (Yeats *et al*., 2012). Quantitative reverse transcription-polymerase chain reaction (qRT-PCR) and protein immunoblotting consistently showed that CD1 transcript and protein load are highest at the rapidly expanding stage of tomato fruit (small green fruit) (Yeats *et al*., 2012). In addition, the young leaf also expresses the second-highest amount of CD1 in the whole plants (Yeats *et al*., 2012), suggesting that CD1 is universal in the whole plant and required during plant growth.

A phylogenetic study of CD1 orthologues revealed that pPCUS1 (a CD1 orthologue in the moss *P. patens*) can also function as a transacylase by using 2-MHG as the substrate, but 14 times slower than CD1 and around 8 times slower than AtCUS1 (a CD1 orthologue in *Arabidopsis thaliana* flower) (Yeats *et al*., 2014). This result may provide a hint for substrate specificity, since both tomato fruit and *Arabidopsis* flower cutin is naturally dominated by diHHA, whereas *P. patens* cutin is dominated by 5-hydroxytetradecane dioic acid (Buda *et al*., 2013). Enzymic products were quantified and characterised by GC-MS, which showed that hydrolytic activity (acyl donor: 2MHG, acyl

acceptor: water, product: diHHA) of these three enzymes was lower than their transacylase activity, especially for CD1, only 4% product attributed to hydrolysis (AtCUS1: 22%, PpCUS1: 13%) (Yeats *et al*., 2014).

CD1 was found to share the same transcription factor, *SHINE3*, with CYP86As which are reported to be involved in cutin precursor intraprotoplasmic biosynthesis as stated above, suggesting that cutin polymer and precursor biosynthesis are co-regulated (Shi *et al*., 2013).

However, some questions remained to be answered: (1) whether there is any hydrolytic activity of CD1 *in planta*, (2) whether CD1 can also use other substrates for transacylation, besides 2-MHG, (3) whether any CD1 paralogues have the same or similar function, but are responsible of incorporating other cutin monomers, and/or re-modelling cutin. Investigating the question (2) and (3) will be the main tasks in this project.

Yeats *et al*. (2010) showed that GDSL family proteins (e.g. Unigene no: SGN-U583101 and SGN-U585129) are expressed higher in epidermis than in underlying collenchyma, and one gene (Unigene no: SGN-U583101) was specifically expressed in small green tomato fruit, consistent with the discovery of CD1 (Yeats *et al*., 2012). Another independent research group found that a cluster of GDSL family enzyme transcripts are localized in outer epidermis of rapid growing tomato (cv. Ailsa Craig) almost exclusively (Matas *et al*., 2011). These findings provide a hint for answering question (3) above: a group of GDSL enzymes genes were co-expressed with *CD1* at the same location and

time, and they may use diverse substrates besides 2-MHG to construct and re-model cutin.

Based on these discoveries, we proposed *in-situ* and *ex-situ* experiments to find out if CD1 and/or other transacylases can use cutins (acyl-R in *Eq. 1*) instead of 2-MHG as acyl donors, capable of transferring fatty acyl groups to acceptor molecules (R–OH in *Eq.1*; and Table 1); and if exogenous glycerol (as a cutin component and a product in *Eq. 1*) (Fang *et al.*, 2001; reviewed by Fich *et al.*, 2016) can be acyl acceptor in the cutin polymerization reactions, and therefore reverse the cutin polymerisation reaction (Table 1).

A hint of that CD1 may be able to use glycerol as a substrate is from Philippe *et al*. (2016), especially they detected that the accumulation of free glycerol in the cutin of *cd1* knockdown tomato fruit. The ratio between non-esterified glycerol at *sn-1,3* and *sn-2* was not altered by mutation (non-esterified *sn-2* was always lower than *sn-1,3*), suggesting that CD1 can transfer acyl groups to all the hydroxy groups of glycerol molecules (acyl acceptor), but preferably to the *sn-2*.

Table 1. Potential acyl donors and acceptors in cutin transacylation reactions.

Acyl **donors**	Acyl **acceptors**
2-mono(10,16-dihydroxyhexadecanoyl)glycerol and other MAGs	2-mono(10,16-dihydroxyhexadecanoyl)glycerol and other MAGs
* Cutin chains (cutin fatty acid residues)	Cutin chains and cutin fatty acids (e.g. HHA)
	* Glycerol
	* Polysaccharides

***** Acyl donors/acceptors proposed by us. Others are proven by Yeats *et al.* (2012).

1.6.2 CD1 and other GDSLs biochemistry background

The GDSL family is widespread in all kingdoms of life (Akoh *et al*., 2004; Yeats *et al.*, 2012). GDSL is a consensus near the N-terminus, and itself is not an absolutely conserved consecutive sequence, because the L can be substituted by threonine (T), tyrosine (Y) or isoleucine (I) (Akoh *et al*., 2004). Proteins in this family usually have a conserved catalytic serine (Ser, the 'S' of GDSL) as a nucleophile near the N-terminus, together with a conserved aspartic acid (Asp, different from the 'D' in GDSL) and a histidine (His) near the C-terminus to form the catalytic triad; and with a conserved glycine (Gly, different from the 'G' in GDSL) and an Asn to constitute the oxyanion hole (a pocket in the active site which uses backbone NH groups to stabilize C=O groups of ester substrates in transition states) (Akoh *et al*., 2004; Simón and Goodman, 2010).

CD1 (SlCUS1; Uniprot: G1DEX3) polypeptide sequence was aligned with selected GDSL enzymes from phylogenetically distant organisms, such as *E. coli* (TEP-I; Uniprot: P0ADA2), *A. thaliana* (Atg33370; Uniprot: Q8LB81), *Homo sapiens* (acyloxyacyl hydrolase; Uniprot: P28039), and showing that it is a classic GDSL enzyme because it contains a GDSL consecutive consensus near N-terminus as others, and its sequence close to C-terminus is similar to other GDSL enzymes to some extent (Fig. 4).

Figure 4. Comparison of polypeptide sequences between CD1 (SlCUS1) and other GDSLs in phylogenetically distant organisms. G1DEX3: SlCUS1 (CD1 in tomato fruit); P28039: an annotated acyloxyacyl hydrolase in *Homo sapiens*; Q8LB81: a CD1 orthologue (Atg33370) in *A. thaliana*; P0ADA2: a GDSL enzyme (TEP-I) in *E. coli*. This comparison was undertaken via T-coffee server (http://tcoffee.crg.cat/apps/tcoffee/do:regular). The black squares indicated by a black triangle highlight the conserved GDSL consensus.

The induced-fit catalytic mechanism can allow a single enzyme to utilise various substrates and thus to have diverse activities, thereby increasing the GDSL enzymes' versatility (e.g. the TEP-I protein from *E. coli* is multi-functional as protease and thioesterase etc.) (Akoh *et al*., 2004). The structural background of CD1 requires investigations, but we proposed that CD1's active site also undergoes induced-fit changes (promiscuity) to enable the binding of bulky molecules based on the hypothesis of that CD1 also uses cutin as the acyl donor (Table 1). Also, the Ser residue at the catalytic triad forms ester bond with the carboxy groups in esters (Akoh *et al*., 2004), enabling CD1 to specifically use esters (probably regardless of size) as the substrates as we proposed (Fig. 5).

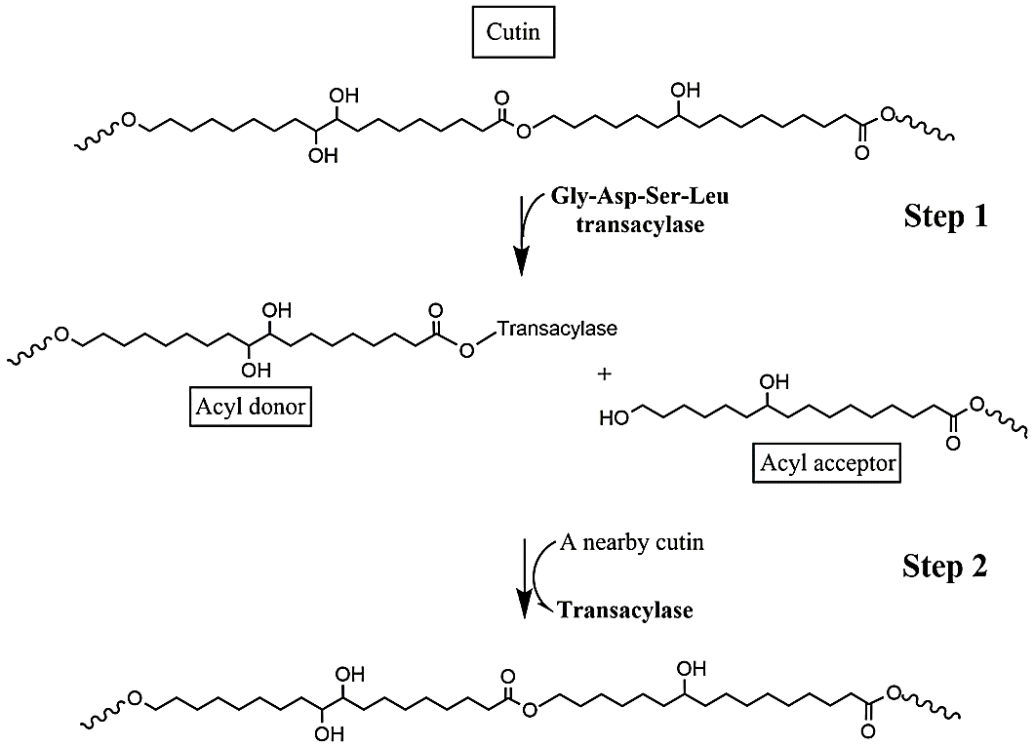

Figure 5. The proposed CD1 transacylase activity (e.g. cutin-to-cutin transacylation) mechanism. Cutin chain is proposed to be transiently cut by a

GDSL transacylase (Gly-Asp-Ser-Leu transacylase) during cell expansion, producing an acyl donor and an acyl acceptor. The acyl donor is produced because the carboxy terminus is ester-bonded with the hydroxy group of serine (not shown) at the catalytic triad, whereas the acyl acceptor does not contain the activated acyl group, only a hydroxy terminus. After incremental expansion ceases, the transacylase-bonded cutin molecule is then transacylated onto a nearby (the original or another) one with a hydroxy terminus (acyl acceptor) or secondary hydroxy groups, resulting in an intact cutin molecule again and the released transacylase is available for the next cycle.

Only a few GDSLs' functions in plants are understood (Akoh *et al*., 2004). In addition to the cutin synthase CD1, some GDSLs (xenobiotic-hydrolysing carboxyesterases) can metabolize herbicide esters (Gershater *et al*., 2006). For example, one of the apoplastic GDSL hydrolase in black-grass (*Alopecurus myosuroides*) was identified to hydrolyse aryloxyphenoxypropionate (AOPP) graminicides, and in turn activate it (Cummins and Edwards, 2004).

Different from the expectation, although CD1 has diverse proposed substrates (Table 1), transacylation is its only known function, since cutin hydrolysis activity is almost negligible *in vitro* (Yeats *et al.*, 2014). When a GDSL enzyme is working as a transacylase (e.g. CD1), the acyl-Ser bonds formed from the donor substrate (ester/peptide/thioester) will be attacked by an alcohol (or amine/thiol), resulting in a new ester or peptide bond.

1.7 Cutin re-modelling *in vivo*

As being stated above, cutin appears to play a role in constraining epidermal cell growth (Hoffmann-Benning and Kende, 1994), suggesting that cutin may be a net-like molecule that covers cells. Since cutin is an important barrier to

prevent plants from environmental damages as stated in '***Cutin Function***' section, and therefore its intact during cells expansion without rupturing is important. The putative strategies are either biosynthesis or re-modelling, a synergy of both is also very likely.

In sweet cherries (*Prunus avium*), the cutin load per fruit increased 115% throughout the expansion (measured at 85 days after full blossom, fully expanded compared with small fruit at 22 days after full blossom). In this case, cutin biosynthesis was used to accommodate cell expansion. From a biomechanical angle, the viscoelastic property of cutin is suggested to contribute in allowing medium-sized tomato fruit enlargement (España *et al*., 2014).

However, the surface area of the sweet cherries increased 311% in the meantime, resulting in the cutin load per cm^2 decreasing 63% (Peschel *et al*., 2007). The slow biosynthesis compared with the fast expansion might suggest that it may not the only strategy, other mechanisms, e.g. loosening of the existing cutin may be also involved in, as it is widely reported in another epidermal layer, cell wall (e.g. Fry *et al*., 2012). From another perspective, the thin cutin may require mechanical support before ripening, and therefore a reinforcement reaction cannot be excluded.

These two hypotheses were not proved yet and will be deeply investigated in this project by using three plant models (***'Studying models'***).

1.7.1 Post-synthetical loosening (**hypothesis**: cutin can be the acyl donor; hydroxy fatty acid, glycerol or water can be acyl acceptors)

Polysaccharide networks in plant cell walls are believed to be reversibly loosened by transglycanases to allow cell expansion (reviewed by Cosgrove 2005; Franková and Fry 2013). Similarly, cutin as a net-like polymer outside the cell wall may also need to be reversibly loosened to enable growth without cutin rupture.

CD1 and/or other unknown cutin transacylase(s) were proposed by us to cut cutin chains transiently via transacylation. After incremental cell expansion, the broken cutin chain may be re-linked to another cutin chain. This behaviour would resemble that of xyloglucan (an abundant polysaccharide component of primary cell walls) in reactions catalysed by xyloglucan endotransglucosylase (XET) activity (Fig. 6) (Thompson and Fry, 2001). Our lab has studied XET very intensively, so we are curious if any transacylase in cuticle and XET in cell wall work in parallel during cell expansion.

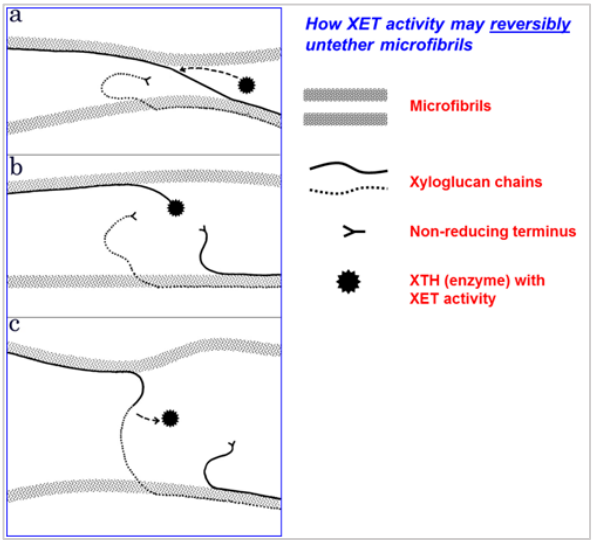

Figure 6. Xyloglucan endotransglucosylase (XET) action *in vivo*. Microfibrils (cellulose) are proposed to be tethered by xyloglucan. To allow cell expansion, polysaccharides need to be loosened transiently (e.g. cut by XET action). After incremental expansion, the broken xyloglucan will be re-linked to another (newly synthesised or pre-existing one) (Thompson and Fry, 2001).

We also proposed that free glycerol may be able to loosen cutin in the presence of CD1 as at high levels it can theoretically drive the reverse reaction of *Eq.1* (i.e. an 'idling' reaction), though glycerol may have versatile functions *in vivo*. For example, it has been suggested that one glycerol molecule may can be esterified with multiple cutin hydroxy-fatty acid chains, and hydrogen bonds between the attached fatty acids can tighten cutin (Graça *et al.*, 2002). The mysterious effects of glycerol led us to explore if the exogenous glycerol can influence cutin structure *in vivo*.

Another important mechanism of loosening cutin is hydrolysis, despite that it will not be studied in this project. Hydrolysis mechanism uses water as the acyl acceptor instead of a hydroxy fatty acid or glycerol. This mechanism is essential when cutin is unnecessary, such as the one on stigma is hydrolysed by pollen secreted cutinase (Shayk and Kolattukudy, 1977). Another example is in fruit: a significant decrease of cutin esterification index in fully ripened tomato fruit than small green stages was observed (España *et al.*, 2014).

1.7.2 Post-synthetical mechanical reinforcement (**hypothesis**: polysaccharides can be the acyl acceptors)

Cutin is located next to polysaccharides in cell walls, as shown by immunolocalization (Jeffree 2006; *Segado et al*., 2016; Mazurek *et al*., 2017) and co-extraction of cutin and polysaccharide components (Fang *et al.*,2001), suggesting a potential interaction between cutin and wall polysaccharides (e.g. pectin) (Fang *et al.*,2001; reviewed by Fich *et al*., 2016).

Polysaccharides have been suggested to provide mechanical support to the cuticle by stiffening it and contributing to elasticity (López-Casado *et al*., 2007; Takahashi *et al*., 2012; España *et al.*, 2014). Moreover, the cutin:polysaccharides ratio may determine the stress (turgor pressure) required for tomato fruit expansion (Peschel *et al.*, 2007).

Wall polysaccharides are diverse: some are composed of monomers dominated by hydroxy groups (Fig. 5a: e.g. cellulosic glucose and hemicellulosic xylose) and some have both carboxy and hydroxy groups (Fig. 5b: e.g. pectic galacturonic acid). There are two possible mechanisms of polysaccharide–cutin cross-linking: (1) cutin elongation starts at the cross-linking point [i.e. esterified hydroxy fatty acid –COOH groups (acyl donor) are transacylated to polysaccharide –OH groups (acyl acceptor)] (Fig. 7a); (2) cross-linking terminates cutin elongation [i.e. pectin's methyl esterified carboxy groups (–$COOCH_3$, acyl donor) are transacylated to a hydroxy-fatty acid's –OH group(s) (acyl acceptor)] (Fig. 7b).

We proposed the later mechanism because the galacturonic acid with an active –COOH (esterified with methanol) is completely different from the CD1 acyl donor, 2-MHG, and therefore CD1 may cannot use pectin as an acyl donor. Despite that plant has pectin methylesterases (PMEs) to assist pectin loosening in response to fruit ripening (reviewed by Brummell and Harpster, 2001) via transferring the acyl group at C-6 to water, this enzyme is not in the GDSL family as CD1 is, and therefore the PMEs are not expected to transfer pectin to cutin. However, the –OH groups of galacturonic acid and any other sugar residue may act as acyl acceptor since GDSL-type transacylases may

not have strict acceptor substrate specificity (i.e. diverse acceptors: 2-MHG, cutin, H_2O etc.).

In reality, only small numbers of cutin and polysaccharide monomer residues may be cross-linked via covalent bonds (i.e. ester bonds and/or ether bonds etc.) (reviewed by Fich *et al*., 2016), which are thus difficult to test for.

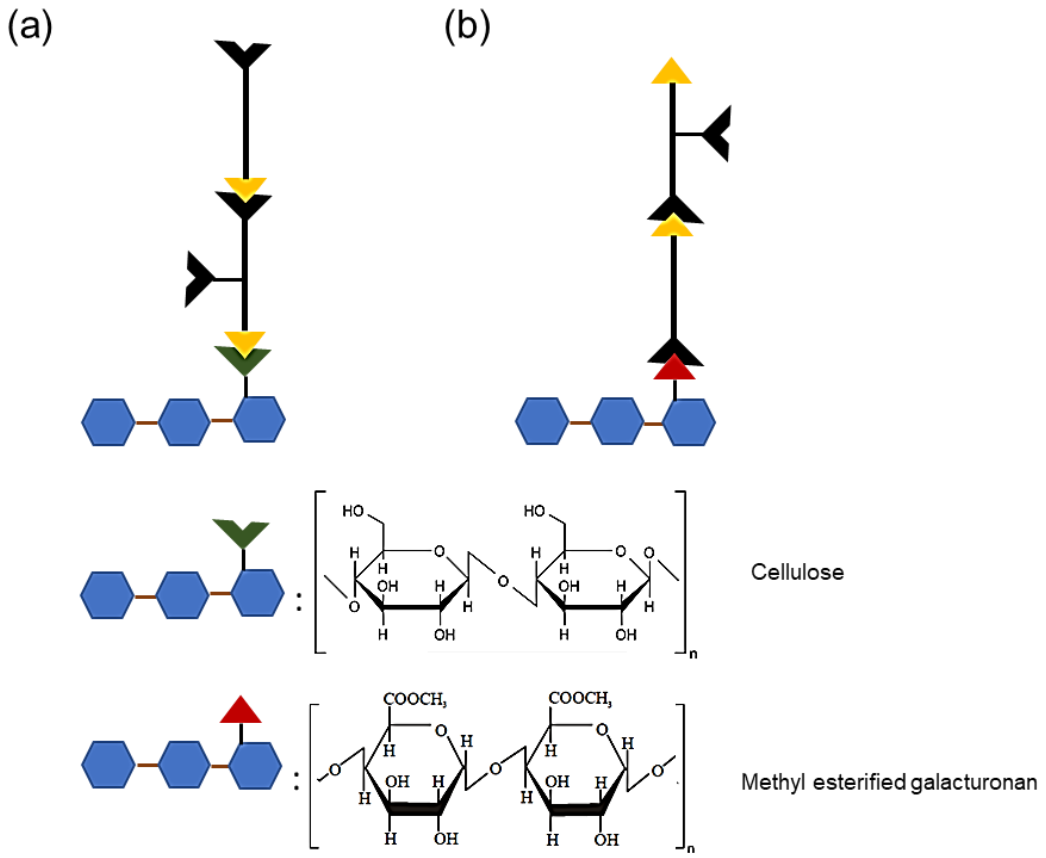

Figure 7. Proposed linking patterns of cutin and polysaccharides. Two possible cutin-polysaccharide cross-linking mechanisms: (a) cutin carboxy group (▲) is the acyl donor, polysaccharide hydroxy group (⌄) is the acceptor, cutin hydroxy groups are represented in (⌄); (b) polysaccharide carboxy group (▲) is the acyl donor, cutin hydroxy group (⌄) is the acceptor. Thick black lines (▬) represent the backbone of a cutin fatty acid. Blue hexagons (⬢) represent polysaccharide building blocks. Thin black lines (—) represent the C–C bonds with in a cutin fatty acid molecule. Brown lines (▬) represent glycosidic bonds between polysaccharide building blocks. Chemical structure of examples of (a) polysaccharide acyl donor and (b) polysaccharide acyl acceptor was illustrated.

1.8 Studying models

Tomato (*Solanum lycopersicum*) is an emerging model in which to study cutin because its fruit cuticle is thick and the major building blocks are 10,16-dihydroxyhexadecanoic acid as in most other plants (Girard *et al.*, 2012). In contrast, the traditional genetic model, *Arabidopsis,* has thin cuticles which are hard to isolate, and the dominant cutin components in leaves and stems are atypical (unsaturated dicarboxylic acids) (Franke *et al*., 2005).

My experiments focused on tomato fruit and two other easily-peeled models: *Hylotelephium spectabile* (ice plant) leaves and *Pisum sativum* (pea) epicotyl.

1.9 Main goals of the thesis

1. Test and validate cutin re-modelling transacylase activity: enzyme activity will be assayed with cutin (from all the three plants) as acyl donor, and a portfolio of radio-labelled fatty acids and mono-/oligo-/poly-saccharides as acyl acceptors *in situ* (with endogenous enzymes) and *ex situ* (with crude enzyme extract). Assay conditions will be optimized and any enzymic products will be analysed.

2. Test factors that affect the discovered transacylase activities, e.g. environmental stresses (humidity, temperature and light) and age *in situ* and *ex situ*.

3. Identify novel activities of CD1: CD1 will be heterologously produced and purified, and its activity with various substrates will be tested *in vitro*.

Chapter 2. Materials and methods

Materials

2.1 Biochemistry

2.1.1 Chemicals

All the chemicals used for this research were mainly obtained from Sigma (St. Louis, USA), Fisher (Hampton, USA), VWR (Radnor, USA), New England Biolabs (Ipswich, USA), Thermo Scientific (Waltham, USA), Merck (Kenilworth, USA) and Bio-Rad (Hercules, USA).

2.1.2 Plant material

Hylotelephium spectabile (*Sedum*; ice plant) was kindly donated by Prof. Stephen Fry (University of Edinburgh, UK); *Pisum sativum* (pea; cv. meteor) and *Solanum lycopersicum* (tomato, cv. Alisa Craig) were commercially available. Tomato (cv. M82) was kindly donated by Prof. J.K.C. Rose (Cornell University, USA). These three species were used as sources of epidermis and transacylases. Ice plant and tomatoes were grown in greenhouse with 16 hours light (21°C) and 8 hours dark (18°C). Peas were grown with or without (covered in aluminium foil) light for 4–10 days at different temperatures, usually at 25°C.

2.1.3 Enzyme assay buffers

All the buffers used in enzyme assays are shown in Table 2.

Table 2. Details of enzyme assay buffers

pH	Name*	Additional ingredients	Purpose
3.5	25 mM Formate (Na^+)		*In-situ*, *ex-situ* and *in-vitro* cutin re-modelling transacylase assays
4.5	25 mM Acetate (Na^+)		
5.5-6.5	25 mM Succinate (Na^+)		
6.5	25 mM Phosphate (Na^+) or 40 mM lutidine (acetate)		
7.5	25 mM Tris(Cl^-)		
5.5	350 mM Succinate (Na^+)	1% Triton-X100 (v/v), 10 mM DTT or 5 mM 2-mercaptoethanol	Cutin-to-cutin transacylase extraction
6.5	350 mM Succinate (Na^+)	1% Triton-x100 (v/v)	Cutin-to-polysaccharide transacylase extraction
8.8	50 mM Ammonium (acetate)		Proteinase K (from *Tritirachium album*)
7.5	50 mM Collidine (acetate)		Lipase (from *Aspergillus niger*)
8.0	50 mM Collidine (acetate)		Cutinase (from *Aspergillus nidulans)*
4.5	Pyridine/acetate/water (1/1/98, v/v/v)		Xyloglucan endoglucanase (XEG)

* For example, “25 mM Formate (Na^+)” implies “25 mM formic acid, adjusted to pH 3.5 with NaOH”.

2.1.4 Radioactive materials

All the radioactive substrates used for enzyme assays are shown in Table 3.

Table 3. Details of radioactive substrates

Category	Name	Origin
Fatty acid	16-Hydroxy-[16-^{3}H]hexadecanoic acid (HHA)	From EDIPOS http://fry.bio.ed.ac.uk//edipos.html
	[1-^{14}C]Hexadecanoic acid (HA)	Purchased from American Radiolabeled Chemicals, Inc. (St. Louis, USA)
Glycerol	[^{14}C]Glycerol	Purchased from American Radiolabeled Chemicals, Inc.
Oligosaccharide	[^{3}H]XXXGol	From EDIPOS http://fry.bio.ed.ac.uk//edipos.html
	[^{3}H]XXGol	
	[^{3}H]XGol	
	[^{3}H]Cellobiiotol	
	[^{3}H]Glucitol	
	[^{3}H]XXFGol	
	[^{3}H]Arabino-octaitol (Ara_8-ol)	
	[^{3}H]Galacturono-octaitol($GalA_8$-ol)	
	[^{3}H]Mannotriitol (Man_3-ol)	
	[^{3}H]Xylopentaitol (Xyl_5-ol)	

2.1.5 Enzymes for transacylase product identification

Proteinase K (from *Tritirachium album*), lipase (from *Aspergillus niger*), Driselase (from Basidiomycetes) were obtained from Sigma. Xyloglucan-specific endo-β-1,4-glucanase (XEG) was obtained from Novo Nordisk (Bagsværd, Denmark).

Pichia pastoris (strain SB), which produced the recombinant *Aspergillus nidulans* cutinase (AN7541.2), was obtained from Fungal Genetics Stock Center (FGSC, US). Cultivation and induction media recipes were obtained from Bauer *et al.* (2006) (Appendix 1).

2.1.6 Chromatography techniques for qualitative analysis

Diverse chromatography techniques were used in this thesis to identify fatty acids, oligosaccharides and proteins. Their details are described in Table 4 below.

Table 4. Details of chromatography techniques used for qualitative analysis

Name	Solvent migration direction	Resolving mechanism
Thin-layer chromatography (TLC)	Bottom to top (ascent)	● Molecular weight ● polarity
Paper chromatography (PC)	Top to bottom (descent)	● Molecular weight ● Polarity
Paper electrophoresis (PE)	Top (cathode) to bottom (anode) (descent)	Charge-to-mass ratio
Size-exclusion column	Alone gravity	Molecular weight
SDS-PAGE	Cathode to anode	Charge-to-mass ratio

2.2 Gene (*CD1*) cloning

2.2.1 Chemicals

All the chemicals used for this research were of molecular biology grade obtained from New England Biolabs (Ipswich, USA), Thermo Scientific (Waltham, USA), Qiagen (Hilden, Germany), Sigma (St. Louis, USA) and Invitrogen (Carlsbad, USA).

2.2.2 Home-made buffers

Commercial buffers are not listed; all the home-made buffers are listed in Table 5.

Table 5. Details of home-made buffer for *CD1* cloning and expression

pH	Ingredients	Function
9.5	10X extraction buffer: 1 M glycine (Na^+), 100 mM EDTA, 1 M NaCl,	RNA extraction
7.3	2% v/v 0.5 M filter-sterilized MES pH 5.6, 0.05% acetosyringone and 1% 1 M $MgCl_2$	Tobacco infiltration buffer
8.3	180 mM Tris (borate) and 5 mM EDTA	1X TBE, agarose gel running

2.2.3 Plasmid

pEAQ-HT plasmid and the construct pEAQ-HT-GFP (as a positive control) were kindly donated by Prof. George Lomonossoff, John Innes Centre, UK.

2.2.4 Bacteria

E. coli (DH5α) and *Agrobacterium tumefaciens* (GV3101) were kindly donated by Dr. Attila Molnar (University of Edinburgh, UK).

2.2.5 Antibiotics

Both pEAQ-HT and *Agrobacterium* GV3101 contained antibiotic sensitive genes, and the antibiotics used are listed in Table 6.

Table 6. Details of antibiotics for *CD1* cloning and expression

Antibiotic	Solvent	Purpose	Stock conc.	Working conc.
Kanamycin	H_2O	*E. coli* and *Agrobacterium* selection	50 mg/ml	50 µg/ml
Rifampicin	DMSO	*Agrobacterium* selection	50 mg/ml	50 µg/ml
Gentamycin	H_2O	*Agrobacterium* selection	25 mg/ml	25 µg/ml

2.2.6 Primers

Manually designed primers based on *CD1* and pEAQ-HT sequences are listed in Table 7.

Table 7. Details of primers for *CD1* cloning

Name	Restriction enzyme cutting site attached to 5'	Sequence	Purpose	% GC content
Sl_CD1_ATG_for	TTTACCGGT	ATGGCCAC ACCTACTA TTATTTTG AG	CD1 coding sequence PCR	39
Sl_CD1_noStop_ rev	AATCCCGGG	TGCATGTG AATCCATA GCCAG		48
CPMV_prom_min1 00_for		GACGAGGT ATTGTTGC CTGTACTT C	pEAQ-HT-CD1 transformed *Agrobacterium* colony PCR	48
CPMV_prom_min1 00_rev		GAGCACAG AAAACCGC TCACC		57

2.3 Protein (CD1) extraction and purification

2.3.1 Plants

Nicotiana benthamiana (1-month-old) was grown at 21°C day (16 h) and night (8 h). It was used as a recipient for agroinfiltration and was kindly donated by Dr. Attila Molnar (University of Edinburgh, UK).

2.3.2 Immobilized metal affinity chromatography

HisPur™ Cobalt Resin (Thermo Scientific) and column extender were kindly donated by Dr. Attila Molnar (University of Edinburgh, UK).

2.3.3 Buffers

All the buffers used to extract and purify CD1 were modified based on Yeats *et al*. (2012) in Table 8.

Table 8. Details of buffers for CD1 extraction and purification

4.5	5 mM sodium acetate, 500 mM NaCl, 0.1% (v/v) Triton X-100, 0.5 mM PMSF, 1 mM 2-mercaptoethanol	Protein extraction from tobacco leaves
7.0	50 mM Phosphate (Na^+), 300 mM NaCl	Co^{2+} column wash buffer
7.0	50 mM Phosphate (Na^+), 300 mM NaCl, 10 mM imidazole	Co^{2+} column elution buffer 1
7.0	50 mM Phosphate (Na^+), 300 mM NaCl, 30 mM imidazole	Elution buffer 2
7.0	50 mM Phosphate (Na^+), 300 mM NaCl, 90 mM imidazole	Elution buffer 3
7.0	50 mM Phosphate (Na^+), 300 mM NaCl, 270 mM imidazole	Elution buffer 4
5.0	20mM MES, 0.1M sodium chloride	Co^{2+} column clean-up buffer

2.3.4 Home-made SDS-PAGE recipe

SDS-PAGE gels used in this project were all home-made; the recipes are as follows:

Resolving gel (15%): 1.5 mm thickness

1.5 M Tris (Cl^-) (pH 8.8)	2.6 ml
10% SDS	100 µl
Acrylamide/bis (29/1, w/w) solution (40%)	3.75 ml
10% Ammonium persulfate (AMPS)	100 µl
Tetramethylethylenediamine (TEMED)	10 µl
Water	3.44 ml

Stacking gel (4%): 1.5 mm thickness

0.5 M Tris (Cl^-) (pH 6.8)	1.25 ml
10% SDS	50 µl
Acrylamide/bis (40%)	0.5 ml
10% AMPS	50 µl
TEMED	5 µl
Water	3.145 ml

4X Laemmli buffer, pH 6.8

Glycerol	40% (v/v)
SDS	8% (w/v)
Tris (Cl^-)	20% (w/v)
Bromophenol blue	0.4% (w/v)
DTT	0.4 M

5X SDS-PAGE running buffer, pH 8.3

Tris (glycinate)	125 mM
SDS	0.5% (w/v)

2.4 Cutin re-modelling transacylase assays

2.4.1 Radio-labelled transacylase substrates preparation and qualitative analysis

[^{3}H]Fatty acids qualification

The purity of each fatty acid used was checked by loading an aliquot, together with appropriate markers on thin-layer chromatography (TLC) plates (Silica gel 60, Merck) (Table 4), which were developed in toluene/acetic acid (9/1, v/v) for 1 h (1–3 ascents), followed by being scanned (AR2000 TLC radio-scanner). Non-radioactive markers were stained in 0.0065% (w/v) rhodamine 6G dissolved in 96% ethanol (Sigma), their migration distances (R_F) were compared to the radioactive samples. For the impure radioa-labelled fatty acids, a big quantity of the sample was analysed by TLC, and the band at the expected position was carefully cut down and eluted in ethyl acetate. The eluent was then dried in SpeedVac (ThermoFisher) and then re-dissolved in dimethyl sulfoxide (DMSO), which is an amphiphilic solvent can dissolve fatty acids and mixed well with aqueous buffer in downstream enzyme assays. The pure stocks (usually dissolved in volatile organic solvents) were directly dried and re-dissolved in DMSO.

Methyl esterified [^{3}H]GalA$_8$-ol preparation

[^{3}H]GalA$_8$-ol was dried in SpeedVac and re-dissolved in 0.1 ml 50 mM MES buffer, pH 6.5. The same volume of methanol was added (final conc. = 50%

MeOH) and mixed well. Right before the incubation, 3 mg *N*-hydroxysuccinimide (NHS) was dissolved in 1 ml MeOH/MES (1/1), and then 45 mg ethyldimethylaminopropylcarbodiimide (EDC) was added and dissolved in the same tube. This solution was added to the [^{3}H]GalA$_8$-ol solution immediately after being prepared. After a thorough mix, the reaction mixture was incubated on bench overnight at room temperature. The methyl esterification reaction was stopped by adding 100 µl acetic acid, which competes with [^{3}H]GalA$_8$-ol to react with methanol.

The complete methyl esterified [^{3}H]GalA$_8$-ol was purified as follows: the final incubation mixture was loaded onto a Whatman no. 3 chromatography paper, together with three external markers: glucose, galacturonic acid and [^{3}H]GalA$_8$-ol. The compounds were separated according to their charge-to-mass ratio by paper electrophoresis (in acetic acid/pyridine/water, 1/33/300, v/v/v, pH 6.5, 3 kV, 90 min) (Table 4). The paper was then dried, and the lanes with radio-labelled samples on were scanned as above, whereas the non-radio-labelled markers were stained by silver nitrate (Partridge, 1946). The complete methyl esterified [^{3}H]GalA$_8$-ol was expected to stay at the loading origin, which was then cut off and eluted in 50% MeOH, finally dried in SpeedVac and re-dissolved in appropriate volume of 0.5% chlorobutanol.

[^{3}H]Xyl$_5$-ol preparation

[^{3}H]Xyl$_6$-ol was dried in SpeedVac and re-dissolved in 20 µl 0.1 M trifluoroacetic acid (TFA), which was then incubated at 85°C for 1 h. Hydrolysed products were identified by TLC [butan-1-ol/acetic acid/water

(BAW), 2/1/1, v/v/v, 2 ascents)]. Hydrolysed products were identified by being scanned as above, with [^{3}H]Xyl$_6$-ol and [^{3}H]xylitol as external markers. [^{3}H]Xyl$_5$-ol was chosen to be used as a transacylase substrate because it is satisfyingly long enough to mimic polysaccharide *in planta*, but not long enough to cause artefact due to non-specific hydrogen bonds. The [^{3}H]Xyl$_5$-ol was eluted down by 0.5% chlorobutanol, followed by dried in SpeedVac and re-dissolved in appropriate volume of 0.5% chlorobutanol.

2.4.2 Cutin re-modelling transacylase assays *in situ*

***In situ*: endogenous enzymes and cutin**

Preparation of epidermis with endogenous enzyme

Epidermis was isolated from plant models manually (ice plant leaf and tomato fruit epidermis was peeled off directly; scalpel was used for removing mesophyll if necessary), then immediately frozen at –80°C for long-term use. Frozen epidermis was thawed on ice before use, followed by either washing in cold buffer or boiling in water for 1 h. Pea epicotyl was frozen and thawed prior to epidermis isolation, which was undertaken by rolling a glass rod on the frozen and thawed pea epicotyls; the epidermal samples were used on the day. The same washing procedure was the same as above.

Transacylase assay set up

For assays, epidermis was blotting dried and cut into small pieces, and then incubated with 0.25–1 kBq radio-labelled substrates (e.g. [^{3}H]HHA and

[^{3}H]XXXGol) (Table 3) in buffers (Table 2) at room temperature for 24 h. Epidermis weight to incubation mixture volume was usually 1/6 (g/ml).

The reaction was stopped by adding 10 volumes of freshly prepared methanol/formic acid/water (MFW) (9/1/1 or 5/1/5, v/v/v), which lowered the pH dramatically (~pH 1.7) to inhibit enzyme activities.

Epidermis was then either washed in tubes by periodically changing MFW or transferred onto chromatography papers (Whatman No. 1), which were run in MFW for 5–9 days.

2.4.3 Cutin re-modelling transacylase assays *ex situ*

***Ex situ*: exogenous enzymes, but endogenous acyl donors**

Preparation of epidermis without endogenous enzyme

Epidermis containing cutin was prepared as follows: frozen and thawed epidermis was boiled in water for 1 hour, and then washed in acetone for 3 x 1 h, boiled in chloroform for 90 seconds (Szafranek *et al*., 2008), followed by being washed in chloroform/methanol (CM) (2/1, v/v) overnight. These steps were designed to denature endogenous enzymes, remove intracellular interferences and cuticle wax. Polysaccharide was removed in some experiments by incubating epidermis with 0.1% (w/v) Driselase in pH 4.5 buffer (Table 2) at 37°C for 5 days or 0.2 M ammonium oxalate (pH 4.3) at 100°C overnight. Acetone was used to finalize the wash procedure, and epidermis was completely dried in a fume hood.

Enzyme extraction

Apoplastic enzyme was extracted as follows: the freshly isolated pea epicotyl epidermis was ground in liquid nitrogen into small pieces, and then ground thoroughly in the extraction buffer (Table 2) with a 1/2 (w/v) ratio; 10% weight of PVPP (preventing the denaturation of enzymes in the presence of natural tannins etc.) and a pinch of sand (Bio-Rad) were added during grinding. Triton X-100 (1% v/v), 10 mM DTT and 5 mM EDTA were included in some experiments.

The extraction mixture was shaken at 4°C for 2 h, followed by centrifuging at 4°C for 15 min at full speed. The supernatant containing apoplastic enzymes was used for cutin re-modelling transacylase *ex-situ* assays.

The following metal salts were added to the enzyme extract in some cutin-to-[^{3}H]HHA experiments: $CaCl_2$, $MgCl_2$, $MnCl_2$, $FeSO_4$, $NiSO_4$, $CuCl_2$, $ZnCl_2$, $CoCl_2$ and KCl (final conc. = 10 mM).

Transacylase assay set up

For assays, the prepared epidermis (2–10 mg) was incubated with ~0.25–1 kBq radioactively-labelled substrate in 100–300 µl enzyme extract for 3–24 hours at room temperature. Reaction termination and wash procedures were the same as *in-situ* experiments above.

2.4.4 Cutin synthase, CD1 transacylase assays *in vitro*

***In vitro*: exogenous enzymes and acyl donors**

The cutin synthase, CD1, was heterologously produced in *N. benthamiana*, purified (Table 8) and assayed radio-chemically and spectrophotometrically.

Radio-chemistry

Epidermis (10 mg) without endogenous enzymes was prepared as above, followed by being incubated with ~1 kBq [^{3}H]HHA or [^{3}H]XXXGol in 300 µl pH 5.5 or 6.5 buffers (Table 2) with or without the purified His_6-tagged CD1 (1 µg) at room temperature for one day. Reaction termination, washing and CD1 product quantification were as above.

Spectrophotometry

A stock solution of the potential acyl donor, *p*-nitrophenyl palmitate was prepared by emulsification in 5% (v/v) Triton X-100 first, then dilution into water to achieve the desired final concentration (5 mM). Mild heat (~40°C) was used for thorough dissolution. Stock solutions (1% w/v) of proposed acyl acceptors (e.g. HHA, xyloglucan oligomers) were dissolved in water containing 5% (v/v) Triton X-100. For assays, both acyl donor and acceptor were diluted 10-fold, and incubated with or without 1 µg His_6-tagged CD1 in 100 µl pH 6.0 buffer (Table 2) at 25°C for 2 days. CD1 product, *p*-nitrophenol, was detected by adjusting the pH to 7.15 ± 0.02 by adding 20 µl pH 8.0 buffer (50 mM collidine acetate), followed by measuring the absorbance at 405 nm (PerkinElmer).

2.4.5 Transacylase product quantitative and qualitative analysis

Crude enzymic product quantification

The thoroughly washed epidermis, which may contain a mixture of enzymic products was dried and transferred into scintillation vials, containing either 2 ml of home-made scintillation fluid (0.5% PPO w/v and 0.05% POPOP w/v dissolved in toluene) or OptiScint HiSafe (Fisher Scientific Ltd.), and mixed well by rocking or wheeling overnight to improve counting efficiency. The former toluene-based scintillation fluid was preferred in most experiments because the later one may cleave ester bonds (the predicted transacylase products).

For liquid or wet samples, the procedures were the same, except that 10 volumes of OptiPhase HiSafe (Fisher) scintillation fluid was added, and there was no necessity to mix overnight. Counting efficiency index (H#) was usually on for liquid samples to monitor the counting efficiency.

In most experiments, each sample was scintillation-counted for 5 minutes, 2-4 times, in Beckmann LS6500 or LS5000 scintillation counters.

Chemical degradation: isolate the transacylase products from others

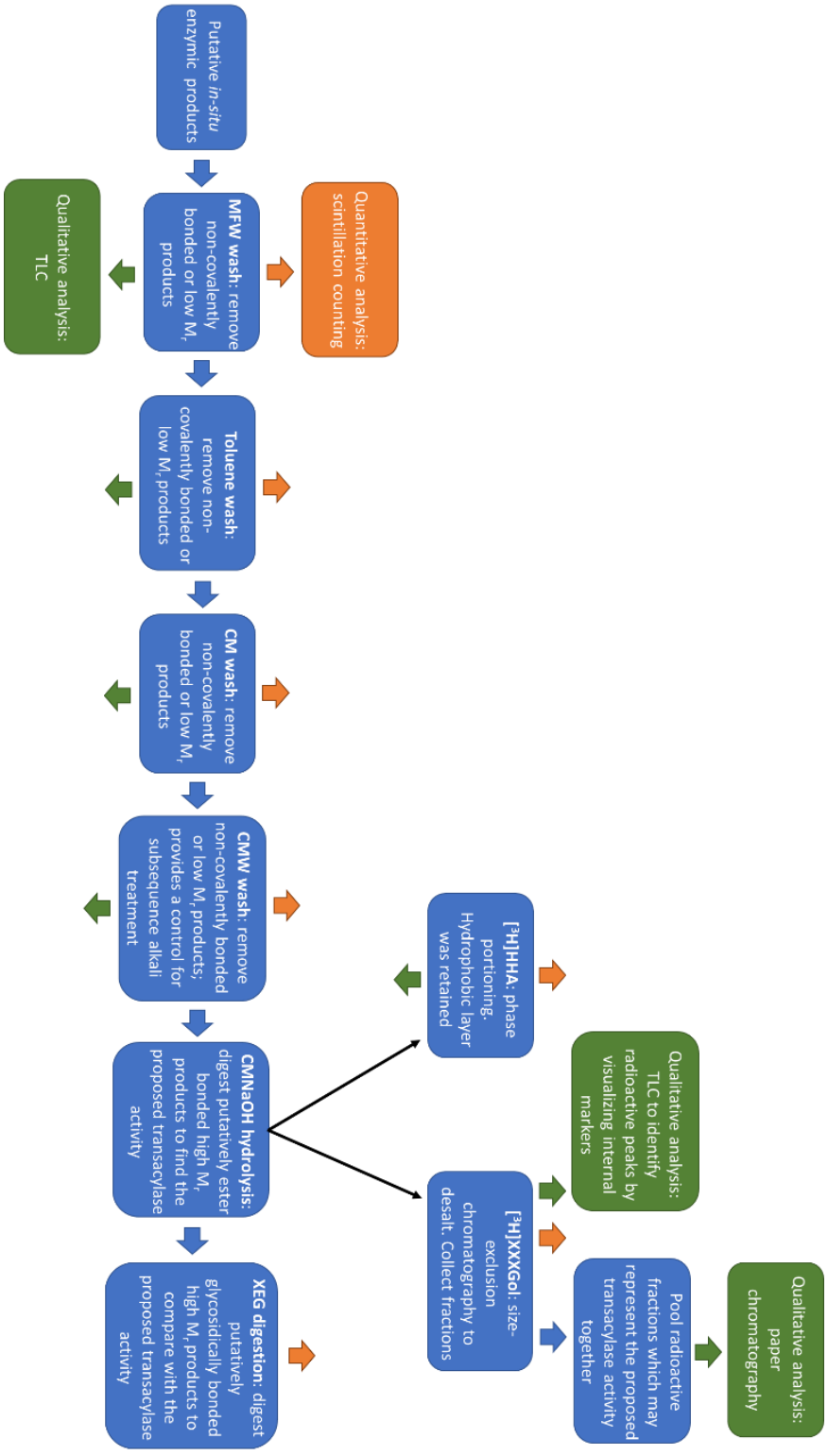

Figure 8. Flowchart of chemical degradation procedure to isolate the transacylase products. Blue squares: main degradation steps being employed.

Orange arrows and squares: quantitative analysis (= scintillation counting). **Green arrows and squares**: qualitative analysis (= TLC and paper chromatography). **Black arrows**: divergent experimental steps for different exogenous substrates.

To look for the transacylase products we were interested in, chemical degradation strategy was employed.

The MFW washes, which were used to remove un-bound radioactivity was collected for later analysis.

Sequentially, the MFW-washed epidermis samples were then washed in toluene, CM (2/1, v/v) and chloroform/methanol/water (CMW, 10/10/3, v/v/v) to remove hydrophobic interferences thoroughly. Supernatants were collected for later analysis.

To remove the possible cell wall protein–radioactivity conjugates, ≥ 3 U/ml proteinase K from porcine liver (Sigma) was incubated with the MFW etc.-washed epidermis samples at pH 8.8 (Table 2) at 37°C for 3 days, to cleave peptide bonds. Supernatant was collected for later analysis.

To look for cutin-to-radioactivity transacylase product, ester bonds were cleaved by incubating the proteinase K-digested epidermis samples with 0.02 U/ml lipase from *Aspergillus niger* (Sigma) at pH 7.5 (Table 2) at 25°C for 2 days. Another enzyme used to cleave the ester bonds was an annotated cutinase (*AN7541.*2) from *Aspergillus nidulans*, which was heterologously expressed in *Pichia* pastoris (SB, FGSC) (induction protocol see Appendix). The freeze-dried culture media containing the cutinase (final conc. = 0.45%, w/v) was incubated with the lipase-digested epidermis samples at pH 8.0

(Table 2) at 37°C for 2–3 days. Supernatants for both digestions were collected for later analysis.

The ester bonds were also hydrolysed chemically: chloroform/methanol/4M NaOH (CMNaOH, 10/10/3, v/v/v, ~pH 14). The cutinase-digested epidermis samples were hydrolysed in CMNaOH at room temperature for 1 day. The reaction was stopped by adding 5 times moles of acetic acid to NaOH. More details in this step will be explained in the next two sections.

Another possible enzymic product, cell wall polysaccharide–radioactivity conjugates were tested by incubating the CMNaOH-hydrolysed epidermis with 0.1% (w/v) XEG in pH 4.5 buffer (Table 2) at room temperature overnight, or alternatively, incubating with 2 M TFA for 1 h at 120°C to hydrolyse glycosidic bonds generally. Supernatant was collected for later analysis.

Cutin-to-[^{3}H]fatty acids transacylase products quantification and qualitative analysis

For **cutin-to-[^{3}H]fatty acids** assays, the supernatant of CMNaOH hydrolysis was transferred to another fresh tube, phase partitioning was performed by the modified Folch lipid extraction procedure (Folch *et al*., 1957): 0.8 volume of 0.9% NaCl (w/v) was added gently to the supernatant, upper aqueous was removed after a gentle mixing and centrifugation; a mixture of 0.9% NaCl solution and methanol (1/1, v/v) was added gently to replenish the methanol lost in last step, upper aqueous was removed after centrifugation. The left

hydrophobic layer was dried in fume hood, and re-dissolved in MFW (9/1/1, v/v/v) for later analysis.

An aliquot of each treatment's supernatant was assayed by scintillation counting as above to quantify transacylase products if any.

The rest of the supernatants were dried in SpeedVac, and re-dissolved in CMW (10/10/3, v/v/v) and MFW (9/1/1, v/v/v), which were then loaded onto TLC plates (toluene/acetic acid, 9/1, v/v, 3 ascents). Substances solubilized in/released into the supernatant was qualified by scanning the TLC plates as above. In the cases that radioactivity was too low for the TLC scanner, the sample-loading track on the TLC plate was cut into small streaks with 1-cm width along the migration distance, followed by scintillation counting by mixing with OptiScint HiSafe scintillant as above.

Cutin-to-[^{3}H]oligosaccharides transacylase products quantification and qualification

For **cutin-to-[^{3}H]oligosaccharides** assays, the chemical degradation procedure was the same as above, except that the supernatant of CMNaOH hydrolysis experiment was not phase partitioned, because oligosaccharides were hydrophilic. Instead, an aliquot of the neutralized CMNaOH supernatant (re-dissolved in MFW, 5/1/5, v/v/v) was directly scintillation counted together with all the other treatment's supernatants, to quantify the transeacylase products if any.

The rest of the neutralized CMNaOH supernatant was dried in SpeedVac and the residues were re-dissolved in 3 ml 0.5% chlorobutanol (**transacylase**

product stock). The sodium succinate formed during neutralization was removed by passing the stock through Bio-gel column P-2 (size-exclusion chromatography, 3 ml/fraction, 50 fractions) (Table 4) with 6 mg glucose, xyloglucan oligomer mixture and dextran as internal markers. A small aliquot (2–4 µl) of each fraction was loaded onto TLC plates (BAW 2/1/1, v/v/v, 3 ascents) to look for the fractions containing the proposed transacylase product by visualising internal markers through Thymol staining (Jork *et al*., 1994), and then those fractions were pooled, dried in SpeedVac and the compound mixture was resolved by paper chromatography [Whatman No. 3, butan-1-ol/pyridine/water (BPW), 4/3/4, v/v/v, 46–46.5 h] (Table 4). The transacylase product was looked for by scanning the chromatography paper as above, or cut the sample lane into small strips, which were then scintillation counted as above.

All the other supernatants from each treatment were also dried in SpeedVac, and the residues were re-dissolved in small volume of MFW, which was then analysed by paper chromatography as above, but with Whatman No. 1 paper.

For the assays (e.g. characterisation of un-bound [^{3}H]XXXGol) which require visualising bands, a fluorography was undertaken. The TLC plates were developed (BAW 2/1/1, v/v/v, 3 ascents) as above, and then they were dipped into 7% PPO (w/v) dissolved in diethyl ether. After dried completely, they were fixed in a development cassette by tapes at corners, and then overlapped with an X-ray film (Kodak, Rochester, USA) in dark. The cassette was stored in dark at –80°C for 6 weeks.

2.4.6 Data analysis

The putative cutin-to-radiolabelled fatty acids, oligosaccharides and glycerol activities were expressed as alkali (CMNaOH)-releasable radioactivity (cpm)/supplied radioactivity (cpm) x 100%, usually per 50 mg fresh weight (FW) of epidermis (putative transacylase activity/50 mg FW) or per ~10 mg dry weight (DW) of epidermis (putative transacylase activity/10 mg DW). All the statistical analysis was achieved by independent student t-test.

2.5 Gene (*CD1*) cloning

2.5.1 Crude RNA extraction and purification

M82 15-Days after anthesis (DAA) (2-cm) tomato fruit pericarp was homogenized to a fine powder by punching and grinding in liquid nitrogen. Pericarp (150 mg) was vortexed vigorously with 600 µl pre-cooled 1X extraction buffer (Table 5) containing 2% SDS (w/v), followed by addition of 600 µl 'phenol' [≥ 90%, saturated with 10 mM aqueous Tris (Cl^-), pH 8.0]. The mixture was centrifuged at 4°C for 10 min. The upper layer (aqueous, total nucleic acid layer, ~600 µl) was mixed thoroughly with 600 µl 'phenol'/chloroform/isoamyl alcohol (25/24/1, v/v/v), and centrifuged as before. This step was repeated. The upper layer was then combined with an equal amount of chlroroform/isoamyl alcohol (24/1, v/v), mixed thoroughly and centrifuged as above. The above partitioning steps were aimed to separate nucleic acid from other components of the cell lysates, such as proteins. Upper layer was mixed gently with 2.5 volume of absolute ethanol plus 1/10 volume of 3 M sodium acetate (pH 5.2) and left on ice for 30 min, to

precipitate total nucleic acid. After being centrifuged at 4°C for 10 min, the supernatant was discarded, and the pellet was aspirated in fume hood. A brief centrifugation usually followed to remove more supernatant. DEPC-treated water (30 µl, Thermo Scientific) was added to the white precipitate after a thorough aspiration.

Extracted RNA was visualized on a 1% agarose gel (1% w/v agarose powder was dissolved in 1X TBE buffer by heating in microwave, and 2 µl SYBR dye was added after cooling down) in 1X TBE buffer. Total nucleic acid was quantified by A_{260}; contamination was checked by A_{260}/A_{280} and A_{260}/A_{230} (Desjardins and Conklin, 2010).

To remove DNA contamination, 3 µg of total nucleic acid (according to A_{260}) was incubated with 2.5 µl 10X TURBO DNAse and 7.5 µl DEPC-treated water at 37°C for 30 min. The reaction was stopped by adding 2 µl TURBO DNAse inactivation reagent, followed by centrifuging at 4°C for 5 min. The supernatant was transferred to a fresh tube, and RNA was precipitated by addition of 2.5 volume of 80% ethanol plus 1/10 volume of 3M sodium acetate (pH 5.2), and the mixture was stored on ice for 30 minutes. Supernatant was discarded after centrifuging at 4°C for 5 min. Remaining salts were removed by washing in 100 µl 80% ethanol, followed by centrifuging at 4°C for 5 min. The supernatant was discarded as before, 15 µl DEPC water was used to re-dissolve the pure RNA, and its quantity and quality were checked by A_{260} and A_{260} ratios respectively.

2.5.2 *CD1* mRNA reverse transcription

Primers were designed manually by following several principles: the optimal length is 20–28 base pair (bp); the 3' end was designed to terminate with G or C to stabilize primers; T_m should be around 60°C with GC content from 40–60%; no complementary sequences between forward and reverse primers or in a single primer.

Reverse transcription was achieved by incubating 1 µg RNA with 1 µl 10 mM dNTP (a mixture of nucleoside triphosphates containing deoxyribose, e.g. dTTP) and 1 µl 100 µM CD1 cDNA primers (Table 7) 5 min at 65°C. It was then transferred to ice immediately, to allow dNTP to bind onto target RNA after its secondary structure had been denatured. Subsequently, a reverse transcription reaction was carried out according to the Superscript III protocol (Thermo Scientific).

2.5.3 *CD1* cDNA amplification

PCR incubation mixture consisted of 400 ng CD1 DNA template in a final volume of 50 µl; Q5® High-Fidelity DNA Polymerase (NEB) reaction protocol was followed.

The PCR protocol was as follows: initial denaturation (30 s at 98°C), followed by 35 cycles of denaturation (5–10 seconds at 98°C), annealing (30 s at 66°C), extension (30 s at 72°C), and final extension (5 min at 72°C).

PCR product was visualised on a 1% agarose gel as above. The fluorescent band with the expected size was cut out under blue light, and the amplified cDNA template was eluted by following QIAGEN gel elution kit instructions.

2.5.4 Plasmids replication

Home-made competent *E. coli* (DH5α) (50 µl) was mixed with 20 ng pEAQ-HT and pEAQ-HT-GFP in two ice-cold tubes, and then the mixtures were placed on ice for 30 minutes. Cells were heat-shocked for transformation in a water bath at 42°C for 1 minute, and then combined with 500 µl liquid Luria broth (LB) media. Cells were grown at 37°C for 45 minutes, followed by transferring aliquots onto LB agar plates with 50 µg/ml kanamycin (Kan^+) (Table 6). Plates were incubated at 37°C overnight.

Selected individual colonies were replicated onto a fresh LB Kan^+ plate with the same recipe as above and inoculated into fresh liquid LB Kan^+ medium. pEAQ-HT and pEAQ-HT-GFP plasmids were harvested from the liquid LB Kan^+ medium after overnight incubation at 37°C, by using a QIAGEN miniprep kit. Plasmid quantity and contamination were checked by A_{260} and its ratios to A_{280} and A_{230} (Parodi *et al*., 1975). Sequence mutation was checked by digesting plasmids with PVUII and XbaI as follows: 1 µl plasmid, 0.2 µl PVUII or Xbal, 2 µl 10X CutSmart buffer [500 mM potassium (acetate), 200 mM Tris (acetate), 10 mM magnesium (acetate), 100 µg/ml BSA, pH 7.9], 17.8 µl DEPC-treated water (21 µl in total). Products were visualized on a 1% agarose gel as above.

2.5.5 pEAQ-HT-CD1 ligation

To produce one sticky end (5') and one blunt end (3'), amplified CD1 coding sequence and pEAQ-HT plasmid were digested by endonucleases, SmaI (producing blunt ends) was applied separately as follows: 10 µl purified CD1 DNA template, 1 µl SmaI solution (final conc. = 1.25 U/µl), 1.5 µl 10X CutSmart buffer, 2.5 µl water (16 µl in total); 20 µl pEAQ-HT, 2 µl SmaI (final conc. = 2 U/µl), 5 µl 10X CutSmart buffer as above, 13 µl water (40 µl in total). Both mixtures were incubated at 25°C for 30 min, and then 1 µl AgeI (producing sticky ends) solution (final conc. = 0.3 U/µl) was directly added to the CD1 DNA template tube, whereas 2 µl AgeI solution (final conc. = 0.12 U/µl) to the plasmid tube; both were then incubated at 37°C for 30 minutes. Digestions were stopped on ice.

Restriction-enzyme digested CD1 coding sequence was purified by QIAquick PCR clean-up kit. The digested pEAQ-HT was de-phosphorylated by incubating with 2 µl rSAP at 37°C for 30 minutes, and then purified by gel elution as CD1 coding sequence.

Prepared pEAQ-HT and CD1 coding sequence were ligated as follows: 8 µl of the digested and purified CD1 cDNA, 1 µl digested and purified plasmid, 0.5 µl T4 DNA ligase, 1 µl T4 buffer; a negative control was prepared with the same recipe except water was added instead of CD1 DNA. The ligation mixtures were incubated at room temperature overnight.

The whole amount of the ligation mixture was introduced into *E.coli* (DH5α) by chemotransformation as before. A positive control (non-digested pEAQ-

HT) was also included. After being incubated at 37°C for 45 minutes, 50 µl of each group was spread on LB Kan$^+$ plates and kept at 37°C overnight.

2.5.6 Ligation quality control

Individual colonies from the pEAQ-HT-CD1 plate were picked up by pipette tips, which were then streaked onto a fresh LB Kan$^+$ plate and then inserted rejected into PCR tubes containing 1 µl 10X Taq buffer, 0.2 µl 10 mM dNTP, 1 µl of each primers (10 µM forward colony primer and 10 µM reverse CD1 primer), 0.1 µl Taq DNA polymerase and 6.7 µl DEPC-treated water (10 µl in total). Tips were removed from PCR tubes before the colony PCR programme started, which was as follows: initial denaturation (30 s at 95°C), followed by in 35 cycles of denaturation (30 s at 95°C), annealing (45 s at 61°C), extension (70 s at 68°C); and final extension (5 min at 68°C).

The success of ligation was validated by the right size of the CD1 cDNA, visualized on a 1% agarose gel as above.

The freshly grown colonies (from the streaking above) containing pEAQ-HT-CD1 were inoculated into 5 ml liquid LB Kan$^+$ medium, incubated at 37°C for 45 min. Aliquots of these cell cultures were spread onto fresh LB Kan$^+$ plates for replicating this construct. The rest of the culture was incubated at 37°C overnight for more tests.

The freshly replicated pEAQ-HT-CD1 construct was harvested with a QIAGEN Miniprep kit again. Tandem insertion was tested by following the same protocol as above, except that only plasmid primers were used.

2.5.7 Transformed *E. coli* genotyping

The best two colonies were inoculated into LB Kan^+ media, and the high-quality pEAQ-HT-CD1 constructs were harvested again by QIAGEN Miniprep kit. Sequencing PCR was set up as follows: 4 µl construct, 1.6 µl 2 µM primer (either forward or reverse plasmid primer), 2 µl 5X BigDye buffer + 0.5 µl BigDye 3.1 ready reaction premix, 1 µl DEPC water (9 µl in total). CD1 insert was sequenced by Edinburgh Genomics.

2.6 CD1 production, extraction and purification

2.6.1 *Agrobacterium* transformation and *N. benthamiana* infiltration

GV3101 cells (50 µl) was homogenized with pEAQ-HT-CD1 constructs (with the correct sequence, 2 µl) and the same amount of pEAQ-HT-GFP (a positive control) in two tubes. Cells were transformed by electroporation at 1800 V for ~5 s. The transformed GV3101 was spread on fresh yeast extract peptone (YEP) plates containing 50 µg/ml kanamycin, 50 µg/ml rifampicin and 25 µg/ml gentamicine (Table 6) and incubated at 28°C for 2 days.

Individual colonies were inoculated into 5 ml liquid YEP broth with the same antibiotics as above, to grow at 28°C (200 rpm) overnight. The cells were sub-cultured by homogenizing 0.3 ml cells with 10 ml YEP broth with the same antibiotics and grown overnight at 28°C (200 rpm). Cells were centrifuged at 4000 rpm for 20 min. Supernatant was discarded, and cell pellets were re-suspended in infiltration buffer (Table 5) to achieve A_{600} = 0.5.

N. benthamiana plants (24–30 days old) were kept in a humid environment for 2 hours to help stomata open. The *Agrobacterium* GV3101 containing pEAQ-HT-CD1 and pEAQ-HT-GFP was infiltrated into leaves from the abaxial side. The infiltrated tobaccos were grown under the same conditions as before for 5 days.

2.6.2 His_6-tagged CD1 extraction and purification

Agroinfiltrated tobacco leaves were harvested, ground in liquid nitrogen and stored at –80°C for future use.

Leaf weight and the pre-cold extraction buffer (Table 8) were mixed at a 1:3 (w/v) ratio at 4°C. Sand was added to help grinding. After being shaken vigorously in the cold room (4°C) for 0.5 h, the extraction mixture was centrifuged at 4°C for 25 min. The supernatant was then transferred to another fresh tube, followed by adjusting the pH to 7.0 by adding 1/20 vol. 1 M sodium phosphate, pH 7.8, for being consistent with Co^{2+} column equilibration/wash buffer. The mixture was centrifuged as before, the supernatant was filtered through 0.45-µm cut-off filters or glass fibre. An equal volume of wash buffer (Table 8) was mixed with the extract, and then the mixture was applied onto a Co^{2+} gravity-flow column (1 ml bed resin).

The flow through was collected and re-applied to the column to maximize His-tagged protein binding. Wash buffer (Table 8) (2×1 ml) was applied to the column to remove non-specifically bound proteins; both washes were collected in the same tube. Elution buffers from 1–4 with low–high imidazole

concentrations (Table 8) were subsequently applied to column as for the wash buffer.

Eluents were dialyzed (12–14 kDa cut-off, Medicell Membranes Ltd., London, UK) against water in the cold room for one day (3 water changes), followed by freeze-drying (–60°C). Protein was re-dissolved in a small volume of water and quantified by A_{280}. Desired concentrations were adjusted by adding water.

2.6.3 His_6-tagged CD1 identification

SDS-PAGE running

Resolving gel (15%, 1.5 mm) was made first; after AMPS being added (3.4), the mixture was immediately poured into a set cassette, and bubbles were eliminated by immediately adding isopropanol. After the gel was solidified, the isopropanol was poured off, and then the stacking gel (4%) mixture was poured into the cassette immediately after the addition of AMPS as before, a comb was also added into the cassette immediately before the stacking gel being solidified.

The dialyzed/freeze-dried protein samples were mixed with 4X Laemmli buffer (3.4) (final conc. = 1X) and DTT solution (final conc. = 100 mM), followed by incubation at 95°C for 5 min before being loaded onto the home-made SDS gel (Table 4). The gel was run in 1X running buffer (3.4): 80 V at stacking gel for 25 min, 120 V at resolving gel for 1.5 h (stacking gel pores were bigger than the resolving one, lower voltage can achieve sharp protein bands at the same line in the stacking gel).

SDS-PAGE stain

Gels were stained with 0.006% Coomassie Brilliant Blue R-250 (dissolved in 10% acetic acid) overnight, and then remove the background staining in the same solvent the day after.

Western blot

SDS-PAGE gels were also immuno-stained instead of chemical staining to obtain a more precise result (i.e. the protein does not only have the correct size, but also has a His_6-tag).

The stacking gel was cut off after running and the resolving gel was soaked in 1X running buffer. Proteins were transferred onto a nitrocellulose membrane for 7 min according to iBlot 2 NC Transfer Stacks protocol. The membrane was then washed with PBS for 5 min at room temperature, followed by incubating with 5% milk powder (w/v) suspended in PBS with 0.1% (v/v) TWEEN-20 (PBST) for 1 h at room temperature, to block non-specific binding for antibody. Monoclonal anti-poly-His–HRP (Alpha Diagnostic International, San Antonio, USA) was diluted (1:1500) in PBST, and incubated with membrane overnight at 4°C. Un-bound antibody was washed with PBST numerous times at 4°C. SuperSignal West Dura Extended Duration Substrate (Thermo) (250:250) was applied onto the membrane for 1 minute, followed by covering the membrane in polythene film and placing it into a cassette, and exposing to an X-ray film (Kodak, Rochester, USA) for 1 s to 5 min.

Chapter 3. Cutin-to-fatty acid transacylation

Introduction

We proposed that during cell expansion, not only new cutin is synthesized (Kosma *et al*., 2010), but also existing cutin could be remodelled to accommodate the dramatic structural change. This remodelling mechanism could be conferred by a transacylase to cut cutin transiently to allow expansion first, and then re-form an ester bond back to another or the original cutin chain after the incremental expansion ceased. This reaction is named 'cutin-to-cutin transacylation' (Fig. 5) in this project.

I looked for this reaction by carrying out *in-situ*, *ex-situ* and *in-vitro* assays of the selected plant epidermis containing cutin (acyl donor) with exogenous radio-labelled hydroxy-fatty acids (acyl acceptors), which were models of a polyester cutin chain (Fig. 5). Hydroxy-fatty acids were chosen because the polymeric cutin is insoluble in aqueous buffers. The proposed transacylase activity was monitored by scintillation counting (standard unit: counting per minute, cpm) of the methanol-insoluble radioactive epidermis (details in Chapter 2 and in e.g. Fig. 11 legends).

I started with 16-[^{3}H]hydroxyhexadecanoic acid ([^{3}H]HHA) as the acyl acceptor (Fig. 5), which has the same chain length as the very abundant residue in vascular land-plant cuticle, 10,16-dihydroxyhexadecanoic acid (diHHA), but only contains one hydroxy group. [^{14}C]hexadecanoic acid ([^{14}C]HA) was a control 'substrate' tested, which has the same length of the carbon chain as the other two above, but no hydroxy groups and was

therefore not expected to serve as an acyl acceptor substrate. DiHHA was not commercially available, and the purification via HPLC was not successful, resulting in no radio-labelled diHHA being available to test in this project.

The exogenous radio-labelled fatty acids were hypothesized to serve only as acyl acceptors, because their –COOH groups were not activated [i.e. the OR groups in the carboxy-esters of cutin (–COOR) tend to be better leaving groups than the OH in unsubstituted carboxy groups (–COOH), because of lower stability]. Thus, fatty acids cannot be donor substrates. Their acceptor substrate ability depends on whether they contain –OH groups; for example, HHA can be an acyl acceptor because it contains a hydroxy group, whereas HA does not.

The transacylase we are interested in was proposed to be apoplastic since it catalyses epidermal cutin re-structuring. Thus, for *in-situ* assays, epidermis samples were frozen, thawed and washed in buffers to burst epidermal cells and remove cytoplasmic interferences (e.g. ATP is involved in *de-novo* synthesis of non-radioactive transacylase substrate), but enzymes, bonded to the cell wall/cutin/wax, would be left. The technical details are described in Chapter 2.

The putative transacylase activity was further validated by *ex-situ* assays: the prepared de-waxed cuticle without endogenous un-denatured enzymes was incubated with crude enzyme extract. *In-vitro* experiments involving the purified enzyme aimed to identify the putative cutin-to-radio-labelled fatty acid transacylase.

Results

3.1 Optimization of *in-situ* assays

Adaxial epidermis of young ice plant leaves (3–5 cm lamina length) and epicotyl epidermis of pea seedlings (default growth conditions: in continuous dark at 25°C for 7 days) were used in the pH optimization experiments. Both were harvested at the young stage because the proposed transacylation reaction was hypothesized to be involved in rapid expansion. Adaxial epidermis of ice plant leaves was chosen because it is easy to peel off and contains more cutin fatty acid residues than abaxial does, based on preliminary experiments (Appendix 3). Tomato fruit epidermis was used to compare with them to select the best plant model.

In addition, pre-incubation treatment was also optimized. As mentioned above, epidermis consists of one layer of cells, which may release some potential transacylase substrates (e.g. *de novo* synthesized acyls) after bursting due to the freeze/thawing treatment, and therefore a pre-incubation wash is thought to be important for removing such interference. However, this wash process may also remove the enzyme we are interested in. Thus, washed and un-washed epidermis were compared.

3.1.1 The optimum pH of the possible cutin-to-HHA transacylase activity (*in situ*)

We hypothesized that the proposed cutin-to-cutin transacylation (Fig. 5) allows cell expansion during rapid growth, and therefore we expected that the

pH optimum window is 4.5–6, which is the apoplastic pH of rapidly expanding cells (reviewed by Cosgrove, 2005).

Pea epicotyl was chosen for this experiment because it was thought to provide enough cutin (Rogers *et al*., 1994). The epidermis was frozen, thawed and washed before incubation as mentioned above.

The blot-dried epidermis was then assayed *in situ* at pH 3.5–7.5. After being incubated for 24 h and thoroughly washed in acidified methanol to terminate enzyme reactions and remove un-bonded [^{3}H]HHA, un-denatured epidermis samples showed significantly more ^{3}H incorporation than denatured ones ($P < 0.05$) at all the pH values tested (Fig.9a), providing preliminary evidence that this is an enzymic incorporation.

Chloroform/Methanol/4 M NaOH (CMNaOH, 10/10/3, v/v/v ≈ 0.5 M NaOH) was a pH~14 hydrophobic mixture employed to hydrolyse ester bonds in all the experiments, enabling us to find out the whether [^{3}H]HHA was incorporated by ester bonds preliminarily. Consistent with the Fig. 9a, un-denatured epidermis samples released significantly more ^{3}H in CMNaOH than the denatured control ($P < 0.05$) (Fig.9b), further confirming that the incorporation was enzymic, and ^{3}H was very likely being incorporated via ester bonds, catalysed by the proposed transacylase activity. Thus, the amount of radioactivity released in CMNaOH can potentially represent the putative transacylase activity.

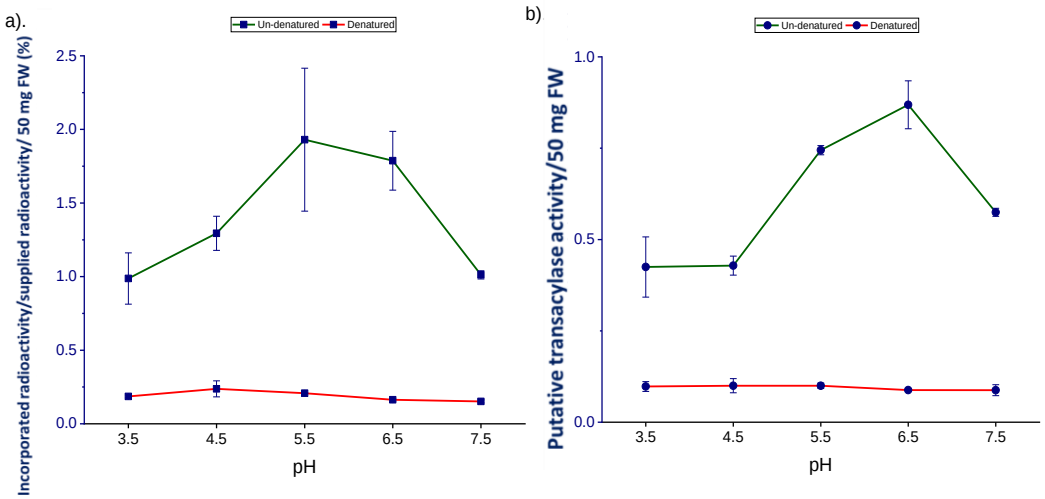

Figure 9. pH optimization of the putative cutin-to-[^{3}H]HHA transacylase activity in pea epicotyl epidermis *in situ*. The blot-dried epidermis samples (50 mg; acyl donor) with (cold buffer-washed) or without (boiled) active endogenous enzymes were incubated with 0.42–0.58 kBq (4 µl) exogenous [^{3}H]HHA (acyl acceptor) in 300 µl buffers at room temperature for 1 day. Followed by intensive MFW wash to remove non-covalently bonded radioactivity and possible low-M_r products before scintillation counting. (a) The total incorporated and (b) CMNaOH-releasable radioactivity ratios (%) were calculated as follows: obtained radioactivity (cpm/ 50 mg epidermis) / initially supplied radioactivity (cpm) × 100%. Green line: un-denatured epidermis samples. Red line: denatured epidermis samples (control). Bars indicate standard errors (n=3).

A value of 1% total incorporated or CMNaOH-releasable radioactivity/50 mg epidermis/supplied radioactivity corresponds to an absolute incorporation of 80–110 cpm/50 mg epidermis.

The total incorporated ^{3}H ratio was significantly increased at pH 4.5 compare with at pH 3.5 ($P < 0.05$), and then gradually increased to reach the highest value at pH 5.5, followed by decreasing gradually with pH increase ($P_{(\text{incorporation \% at pH 6.5 vs. at pH 7.5})} < 0.05$) (Fig. 9a). The putatively ester-bonded (= CMNaOH-releasable) ^{3}H showed the similar pattern: the value started to be significantly higher at pH 5.5 than at more acidic pH values ($P < 0.01$), and reached the summit at pH 6.5, and then decreased again at pH 7.5 ($P_{(\text{CMNaOH-releasable radioactivity \% at pH 6.5 vs. at pH 7.5})} < 0.05$) (Fig.9b). These results

suggested that the possible cutin-to-HHA transacylase activity prefers pH 5.5–6.5, which is consistent with our hypothesis; and the higher CMNaOH-releasable ^{3}H ratio at pH 7.5 than at 3.5–4.5 may suggest that this transacylase is involved in responding to other stimuli, besides cell expansion because pH 7.5 is out of the physiological range of a rapidly expanding cell apoplast (reviewed by Cosgrove, 2005).

The CMNaOH-releasable ^{3}H was around 50% of the total incorporated ^{3}H in most cases, possibly due to loss during processing, and/or some [^{3}H]HHA was incorporated by bonds other than ester bonds. The latter possibility will be investigated later in this chapter.

To test whether the results above can also be observed in other plants, epidermis from rapidly expanding ice plant leaves (lamina length: 3–5 cm) was also assayed. Similarly, the un-denatured epidermis incorporated and released significantly more ^{3}H than the denatured control ($P < 0.05$), indicating that [^{3}H]HHA can also be incorporated into ice plant leaf epidermis enzymically (Fig. 10). Moreover, both the total incorporated and CMNaOH-releasable ^{3}H at pH 4.5–5.5 were slightly higher than at other pH values (Fig. 10), supporting that the putative cutin-to-HHA transacylase prefers mildly acidic pH values, which were again consistent with our hypothesis.

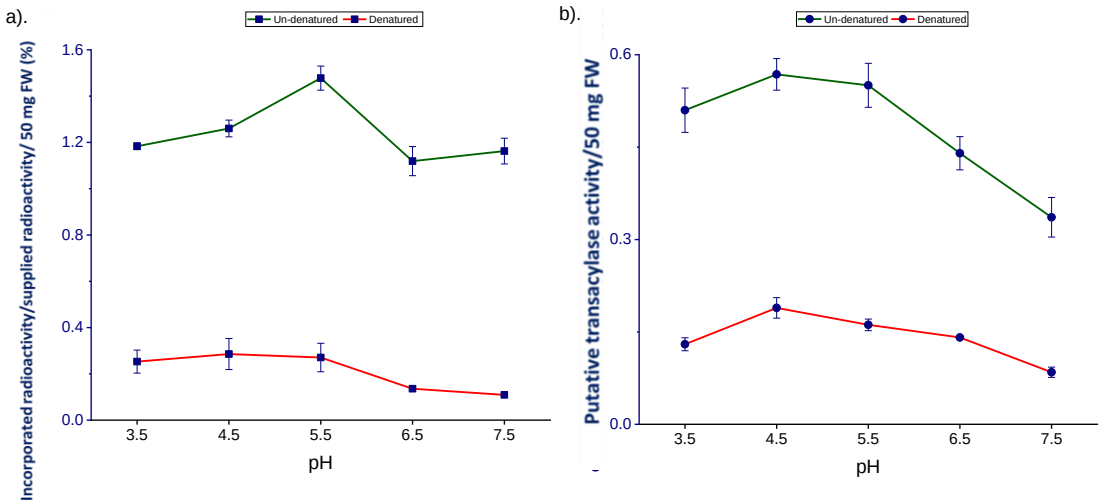

Figure 10. pH optimization of the putative cutin-to-[^{3}H]HHA transacylase activity in ice plant leaf epidermis *in situ*. Experimental details were as in figure 6, except 50 mg ice plant leaf epidermis was used as the acyl donor. (a) The total incorporated and (b) CMNaOH-releasable radioactivity ratios (%) were calculated as above. Green line: un-denatured epidermis samples. Red line: denatured epidermis samples (control). Bars indicate standard errors (*n*=3).

A value of 1% total incorporated or CMNaOH-releasable radioactivity/50 mg epidermis/supplied radioactivity corresponds to an absolute incorporation of 80–110 cpm/50 mg epidermis.

From the overall results, pH 5.5 was chosen for subsequent experiments because it is within the optimum range of the two plant species, and within the apoplastic physiological pH range of expanding cells (reviewed by Cosgrove, 2005), enabling us to investigate our hypothesis further.

3.1.2 The best plant to study the putative cutin-to-HHA transacylase activity (*in situ*)

Ice plant *leaf vs. pea epicotyl*

As shown in Fig. 9 and 10, the amount of ^{3}H from [^{3}H]HHA incorporated by the putative transacylase in ice plant epidermis samples was only ~0.75 of the pea epicotyl epidermis samples at the optimum pH (5.5) (Fig. 11), and the values were significantly different ($P < 0.05$) (Fig. 11). Thus, pea was preferred over ice plant because of its high putative transacylase activity and fast harvest cycle.

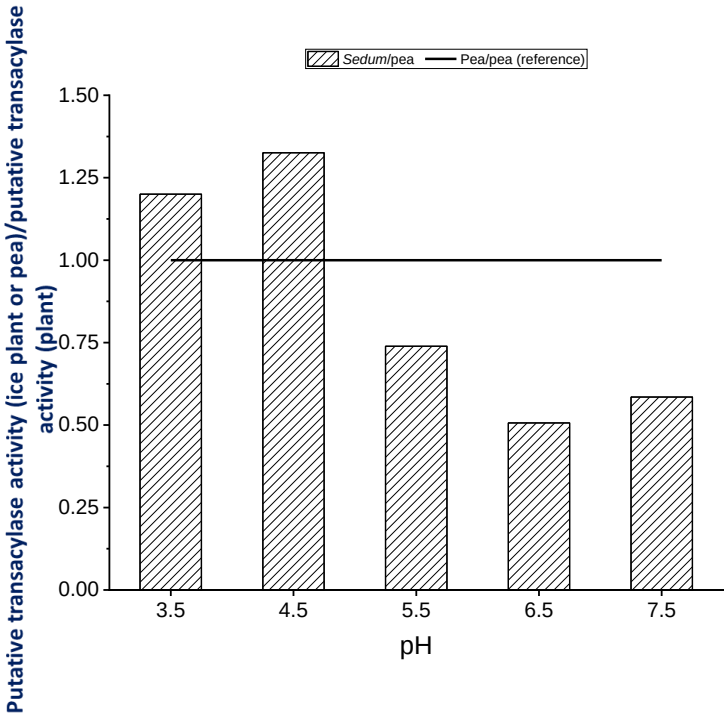

Figure 11. The putative cutin-to-[^{3}H]HHA transacylase activity in rapidly-expanding ice plant adaxial epidermis vs. rapidly-expanding pea epicotyl epidermis *in situ*. Experimental details were the same as figure 7 and 8. The CMNaOH-releasable radioactivity ratio (%) of pea samples was a reference (**black line**) to be compared with the ice plant samples (columns).

Tomato fruit vs. pea epicotyl

Tomato fruit was also predicted to be a good model because its epidermis has enough cutin, and Yeats *et al*. (2012) used it as a model to find how cutin was synthesized, indicating that our proposed GDSL transacylase activity may also be found. Epidermis of tomato fruit at the rapidly expanding stage (10–21 days after anthesis, DAA) was chosen to be assayed because the pH optima above suggested that the possible cutin-to-HHA transacylase is highest during rapid expansion, and also because it contains the highest amount of CD1 (Yeats *et al*., 2012), which might also catalyse the observed cutin-to-[^{3}H]HHA transacylation reaction.

However, comparing with pea epicotyl epidermis samples, there was only negligible ^{3}H incorporated enzymically (8 cpm) ($P_{\text{(tomato fruit vs. pea epicotyl)}} < 0.01$) (Fig. 12 and 34), even much lower than the ice plant adaxial leaf epidermis ($P_{\text{(tomato fruit vs. ice plant leaf)}} < 0.01$) (Fig. 11 and 12). Thus, tomato fruit epidermis was not used routinely in this project.

This unexpected result might be because of the endogenous transacylase substrate specificity: the dominant fatty acid in tomato fruit cutin is diHHA, instead of HHA, which was used as a substrate here.

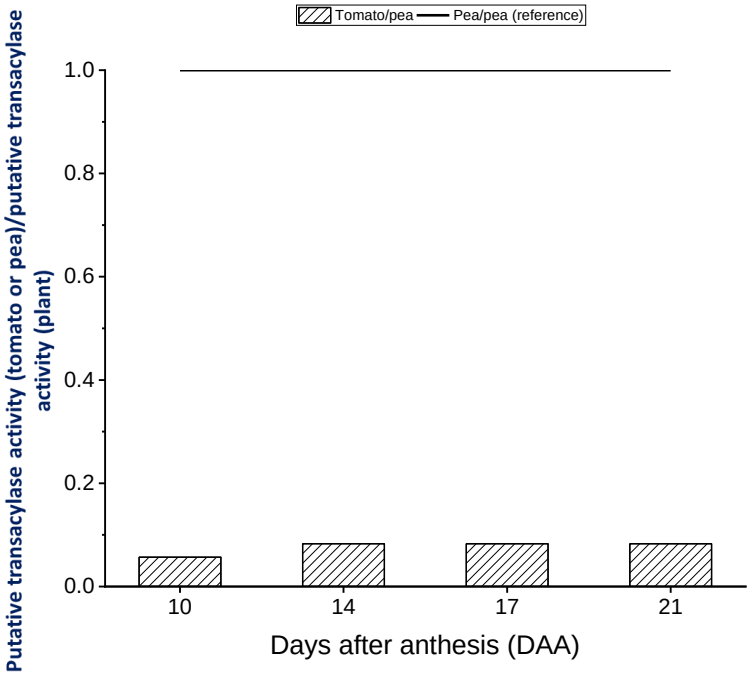

Figure 12. The putative cutin-to-[^{3}H]HHA transacylase activity in rapidly-expanding tomato fruit epidermis vs. rapidly-expanding pea epicotyl epidermis *in situ*. Experimental details were the same as figure 7, except only pH 5.5 was used for incubation, and tomato fruit epidermis was another acyl donor. The CMNaOH-releasable radioactivity ratio (%) of pea samples was a reference (**black line**) to be compared with the tomato samples (columns).

In summary, pea epicotyl, which had grown in continuous dark for 7 days (average ~16 cm) provided higher possibly endogenous cutin-to-HHA transacylase activity than ice plant leaf and tomato fruit. Thus, such pea epicotyl epidermis was used as a standard plant model.

3.1.3 Effects of pre-incubation process on the putative cutin-to-HHA transacylase activity (*in situ*)

The un-denatured epidermis had been washed in cold buffer (4°C) for 1 h (Chapter 2) in all the experiments above, to remove the cutin's intracellular competitors e.g. acyl-CoA compounds, and sources of energy (ATP) that

might drive synthetase reactions involved in acyl-CoAs synthesis (reviewed by Li *et al*., 2010). However, the wash process may also harm the quantity and/or quality of the transacylase that we are interested in.

To investigate the pre-incubation wash effect, I compared un-washed pea epicotyl epidermis (frozen and thawed only) with the pH-5.5 buffer-washed samples (frozen, thawed and washed) *in situ* at pH 5.5 (the same buffer, Chapter 2, Table 1).

The un-washed epidermis samples released slightly less radioactivity in CMNaOH than the pre-washed ones (Fig. 13), indicating that the possible cutin-to-HHA transacylase activity was not harmed by this wash process, and also that this putative transacylase did not use intracellular substrates (e.g. *de-novo* synthesized oligoesters) as the acyl donors.

Both un-washed and pre-washed epidermis samples released significantly more radioactivity than the denatured control did, indicating an enzymic incorporation as above (Fig. 13).

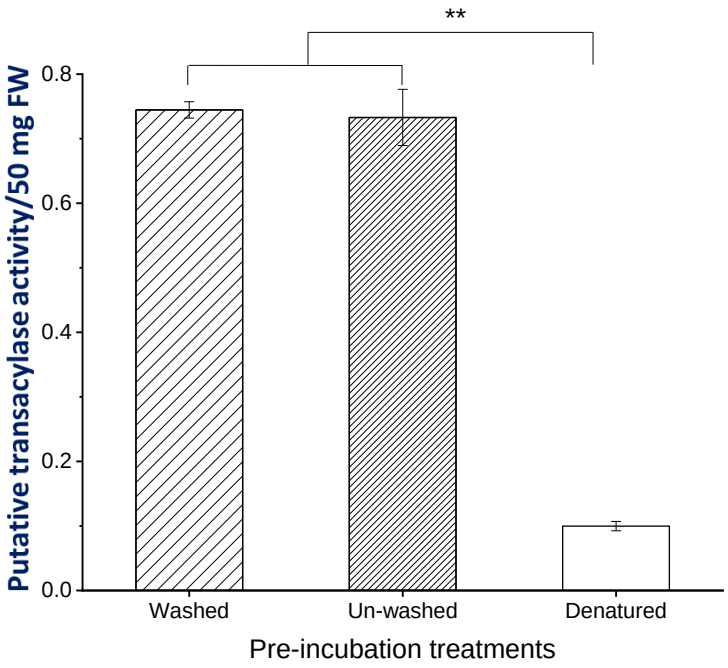

Figure 13. Effects of the pre-incubation wash on the putative cutin-to-[^{3}H]HHA transacylase activity in pea epicotyl epidermis *in situ*. Experimental details were as in figure 7, except a group of epidermis samples, which were not pre-incubation washed by cold buffer was assayed with the washed one. The CMNaOH-releasable radioactivity ratio (%) shows the pre-incubation treatments' effects on the cutin-to-[^{3}H]HHA transacylase activity. Bars indicate standard errors (n=3). **: $P < 0.01$.

A value of 1% CMNaOH-releasable radioactivity/50 mg epidermis/supplied radioactivity corresponds to an absolute incorporation of 80–110 cpm/50 mg epidermis.

To check the consistency, rapidly expanding ice plant leaf epidermis was assayed in the same way. Consistently, un-washed epidermis samples only released slightly more ^{3}H in CMNaOH than the pre-washed samples (Fig. 14). Together with the pea results (Fig. 13), we conclude that the wash in cold pH 5.5 buffer was not harmful.

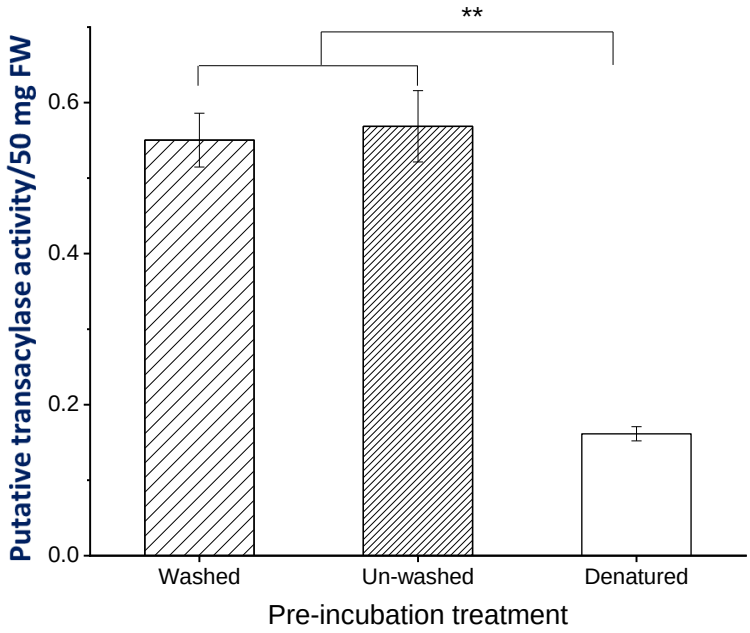

Figure 14. Effects of the pre-incubation wash on the putative cutin-to-[^{3}H]HHA transacylase activity in ice plant leaf epidermis *in situ*. Experimental details were the same as figure 11, except that ice plant leaf epidermis was used as the acyl donor. Bars indicate standard errors (*n*=3). **: P < 0.01.

A value of 1% CMNaOH-releasable radioactivity/50 mg epidermis/supplied radioactivity corresponds to an absolute incorporation of 80–110 cpm/50 mg epidermis.

In conclusion, the pre-wash in cold pH 5.5 buffer not only helped in removing potentially interfering cytoplasmic substrates, but also did not harm the transacylase activity which we were interested in. Thus, this procedure was kept throughout the thesis.

3.2 Further investigation of cutin-to-HHA transacylase activity under the optimized conditions

3.2.1 Cutin-to-HHA and HA transacylase activity *in situ*

Removal of Un-bonded radioactivity

The experiments above all showed that the un-denatured epidermis samples incorporated significantly more radioactivity than the denatured control, providing a piece of evidence that [^{3}H]HHA was incorporated enzymically. Based on this observation, we expected that the [^{3}H]HHA incorporation increases with time, which is another signature of an enzyme-catalysed reaction.

The MFW (9/1/1, v/v/v) wash was scintillation monitored to track whether the un-bonded radioactivity was removed efficiently. Similar results were observed in all such experiments; here is an example: the dramatic decrease of the un-bonded radioactivity started from the second wash, and the value was reduced to background from the third change, indicating that the epidermis was thoroughly washed in MFW before being subjected to further investigations (Fig. 15).

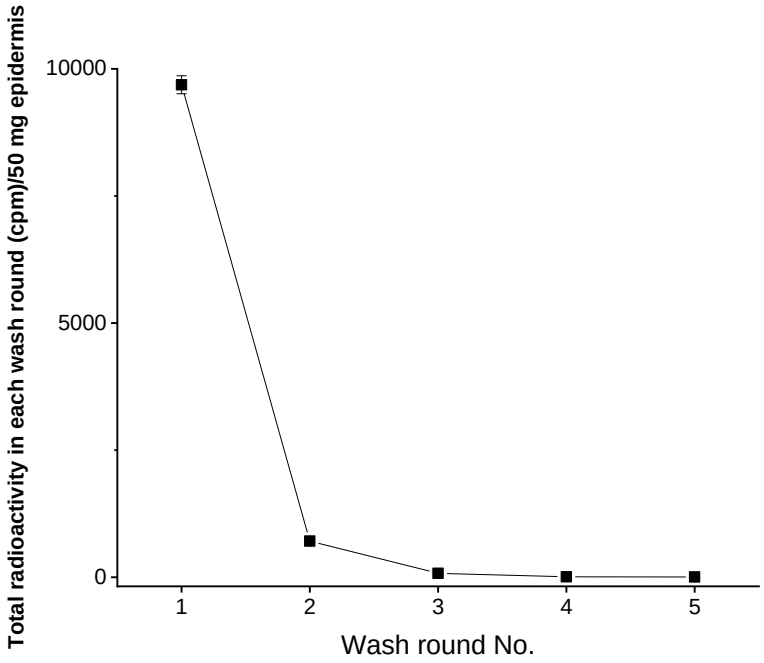

Figure 15. Washing efficiency of un-bonded ^{3}H from [^{3}H]HHA in acidified methanol. Pea epicotyl epidermis (50 mg; acyl donor) containing endogenous enzymes was incubated with 0.55 kBq exogenous [^{3}H]HHA (acyl acceptor) under the standardized conditions for 1 day. The samples were then washed in MFW (9/1/1) for multiple rounds. Aliquots of the supernatant of each round were scintillation counted. Bars indicate standard errors (*n*=3).

Detection of covalently bonded radioactivity

Pea epicotyl epidermis was assayed for the cutin-to-HHA transacylase activity with [^{3}H]HHA as the acyl acceptor *in situ* under the optimized conditions. As we expected, the un-denatured epidermis samples showed an ascending total ^{3}H incorporation with time, and much more incorporation than the denatured ones ($P < 0.01$) (Fig. 16a), indicating that [^{3}H]HHA was incorporated enzymically.

The same pattern was also observed with the CMNaOH-releasable (putatively ester-bonded) radioactive material (Fig. 16b), further suggesting

that the [^{3}H]HHA incorporation was catalysed by a transacylase. The reaction rate slowed down from 12 h maybe because the putative transacylase started to be denatured.

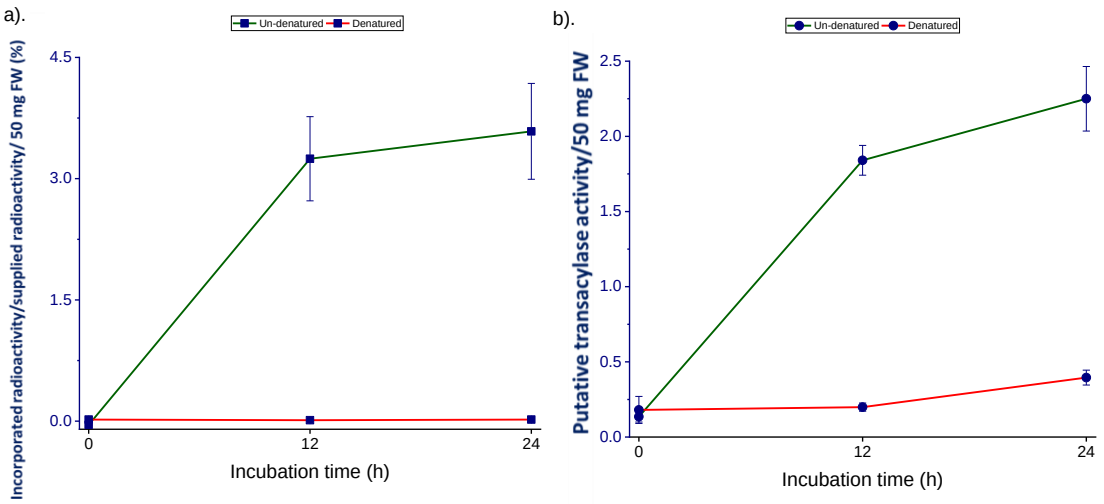

Figure 16. Effects of incubation time on the putative cutin-to-[^{3}H]HHA transacylase activity *in situ*. Experimental details were as in figure 7, except 1.3 kBq exogenous [^{3}H]HHA was supplied as the acyl acceptor at pH 5.5. (a) The total incorporated and (b) CMNaOH-releasable radioactivity ratios (%) illustrate the effects of incubation time on the cutin-to-[^{3}H]HHA activity. Green line: un-denatured epidermis samples. Red line: denatured epidermis samples (control). Bars indicate standard errors (*n*=3).

A value of 1% total incorporated or CMNaOH-releasable radioactivity/50 mg epidermis/supplied radioactivity corresponds to an absolute incorporation of 24 cpm/50 mg epidermis.

Is [^{3}H]HHA the acyl acceptor or donor?

[^{3}H]HHA has both potential acyl acceptor (–OH) and donor (–COOH) groups, even though the latter were not expected to be transferred efficiently because a simple –COOH group is not activated. To test which functional group was involved in the proposed transacylation reactions, I compared [^{3}H]HHA with [^{14}C]HA, which is exactly the same as HHA, except having no hydroxy group.

Only rapid expanding ice plant epidermis was used for this experiment due to material availability. In the [^{3}H]HHA-fed samples, as above, un-denatured epidermis showed significantly higher incorporation ratio than denatured control at 12 h ($P < 0.05$), whereas there was no significant difference at any time point in the [^{14}C]HA group ($P > 0.05$) (Fig. 17a).

The increase of [^{14}C]HA in both un-denatured and control (denatured) samples at 12 h compared with 0 h may be due to HA's hydrophobicity, causing physical adherence onto the cuticle, and therefore difficult to be washed away efficiently. The CMNaOH assay confirmed this speculation: the 24-h un-denatured epidermis samples released significantly more ^{3}H than the denatured control only when the substrate was [^{3}H]HHA ($P < 0.05$); no [^{14}C]HA was released (Fig. 17b).

The results above supported our hypothesis: −OH groups of [^{3}H]HHA were the transacylation sites, and fatty acids which do not have an activated carboxy group cannot be the acyl donor.

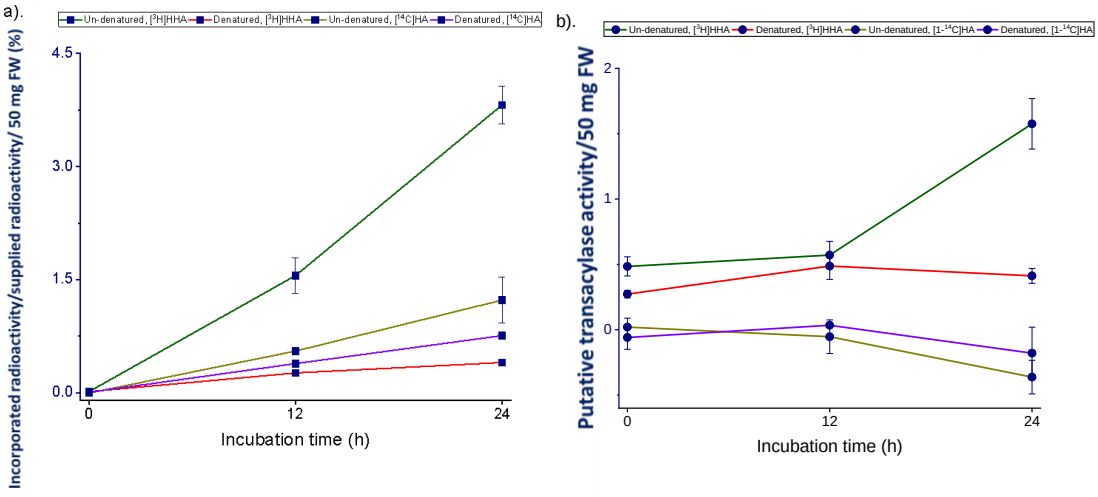

Figure 17. Transacylation substrate abilities of [^{3}H]HHA and [^{14}C]HA in ice plant leaf epidermis *in situ*. Experimental details were as in figure 12, except 0.42

kBq [^{3}H]HHA or [^{14}C]HA were supplied as the acyl acceptors at pH 5.5. (a) The total incorporated and (b) CMNaOH-releasable radioactivity ratios (%) illustrate the cutin-to-[^{3}H]HHA and -to-[^{14}C]HA activity. Un-denatured epidermis samples were in green and brownish-green lines for [^{3}H]HHA and [^{14}C]HA respectively. Red and purple lines are for denatured epidermis samples with [^{3}H]HHA and with [^{14}C]HA respectively. Bars indicate standard errors (n=3).

A value of 1% total incorporated or CMNaOH-releasable radioactivity/50 mg epidermis/supplied radioactivity corresponds to an absolute incorporation of 80 cpm/50 mg epidermis.

In conclusion, exogenous [^{3}H]HHA was the acyl acceptor for the proposed transacylation reaction as we expected. Moreover, the acyl donor was very likely to be cutin, because it is the only feasible epidermis component to form ester bonds with fatty acids (more details will be discussed later).

3.2.2 Cutin-to-HHA transacylase activity *ex situ*

The *in-situ* assays above successfully detected the proposed activity and suggested that a [^{3}H]HHA-incorporating transacylase exists, and the acyl donor is possibly cutin (more in '***3.3***'). To further verify the presence of transacylase in the model plants, I extracted endogenous apoplastic enzymes by homogenizing the frozen and thawed pea epicotyl epidermis with pH 5.5 buffer, and the transacylase activity was assayed *ex situ* (Chapter 2). There are two challenges for the enzyme to be active under these conditions: (1) the enzyme's environment was hydrophobic in *in-situ* assays because the transacylase was surrounded by cutin; (2) the extraction process may harm its activity. Thus, a detectable enzyme activity in *ex-situ* assays would be solid evidence for the cutin-to-HHA transacylase's existence.

Prepared pea epicotyl epidermis (with no endogenous active enzyme, see Chapter 2) was used to provide cutin, the putative acyl donor, and [^{3}H]HHA as the acyl acceptor was supplied as above. The enzyme extract was assumed to contain the proposed transacylase.

At the optimum pH (5.5) for the proposed transacylation reaction, an increase incorporation of ^{3}H into epidermis samples was observed with time, and significantly higher than the control (no enzyme extract, buffer only) ($P < 0.01$), suggesting that the proposed transacylase was extractable and active *ex situ*. However, compared with the *in-situ* assay incorporation ratios (Fig 7 and 14), which are usually 2–4% after 24 h incubation, only ~0.3% ^{3}H was incorporated *ex situ* (Fig. 18), indicating that the extraction process requires to be optimized. In the future experiments, the negative control should be replaced with boiled enzyme extract to further verify the proposed transacylase activity.

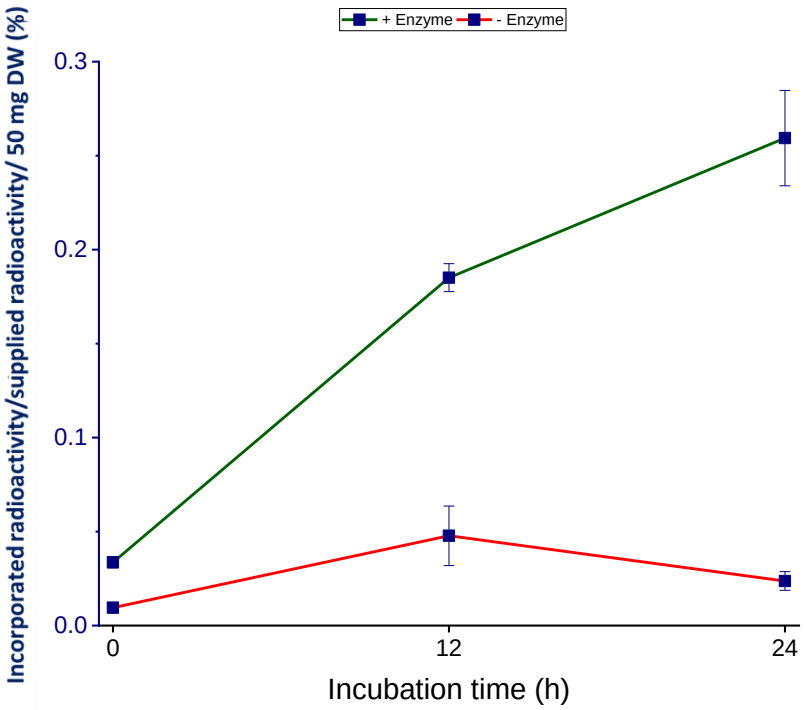

Figure 18. The putative cutin-to-[^{3}H]HHA transacylase activity *ex situ*. 25 mM succinate-Na^+ (pH 5.5) buffer was used to extract apoplastic enzymes from frozen and thawed pea epicotyl. The prepared pea epicotyl epidermis samples (50 mg dry weight; acyl donor) without active enzymes were incubated with 300 µl enzyme extract from the same source and 0.64 kBq exogenous [^{3}H]HHA (acyl acceptor) at room temperature for 1 day. The total incorporated radioactivity ratio (%) illustrates the transacylase activity *ex situ*. Green line: with (+) exogenous enzyme. Red line: without (-) exogenous enzyme. Bars indicate standard errors (*n*=3).

A value of 0.1% total incorporated radioactivity/50 mg epidermis/supplied radioactivity corresponds to an absolute incorporation of 12 cpm/50 mg epidermis.

Optimization of the extraction buffer

Different pH 5.5 extraction buffer concentrations (35- and 350-mM succinate-Na^+) were tested. However, there was no significant difference in the incorporated radioactivity ratios between them, no matter what else was added ($P > 0.05$) (Fig. 19).

The addition of Triton X-100 helped extraction in the high-concentration buffer insignificantly (P > 0.05), compared with the samples in the same buffer but without Triton X-100 (Fig. 19).

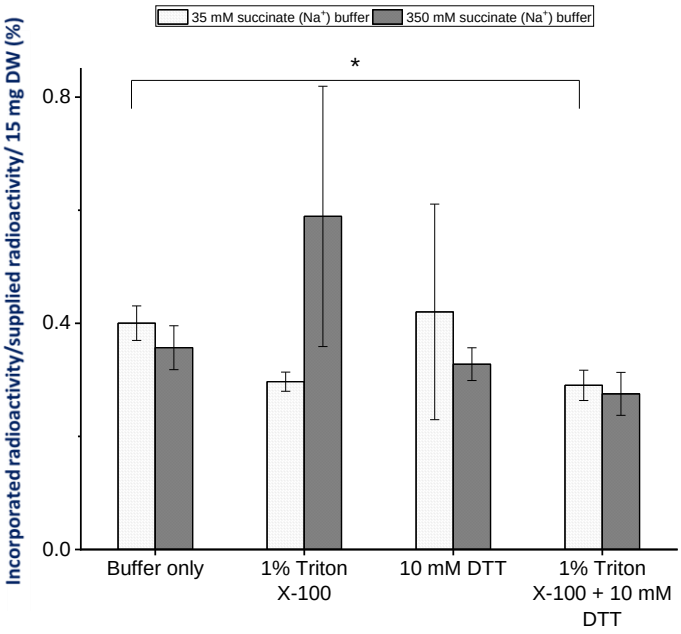

Figure 19. The optimization of the putative cutin-to-[^{3}H]HHA transacylase extraction buffer for *ex-situ* assays. Experimental details were as in figure 16, except two buffer concentrations (35 and 350 mM) were assayed with or without 1% (v/v) Triton X-100 or 10 mM DTT for their abilities in extracting apoplastic enzymes. The prepared pea epicotyl epidermis (15 mg, acyl donor) was incubated with 0.64 kBq exogenous [^{3}H]HHA (acyl acceptor) under the standardised conditions. The total incorporated radioactivity ratio (%) illustrates the effects of buffers on the cutin-to-[^{3}H]HHA transacylase activity. Bars indicate range (n=2). *: P < 0.05.

A value of 0.1% total incorporated radioactivity/15 mg epidermis/supplied radioactivity corresponds to an absolute incorporation of 12 cpm/15 mg epidermis.

Dithiothreitol (DTT), a reducing agent preventing undesired disulphide bond formation was added to some extraction buffers (Konigsberg, 1972), but It had no significant effect ($P_{(+\text{ DTT vs. }-\text{ DTT})} > 0.05$) (Fig. 19). These results demonstrated that the transacylase activity we are interested in was not affected by disulphide bond formation, suggesting that the cysteine residues

are fairly scattered in the transacylase's 3-dimensional (3-D) structure. Another possible explanation is that that DTT does not function properly at pH 5.5, but it has been reported that DTT is still active at pH 5 (Wechtersbach and Cigić, 2007). Thus, only the first explanation was reliable.

DTT and Triton X-100 were also added together to the extraction buffers, but they decreased the ^{3}H incorporation slightly compare with the "buffer-only" group at the high concentration ($P > 0.05$), and the effect was even significant in the low-concentration "buffer-only" group ($P < 0.05$) (Fig. 19).

In summary, both Triton X-100 and DTT provided a hint of improving the possible cutin-to-HHA transacylase extraction efficiency and its subsequent activity, and the high-concentration buffer with Triton X-100 was the best among the tested combinations. The CMNaOH hydrolysis was not carried out for this experiment because of the low incorporated radioactivity.

This *ex-situ* assay was repeated with the high-concentration buffer only, to re-test the effects of Triton X-100 and DTT. Again, DTT did not affect the possible cutin-to-HHA transacylase activity ($P > 0.05$); Triton X-100 improved incorporation around to 150% higher than the buffer-only control, but not significantly ($P > 0.05$) (Fig. 20a). Samples incubated with enzyme extract containing both DTT and Triton X-100 showed incorporation ratios very similar to those containing Triton X-100 only (Fig. 20a), further suggesting that DTT was not required to maintain the proposed transacylase activity. CMNaOH hydrolysis assays showed similar results (Fig. 20b). Thus,

consistent with the last experiment, high-salt buffer with 1% Triton x-100 (v/v) was selected as the best extraction buffer.

The unusually high CMNaOH-releasable radioactivity ratios (Fig. 20b) were very likely to be because a high amount of prepared pea epicotyl epidermis was used (50 mg dry weight instead of 15 mg in Fig. 19).

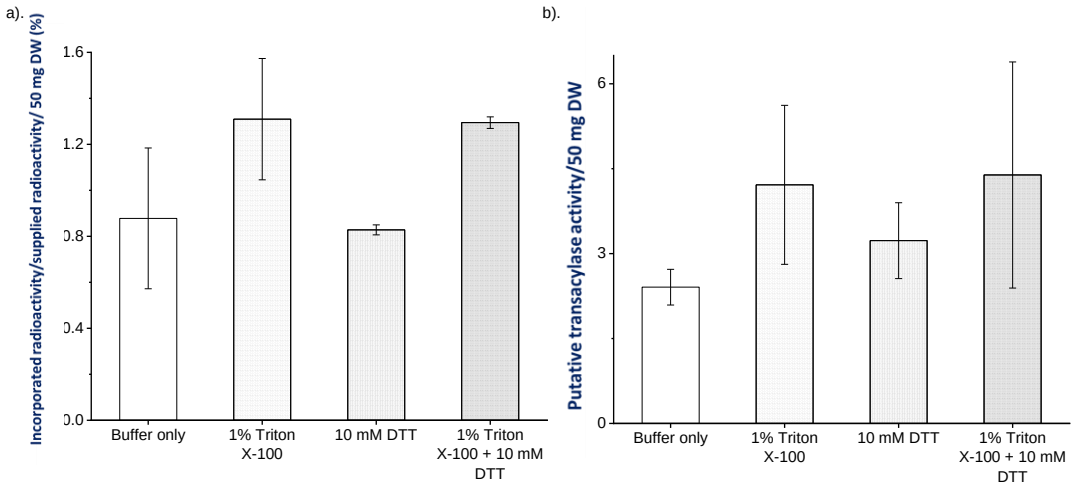

Figure 20. A repeat test of optimizing the putative cutin-to-[^{3}H]HHA transacylase extraction buffers for *ex-situ* assays. Experimental details were as in figure 17, except only the 350 mM succinate (Na^+) buffer was used. The prepared pea epicotyl epidermis (50 mg; acyl donor) was incubated with 0.58 kBq exogenous [^{3}H]HHA (acyl acceptor) under the standardised conditions. (a) The total incorporated radioactivity ratio (%) and (b) CMNaOH-releasable radioactivity ratio (%) illustrate the additives' effects on the cutin-to-[^{3}H]HHA transacylase activity. Bars indicate range (n=2).

A value of 1% incorporated radioactivity/50 mg epidermis/supplied radioactivity corresponds to an absolute incorporation of 110 cpm/50 mg epidermis.

The reproducible *ex-situ* [^{3}H]HHA incorporation provided solid evidence that the proposed cutin-to-HHA transacylase was very likely to exist. Moreover, the *ex-situ* assays enabled us to obtain more hints about the proposed

transacylase's properties, such as that its structure did not allow disulphide bonds formation.

3.2.3 Effects of metal ions on cutin-to-HHA transacylase activity *ex situ*

The cell wall has been believed to contain metal ions based on the finding of ion channels in cell membranes (e.g. Ca^{2+} and K^{+}) (Hedrich, 1989). Moreover, Ca^{2+}, Mg^{2+} and Zn^{2+} have been reported to dimerise rhamnogalacturonan II in cell wall (O'Neill *et al*., 1996; Matsunaga *et al*., 1997). The ions also affect cell wall re-modelling enzymes' activity. For example, the polysaccharide re-modelling enzyme, xyloglucan endotransglucosylase (XET), extracted from pea epicotyl was more active with Ca^{2+}, Mg^{2+} and Mn^{2+} (Fry *et al*., 1992). There was no report about plant GDSLs as were aware, but the ones in bacteria, such as an esterase (estSL3) in *Alkalibacterium*, the activity was reported to be improved with 1 mM Ca^{2+}, K^{+} and Mg^{2+} (Wang *et al*., 2016). Thus, possibly the putative cutin-to-HHA transacylase also requires metal ions, especially the divalent ions to be fully active. Enzymes were extracted by the optimized buffer (350 mM succinate-Na^{+}, pH 5.5 with 1% Triton X-100 v/v), and then divided into aliquots, followed by adding a selected metal ion solution to each one. The only two ions which had big effects on the putative transacylase activity were Cu^{2+} and Ca^{2+}: They decreased and increased the [^{3}H]HHA incorporation respectively ($P > 0.05$) (Fig. 21). The rest of the ions only imposed a mild effect on the transacylase activity insignificantly ($P > 0.05$): the divalent metal ion chelator, EDTA and three heavy metals (Ni^{2+}, Zn^{2+}, Cu^{2+}) slightly reduced compare with the control (Na^{+} from the buffer

preparation only); Mg^{2+} slightly increased the transacylase activity; and Fe^{2+} may did not impact the activity the transacylase activity (Fig. 21).

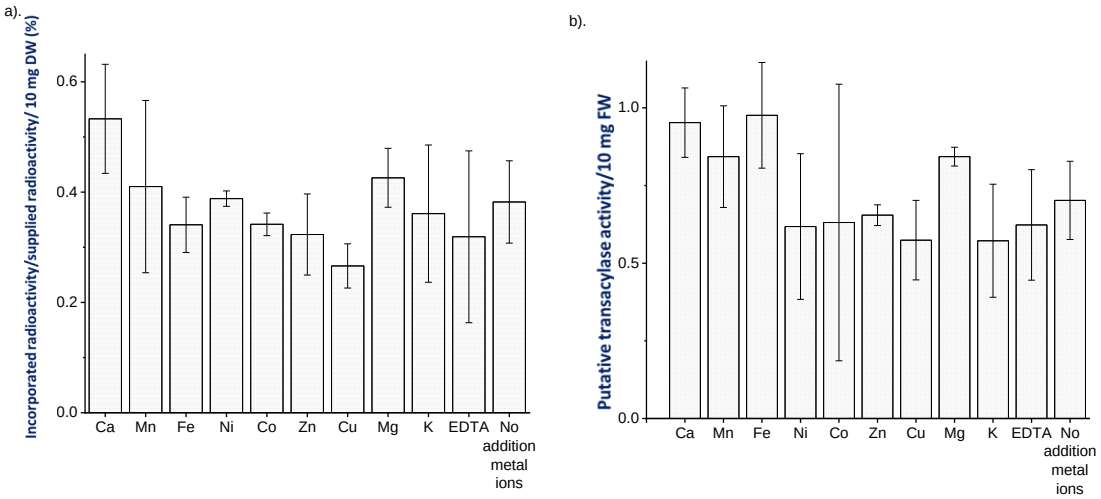

Figure 21. Effects of metal ions on the putative cutin-to-[^{3}H]HHA transacylase activity *ex situ*. Experimental details were as in figure 18, except the only 1% (v/v) Triton X-100 was added to the enzyme extract. The prepared pea epicotyl epidermis (10 mg; acyl donor) without endogenous enzymes was incubated with or without additional metal ions (final conc. = 10 mM) or EDTA (final conc. = 10 mM) and 0.37 KBq exogenous [^{3}H]HHA (acyl acceptor) under the standardised conditions. (a) The total incorporated radioactivity ratio (%) and (b) CMNaOH-releasable radioactivity ratios (%) illustrate the metal ions' effects on the cutin-to-[^{3}H]HHA transacylase activity. Bars indicate range (*n*=2).

A value of 1% incorporated radioactivity/10 mg epidermis/supplied radioactivity corresponds to an absolute incorporation of 70 cpm/10 mg epidermis.

As Ca^{2+} was the ion which had the biggest improving effect on the proposed transacylase's activity, its effect was tested again with more replicates (*n*=6) *ex situ*. Samples with the addition of Ca^{2+} showed ~80% higher ^{3}H total incorporation ratio than the Ca^{2+}-free control in average, but not significantly ($P > 0.05$) (Fig. 22). CMNaOH hydrolysis was not carried out because of the low incorporation ratio compared with the previous experiment (i.e. around 5 times lower), caused by the usage of less epidermis than above.

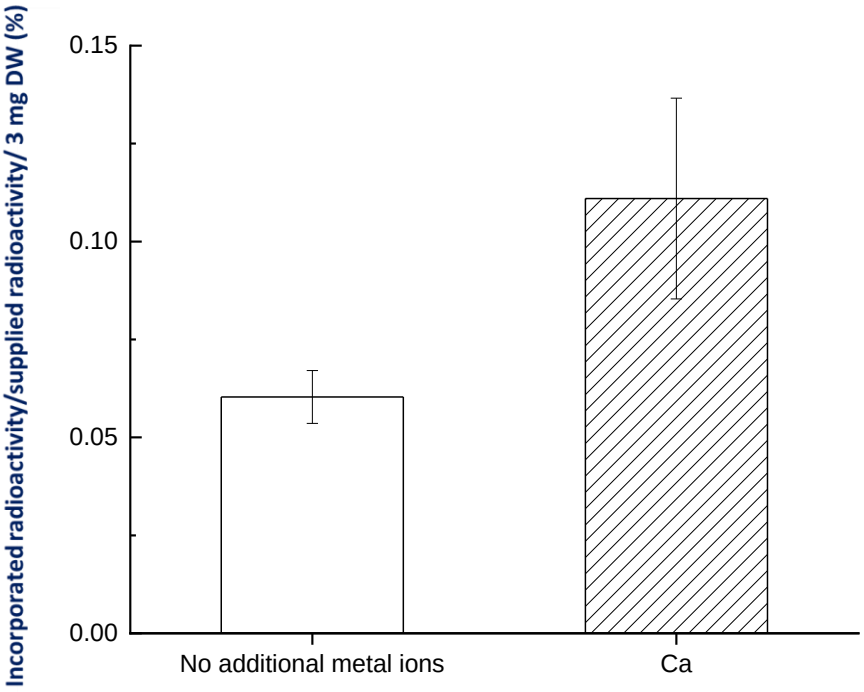

Figure 22. Effects of Ca^{2+} ions on the putative cutin-to-[^{3}H]HHA transacylase activity *ex situ*. Experimental details were as in figure 19, except the prepared pea epicotyl epidermis (3 mg; acyl donor) without endogenous active enzyme was only incubated with or without CaCl (final conc. = 10 mM) and 0.11 kBq exogenous [^{3}H]HHA (acyl acceptor) under the standardised conditions. The total incorporated radioactivity ratio (%) illustrates the effects of Ca^{2+} on the cutin-to-[^{3}H]HHA transacylase activity. Bars indicate standard errors (*n*=6).

A value of 0.1% total incorporated or CMNaOH-releasable radioactivity/3 mg epidermis/supplied radioactivity corresponds to an absolute incorporation of 2 cpm/3 mg epidermis.

In summary, these results suggested that Ca^{2+} can promote the possible cutin-to-HHA transacylase activity, but not dramatically, similar to the reported GDSL enzyme, estSL3 in bacteria (Wang *et al*., 2016). Moreover, it does not require a metal co-factor as some bacteria GDSLs have been reported (Kim *et al*., 2012; Wang *et al*., 2016).

Besides the effects on the transacylase activity, the effects of metal ions on the enzyme extraction efficiency were also investigated. The experimental

procedures were the same as above, but the metal ions were added during extraction.

Similar to the results above (Fig. 21a), only Ca^{2+} and Mg^{2+} slightly improved the extraction efficiency and the activity of the putative cutin-to-[^{3}H]HHA transacylase ($P > 0.05$); and EDTA did not affect either extraction or the transacylase activity, whereas Zn^{2+}, Ni^{2+}, Fe^{2+} and Co^{2+} reduced the extraction efficiency and/or activity; especially the effect of Co^{2+} was significant ($P < 0.01$) (Fig. 23).

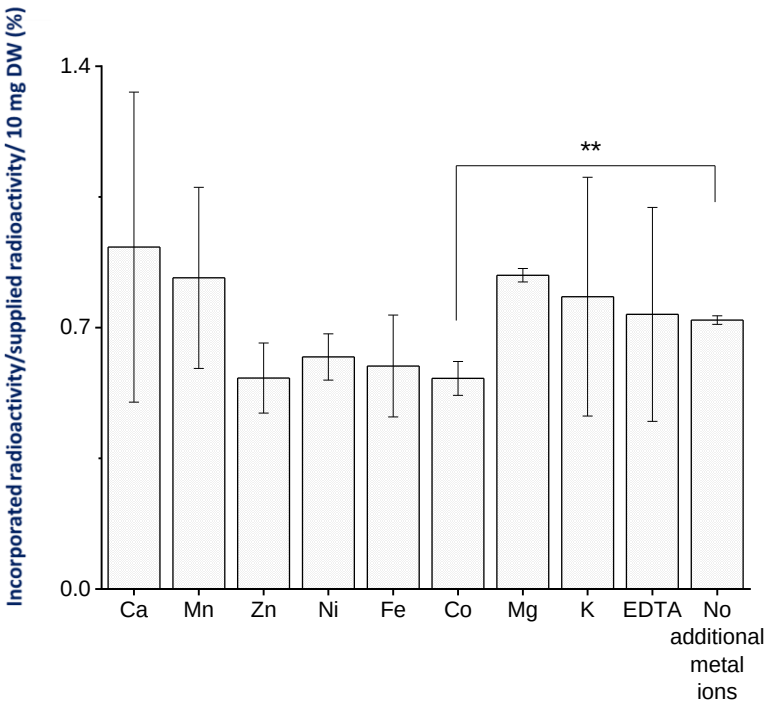

Figure 23. Effects of metal ions on the putative cutin-to-[^{3}H]HHA transacylase extraction efficiency. Experimental details were as in figure 19, except the metal ions and EDTA (final conc. = 10 mM) were added during extraction; and 0.48 kBq exogenous [^{3}H]HHA was supplied as the acyl acceptor. The total incorporated radioactivity ratio (%) illustrates the metal effects on the cutin-to-[^{3}H]HHA transacylase extraction efficiency. Bars range (*n*=2). **: $P < 0.01$.

A value of 1% total incorporated radioactivity/10 mg epidermis/supplied radioactivity corresponds to an absolute incorporation of 90 cpm/10 mg epidermis.

Taken together, the possible cutin-to-HHA transacylase was reproducibly confirmed not require a metal co-factor, but the addition of Ca^{2+} and Mg^{2+} can be beneficial to the activity and extraction efficiency.

3.3 Cutin-to-HHA transacylase product analysis

The significant difference of the incorporation ratio between un-denatured and denatured epidermis samples above have demonstrated preliminarily that the exogenous ^{3}H from [^{3}H]HHA can be incorporated into epidermis enzymically. The hydrophobic alkaline (CMNaOH) hydrolysis assays provided a preliminary indication that [^{3}H]HHA was incorporated by forming ester bonds, very likely to be with cutin. To eliminate all other possibilities, such as wax–[^{3}H]HHA, protein–[^{3}H]HHA and polysaccharide–[^{3}H]HHA, a series of chemical and enzymic treatments was applied.

Pea epicotyl epidermis with or without active endogenous enzymes was incubated with [^{3}H]HHA *in situ* under the standardised conditions as above. The MFW-washed epidermis samples were then subjected to the enzymic product analysis as below.

3.3.1 Modifications of the un-bonded [^{3}H]HHA

The first solvent used to wash away non-bonded radioactivity was the MFW (pH ~1.7), which removed ~70% of the supplied radioactivity in 1 hour (data not shown). The washings were collected and analysed by TLC (Fig. 24), which showed that after 24 h incubation, still some exogenous [^{3}H]HHA had not been incorporated, indicating that the supplied [^{3}H]HHA was adequate.

The free [^{3}H]HHA was metabolised into 6 other compounds (Fig. 24). Most of them were un-identified, so I roughly divided the metabolites into two classes: the ones that migrated further than [^{3}H]HHA did were “hydrophobic metabolites”, and the ones nearer the origin were “hydrophilic metabolites”, because the more hydrophobic compounds migrate further in this TLC developing system (exemplified in Fig. 25: TLC staining of HA and HHA markers).

Based on the R_F of di-[^{3}H]HHA ester (R_F = 0.25±0.01), which we synthesized in the lab (Appendix 4), there was no di-ester, such as a fatty acid–[^{3}H]HHA conjugate (produced with cutin precursor, 2-MAG, as the acyl donor, and exogenous [^{3}H]HHA as the acceptor) dissolved in the MFW (Fig. 24). Nevertheless, we cannot exclude that oligoesters with other lengths were formed and dissolved. For example, the peaks near the origin (R_F = 0.017–0.141) may represented high-M_r products. Another unknown peak (R_F = 0.644) was annotated as putative 16-oxohexadecanoic acid (OHA) based on our chemical synthesis tests (Appendix 5). It may have been generated because of the overnight drying process in the SpeedVac, which produces a mild heat and may have oxidized the [^{3}H]HHA (Appendix 5).

The total radioactivity solubilised in the MFW from the un-denatured epidermis samples was ~0.8× that from the denatured control [Fig. 24: [^{3}H]HHA (R_F = 0.387); [^{3}H]OHA (R_F = 0.644)] because of the enzymic incorporation.

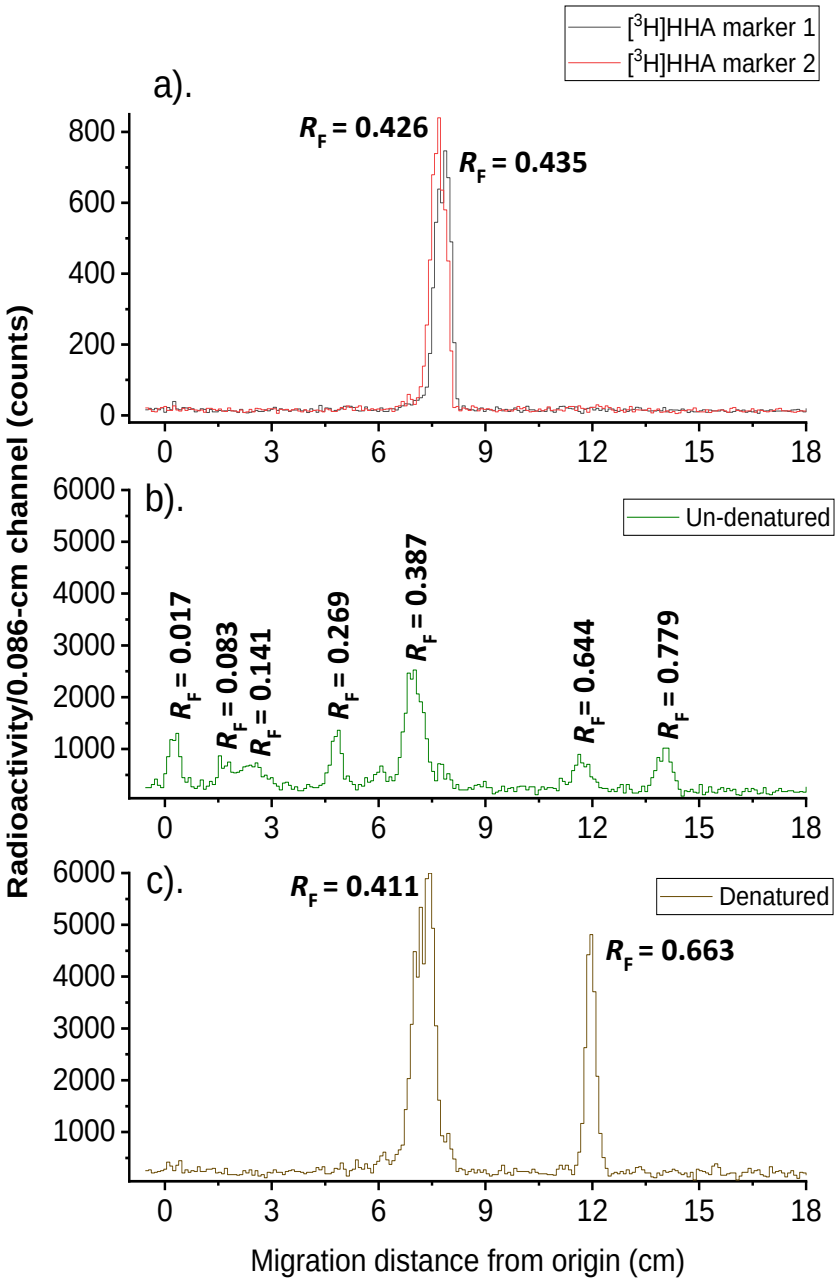

Figure 24. Chromatographic analysis of the acidified methanolic wash of [^{3}H]HHA-incubated epidermis samples. Blot-dried pea epicotyl epidermis (100 mg; acyl donor) with or without active endogenous enzymes was incubated with exogenous 12.7 kBq [^{3}H]HHA (acyl acceptor) in 600 µl pH 5.5 buffer for 24 h under the standardised conditions. MFW (9/1/1) was used to stop reactions and the supernatant was dried, and the residue was re-dissolved in a small volume of MFW, which was then loaded onto TLC plates (toluene/acetic acid, 9/1 v/v, 3 ascents). (a) Two external [^{3}H]HHA markers. (b). MFW of un-denatured epidermis samples. (c). MFW of denatured (control) epidermis samples. The solubilised substances were localised by radio-scanning the TLC plates for 1 h per lane (spatial resolution: 0.086

cm) (unit: counts). R_F values annotated to each peak were calculated as follows: migration distance of a peak / distance from the loading origin to the solvent front.

3.3.2 Wax–[^{3}H]HHA conjugates in the enzymic products

Different from cutin, wax lipids can be dissolved in neutral organic solvents, because it is dominated by very long alkane (e.g. C_{29} *n*-alkanes in *Arabidopsis* stem cuticle); and only 1% is oligoester e.g. in *Arabidopsis* stem wax (reviewed by Kunst and Samuels, 2003). Noticeably, the wax oligoester is also a potential transacylase donor, so its conjugate with [^{3}H]HHA and the product we were interested in, cutin–[^{3}H]HHA, should be carefully distinguished from each other.

More neutral hydrophobic solvents were applied after the MFW wash: toluene and CM (2/1, v/v), especially the latter, has been reported to be able to remove wax (Yeats *et al*., 2010).

Toluene was applied to epidermis samples after the MFW, and it dissolved ~11% of the supplied radioactivity from the un-denatured epidermis samples, but only 0.92% from the denatured control (Fig. 25a), indicating that some enzymic products were being dissolved in the toluene. The toluene extract was analysed by TLC as well, showing that toluene mainly dissolved the most hydrophobic [^{3}H]HHA metabolite (R_F = 0.778), which co-migrated with HA; and the majority of other metabolites had already been removed by MFW (Fig. 26a). The negligible peaks from the denatured control further confirmed that the compound solubilised in toluene from un-denatured samples was an enzymic product (Fig. 26b).

This solubilised compound was not identified in this project, even though it shared the same R_F with HA (i.e. removal of the terminal –OH group by a hydratase may turn [^{3}H]HHA into [^{3}H]hexadecenoic acid).

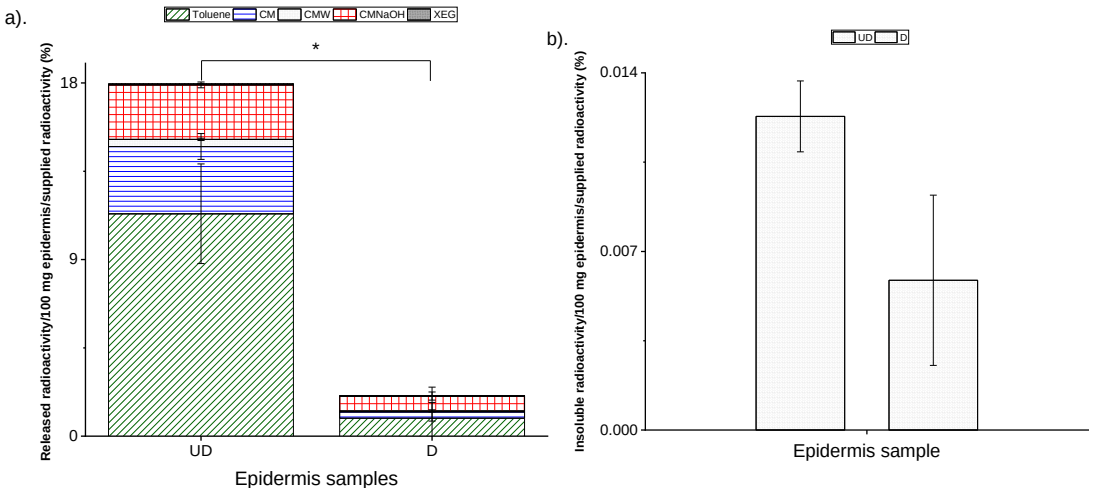

Figure 25. Quantification of all the chemical extractions and MFW-insoluble residues of [^{3}H]HHA-incubated pea epicotyl epidermis. (a). After MFW wash, aliquots of the supernatants of the toluene, CM (2/1, v/v), CMW (10/10/3, v/v/v), CMNaOH (10/10/3, v/v/v) and 0.1% (w/v) XEG treatments of the [^{3}H]HHA (12.7 kBq)-incubated pea epicotyl epidermis (100 mg) were scintillation counted. (b). The insoluble residues were scintillation counted after all the extraction and degradation treatments. UD: un-denatured pea epicotyl epidermis samples. D: denatured (control) epidermis samples. Bars indicate range. *: $P < 0.05$.

A value of 1% incorporated radioactivity/100 mg epidermis/supplied radioactivity corresponds to a calculated (for CMNaOH) or absolute (for toluene etc.) incorporation of 2400 cpm/100 mg epidermis.

The peak near origin in the toluene may represent cutin-related oligoester–[^{3}H]HHA conjugates, because it was not released from the denatured control, and the migration was expected to be slow (Fig. 26). Thus, the peak (R_F = 0.017) in MFW (Fig. 24) was also likely to represent oligoester–[^{3}H]HHA conjugates.

a).

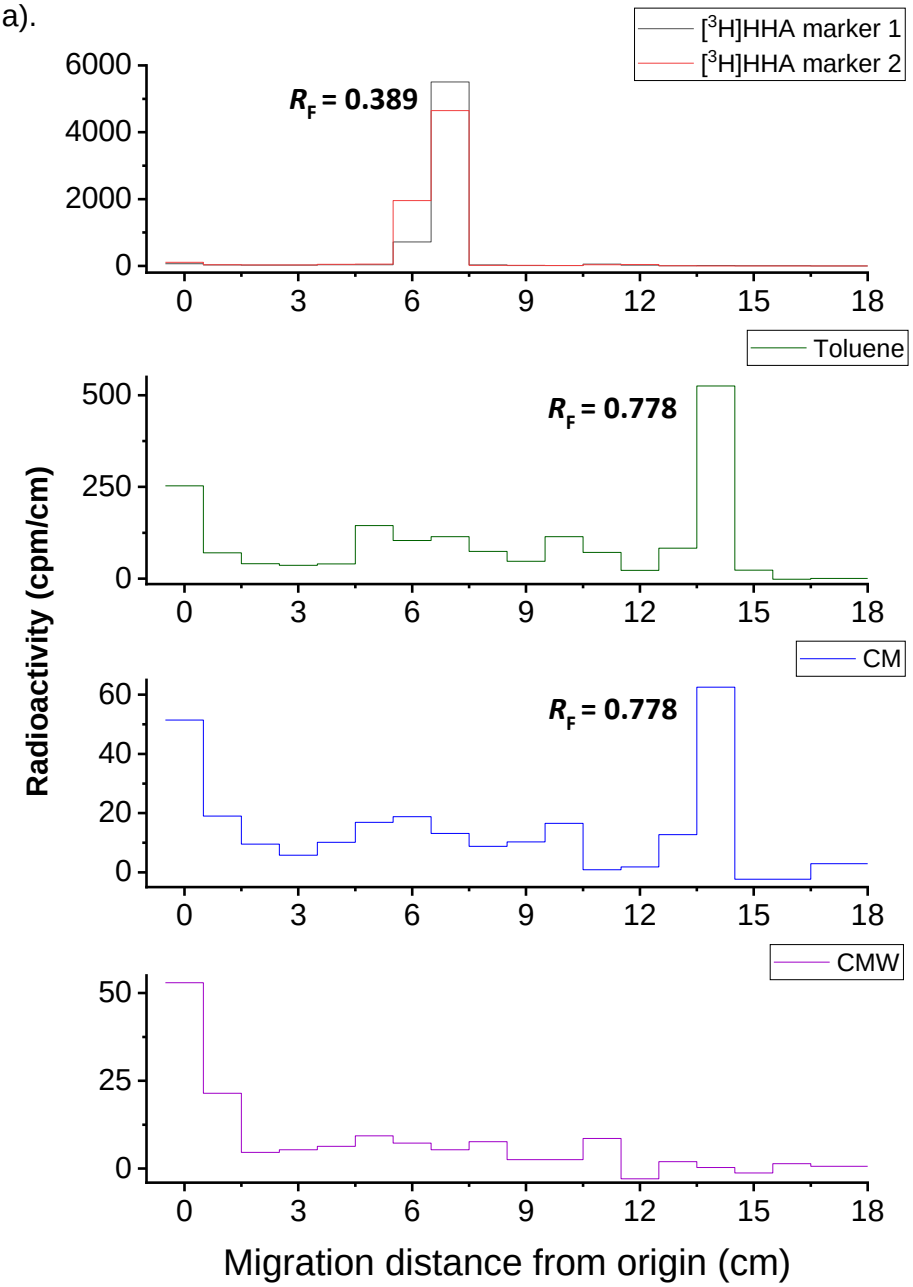
[3H]HHA marker 1
[3H]HHA marker 2
RF = 0.389
Toluene
RF = 0.778
CM
RF = 0.778
CMW
Radioactivity (cpm/cm)
Migration distance from origin (cm)


HHA
HA

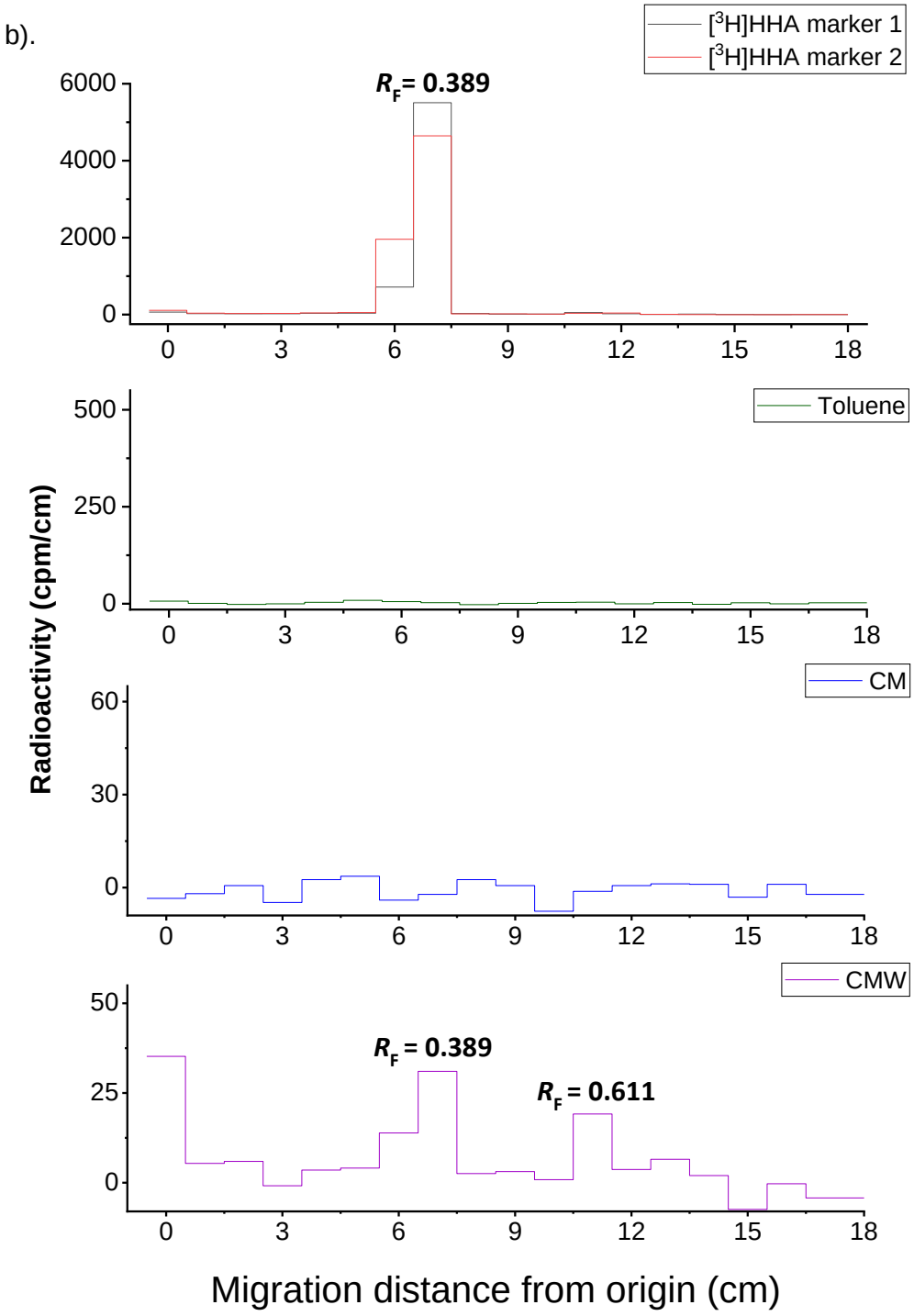

Figure 26. Chromatographic analysis of the neutral hydrophobic solvent washes of [^{3}H]HHA-incubated pea epicotyl epidermis. The toluene, CM (2/1, v/v) and CMW (10/10/3, v/v/v) washes of the [^{3}H]HHA (12.7 kBq)-incubated pea epicotyl epidermis (100 mg) were subjected to TLC as above. The TLC plates were then cut into 1-cm (migration distance) strips, which were scintillation counted (unit: cpm). Supernatants from both un-denatured pea epicotyl epidermis samples (a) and the denatured control (b) were analysed.

The external markers (non-radioactive HHA and HA) were revealed by staining with iodine-vapour.

In summary, toluene removed the most hydrophobic [^{3}H]HHA metabolites and putative oligoester–[^{3}H]HHA conjugates, which were not removed by MFW efficiently.

Some enzymic products were also found to be dissolved in the following CM wash, because ~3% of the supplied radioactivity was detected from the un-denatured epidermis samples, but only a negligible amount from the denatured control (Fig. 25a). CM also mainly dissolved the same hydrophobic [^{3}H]HHA metabolite and the putative oligoester–[^{3}H]HHA conjugates as toluene did (Fig. 26a), but the quantity was much smaller. Together with the negligible radioactivity released from the denatured control (Fig. 25 & 24b), the results indicated that these solvents removed un-bonded radioactivity efficiently.

CMW (10/10/3, v/v/v) was another hydrophobic solvent mixture, but more hydrophilic than the CM above. It was applied after the above washes, to remove [^{3}H]HHA and its relatively hydrophilic metabolites, and in the meanwhile also acted as a control for later CMNaOH hydrolysis (10/10/3, v/v/v).

Only a trace (~0.4%) radioactivity was dissolved in CMW from un-denatured epidermis samples (Fig. 25a), and the TLC analysis showed that the hydrophobic [^{3}H]HHA metabolite cannot be detected in this solvent mixture, only a small peak (~50 cpm) near the origin, which was also found in the

denatured control (~40 cpm) (Fig. 26). These results may suggest that this peak actually represents a hydrophilic metabolite of [^{3}H]HHA or an artefact, because the putative wax oligoester–[^{3}H]HHA conjugates should be totally removed by more hydrophobic solvents than CMW, as the most hydrophobic metabolite was (Fig. 26).

The denatured control released even less radioactivity into CMW (10/10/3) (0.05%) than the un-denatured epidermis samples, and besides the peak near the origin, it also released a trace of un-bonded [^{3}H]HHA (R_F = 0.389) (evidenced by the staining of non-radioactive markers and counting of radioactive markers), which was not observed in the toluene and CM, providing evidence that the CMW dissolves [^{3}H]HHA efficiently (Fig. 26b), thus a good solvent for the subsequently used NaOH hydrolysis. Another peak (R_F = 0.611) was unidentified (Fig. 26b).

In conclusion, four acidic or neutral hydrophobic solvent mixtures were used to remove [^{3}H]HHA and its metabolites, which were not bonded to polymeric cutin. The potential wax oligoester–[^{3}H]HHA conjugates were concluded not to be found because the possibly representative peak nearby origin was not dissolved in hydrophobic solvents (e.g. CM) efficiently as expected. The amount of dissolved radioactivity was decreasing from the first applied mixture (MFW) to the last (CMW), indicating that these washes thoroughly removed un-cutin-bonded radioactivity.

3.3.3 Possible protein–[^{3}H]HHA conjugates in the enzymic products

Even though the protein-to-[^{3}H]HHA transacylation reaction has never been reported, β-carboxy groups of asparagine and γ-carboxy group of glutamine (activated acyl groups by $–NH_2$), as well as the C-terminal carboxy groups of amino acids can potentially act as the donor (reviewed by Lamport, 1970), forming protein–HHA ester bonds.

In the preliminary experiments, proteinase K (from porcine liver) was applied to the thoroughly washed (by toluene etc.) epidermis samples to hydrolyse proteins (Chapter 2, Table 1), which in turn may release any amino acid–^{3}H conjugates, if the incorporation was catalysed by a protein-to-HHA transacylase. Free ^{3}H may also be released by proteinase K if it can catalyse ester hydrolysis (reviewed by Hedstrom, 2002).

The amount of proteinase K-releasable radioactivity from un-denatured epidermis samples was equally negligible (~0.25% of supplied radioactivity) as the buffer (without proteinase K, control) alone, indicating that essentially no [^{3}H]HHA was covalently bonded to cell wall proteins (Fig. 27). Both un-denatured samples released much more (~8-fold) ^{3}H than the denatured samples with proteinase K may be because the buffer (pH 8.8) is basic enough to break some ester bonds between cutin and ^{3}H in un-denatured samples (Fig. 27).

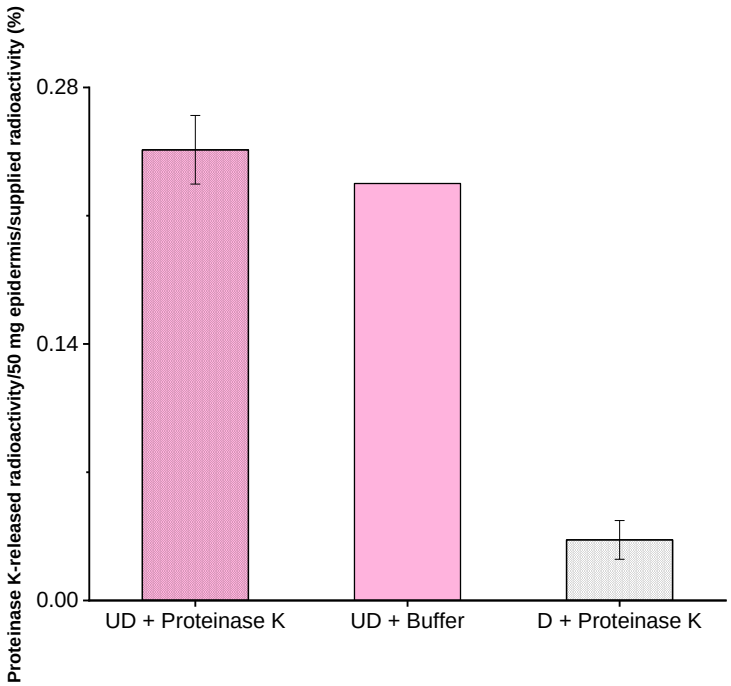

Figure 27. Quantification of cell wall protein–[^{3}H]HHA conjugates of [^{3}H]HHA-incubated pea epicotyl epidermis. Blot-dried pea epicotyl epidermis (50 mg; acyl donor) with or without active endogenous enzymes was incubated with 1.2 kBq exogenous [^{3}H]HHA in 300 µl pH 5.5 buffer at room temperature for 24 h. After all the MFW (9/1/1), toluene, CM (2/1) and CMW (10/10/3) extraction, the insoluble residue was incubated with or without 3 U proteinase K in 1 ml of pH 8.8 (50 mM ammonium-acetate) buffer 37°C for 3 days. The supernatant was scintillation counted as above. UD: un-denatured pea epicotyl epidermis samples. D: denatured (control) epidermis samples. Bars indicate standard errors (*n*=3) for the 'UD + Proteinase K' group. Bars indicate range (*n*=2) for the 'D + Proteinase K' group.

A value of 0.1% proteinase K-releasable radioactivity/50 mg epidermis/supplied radioactivity corresponds to an absolute incorporation of 23 cpm/100 mg epidermis.

The results above was reproducibly observed in other preliminary experiments, demonstrating that no ^{3}H from [^{3}H]HHA was not covertly bonded with proteins, and therefore this treatment was neglected in rest of the experiments.

3.3.4 Probable cutin–[^{3}H]HHA conjugates in the enzymic products

Lipase in general hydrolyses water-insoluble esters (Chahinian and Sarda, 2009), so a lipase from *Aspergillus niger* was applied to the epidermis samples, which had been washed and digested in the organic solvent treatments and Proteinase K above, in order to release the putatively cutin-ester-bonded [^{3}H]HHA.

However, even though the lipase activity was detectable by using commercial *p*-nitrophenyl palmitate (*p*-NPP) as the substrate (Appendix 2), it only released negligible amount of incorporated ^{3}H from both un-denatured and denatured epidermis samples (~0.16 and 0.13% of the supplied radioactivity) ($P_{\text{(un-denatured vs. denatured)}} > 0.05$) (Fig. 28a). Thus, the *Aspergillus* lipase is not an efficient enzyme with which to look for the cutin–[^{3}H]HHA conjugates.

Cutinase (*AN7541.2*) from *A. nidulans* was predicted to function as a cutin hydrolase because its nucleotide sequence aligned with identified cutinases from *A. fumigatus* and *A. oryzae* (Liu *et al*., 2009; Baker *et al*., 2012; Ping *et al*., 2017).

I cultivated the engineered *Pichia pastoris* (strain: SB), which produced the secretory cutinase heterologously (Bauer *et al*., 2006) (Appendix 1), and the culture medium containing cutinase was then isolated and freeze-dried to be used for the cutin–[^{3}H]HHA hydrolysis experiment. However, even though the cutinase can hydrolyse *p*-NPP very efficiently (Appendix 1), it was unable to release the cutin-bonded [^{3}H]HHA from un-denatured epidermis (~0.07% of supplied radioactivity), and not significantly different from the denatured

control (P > 0.05) (Fig. 28b). Moreover, cutinase essentially released less radioactivity than the buffer alone (pH 8.0) (Fig. 28b), further indicating that it cannot be used in hydrolysing cutin–^{3}H ester bonds.

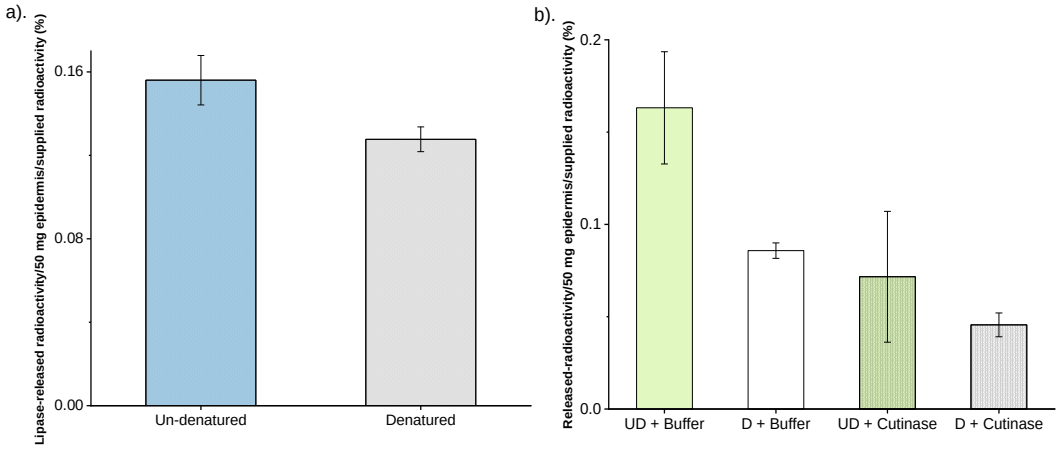

Figure 28. Quantification of cutin–[^{3}H]HHA conjugates of [^{3}H]HHA-incubated pea epicotyl epidermis by enzyme degradations. Experimental details were as in figure 25, except 0.85 kBq exogenous [^{3}H]HHA was supplied as the acyl acceptor, and the CMW-insoluble residue was incubated with 0.02 U lipase in 1 ml of pH 7.5 (50 mM collidine-acetate) buffer at 25°C for 3 days. (b). After the lipase digestion, the insoluble residue was incubated with or without 0.45% (w/v) cutinase in 1 ml of pH 8.0 (50 mM collidine-acetate) buffer at 37°C for 3 days. UD: un-denatured pea epicotyl epidermis samples. D: denatured (control) epidermis samples. Bars indicate standard errors (*n*=3).

A value of 0.1% releasable radioactivity/50 mg epidermis/supplied radioactivity corresponds to an absolute incorporation of 16 cpm/100 mg epidermis.

Thus, this annotated cutinase does not function as the prediction, at least not detectable by using the radio-chemical technique. Another explanation is that ^{3}H was not incorporated into cutin. This possibility was further investigated below.

In summary, two lipases were tested, but neither the general nor the more specific one hydrolysed the putative cutin–[^{3}H]HHA *in vitro*.

Alternatively, the CMNaOH mixture used in the earlier experiments was employed to find out whether ^{3}H from [^{3}H]HHA was incorporated via ester bonds. The advantage of CMNaOH compared with the lipases is that it hydrolyses esters more efficiently, but also less specific as a disadvantage.

As Figures 23a and 24a show, negligible [^{3}H]HHA was extracted from un-denatured epidermis samples by neutral CMW, but CMW containing 0.5 M NaOH, released ~2.8% of the supplied radioactivity from un-denatured epidermis samples, and only 0.8% from the denatured epidermis samples (Fig. 25a), suggesting that some enzymically incorporated radioactivity was released by alkali. Moreover, the majority of the released radioactivity was identified as [^{3}H]HHA (R_F = 0.359–0.364) (Fig. 29: TLC staining and radio-scanning of external markers), which was only a negligible peak from the denatured control, providing solid evidence that the exogenous [^{3}H]HHA was incorporated via ester bonds without otherwise being modified (Fig. 29).

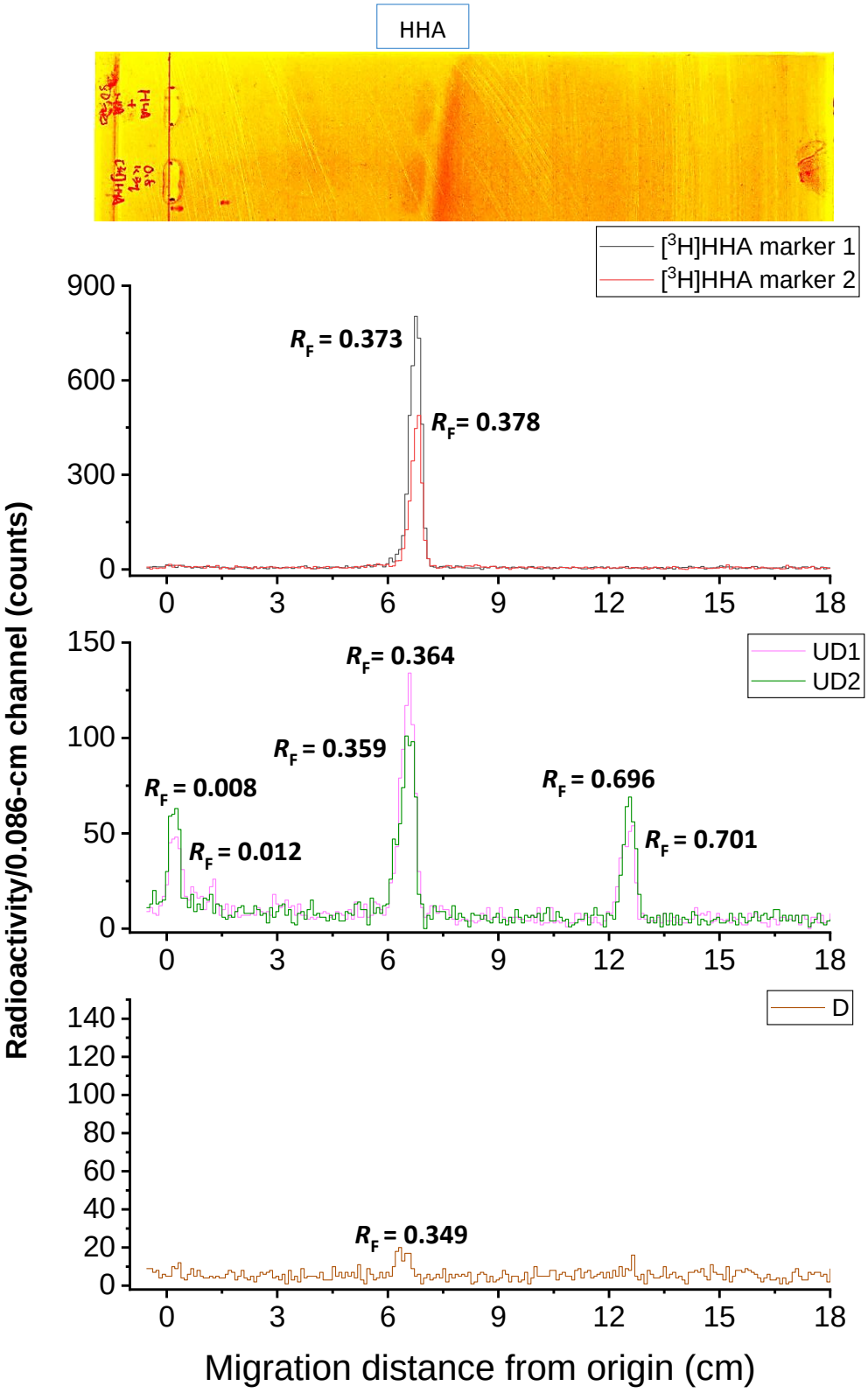

Figure 29. Chromatographic analysis of the CMNaOH-hydrolysed radioactivity from [^{3}H]HHA-incubated pea epicotyl epidermis. The CMNaOH supernatant

from the [^{3}H]HHA (12.7 kBq)-incubated pea epicotyl epidermis (100 mg) was acidified and then phase-partitioned between hydrophobic solvents and water to remove salts, and the hydrophobic layer containing any [^{3}H]HHA-related compounds was subjected TLC as above, which were then radio-scanned for 1 h per lane (spatial resolution: 0.086 cm) (unit: counts). R_F values are annotated to each peak, calculated above. UD: un-denatured pea epicotyl epidermis samples. D: denatured (control) pea epicotyl epidermis samples.

The external HHA markers were revealed by staining with iodine vapour.

The peak near the origin (R_F = 0.008–0.012) was also found in the neutral CMW extract (Fig. 25a), but more of it was released by CMNaOH because the radio-scanner (unit: counts) (Fig. 29) is less sensitive than scintillation counting with scintillation fluid (unit: cpm) (Fig. 25a). Furthermore, this peak was absent in the control sample (denatured epidermis), indicating that it is an enzymic product (Fig. 29). Even though it was unidentified in this thesis, it further confirmed that it does not represent wax oligoester–[^{3}H]HHA conjugates, which should not be intact after CMNaOH hydrolysis.

The other peak (R_F = 0.696–0.701), which had been predicted to be OHA above, was not seen in CMW and other neutral organic solvents, but only emerged in CMNaOH of un-denatured epidermis samples, (Fig. 21a, 20 and 27). It was proposed to be produced by oxidizing the CMNaOH-releasable [^{3}H]HHA during SpeedVac drying process as above (Fig. 24).

In summary, these results indicate that [^{3}H]HHA together with its two putative metabolites were ester bonded within the epidermis, possibly to cutin.

Since the possibility of wax oligoester being an acyl donor was not supported, and its absolute quantity in the epidermis is much smaller than that of cutin, and hence the most plausible remaining epidermal components to form ester

bonds with the –OH group of [^{3}H]HHA and its metabolites were cutin and methyl esterified galacturonic acid, because they both have activated acyl groups. However, the later possibility was not very likely, because as I have stated in Chapter 1, PME, the enzyme that transfers the acyl group of a methyl esterified galacturonan to a water molecule (in hydrolysis) is not in the same family as CD1, differentiating the substrate specificities; and the methyl esterified [^{3}H]GalA$_8$-ol did not have detectable acyl donor ability *in situ* under comparable conditions (Chapter 4).

Thus, cutin was the most feasible candidate to form ester bonds with exogenous [^{3}H]HHA and its metabolites. This is the first experimental evidence that the cutin-to-hydroxy fatty acid transacylase activity exists.

3.3.5 Possible polysaccharide–[^{3}H]HHA conjugates in the enzymic products

Another big class of epidermal components are cell wall polysaccharides. One of the possible scenario is that the reducing ends of polysaccharides form glycosidic bonds with [^{3}H]HHA as in the glycosidic bonds in XET product (Thompson and Fry, 2001); a less feasible possibility is that the inactivated carboxy group of [^{3}H]HHA form ester bonds with the hydroxy groups of xyloglucan. To eliminate these possibilities, I digested the insoluble residue of the CMNaOH-hydrolysed epidermis samples with 0.1% (w/v) XEG (Pauly *et al*., 1999) (Chapter 2, Table 1).

Only equally negligible radioactivity (0.04% of supplied radioactivity) was released from both un-denatured and denatured epidermis samples (Fig. 25a), indicating that not only xyloglucan, but also other polysaccharide were

not involved in the observed radioactivity incorporation, because XEG released almost the whole CMNaOH-insoluble ^{3}H (Fig. 25b). This result further supported the suggestion that cutin was the only epidermal component, which was covalently bonded with ^{3}H from [^{3}H]HHA.

3.3.6 Possible cutan–[^{3}H]HHA conjugates in the enzymic products

Cutan is a non-hydrolysable aliphatic polymer in land plants, composed of *n*-alkane or alkene units ($C_{8–35}$) interlinked by ether bonds, but it is unknown whether it exists in pea epicotyl epidermis since it is less common than cutin (Gupta *et al*., 2006). To test the presence of cutan–[^{3}H]HHA (i.e. the alkali-insoluble residues), the residues left after the chemical and enzymic treatments above were scintillation counted. Only background radioactivity was detected in both un-denatured epidermis samples and the denatured control, indicating that there was no cutan–[^{3}H]HHA conjugate in pea epicotyl epidermis (Fig. 25b). In future experiments, the CMNaOH-insoluble residues could be combusted for scintillation counting to achieve a higher counting efficiency.

Taken together, a series of degradation treatments was applied to *in-situ* assayed epidermis samples (acyl acceptor: [^{3}H]HHA), to remove interferences and identify the cutin-to-HHA transacylase product. The chemical analysis (TLC method) showed that exogenous [^{3}H]HHA was metabolised into different compounds, most of which were washed away by the MFW, the rest were removed by toluene, CM and CMW. The CMNaOH hydrolysis enabled us for the first time to demonstrate that [^{3}H]HHA and its

metabolites were incorporated via forming ester bonds, likely with cutin, *in situ*. This novel transacylase activity was thus named as cutin-to-HHA transacylase in this chapter.

3.4 Attempts to identify the putative cutin-to-HHA transacylase

3.4.1 CD1 activity on [^{3}H]HHA *in situ*

Cutin-to-HHA transacylase activity was found for the first time, but the transacylase protein was not identified. As the only well-known cutin transacylase, CD1 (Yeats *et al*., 2012) was proposed to be a candidate. Thus, even though tomato fruit was not a good model for testing cutin-to-HHA transacylase activity, *cd1*-knockout M82 tomato fruit epidermis was compared with the WT fruit epidermis in the *in-situ* cutin-to-HHA transacylase assay.

The incorporation was very low in both samples, but not absolutely nothing because the un-denatured samples of both genotypes incorporated more ^{3}H than the denatured control did ($P_{(\text{WT un-denatured vs. WT denatured})} < 0.05$; $P_{(cd1\text{-knockout un-denatured vs. WT denatured})} < 0.01$) (Fig. 30). However, the WT epidermis only incorporated slightly higher [^{3}H]HHA than *cd1* mutant did ($P > 0.05$) (Fig. 30), suggesting that CD1 was at least not the sole enzyme for the cutin-to-HHA transacylation reaction.

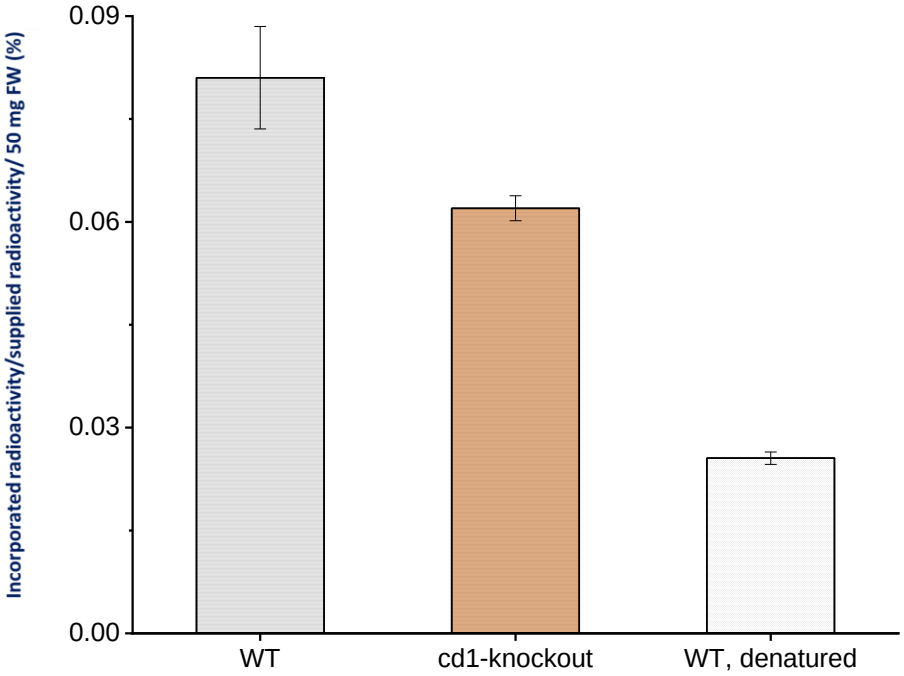

Figure 30. The comparison between the putative cutin-to-[^{3}H]HHA transacylase activities in WT and *cd1*-knockout tomato fruit (cv. M82) epidermis *in situ*. The epidermis samples (50 mg; acyl donor) with or without endogenous active enzymes were incubated with 0.95 kBq exogenous [^{3}H]HHA (acyl acceptor) under the standardised conditions as all the *in-situ* experiments above. The incorporated radioactivity ratio (%) illustrates the endogenous cutin-to-[^{3}H]HHA transacylase activity. Bars indicated standard errors (*n*=3). For 'WT, denatured' samples, bars indicate range (*n*=2).

A value of 0.1% total incorporated radioactivity/50 mg epidermis/supplied radioactivity corresponds to an absolute incorporation of 18 cpm/50 mg epidermis.

3.4.2 His$_6$-tagged CD1 transacylase activity on HHA and [^{3}H]HHA *in vitro*

CD1 was also heterologously expressed in *Nicotiana benthamiana* (Appendix 7) with a C-terminal His$_6$-tag (because it is a secreted apoplastic enzyme, an N-terminal His$_6$-tag might interfere with the secretory signalling peptide). The His$_6$-tagged CD1 was extracted by a modification of the published protocol (Yeats *et al*., 2012, supplementary), purified by immobilised metal affinity chromatography (Co^{2+}), dialyzed against water to de-salt, and freeze-dried. The purified His$_6$-tagged CD1 (native size = 40 kDa; His$_6$-tag = 1 kDa) in the last two eluents was identified on SDS-PAGE, via Coomassie blue staining

and immuno-staining (western blot) (Fig. 31a and b). WT samples (without transformation) did not show the 41 kDa band in the last two eluents (Fig. 31c) and no such bands by Western-blot as well (Fig. 31d), providing evidence that CD1 was specifically produced in *CD1*-transformatted tobacco. However, the transformation step seems enhances other unspecific protein productions (Fig. 31c and d). Its activity was assayed spectrophotometrically and radio-chemically as below.

a).

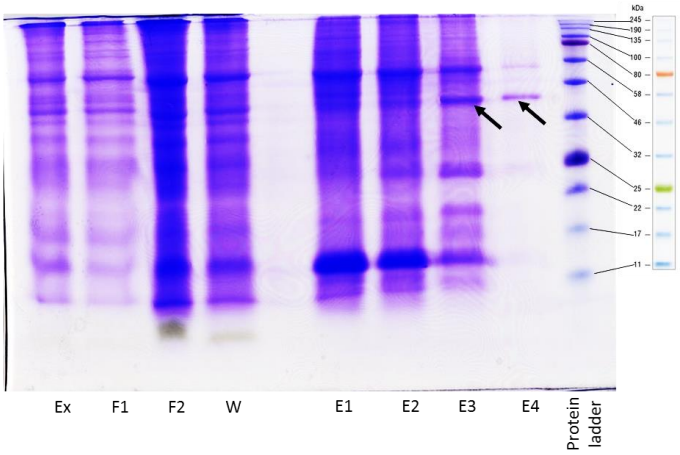

b).

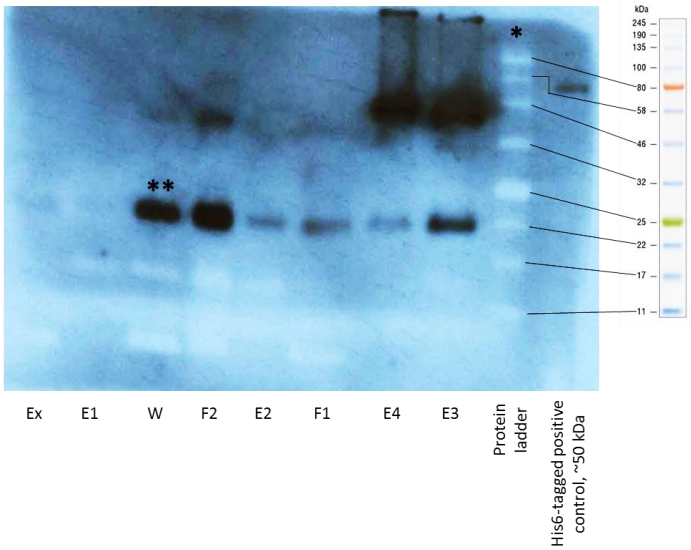

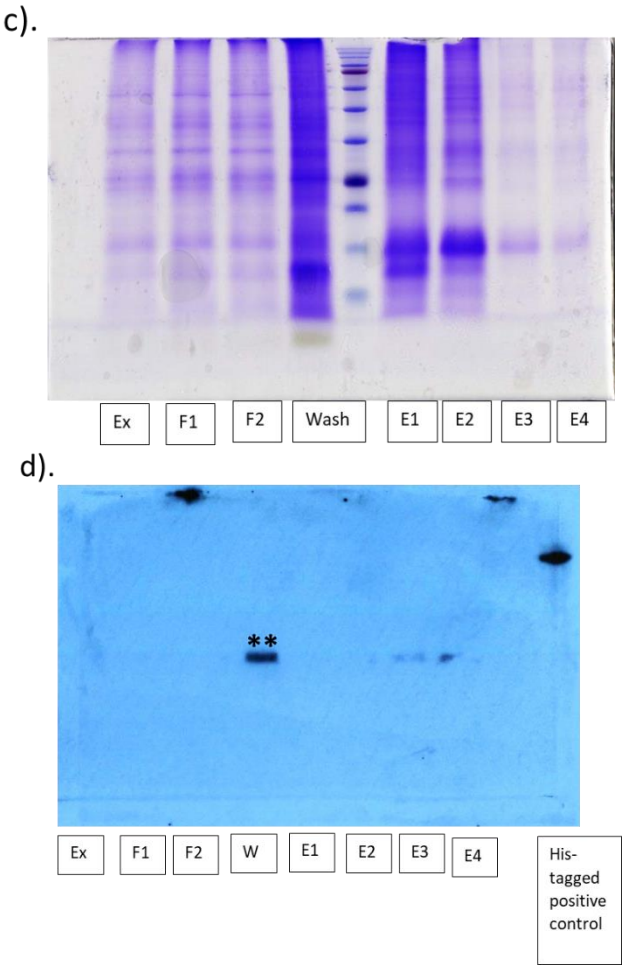

Figure 31. The detection of His_6-tagged CD1 by Coomassie and immune-staining. The immobilized metal affinity column-purified His_6-tagged CD1 was concentrated 100-fold after dialysis and freeze-drying. It was analysed by SDS-PAGE (discontinuous system), and then one of the gels was stained by 0.006% Coomassie Brilliant Blue R-250 (dissolved in 10% acetic acid) overnight (a); the other one was stained by monoclonal anti-poly-His–HRP antibody, and visualized by exposing to an X-ray film for 1 s (b). The E3 and E4 containing a His_6-tagged protein at ~40 kDa (a) (b), compared with the protein ladder. Ex: crude extract. F1–F2: flowthrough 1–2. W: wash. E1–E4: eluents 1–4 (50 mM phosphate-Na^+, 300 mM NaCl and 10–270 mM imidazole). (c) and (d) were obtained by the same experimental steps as (a) and (b) respectively, but with WT samples.

*: The protein ladder was not His_6-tagged, so not stained by the anti-poly-His–HRP antibody.

**: The non-His_6-tagged proteins were stained by the anti-poly-His–HRP antibody probably due to the high concentration of antibody (1:1500), and/or of the high concentration of the unspecified protein.

Assay His$_6$-tagged CD1's transacylase activity spectro-photometrically

The purified His$_6$-tagged CD1 (E3 and E4; Fig. 31) was incubated with *p*NPP as the acyl donor, and each of various cutin components: non-radiolabelled HHA, HA (a control as in Fig. 17), *p*-coumaric acid and ferulic acid (Hunt and Baker, 1980; Kosma *et al.*, 2010; Rautengarten *et al*., 2012; reviewed by Fich *et al*., 2016) as the acyl acceptors (exemplified by Fig. 32). However, CD1 activities in the presence of these four compounds were even lower than with water only ($P < 0.01$). I hypothesized that it might be because they were not completely dissolved in the aqueous buffer like isopropanol and propanol were (Fig. 33), resulting in a suspension (invisible particles), which may impede the mobility of CD1. In addition, the insignificant difference ($P > 0.05$) between HHA and HA indicated that as HA, HHA was also not the acyl acceptor under the catalysis of CD1 (Fig. 33). This result suggested that CD1 did not use HHA or the other tested compounds as the acyl acceptors, but a potential hydrolysis reaction was detected (~27% *p*NPP was hydrolysed).

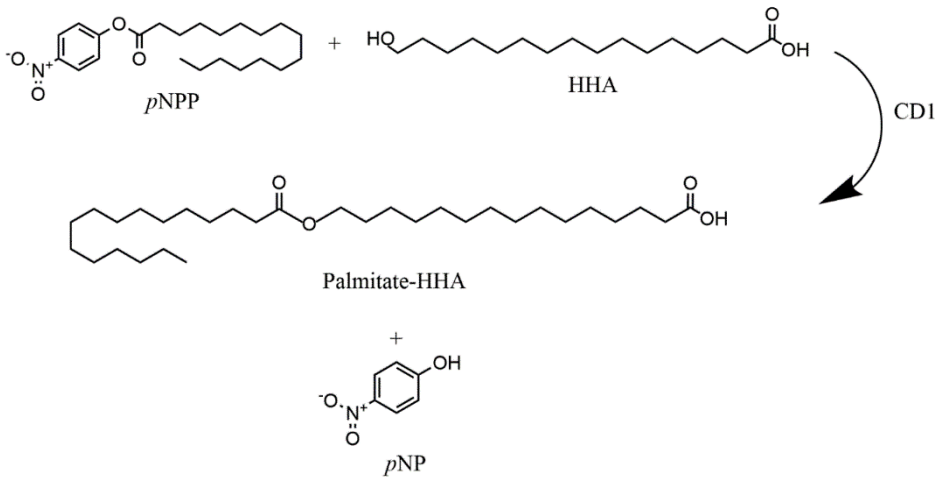

Figure 32. The proposed *p*NPP-to-HHA transacylation reaction mechanism. The palmitic acid residue in the *p*NPP (acyl donor) was hypothesized to be transacylated onto the terminal hydroxy group of the HHA (acyl acceptor), under the catalysis of

purified His_6-tagged CD1, producing a palmitate-HHA ester molecule and a free *p*NP molecule per reaction. *p*NPP: *p*-nitrophenyl palmitate; *p*NP: *p*-nitrophenol.

Isopropanol and propanol were also assayed as acyl acceptors, since their free hydroxy groups might have enabled them to be acyl acceptors. The CD1 activity with these two compounds was not significantly different from with water only ($P > 0.05$) (Fig. 33), so they were also not substrates of CD1.

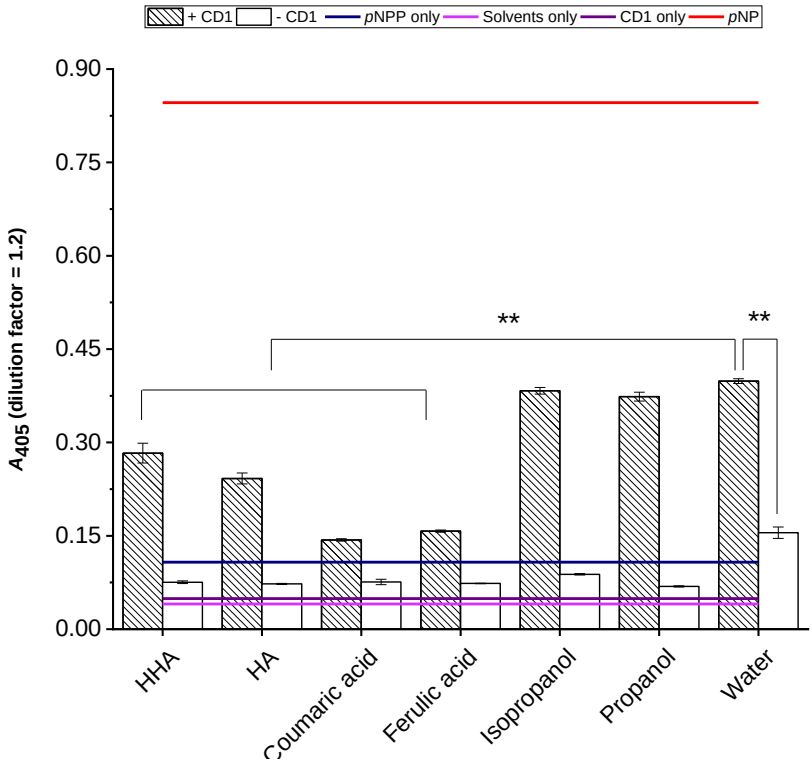

Figure 33. The CD1 *in-vitro* activity on *p*NPP with various acyl acceptors (cutin components). The artificial acyl donor, *p*NPP (final conc. = 5 mM) was incubated together with potential acceptors (natural cutin components and alcohols; final conc. = 0.1% w/v) with or without the purified His_6-tagged CD1 (1 µg) in 100 µl pH 6.0 buffer at 25°C for 3 days. The CD1 activity was illustrated by quantifying one of the products, *p*NP by A_{405} at pH 7.15±0.02 (dilution factor = 1.2). The actual CD1 activity was calculated as follows: reaction mixture A_{405} – the sum of (*p*NPP-only A_{405} and CD1-only A_{405}). The solvents-only A_{405} provided a blank, and the *p*NP A_{405} provided a reference if the *p*NPP was completely hydrolysed. *p*NPP: 0.5 mM *p*-nitrophenyl palmitate; *p*NP: 0.5 mM *p*-nitrophenol. Bar indicate standard errors (n=3). **: $P < 0.01$.

The observed potential ester (*p*NPP) hydrolysis activity of CD1 was further validated by comparing activities of the purified His_6-tagged CD1 with the same amount of proteins (extracted and eluted from the same Co^{2+} column as the CD1; E3 and E4 were used) from WT tobacco leaves. Unlike CD1, which hydrolysed ~18% of the *p*NPP in this experiment, the same amount of the WT proteins (measured by A_{280}) did not have any ester hydrolysis activity ($P_{(+\text{ WT protein vs. } -\text{ WT protein})} > 0.05$), not even with the 10 times more concentrated WT proteins (Fig. 34).

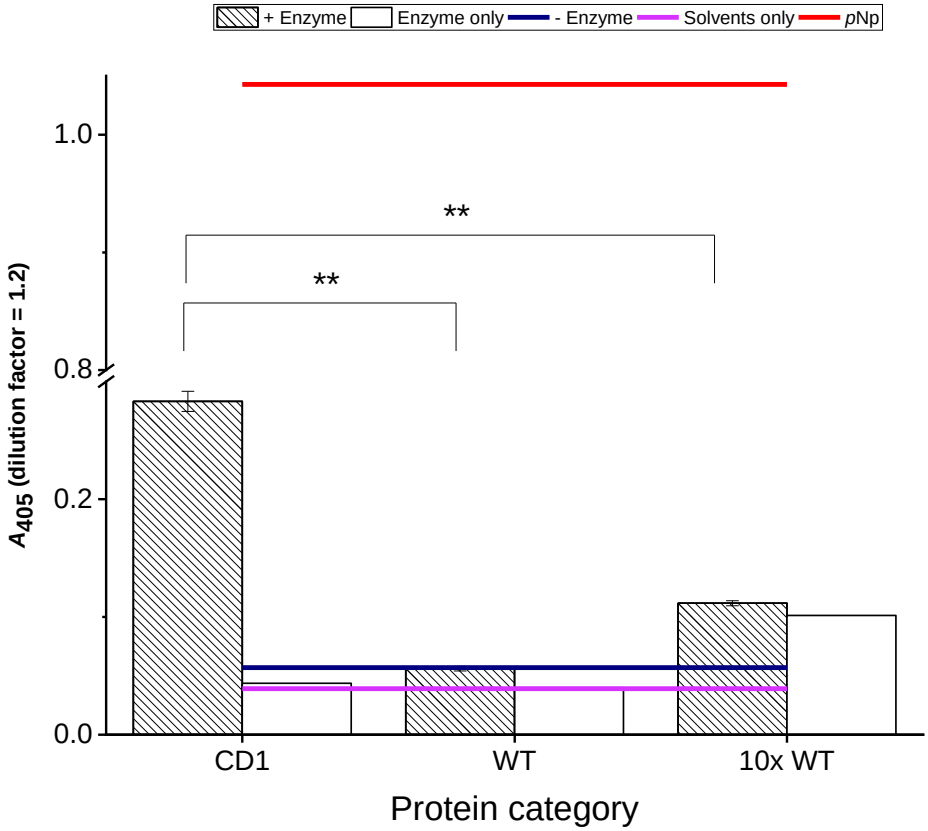

Figure 34. CD1 vs. WT proteins compared for their *p*NPP hydrolysis activity *in vitro*. Experimental details were as in figure 31, except native proteins from WT *N. benthamiana* leaves (1 or 10 µg; obtained by pooling the 3rd and 4th eluent from Co^{2+} column) were also assayed with His_6-tagged CD1 (1 µg) as a control. Any enzyme-catalysed hydrolysis activity was calculated as follows: reaction mixture A_{405} – the sum of [- Enzyme (*p*NPP-only) A_{405} and enzyme-only A_{405}). The solvents-only A_{405} provided a blank, and the *p*NP A_{405} provided a reference as figure 31. *p*NPP: 0.5 mM

p-nitrophenyl palmitate; *p*NP: 0.5 mM *p*-nitrophenol. Bars indicate standard errors (*n*=8). **: P < 0.01.

Assay His_6-tagged CD1's transacylase activity radio-chemically

The purified His_6-tagged CD1 was also incubated with prepared pea epicotyl epidermis (no active endogenous enzymes; see Chapter 2), which acted as the acyl donor, and [^{3}H]HHA was the acyl acceptor as in most other experiments. Consistent with the *in-situ* and *in-vitro* spectrophotometry assays, CD1 did not catalyse the [^{3}H]HHA incorporation, as shown by the negligible difference between the samples with and without CD1 (Fig. 35). The same results were reproducibly observed in two other independent experiments (Table 9).

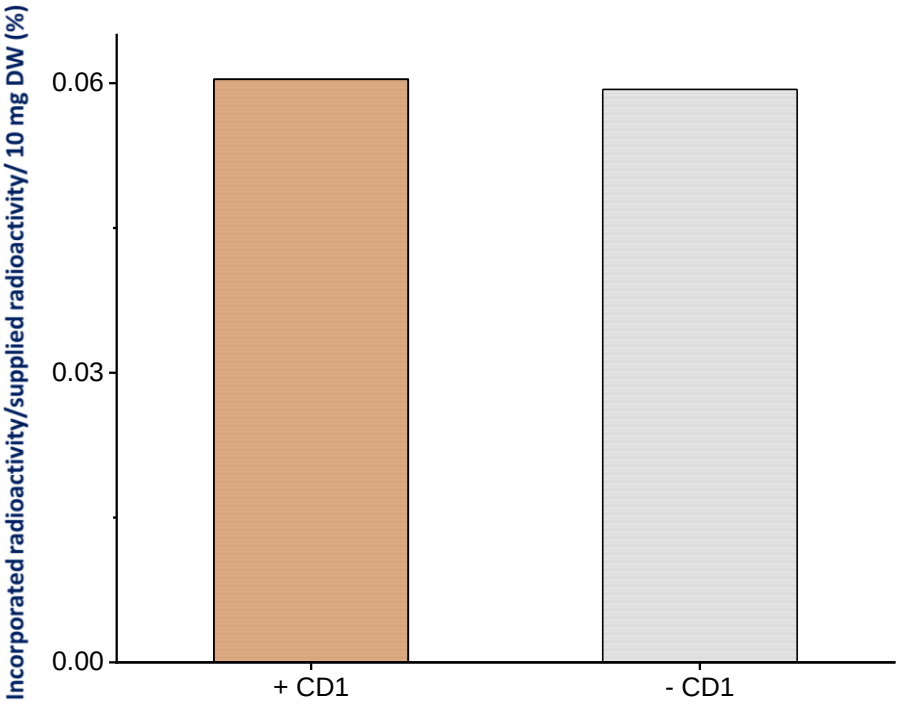

Figure 35. CD1 shows negligible cutin-to-[^{3}H]HHA transacylase activity *in vitro*. The prepared pea epicotyl epidermis (10 mg; acyl donor) without active endogenous enzymes was incubated with 1.1 kBq exogenous [^{3}H]HHA (acyl acceptor) with or

without CD1 (1 µg) in 300 µl pH 5.5 buffer at room temperature for 1 day. The incorporated radioactivity ratio (%) illustrates the CD1's cutin-to-[^{3}H]HHA transacylase activity. No bars (*n*=1).

A value of 0.1% total incorporated radioactivity/10 mg epidermis/supplied radioactivity corresponds to an absolute incorporation of 20 cpm/10 mg epidermis.

Table 9. CD1 shows negligible cutin-to-[^{3}H]HHA transacylase activity in three *in-vitro* experiments.

Acyl donor	Acyl acceptor	+ CD1 incorporated ^{3}H of the supplied ^{3}H ratio (%)	- CD1 incorporated ^{3}H of the supplied ^{3}H ratio (%)
Pea epicotyl cutin	[^{3}H]HHA	0.02% (*n*=1)	0.01% (*n*=1)
Pea epicotyl cutin	[^{3}H]HHA	0.1 % (*n*=1)	0.13% (*n*=1)
Pea epicotyl cutin	[^{3}H]HHA	0.06% (*n*=1)	0.06% (*n*=1)

All the results clearly indicated that CD1 is not the cutin-to-HHA transacylase we observed, which requires to be identified in the future. The ester hydrolysis activity was also reported by Yeats *et al*. (2014), but the cutin precursor, 2-MHG was used, instead of the *p*NPP here.

3.5 Age effect on cutin-to-HHA transacylase activity

In the cutin-to-HHA *in-situ* assays above, I used young, rapidly expanding epidermis, such as from the 7-day pea epicotyls. However, screening more developmental stages might provide a hint for the newly discovered cutin-to-HHA transacylase's physiological function.

3.5.1 Cutin-to-HHA transacylase activity through tomato fruit development

The whole developmental progress of cv. Ailsa Craig tomato fruit epidermis was assayed with [^{3}H]HHA as the acyl acceptor *in situ*. The cutin-to-HHA transacylase activity peaked on 14 DAA (Fig. 36), and then gradually went down, indicating that tomato fruit mainly has it at young, rapidly expanding stages. Moreover, this age was consistent with the peak of CD1 protein (15 DAA; Yeats *et al*., 2012). This correlation might indicate that even though the cutin-to-HHA transacylase was not CD1, they may share the same promoter, providing additional information for future identification. CMNaOH hydrolysis was not undertaken because the incorporation ratio of ^{3}H was very low; and the possible reason has been discussed in the '***Optimization***' section.

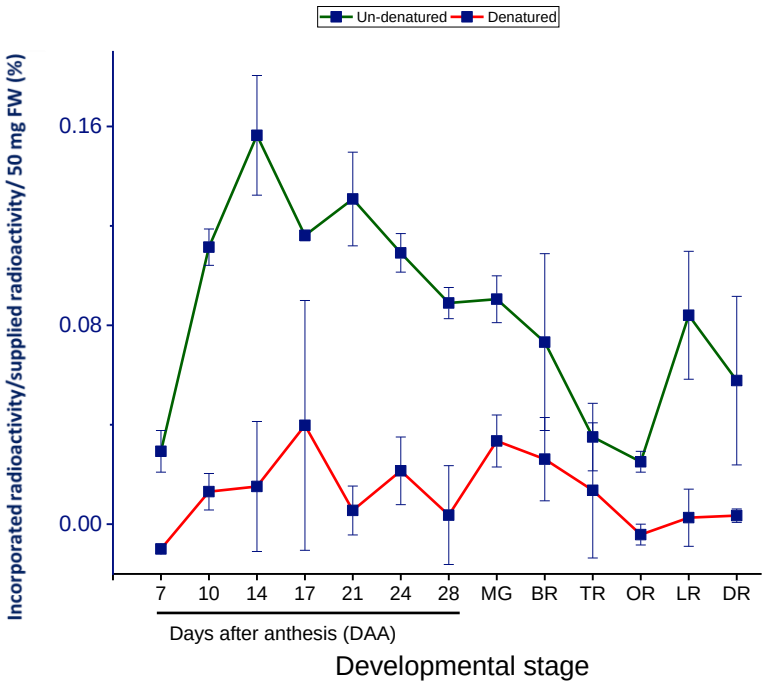

Figure 36. Effects of tomato fruit development on the putative cutin-to-[^{3}H]HHA transacylase activity *in situ*. Tomato (cv. Ailsa Craig) fruit epidermis samples (50 mg; acyl donor) with or without active endogenous enzymes were incubated with 0.26 kBq exogenous [^{3}H]HHA (acyl acceptor) in 300 µl pH 5.5 buffer at room temperature for 1 day. The CMNaOH-releasable radioactivity ratio

(%) illustrates the effects of development on the endogenous cutin-to-[^{3}H]HHA transacylase activity. MG: mature green (growth stopped). BR: breaker (10% colour change). TR: turner (30% colour change). OR: orange. LR: light red. DR: deep red. Bars indicate range (*n*=2).

A value of 0.1% total incorporated radioactivity/50 mg epidermis/supplied radioactivity corresponds to an absolute incorporation of 5 cpm/50 mg epidermis.

3.5.2 Cutin-to-HHA transacylase activity through ice plant leaf expansion

The same trend was also observed in ice plant leaf adaxial epidermis: the transacylase activity decreased with leaf expansion, evidenced by 10–30% higher ($P > 0.05$) ^{3}H incorporation in the un-denatured epidermis from smaller leaves than in the bigger leaves' epidermis, and the quantity of cutin-bonded ^{3}H incorporated decreased linearly with age (Fig. 37a). In another comparable experiment, young, rapidly expanding ice plant leaves' adaxial epidermis incorporated >2-fold more ^{3}H enzymically than the fully expanded leaves' epidermis did ($P < 0.01$) (Fig. 37b).

The un-denatured epidermis samples produced significantly more CMNaOH-releasable ^{3}H than the denatured control in both experiments (Fig. 37), indicating that the incorporation was enzymic.

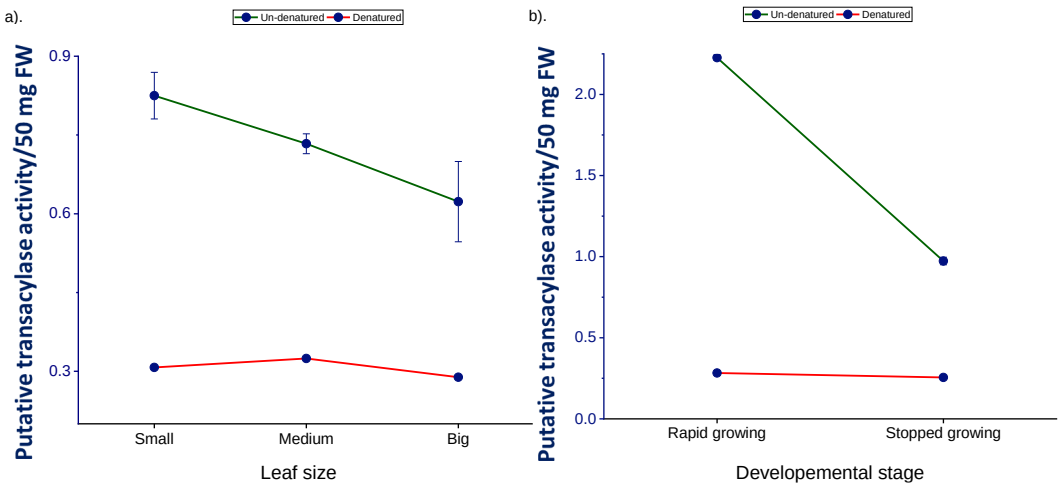

Figure 37. Effects of ice plant leaf expansion on the putative cutin-to-[^{3}H]HHA transacylase activity *in situ*. (a). Epidermis (50 mg; acyl donor) from different sizes of expanding ice plant leaves was compared by incubating with 0.67 kBq exogenous [^{3}H]HHA (acyl acceptor) in 300 µl pH 5.5 buffer at room temperature for 1 day. (b). Experimental details were as in (a), except epidermis samples from expansion-ceased leaves were assayed as well as the rapidly-expanding samples by incubating with 0.14 kBq exogenous [^{3}H]HHA (acyl acceptor). The CMNaOH-releasable radioactivity ratio (%) illustrates the effects of development on the endogenous cutin-to-[^{3}H]HHA transacylase activity. Small: 3–5 cm lamina length; medium: 5–8 cm lamina length; big: 12 cm lamina length. Bars indicate standard errors (*n*=3) for the un-denatured group, no bars for the denatured control (*n*=1).

A value of 1% CMNaOH-releasable radioactivity/50 mg epidermis/supplied radioactivity corresponds to an absolute incorporation of 142 cpm/50 mg epidermis in (a), and 29 cpm/50 mg epidermis in (b).

3.5.3 Cutin-to-HHA transacylase activity during pea epicotyl elongation

The same experimental procedure was also applied to pea epicotyl epidermis, however, the “decreasing with age” phenomenon was not observed (Fig. 38). There was no significant difference of the enzymically incorporated ^{3}H quantity between 4, 7 and 10 days after sowing (DAS) ($P > 0.05$), even though the epicotyl length at 4 DAS was ~5 times shorter than at the older ages (i.e. ~3 cm vs. ~16 cm).

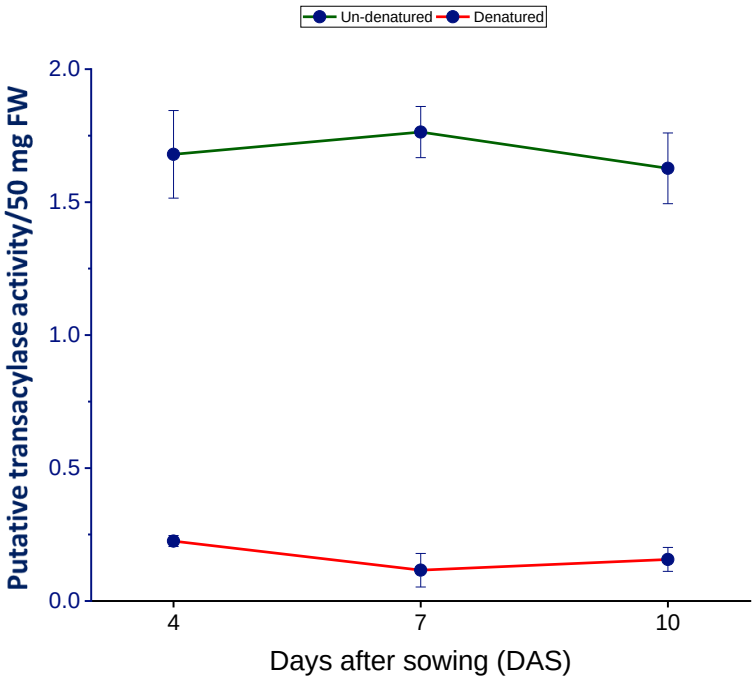

Figure 38. Effects of pea epicotyl elongation on the putative cutin-to-[^{3}H]HHA transacylase activity *in situ*. Epidermis (50 mg, acyl donor) from different lengths (4-, 7- and 10-DAS) of the expanding pea epicotyl with or without active endogenous enzymes were incubated with 0.74 kBq exogenous [^{3}H]HHA (acyl acceptor) under the standardised conditions as in figure 7. The CMNaOH-releasable radioactivity ratio (%) illustrates the effects of development on the endogenous cutin-to-[^{3}H]HHA transacylase activity. Bars indicate standard errors (*n*=3).

A value of 1% CMNaOH-releasable radioactivity/50 mg epidermis/supplied radioactivity corresponds to an absolute incorporation of 140 cpm/50 mg epidermis.

This inconsistency between pea epicotyl and other two plants might be because the pea epicotyl was still in rapid growing stages at 10-DAS (maximum length: 45 cm+; https://www.simplyseed.co.uk/pea-seeds/meteor.html), and therefore the putative transacylase activity was not decreased. In contrast, the whole developmental progress was screened for other two models, allowing us to have a good comparison between ages.

In conclusion, the results above together with the pH optimum range indicated that the cutin-to-HHA transacylase activity may be involved in cell

expansion as we hypothesized (i.e. loosening cutin matrix to allow expansion).

3.6 Effect of environmental stresses on cutin-to-HHA transacylase activity

Besides age, studying how the cutin-to-HHA transacylase activity responds to environmental stresses may also provide background knowledge for its physiological functions.

3.6.1 Effects of light on the cutin-to-HHA transacylase activity *in situ*

All the pea epicotyl epidermis used in assays above were sampled from dark-grown (etiolated) pea seedlings, whose growth condition was different from in light-grown (de-etiolated) seedlings. Moreover, the cutin load is reported to be higher in *Hedera helix* leaves under sunshine (Skoss, 1955), suggesting that cutin metabolism, at least the synthesis, was affected by light.

To investigate whether any artefact was imposed by the artificially dark environment on the newly discovered cutin re-modelling transacylase activity, the same age of continuously dark- and light (resource: bulb)-grown pea epicotyl epidermis was compared *in situ*. Fig. 39 shows no significant difference between the two groups at any time point ($P > 0.05$): the activity was 1.1- and 1.3-fold higher in the ‘dark’ samples than in the ‘light’ ones, indicating that the cutin-to-HHA transacylase activity was little affected by light. Furthermore, the data showed that the growth rate of pea epicotyls did not correlate with the transacylase activity: the light-grown pea was only 4 cm long after 7 days, whereas the dark group was 16 cm.

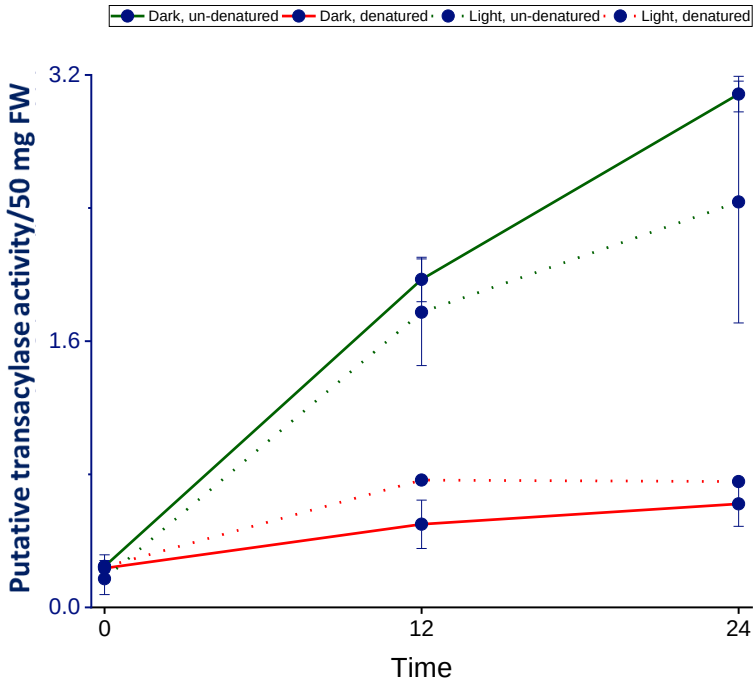

Figure 39. Effects of light on the putative cutin-to-[^{3}H]HHA transacylase activity in pea epicotyl epidermis *in situ*. Experimental details were as in figure 36, except epidermis samples from pea epicotyl, which grown in different light conditions were incubated with 0.1 kBq exogenous [^{3}H]HHA (acyl acceptor). The CMNaOH-releasable radioactivity ratio (%) shows the effects of light on the endogenous cutin-to-[^{3}H]HHA transacylase activity. Dark: grew in continuous darkness for 7 days at 25°C; light: grew in continuous bulb light (intensity: µmol/m^2/s) for 7 days at 25°C. Bars indicate range (*n*=2); except that no bars for the 'light, denatured' samples (*n*=1).

A value of 1% CMNaOH-releasable radioactivity/50 mg epidermis/supplied radioactivity corresponds to an absolute incorporation of 18 cpm/50 mg epidermis.

Overall, this result not only showed that dark-grown pea is a validated model for this project, but also suggested that growth rate did not affect the cutin-to-[^{3}H]HHA transacylation reaction *in situ*. Noticeably, the *in-situ* observation is determined by both substrate (cutin) and enzyme (the putative cutin-to-HHA transacylase), and therefore the non-affected cutin-to-[^{3}H]HHA transacylation products here may be a synergic result of increased cutin availability and decreased cutin-to-HHA transacylase activity, and *vice versa*. Thus, to obtain

a more detailed overview of the correlation between growth rate and the cutin-to-HHA transacylase activity, more approaches should be employed (discussed in Chapter 6).

3.6.2 Effects of humidity on the cutin-to-HHA transacylase activity *in situ*

Environmental humidity usually affects plant water loss. For example, serving to prevent water loss, epidermal wax load tends to increase in response to low humidity (Baker, 1974). Even though independent studies suggested that cutin does not play an important role in controlling water permeability (Schönherr and Riederer, 1989; Isaacson *et al*., 2009), suggesting that cutin would not be affected by humidity, we attempted to study whether the newly discovered cutin-to-HHA transacylase activity responds to humidity change.

To investigate this question, I grew pea seedlings in continuous light for 7 days at 25°C either isolated in a plastic bag (humidity: 80–90%) or exposed to the normal Edinburgh atmosphere (humidity: 40–45%).

In-situ (acyl acceptor: [^{3}H]HHA) results showed no significant difference in enzymically-incorporated ^{3}H quantities between the normal-humidity plants and the humid ones ($P > 0.05$): the ‘normal’ group cutin incorporated 1.2-fold higher ^{3}H than the ‘humid’ group (Fig. 40). This might support biochemically the biophysical point of view that cutin is not essential in response to humidity, but in future studies we cannot exclude the possibility that cutin morphology may be important in regulating water permeability: e.g. cutin’s 3-D structure may affect the shape of the wax layer, resulting in affecting water permeation physically (reviewed by Fich *et al*. 2016).

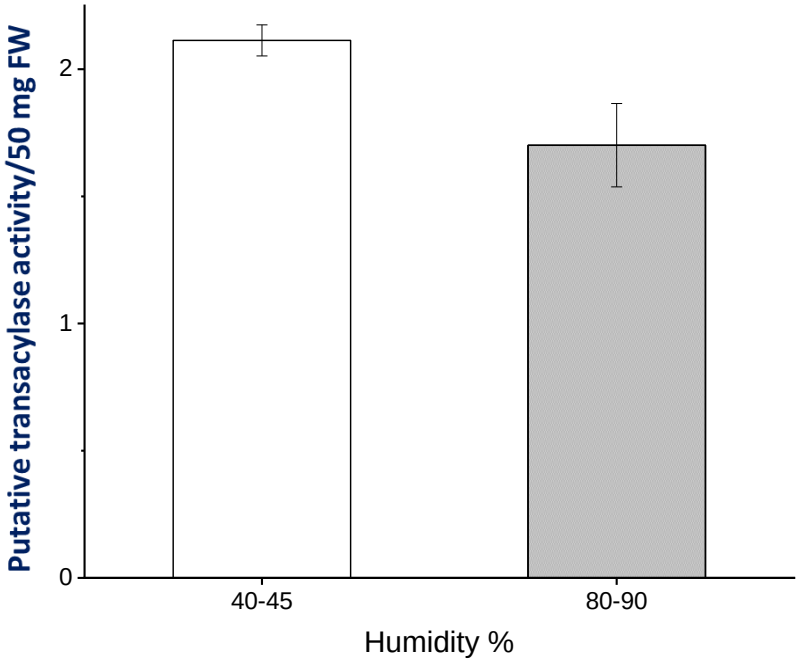

Figure 40. Effects of humidity on the putative cutin-to-[^{3}H]HHA transacylase activity in pea epicotyl epidermis *in situ*. Experimental details were as in figure 36, except epidermis samples from 7-day dark-grown pea epicotyl under high- (80–90%) and normal- (40–45%) humidity conditions were incubated with 0.12 kBq exogenous [^{3}H]HHA (acyl acceptor). The CMNaOH-releasable radioactivity ratio (%) illustrates the effects of humidity on the endogenous cutin-to-[^{3}H]HHA transacylase activity. Bars indicate standard errors (*n*=3).

A value of 1% CMNaOH-releasable radioactivity/50 mg epidermis/supplied radioactivity corresponds to an absolute incorporation of 23 cpm/50 mg epidermis.

Noticeably, the 'humid' samples released much less ^{3}H in toluene and chloroform mixtures than the 'normal' one did ($P < 0.01$) (Fig. 41), which might be because the hydrophobic [^{3}H]HHA metabolite was a wax component, and its formation was inhibited by high humidity (Baker, 1974).

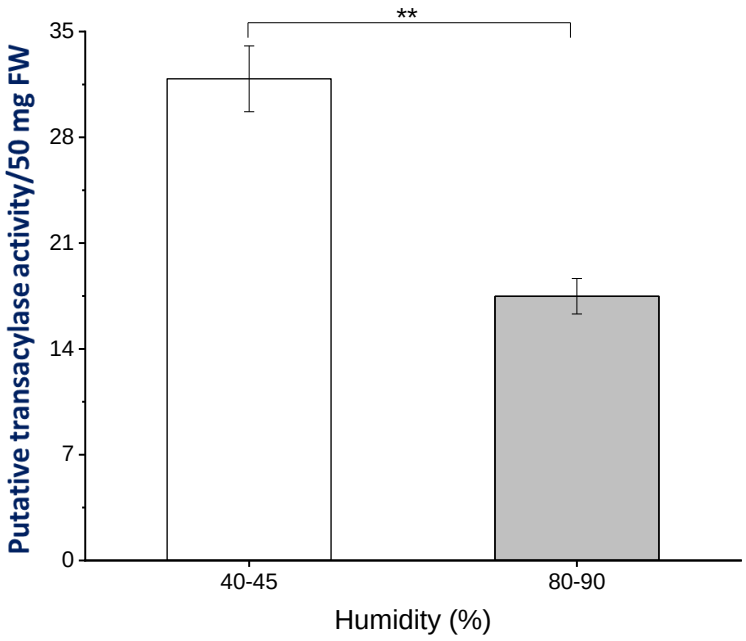

Figure 41. Effects of humidity on the production of the proposed wax components in pea epicotyl epidermis i*n situ*. Experimental details were as in figure 38, except that toluene-, CM (2/1)- and CMW (10/10/3)-extractable radioactivity was scintillation counted. The neutral hydrophobic solvents-releasable radioactivity ratio (%) was used to illustrate the effects of humidity one of the [^{3}H]HHA metabolic mechanism. Bars indicate standard errors (*n*=3). **: P < 0.01.

A value of 10% neutral hydrophobic solvents-releasable radioactivity/50 mg epidermis/supplied radioactivity corresponds to an absolute incorporation of 230 cpm/50 mg epidermis.

No dry condition was tested due to technical limitations, but it will be considered by Prof. Stephen C. Fry's lab in future.

3.6.3 Effects of pre-growth temperature on the cutin-to-HHA transacylase activity *in situ*

Temperature is another important environmental factor. Differently from humidity, cutin responds to it. For example, cutin load increased at lower temperatures in tree tobacco (*Nicotiana glauca*) leaves (Skoss, 1955),

suggesting that the cutin re-modelling mechanism, cutin-to-[^{3}H]HHA transacylation reaction might also be affected by temperature changes.

I germinated peas at 25°C in dark for 4 days, then harvested some and transferred the rest to 4°C for further growth. Epicotyl epidermis was isolated as above and assayed for cutin-to-HHA transacylase activity under the standardised conditions *in situ*. The factors of age and growth rate can probably be neglected, because the data above suggested they do not affect the transacylase activity *in situ* (Fig. 38 and 37).

The rate of ^{3}H incorporation into CMNaOH-releasable ^{3}H decreased with the duration the plants had been held at 4°C (Fig. 42), indicating that the transacylase activity was not involved in response to cold stress, because otherwise it would have been promoted.

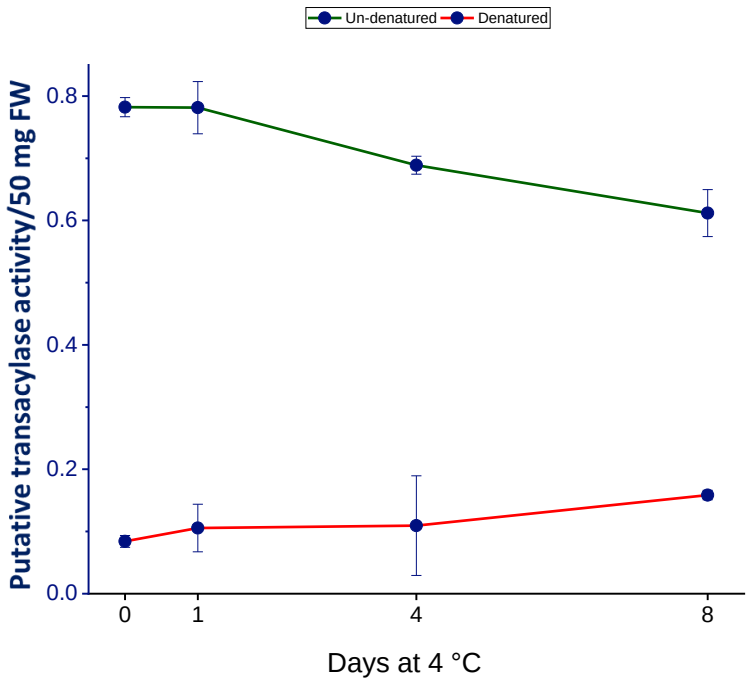

Figure 42. Effects of pre-growth temperature on the putative cutin-to-[^{3}H]HHA transacylase activity in pea epicotyl epidermis *in situ*. Experimental details were as in figure 36, except epidermis samples from dark-grown pea epicotyls exposed to

4°C for different durations were incubated with 1.2 kBq exogenous [^{3}H]HHA (acyl acceptor). The CMNaOH-releasable radioactivity ratio (%) illustrates the effects of temperature on the endogenous cutin-to-[^{3}H]HHA transacylase activity. Bars indicate standard errors for the un-denatured group (*n*=4). Bars also indicated range for the denatured control (*n*=2).

A value of 1% CMNaOH-releasable radioactivity/50 mg epidermis/supplied radioactivity corresponds to an absolute incorporation of 220 cpm/50 mg epidermis.

Moreover, the amount of ^{3}H produced into toluene- and CMW-releasable radioactivity was decreased after 4 days at 4°C ($P < 0.01$) (Fig. 43). This may support the idea that the toluene- and CMW-solubilized [^{3}H]HHA metabolite was incorporated into wax because it is consistent with the report that the wax load is decreased during growth at low temperature (Skoss, 1955). However, the opposite observations were also reported: wax production in leaves of Brussels sprout (*Brassica oleracea* var. gemmifera) is promoted at lower temperatures (Baker, 1974), indicating that different species reacts differently, and my hypothesis requires further testing.

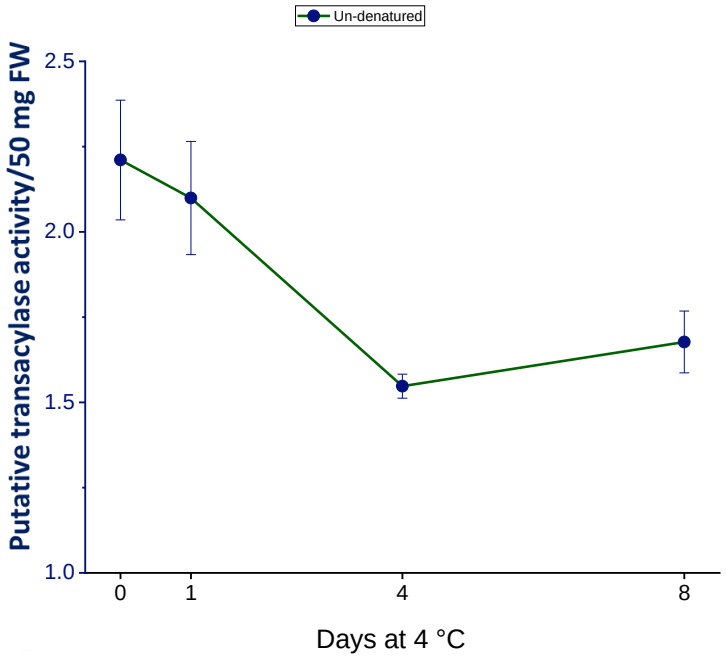

Figure 43. Effects of pre-growth temperature on the production of the proposed wax components in pea epicotyl epidermis *in situ*. Experimental details were as in figure 40, except that toluene- and CMW (10/10/3)-extractable radioactivity was scintillation counted. The neutral hydrophobic solvents-releasable radioactivity ratio (%) was used to illustrate effects of temperature on one of the endogenous [^{3}H]HHA metabolic mechanism. Bars indicate standard errors (*n*=4).

A value of 1% neutral hydrophobic solvents-releasable radioactivity/50 mg epidermis/supplied radioactivity corresponds to an absolute incorporation of 220 cpm/50 mg epidermis.

In summary, the cutin-to-HHA transacylase activity was not altered in response to cold, and the [^{3}H]HHA metabolite extractable in neutral hydrophobic solvents (toluene etc.) was heavily decreased by cold.

Elevated temperatures were not tested due to the technical limitations (e.g. mould development). However, a recent study of pea adaxial leaf cuticle by using attenuated total reflection-Fourier transform infrared spectroscopy

(ATR-FTIR) to quantify ester bonds reported that cutin load was decreased by high temperature (Liu *et al*., 2019).

Discussion

3.7 The discovery of the novel cutin-to-HHA transacylase activity

We hypothesized that cutin (acyl donor) was transiently cut during rapid cell expansion, and then re-joined to another cutin (acyl acceptor) to form an intact matrix again after incremental cell expansion. This reaction was looked for by using [^{3}H]HHA as the model of 'another cutin' to be the acyl acceptor, and verified by analysing the enzymic product via TLC.

Pea epicotyl epidermis was very accessible and incorporated the highest amount of radioactivity among models I tested (i.e. pea, ice plant leaf and tomato fruit epidermis). As the default growing conditions of the standard plant model, dark did not impose a dramatic artefact on the *in-situ* cutin-to-HHA transacylase activity (Fig. 39), and dark-grown peas were used in most experiments.

The reproducibly observed dramatic contrast between the ^{3}H incorporation from [^{3}H]HHA in un-denatured epidermis samples and the denatured controls (*in-* and *ex-situ*) indicated that this incorporation was catalysed by an extracellular enzyme, which was stably associated with the epidermis because it was not lost by the cold-buffer wash (*in-situ*) (Fig. 13), but was extracted out by homogenizing epidermis with Triton X-100 and sands (*ex-situ*) (Fig. 20).

The importance of the –OH group of [^{3}H]HHA was demonstrated by the data showing that [^{14}C]HA (Fig. 17), which does not have –OH group cannot be the substrate.

Enzymic and chemical degradation techniques were employed to look for the *in-situ* cutin-to-HHA transacylase product. Acidified methanol removed the majority of un-bonded [^{3}H]HHA and its metabolites (Fig. 24), evidenced by the scintillation counting (quantification) (Fig. 25) and the TLC analysis (qualitative analysis) (Fig. 26a). The following neutral hydrophobic solvents, especially toluene and CM, exclusively removed the most hydrophobic metabolite (Fig. 26a), which had probably been incorporated into wax.

Enzymic digestions by lipase and cutinase require further optimization to attack the cutin–[^{3}H]HHA conjugate (Fig. 28). A general chemical method, CMNaOH (~0.5 M NaOH) hydrolysis, successfully detected the conjugate, because ester bonds are alkali labile. The CMNaOH-releasable radioactivity was usually ~1–2% of the supplied radioactivity in un-denatured pea epicotyl epidermis after a 24-h transacylase reaction (Fig. 26a), and it was identified as [^{3}H]HHA dominantly (~36%, including the presumed oxidation product, [^{3}H]OHA, ~10% inclusive) without a modification and an unidentified metabolite (~10%) (Fig. 29). These results were reproducibly observed in independent experiments. Thus, at least ~0.72% of the supplied [^{3}H]HHA (excluding the oxidized [^{3}H]HHA) became ester-bonded to epidermis.

Since the possibility of other epidermal components (e.g. wax oligoesters) being the acyl donors was not very likely and/or not detectable, cutin was the

most probable component which can form ester bonds with [^{3}H]HHA. Thus, we can conclude that we have observed the cutin-to-HHA transacylase activity with clear experimental evidence for the first time.

Nevertheless, a low-impact interference by other substrates cannot be excluded: even though there is no evidence to show that free un-bonded [^{3}H]HHA has been methyl esterified after the addition of MFW (i.e. otherwise it will be observed in toluene and chloroform-mixture extractions from the denatured control; Fig. 26b), it is a possibility that we cannot exclude. In fact, the methyl esterified [^{3}H]HHA may be transacylated onto cutin chemically because of its activated acyl group, and on the other hand, the cutin motif in the cutin–[^{3}H]HHA conjugate may also be transacylated onto methanol in MFW, resulting in releasing the enzymic incorporated [^{3}H]HHA back into supernatant. Thus, the observed [^{3}H]HHA released by CMNaOH from denatured epidermis samples might be due to this chemical transacylation; the observed cutin–[^{3}H]HHA transacylation product in un-denatured epidermis might be a result of the two opposite chemical transacylation reactions. Fortunately, the majority was still the pure transacylase products, because the quantity was much higher in un-denatured epidermis samples than the denatured control (Fig. 25 and 27).

It was difficult to identify the [^{3}H]HHA metabolites shown on TLCs, but it was likely that the co-released compound (near origin) (Fig. 29) with [^{3}H]HHA in CMNaOH hydrolysis was also a hydroxy fatty acid (acyl acceptor), and the chance to be the acyl donor was low (i.e. [^{3}H]HHA's carboxy group cannot be activated enzymically, because the compounds, such as acetyl-CoA which

are required for such reaction had been removed by the pre-incubation wash). Furthermore, there was also no di-hydroxy fatty acid formed based on our preliminary experiments (i.e. the R_F of di-HHA was ≤ 50% that of HHA) (Appendix 6). Nevertheless, we cannot exclude the possibility that hydroxylation reactions happened together with other [^{3}H]HHA modifying reactions.

There are no known apoplastic fatty-acid-metabolising enzymes, but a set of cutin-related genes, encoding protoplasmic fatty acids modification proteins were found by transcriptomics (Panikashvili *et al.*, 2010), such as CER4/FAR3 (Eceriferum 4/Fatty acid reductase 3), which reduces fatty aldehydes to alcohols (Jenks *et al.*, 1995; Rowland *et al*., 2006); and MAH1 (mid-chain alkane hydroxylase), which adds hydroxy groups to the middle of an alkane chain (Greer *et al*., 2007). Even though CER4 and MAH1 are both NADPH-dependent (Rowland *et al*., 2006; Greer *et al*., 2007), but it is possible that they have isozymes in apoplast, and they may use different redox substrates. These isozymes may work synergistically to produce the [^{3}H]HHA metabolites.

3.8 Preliminary knowledge of the protein responsible for the cutin-to-HHA transacylase activity

The protein responsible for cutin-to-HHA transacylase activity was not identified in this project, since *in-situ* and *in-vitro* assays clearly showed that CD1, as the only well-studied cutin transacylase, did not catalyse the cutin-to-HHA transacylation reaction (Fig. 30, 31, 33; Table 9). However, the cutin-

to-HHA transacylase activity peaked at the same developmental stage (Fig. 36) as CD1 in tomato fruit epidermis (Yeats *et al*., 2012), suggesting that these two transacylases may be co-regulated. Another consistent piece of evidence was that the pH optima of CD1 and the newly discovered transacylase were very close, pH 5.0 and 5.5 respectively (Fig. 13 and 8; Yeats *et al*., 2014), also suggesting that these two proteins emerge at the same developmental stage. These findings may provide useful information for future cutin-to-HHA transacylase transcriptomic studies.

Ex-situ assays provided additional information for the future cutin-to-HHA identification and characterisation: (1) its 3-D structure did not seem to allow disulphide bond formation (Fig. 19 and 18), unlike CD1, which was predicted by bioinformatics program (DIANA) to have disulphide bonds (Bakan and Marion, 2017); (2) its activity and extraction efficiency were slightly improved by adding Ca^{2+} (Fig. 22 and 21). However, the Ca^{2+} may not be a co-factor, because the transacylase was active without Ca^{2+}, and EDTA did not reduce activity significantly (Fig. 22 and 21). Similarly, the functionally similar xyloglucan re-modelling enzyme activity, XET is also higher with Ca^{2+} (Fry *et al*., 1992), but no co-factor information was given yet (Saladié *et al*., 2006; Maris *et al*., 2009; Maris *et al*., 2011). Noticeably, it has been reported that CaCl solubilises ionically cell-wall-bound proteins better than other salts in *Arabidopsis* rosettes (Boudart *et al*., 2005), probably the cutin-to-HHA transacylase is also ionically bound with cell wall or cutin.

The proposed new enzyme's substrate specificity may be related to the correlation between the low amount of HHA in tomato fruit epidermal cutin

(~1.5–3% of total identified cutin, Kosma *et al*., 2010) and the low [^{3}H]HHA incorporation by tomato epidermis *in situ* (Fig. 36): the endogenous tomato transacylase possibly prefers this species' common endogenous cutin fatty acid residues as the acyl acceptors. Unfortunately, this hypothesis could not be tested in this project because the most common cutin fatty acid in in tomato fruit epidermis, diHHA was not successfully purified via HPLC (Appendix 6), and the cutin components of the pea epicotyl epidermis were not analysed. Another possible scenario is that the abundant cutin provides sufficient viscoelasticity for young tomato fruits to expand (España *et al*., 2014)., taking place the role of the putative transacylase activity.

3.9 Speculation as to cutin-to-HHA transacylase's physiological function

Consistent with our hypothesis that this transacylase activity was required for cell expansion, [^{3}H]HHA *in-situ* incorporation peaked at pH 5.5, which is within the physiological pH range of expanding cells' apoplast (reviewed by Cosgrove, 2005). However, the incorporation was not much less when pH was increased to values such as 7.5, especially in the pea epicotyl epidermis (Fig. 13 and 8). In addition, the activity was still quite high after the ice plant leaf stopped expansion, suggesting that this transacylase activity was not only required for cell expansion, but also played a role for other purposes, such as 'healing' a broken cutin chain after it has been broken by external physical forces. Another possible scenario is that the newly discovered transacylase is only required for cell expansion, but it is not degraded once growth has finished. However, CD1, which may share the same family

(GDSL) as the novel transacylase, is degraded after rapid expansion has finished (Yeats *et al.*, 2012). Thus, I propose that the novel cutin-to-HHA transacylase activity after cell expansion may be required for a specific mechanism.

The 'cutin loosening' function of the cutin-to-HHA transacylase was further hinted by comparing its characteristics with similar, but well-known enzymes. For example, the most functionally comparable enzyme activity to the newly discovered cutin transacylase is XET, extracted from rapidly growing pea internodes, which has been reported to be involved in loosening cell wall during cell expansion, and it also prefers pH 5.5 (Fry *et al*., 1992; Hetherington and Fry, 1993). This putative 'loosening' function of the cutin transacylase was further suggested by the fact that its activity was higher in young, rapidly growing ice plant leaves and tomato fruit epidermis than at later developmental stages. However, a correlation between growth rate and the cutin-to-HHA transacylase activity was not observed *in situ* (Fig. 39), but we cannot exclude that it might be found *in vivo* (more in Chapter 6).

Cutin itself was suggested not to be critical in controlling water loss in response to humidity, except that the interactions between cutin flavonoid residues were proposed to obstruct water permeation (Luque *et al*., 1995). Consistently, the cutin re-modelling, cutin-to-HHA transacylation reaction was only decreased slightly by high humidity *in situ* (Fig. 40). Temperature decrease was reported to increase cutin load, but in this thesis, low temperature pre-growth slightly decreased the cutin-to-HHA transacylase activity (Fig. 42), suggesting that this transacylase was not essential in the

plant's response to cold. It also provided another piece of evidence that the cutin synthase and the cutin-to-HHA transacylase were two separate enzymes.

Taken together, this newly discovered transacylase activity was likely to be involved in re-modelling (e.g. loosening) cutin to accommodate cell expansion but may be not vital in reacting to humidity and temperature changes. These hypotheses can be answered by identifying the transacylase first, and then analysing its physiological functions *in planta*.

Conclusions

The reproducibly observed cutin-to-HHA transacylation reaction in different organs of different plants strongly indicated the transacylase's existence, which was then for the first time demonstrated by our product analysis. We can conclude that the hypothesized cutin-to-cutin transacylation reaction is very likely to occur in nature and may be involved in loosening cutin in parallel with cell wall re-modelling enzyme activities (e.g. XET activity) during rapid cell expansion, based on the pH optimum and correlations with plant development. However, this transacylase is not identified yet, the only solid conclusion is that it is not CD1, the known cutin synthase. Some of the most common environmental stresses, light, temperature and humidity, did not affect the transacylase activity dramatically *in situ*, and thus it may not be essential in the plant's response mechanisms to these stresses.

Future perspectives

Only one hydroxy fatty acid, [^{3}H]HHA, was tested to model cutin-to-cutin transacylation reactions in this project, so more hydroxy fatty acid species should be tested in the future, especially the most dominant one in tomato fruit cutin, di-[^{3}H]HHA. Moreover, a CD1-specific antibody would be more specific to detect the His_6-tagged CD1 than the anti-poly-His–HRP antibody.

In future, pea epicotyl epidermis cutin components could be identified and quantified by LC- and GC-MS; and the actual presence will be verified by e.g. TEM, even though it has been confirmed by previous studies (e.g. Rogers *et al*., 1994). The cutin-to-HHA transacylase could be identified via screening the activities of CD1 homologues in tomato fruit (e.g. *Solyc04g050730.2.1*, a gene expressing a GDSL enzyme with 76% similarity to CD1 polypeptide sequence) and *Arabidopsis* petals (e.g. *At5g33370*, a gene expressing a GDSL enzyme with 73% similarity to CD1 polypeptide sequence), and the correlation between plant cutin components and substrate specificity will be established. No genes have yet been annotated as possessing the cutin-to-HHA transacylase activity (April 2019).

Chapter 4. Cutin-to-oligosaccharide transacylation

Introduction

Putative interactions between cell wall polysaccharides and cutin have been reported from different angles. For example, polysaccharide was found in cuticle of different land plants via biochemical analysis (e.g. 15% dry weight of *Eucalyptus* leaf cuticle; 30–37% dry weight of cherry tomato fruit cuticle) (Domínguez *et al*., 2008; Guzmán *et al*., 2014) and microscopic observations (Jeffree 2006; reviewed by Fernández *et al.*, 2016). A partial hydrolysis of lime fruit cutin released a conjugate composed of a hydroxy fatty acid tetramer *O*-linked to the C-6 position of a hexose disaccharide, but the structure was unclear (Tian *et al*., 2008). Moreover, a co-regulation of cutin and polysaccharide biosynthesis has been suggested: alterations of primary cell wall quantity and morphology were observed in *SHINE3* (a proposed transcription factor of cutin synthase)-silenced tomato fruit epidermis (Shi *et al*., 2013).

Based on the cutin biosynthesis mechanism catalysed by cutin deficient 1 (CD1), we proposed that cutin could be linked to nearby cell wall polysaccharides via ester bonds, thereby reinforcing the epidermis mechanically despite dramatic cell expansion. This hypothesized mechanism is the same as the cutin-to-cutin bonding (i.e. a transient cut of cutin, followed by the reformation of ester bond; Chapter 3), except that the acyl acceptors are polysaccharides, all of which carry –OH groups. As mentioned in Chapter 1, methyl esterified galacturonan (reviewed by Wolf *et al*., 2009) has a

chance to be the acyl donor, because it contains activated acyl groups. Non-esterified galacturonic acid residues are less likely to be acyl donors, because the –OH of a free carboxy group (–COOH) is a poorer leaving group than the $–OCH_3$ of a methyl ester ($–COOCH_3$).

Cutin–polysaccharide hetero-polymers have been proposed for many years (reviewed by Fich *et al*., 2016), but no biochemical study has yet proved their existence. The transacylation mechanism is like the cutin-to-cutin transacylation one (Fig. 5), but the acyl acceptor is replaced with tritiated labelled oligosaccharides, to avoid artefacts [e.g. strong hydrogen bonds (H-bonds) between exogenous radio-labelled polysaccharides and endogenous cell wall polysaccharides in assays]. The radio-chemical technique was employed because the possible hetero-polymer may be in very low quantity, requiring a very sensitive monitoring technique.

All the ^{3}H-labelled oligo- and mono-saccharides I used lacked reducing ends (i.e. a free oxo group at one end, which acts as a reducing agent; Pratt and Cornely, 2013), to mimic the major part of a polysaccharide molecule, whose building blocks do not have free oxo groups since they are involved in glycosidic bonds (Fig. 44).

The default growth conditions for the most frequently used plant model, pea epicotyl, were in continuous dark at 25°C for 7 days as in Chapter 3. Experimental strategies were also similar to those in Chapter 3 (e.g. ~0.5 M NaOH in CMNaOH to hydrolyse ester bonds within the hydrophobic environment of cutin). Importantly, the radio-labelled xyloglucan oligomers

are also xyloglucan endotransglucosylase (XET) substrates (Fry *et al*., 1992). Thus, the transacylase product should be carefully distinguished from XET products; more details will be provided later in this chapter.

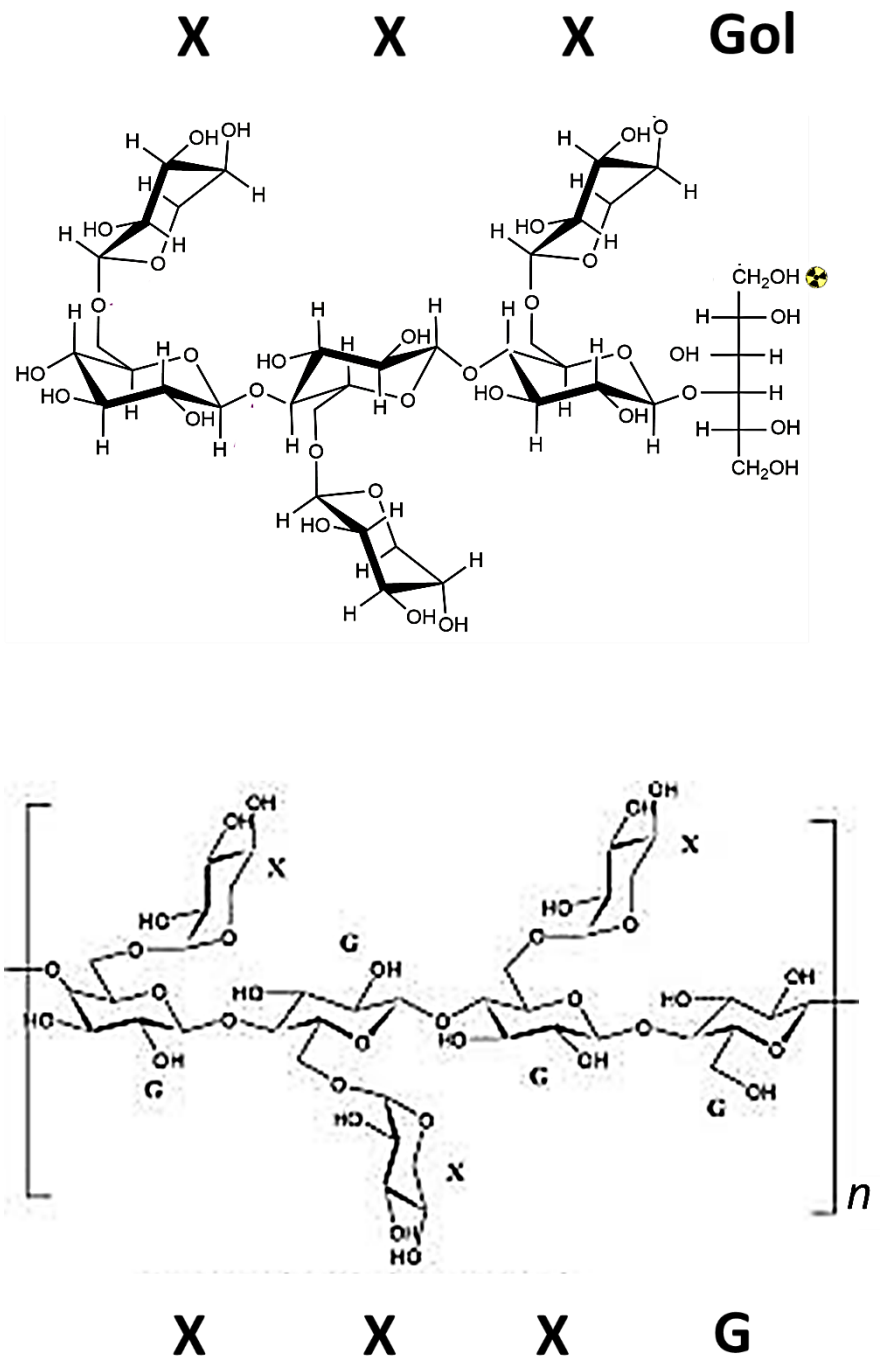

Figure 44. A structural illustration of [^{3}H]XXXGol structure. Glucose residues (hexose) are glycosidically linked to each other via β-1→4 bonds; and a xylose (pentose) is linked to three of them via α-1→6 glycosidic bonds to form a motif (α-D-xylopyranosyl-(1→6)-β-D-glucose), named X. The fourth glucose (from left to right,

G) is the last motif in this xyloglucan building block, and in most cases, it is attached to the next building block *in muro*, resulting in the great majority of the XXXG units lacking a free reducing end (adapted from Bhalekar *et al*., 2013). In the laboratory, we mimicked this situation by reducing the G of the heptasaccharide to glucitol (Gol), which does not have the oxo group at C-1 (XXXGol). The hydrogen atom at C-1 of Gol was radio-labelled, resulting in [^{3}H]XXXGol. [^{3}H]XXXGol and XXXG are assumed to be functionally the same so far as acceptor substrate function is concerned, as is the case when they act as XET acceptor substrates (Fry *et al*., 1992).

Results

4.1 Optimization of *in-situ* assays

I mainly used one of the most common radio-labelled dicot xyloglucan building blocks as the acyl acceptor, [^{3}H]XXXGol (Fig. 44), to optimize the *in-situ* transacylase assays. [^{3}H]XXXGol is a heptasaccharide, where X represents an α-D-xylopyranosyl-(1→6)-β-D-glucopyranosyl segment, and Gol is a D-glucitol unit (Fry *et al*., 1993) (Fig. 44). Pectic oligomers' acceptor abilities were also tested in comparison with the hemicellulosic [^{3}H]XXXGol.

The enzyme assay optimization experiments were designed to look for the best plant model, pH and pre-incubation conditions. Strategies were like those for the cutin-to-[^{3}H]HHA assays (Chapter 3). Furthermore, CMNaOH (~0.5 M NaOH) treatment here not only enabled us to test whether an ester bond had been formed, but also allowed us to distinguish between the activities of XET and the proposed transacylases, because the glycosidic bonds (β-D-glucopyranosyl-(1→4)-β-D-glucose) between endogenous polysaccharide and exogenous [^{3}H]XXXGol should be stable in this alkaline solution, especially since the end is non-reducing (reviewed by Glaus and Van Loon, 2008); and also the polysaccharide–[^{3}H]XXXGol conjugates were

predicted to be insoluble in the hydrophobic CMNaOH solution because of their high molecular weight and hydrophilicity.

4.1.1 The optimum pH of the putative cutin-to-oligosaccharide transacylase activity (*in situ*)

Effects of pH on the putative cutin-to-XXXGol transacylase activity

Pea epicotyl epidermis was obtained from dark-grown pea seedlings, selected because of the fast harvesting cycle and rich cutin (Rogers *et al*., 1994). We hypothesized that the cutin-to-polysaccharide transacylation reaction was required to adjust cutin mechanical strength during rapid growth, and therefore the optimal pH should be 4.5–6.0 (reviewed by Cosgrove, 2005).

However, the total ^{3}H incorporated and incorporated into CMNaOH-releasable ^{3}H ratios of un-denatured epidermis samples increased almost linearly from pH 3.5 to 7.5 (~10-fold, $P < 0.05$) (Fig. 45). This observed incorporation was believed to be enzymic because much more total incorporated and CMNaOH-releasable ^{3}H in un-denatured epidermis samples than in the heat-denatured control at all the pH values ($P < 0.05$) (Fig. 45). Essentially, the total incorporated ^{3}H was proposed to be mainly XET products (Fig. 45a), because the quantity of the hypothesized cutin–xyloglucan hetero-polymer may be very low in nature due to the physical separation of cutin and cell wall layers. The hypothesized cutin–xyloglucan transacylase activity was suggested by the CMNaOH hydrolysis, that at least partial [^{3}H]XXXGol was incorporated by ester bonds (Fig. 45b).

Thus, in summary, a XXXGol-utilising transacylase activity, which possibly uses cutin as the acyl donor does exist in pea epicotyl but prefers a slightly basic pH (7.5), inconsistent with our hypothesis.

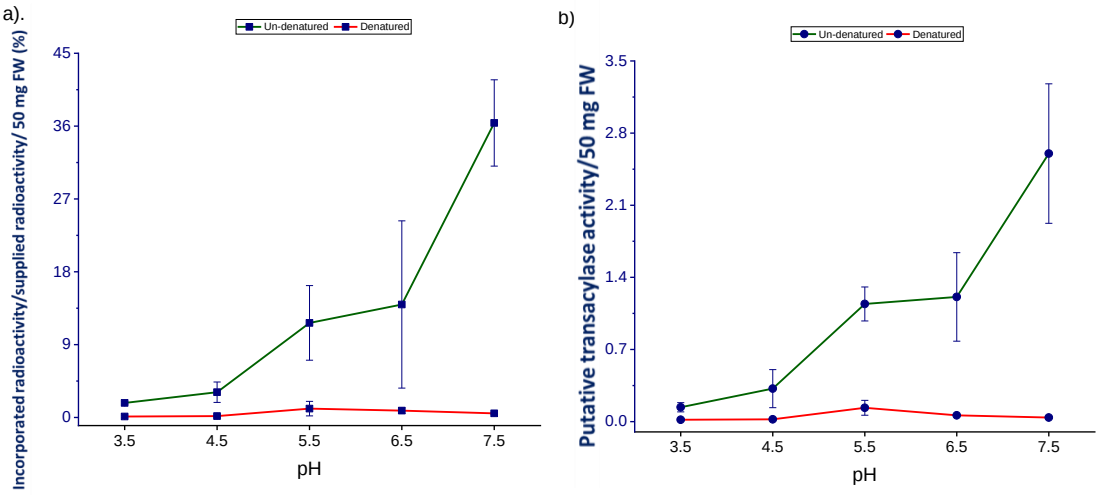

Figure 45. pH optimization of the cutin-to-[^{3}H]XXXGol transcylase activity in pea epicotyl epidermis *in situ*. The blotting dried epidermis samples (50 mg; acyl donor) with (cold buffer-washed) or without (boiled) active endogenous enzymes were incubated with 0.72 kBq exogenous [^{3}H]XXXGol (acyl acceptor) at room temperature for 1 day in 300 µl buffers with different pH values. (a). The total incorporated and (b) CMNaOH-releasable radioactivity ratios (%) were calculated as follows: obtained radioactivity (cpm/50 mg epidermis) / initially supplied radioactivity (cpm) × 100%. Green line: un-denatured epidermis samples. Red line: denatured epidermis samples (control). Bars indicate range (n=2).

A value of 10% total incorporated radioactivity/50 mg epidermis/supplied radioactivity corresponds to an absolute incorporation of 1350 cpm/50 mg epidermis in (a); and 135 cpm/50 mg epidermis is for 1% CMNaOH-releasable radioactivity/50 mg epidermis/supplied radioactivity in (b).

The same assay was carried out with expanding ice plant leaf adaxial epidermis to see if the same trend can be observed in a different plant species. The adaxial epidermis was chosen because it was observed to contain more cutin than the abaxial one does (Appendix 3). This *in-situ* assay showed similar results as above: the total incorporated and CMNaOH-

releasable ^{3}H ratios were significantly higher at higher pH values (e.g. pH 4.5 > 3.5 etc.) ($P < 0.05$) (Fig. 46).

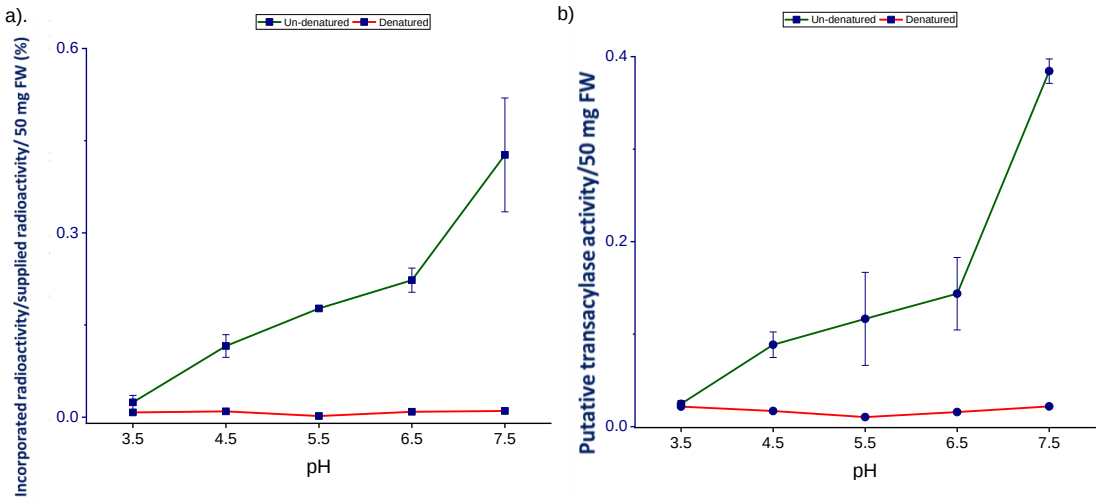

Figure 46. pH optimization of the cutin-to-[^{3}H]XXXGol transcylase activity in expanding ice plant leaf epidermis *in situ*. The experimental procedures were as in figure 43, except that 0.9 kBq exogenous [^{3}H]XXXGol was supplied as the acyl acceptor. (a). The total incorporated and (b) CMNaOH-releasable radioactivity ratios (%) were calculated as above. Green lines: un-denatured epidermis samples. Red lines: denatured epidermis samples (control). Bars indicate range (n=2) for the 'un-denatured' group. No bars for the 'denatured' group (n=1).

A value of 0.1% total incorporated or CMNaOH-releasable radioactivity/50 mg epidermis/supplied radioactivity corresponds to an absolute incorporation of 17 cpm/50 mg epidermis.

The preference for more basic pH values of the possible cutin-to-XXXGol transacylase might indicate that the linking reaction of cutin and polysaccharide occurs at the end of the cell expansion or even after the cessation. This question was answered by studying the putative cutin-to-XXXGol transacylase's change during development (see ***4.6***).

Effects of pH on the putative cutin-to-Ara$_8$-ol transacylase activity

To find out if the obtained results above can also be observed when using other [^{3}H]oligosaccharide as the substrate, the oligomer related to a rhamnogalacturonan I (RG-I, a subdomain of pectin; Fig. 47) side chain, [^{3}H]Ara$_8$-ol (an α-1→5-linked L-arabinosyl oligomer, which does not have a reducing end because the last arabinose unit from the right side was reduced to arabitol) (Øbro *et al*., 2004; reviewed by Harholt *et al*., 2010) was tested. It was chosen because pectin has been detected to be nearby cutin via immunocytochemistry (Guzmán *et al*., 2014; Segado *et al*., 2016), and thus a possible link may be found between them.

a).

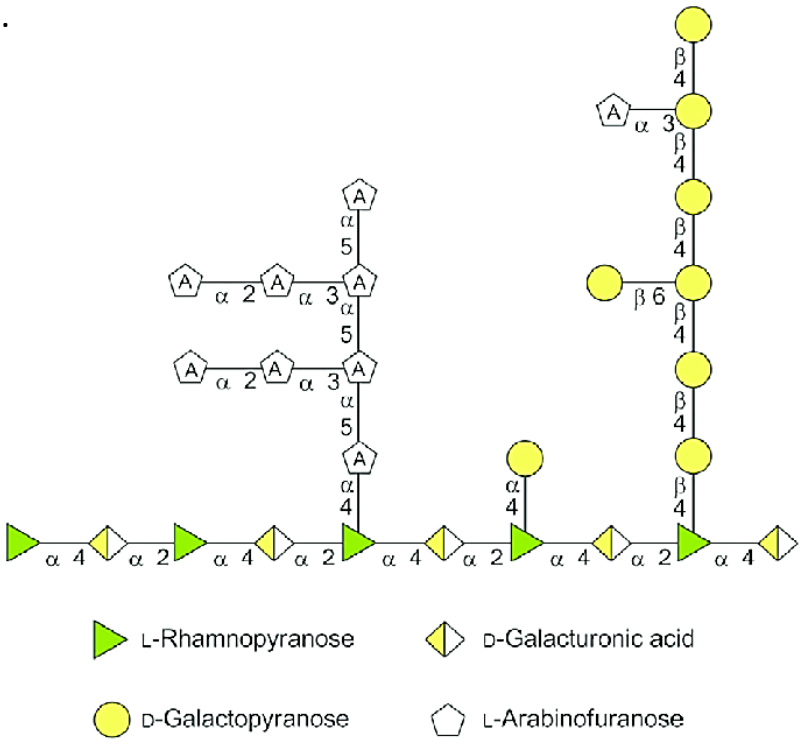

b).

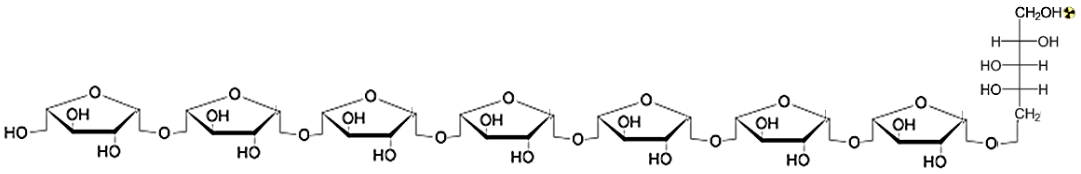

Figure 47. A schematic illustration of RG-I domain in Arabidopsis pectin and chemical structure of the [^{3}H]Ara$_8$-ol. (a) The backbone is composed of α-D-galacturonic acid-(1→2)-α-L-rhamnopyranose-(1→4)-α-D-galacturonic acid repeats. One of the sides chains is made of four 1→5 linked α-L-arabinosyl residues (adapted from Goetz *et al*., 2016). (b) Structural formula of [^{3}H]Ara$_8$-ol: composed of eight 1→5 linked α-L-arabinosyl residues, whilst the last one was reduced to arabinitol and tritiated labelled at C-1.

The same methodologies were used as above. However, the total [^{3}H]Ara$_8$-ol incorporation ratio was much lower (~200-fold) than that of [^{3}H]XXXGol at all the pH values in both pea epicotyl and ice plant leaf un-denatured epidermis (Fig. 46–46). Nevertheless, I was still able to demonstrate pH effects on incorporation, and the incorporation was enzymic ($P_{(\text{un-denatured vs. denatured})} < 0.05$) (Fig. 48 and 46).

In pea epicotyl epidermis samples, the total incorporated and incorporated into CMNaOH-releasable ^{3}H in the un-denatured samples was significantly higher than in the denatured control ($P < 0.05$) at pH 6.5 only, suggesting that the possible cutin-to-Ara$_8$-ol transacylase is only detectably active at pH 6.5 (Fig. 48).

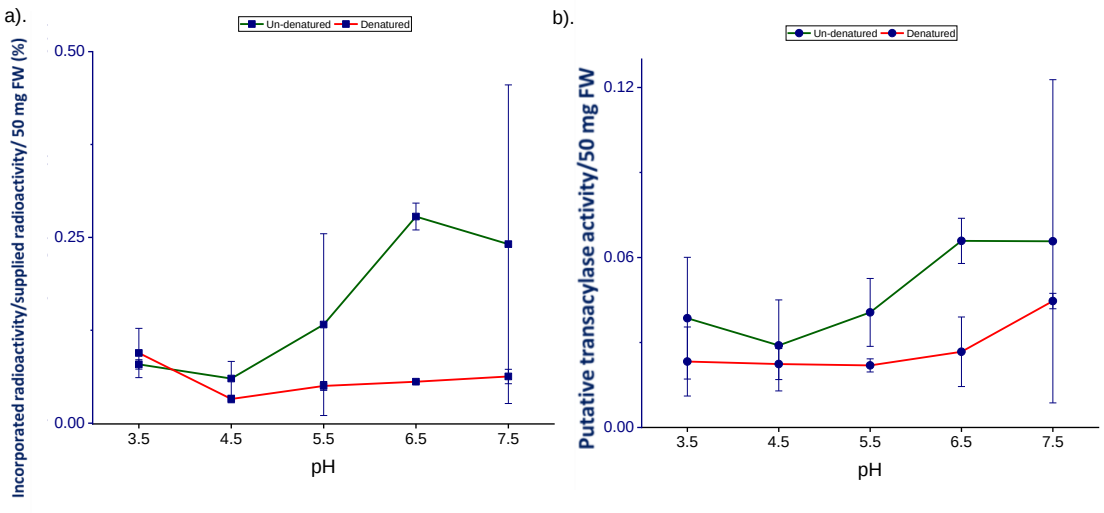

Figure 48. The putative cutin-to-[^{3}H]Ara$_8$-ol transacylase activity in pea epicotyl epidermis at different pH values *in situ*. Experimental details were as in figure 43, except 0.79 kBq exogenous [^{3}H]Ara$_8$-ol (acyl acceptor) was used. (a) The total incorporated and (b) CMNaOH-releasable radioactivity ratios (%) were calculated as figure 43 illustrate the endogenous cutin-to-[^{3}H]Ara$_8$-ol transacylase activity. Green lines: un-denatured epidermis samples. Red lines: denatured epidermis samples (control). Bars indicate range (n=2).

A value of 0.1% total incorporated or CMNaOH-releaseable radioactivity/50 mg epidermis/supplied radioactivity corresponds to an absolute incorporation of 15 cpm/50 mg epidermis.

Ice plant epidermis samples showed very similar results: the total incorporated ^{3}H ratio increased with pH (Fig. 49a). The putative product of the proposed transacylase became detectable at pH 5.5 ($P_{(\text{un-denatured vs. denatured})} < 0.05$), and peaked at pH 7.5, where the CMNaOH-releasable ^{3}H ratio was 1.5 times higher than pH 5.5 and 6.5 ($P > 0.05$) (Fig. 49b).

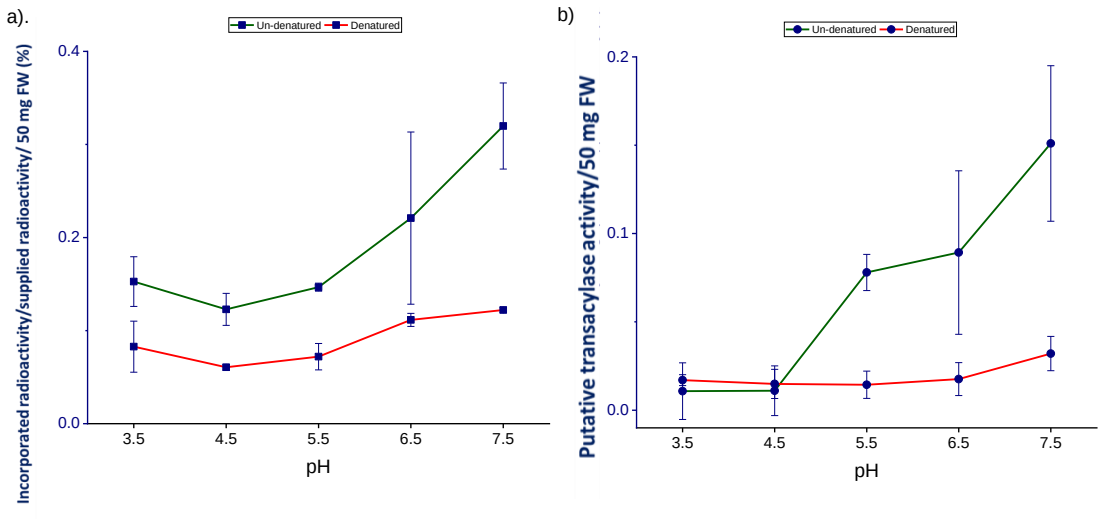

Figure 49. The putative cutin-to-[^{3}H]Ara$_8$-ol transcylase activity in expanding ice plant leaf epidermis at different pH values *in situ*. The experimental procedure was as figure in 45, except 0.68 kBq exogenous [^{3}H]Ara$_8$-ol was supplied as the acyl acceptor. (a) The total incorporated and (b) CMNaOH-releasable radioactivity ratios (%) were calculated as figure 43 and illustrate the endogenous cutin-to-[^{3}H]Ara$_8$-ol transacylase activity. Green lines: un-denatured epidermis samples. Red lines: denatured epidermis samples (control). Bars indicated range (*n*=2).

A value of 0.1% incorporated /50 mg epidermis/supplied radioactivity corresponds to an absolute incorporation of 13 cpm/50 mg epidermis.

Overall, these four [^{3}H]oligosaccharides *in-situ* assays provided preliminary evidence for the existence of the proposed cutin-to-oligosaccharide transacylase, and its pH preference (6.5–7.5), suggesting that the possible cutin-to-XXXGol and -to-Ara$_8$-ol transacylation reactions are not required during rapid growth as we had hypothesised (i.e. rapid expanding cells' apoplast pH is 4.5–6; reviewed by Cosgrove, 2005). Moreover, the big contrast between [^{3}H]XXXGol and [^{3}H]Ara$_8$-ol's acyl acceptor abilities may suggest a substrate specificity, favouring xyloglucan, and the possible linking between cutin and RG-I sidechains may be very rare in nature.

In subsequent experiments, pH 6.5 was chosen for all cutin-to-[^{3}H]oligosaccharide transacylation reactions, because it was not only in the optimized range, but also close to the physiological pH (reviewed by Cosgrove, 2005).

4.1.2 The best plant model to study the putative cutin-to-XXXGol transacylase activity (*in situ*)

Ice plant *leaf vs. pea epicotyl*

Different organs from different plants with thick epidermis were compared to find the best plant model, which can provide the highest amount of cutin and the highest endogenous cutin transacylase activity.

The comparison between expanding pea epicotyl and ice plant leaf epidermis can be seen from the results above (Fig. 46–46): the CMNaOH-releasable ^{3}H (substrate: [^{3}H]XXXGol) from the latter model was only 0.1–0.3 of the former one, indicating that the pea epicotyl epidermis was much more active (Fig. 50). Thus, concerning the growth period, epidermis yield and the performances, pea epicotyl is preferred.

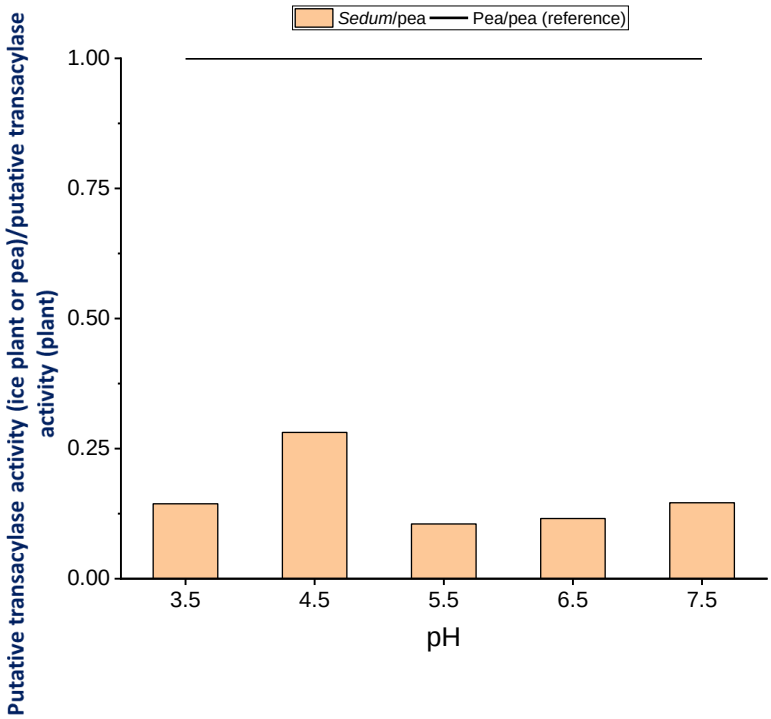

Figure 50. The putative cutin-to-[^{3}H]XXXGol transacylase activity in rapidly-expanding ice plant adaxial epidermis vs. rapidly-expanding pea epicotyl epidermis *in situ*. Experimental details were as in figure 43 and 44. The CMNaOH-releasable radioactivity ratio (%) of pea samples (**black line**) was a reference to be compared with the ice plant samples (**yellow columns**).

Tomato fruit vs. pea epicotyl

Epidermis of medium-sized tomato (cv. Ailsa Craig) fruit as another cutin resource (Girard *et al*., 2012) was also assayed with [^{3}H]XXXGol *in situ*, but only at the chosen pH, 6.5. I screened the 10–21 days after anthesis (DAA) fruit because they were in the rapidly expanding stage, as had been the pea epicotyls and ice plant leaf.

The CMNaOH-releasable ^{3}H ratio was ~1.3–2.0-fold higher than the pea epicotyl epidermis samples under the same conditions (Fig. 46 and 48); in particular, the 21-DAA tomato fruit epidermis released almost 2-fold higher

radioactivity than the pea epicotyl epidermis did (Fig. 51). However, tomato fruit's much longer growth time than the pea epicotyls lowered down experimental efficiency, and therefore compensated this advantage.

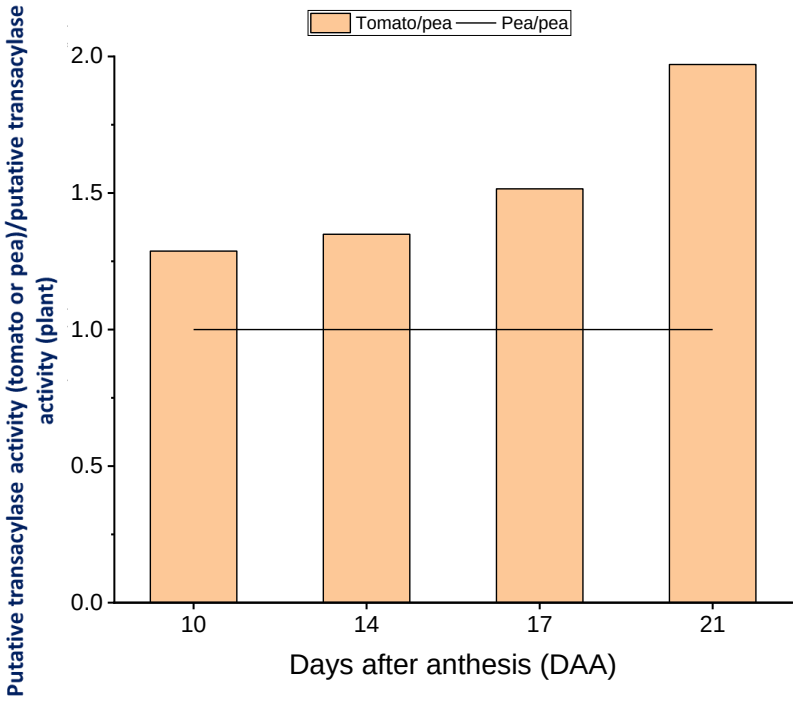

Figure 51. The putative cutin-to-[^{3}H]XXXGol transacylase activity in rapidly-expanding tomato fruit epidermis vs. rapidly-expanding pea epicotyl epidermis *in situ*. Experimental details were the same as figure 43, except only pH 6.5 buffer was used for incubation. The CMNaOH-releasable radioactivity ratio (%) of pea samples (**black line**) was a reference to be compared with the tomato samples (**yellow columns**).

In summary, considering all the factors together, I conclude that the pea epicotyl is the best because of the fastest harvest cycles and a very good putative cutin-to-XXXGol transacylase activity.

4.1.3 Effects of pre-incubation process on the putative cutin-to-oligosaccharide transacylase activity (*in situ*)

In the experiments above, all the un-denatured epidermis samples had been frozen, thawed and then washed in cold buffers (4°C) for 1 h before incubation, because this process was proposed to be important for removing intracellular transacylase substrates, such as ATP and CoA, which can potentially synthesize oligo-esters *de novo*, and therefore compete with extraprotoplasmic cutin transacylation. Nevertheless, the pre-wash procedure might also remove the proposed transacylase. I investigated this question by comparing washed and un-washed pea epicotyl epidermis samples and found that the CMNaOH-releasable ^{3}H ratio was two-fold higher in the un-washed samples (Fig. 52). However, there was no replicate for the un-washed epidermis sample, and therefore the results here only hinted that the cold buffer wash may have removed some putative endogenous cutin-to-XXXGol transacylase.

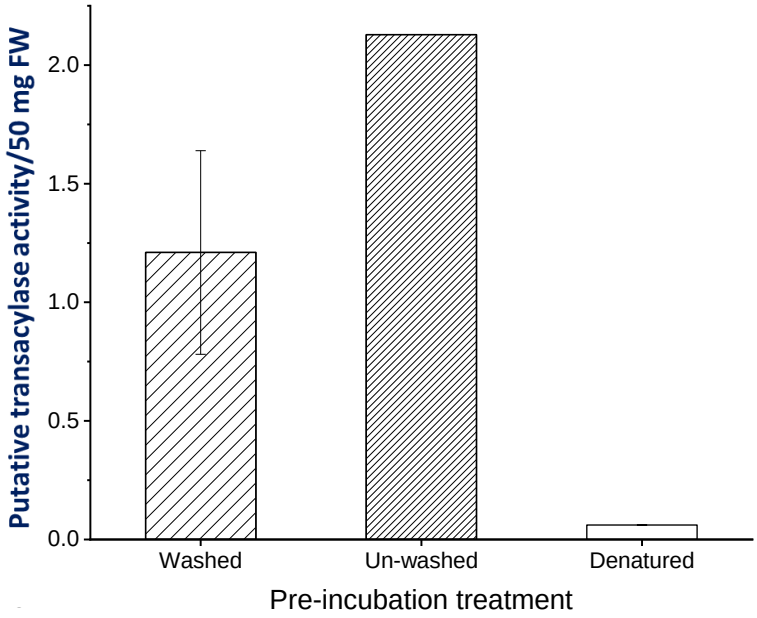

Figure 52. Effects of pre-incubation wash on the putative cutin-to-[^{3}H]XXXGol transacylase activity in pea epicotyl epidermis *in situ*. Experimental details were as in figure 43, except epidermis samples without being pre-incubation cold-buffer washed was added, and only pH 6.5 buffer was used for incubation. The CMNaOH-releasable radioactivity ratio (%) shows the pre-incubation treatments' effects on the cutin-to-[^{3}H]XXXGol transacylase activity. Bars indicate range (n=2) (not visible for the 'denatured' group). No bars for the 'un-washed' sample (n=1).

A value of 1% CMNaOH-releasable radioactivity/50 mg epidermis/supplied radioactivity corresponds to an absolute incorporation of 135 cpm/50 mg epidermis.

The same trend was observed by assaying expanding ice plant leaf adaxial epidermis with [^{3}H]XXXGol: the un-washed epidermis samples released 1.4-fold higher ^{3}H in CMNaOH than the washed one (Fig. 53). However, same as the figure 48, there was no replicate for the un-washed sample (Fig. 53), only providing a hint of the washing procedure's effect.

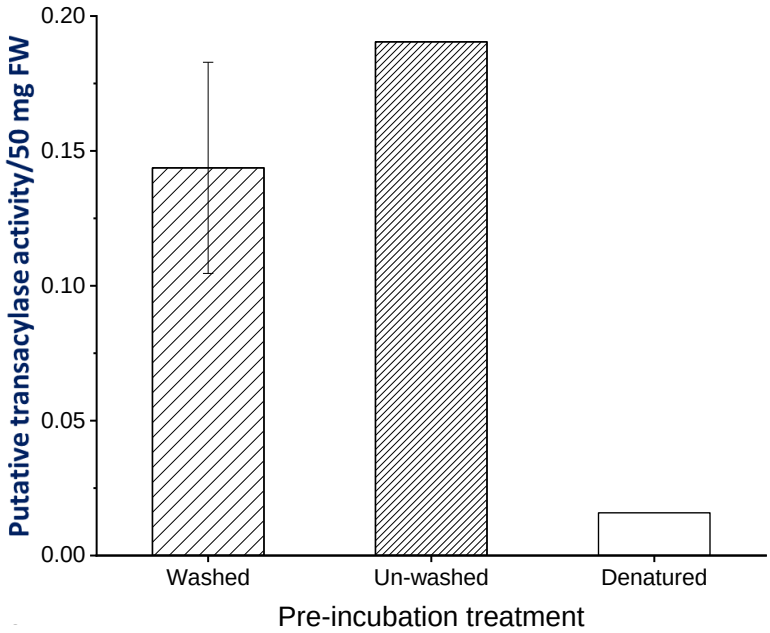

Figure 53. Effects of pre-incubation wash on the putative cutin-to-[^{3}H]XXXGol transacylase activity in expanding ice plant leaf epidermis *in situ*. Experimental details were the same as figure 44 and 49, except that 0.9 kBq exogenous [^{3}H]XXXGol was used. Bars indicate (*n*=2) for the 'washed' group. No bars for other groups (*n*=1).

A value of 0.1% CMNaOH-releasable radioactivity/50 mg epidermis/supplied radioactivity corresponds to an absolute incorporation of 17 cpm/50 mg epidermis.

These observations were unexpected, because in Chapter 3, the pre-incubation wash did not harm the proposed transacylase activity. It might suggest that this possible cutin-to-XXXGol transacylase is a different enzyme from the cutin-to-HHA transacylase, and that their locations *in muro* are different: the former may be located at the interface between cell wall and cutin, such that it was easier to be removed, whereas the latter may be embedded in cutin, making it more stable physically (i.e. cutin is located in the middle of the epidermis, between cell wall and wax; Chapter 1, Fig. 1).

However, since the CMNaOH-releasable ^{3}H ratio after the pre-incubation wash was still reasonably high, and the desire to avoid intracellular interferences, we decided to keep this step in the rest of cutin-to-[^{3}H]oligosaccharide *in-situ* assays.

4.2 Screen of acyl acceptors

4.2.1 Pectic oligosaccharides' acceptor abilities

As stated above, pectin has been observed by microscopy to be physically adjacent to cutin (Guzmán *et al*., 2014; Segado *et al*., 2016), but no biochemical evidence yet exists to prove the links between them yet. To test this, ^{3}H-labelled pectic oligosaccharides (e.g. [^{3}H]Ara_8-ol, [^{3}H]$GalA_8$-ol and methyl esterified [^{3}H]$GalA_8$-ol) were tested *in situ*.

Cutin-to-[^{3}H]Ara_8-ol transacylation

The *in-situ* incorporation of [^{3}H]Ara_8-ol results are shown above, where the CMNaOH-releasable ^{3}H ratio was very low in both rapidly expanding pea epicotyl and ice plant leaf epidermis (e.g. 0.1% in un-denatured expanding ice plant leaf epidermis) (Fig. 48 and 46), indicating that the acyl acceptor ability was only a little.

Cutin-to-[^{3}H]GalA$_8$-ol transacylation

Another radio-labelled pectic component, [^{3}H]GalA$_8$-ol, an oligomer of the backbone of pectin (homogalacturonan), which is composed of α-1→4-linked D-galacturonic acid (reviewed by Harholt *et al*., 2010) (Fig. 54) without a reducing group as the [^{3}H]Ara$_8$-ol. It was assayed with pea epicotyl epidermis at different pH values, but no enzymic incorporation was detected, and only background radioactivity was left after the MFW wash (Fig. 55).

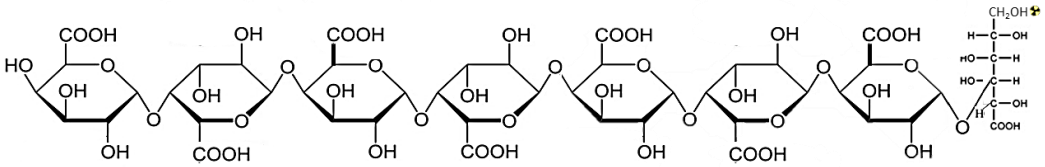

Figure 54. Structural formula of [^{3}H]GalA$_8$-ol. Eight α-1→4-linked D-galacturonic acid residues, the last one was reduced to galacturonitol and tritiated-labelled at C-1.

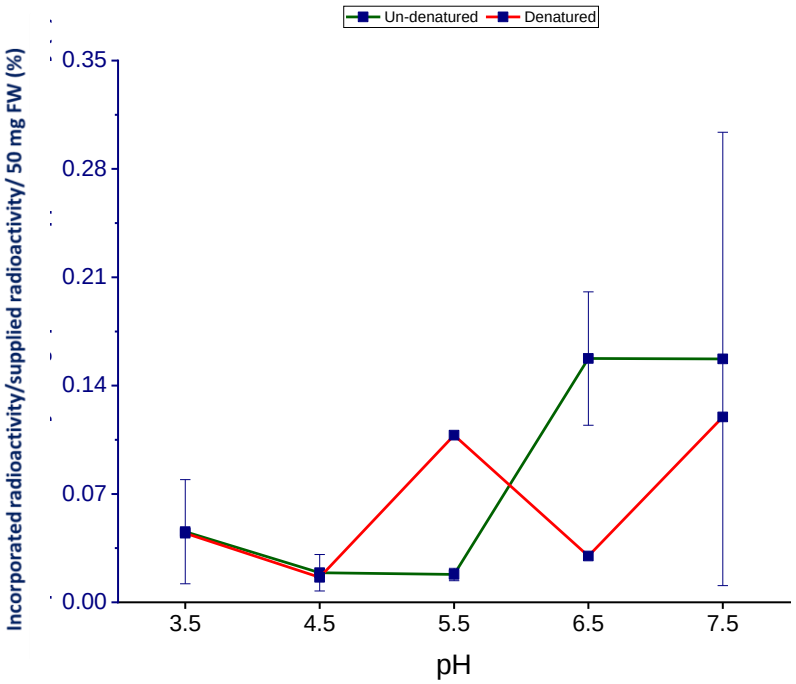

Figure 55. The putative cutin-to-[^{3}H]GalA$_8$-ol transacylase activity in pea epicotyl epidermis at different pH values *in situ*. Experimental details were as in figure 43, except 0.26 kBq exogenous [^{3}H]GalA$_8$-ol (acyl acceptor) under the standardised conditions as above at different pH values. The total incorporated radioactivity ratio (%) was used to illustrate the endogenous cutin-to-[^{3}H]GalA$_8$-ol transacylase activity.

Green line: un-denatured. Red lines: denatured (control). Bars indicate (*n*=2). No bars for the 'denatured' (*n*=1).

A value of 0.1% total incorporated radioactivity/50 mg epidermis/supplied radioactivity corresponds to an absolute incorporation of 5 cpm/50 mg epidermis.

This result was partially expected, because the same as [^{14}C]HA in Chapter 3, the [^{3}H]GalA$_{8}$-ol only has 8 non-activated –COOH groups at C-6, and therefore it cannot act as an acyl donor. However, the fact that it also cannot act as an acyl acceptor (despite possessing a –OH groups at C-2 and C-3) may indicate that cutin does not link to the backbone of pectin, at least not to the un-methyl esterified parts.

Methyl esterified [^{3}H]GalA$_{8}$-ol-to-cutin transacylation

Some homogalacturonan residues are methyl esterified (reviewed by Harholt *et al*., 2010), which in turn activates the acyl groups, –COOH at C-6 (refer to Fig. 55), making the galacturonic acid residue capable of being an acyl donor, which is different from the oligosaccharides tested above. Thus, we methyl esterified the [^{3}H]GalA$_{8}$-ol uniformly at C-6 by the EDC-NHS coupling method (preliminary data not shown) (Sam *et al*., 2010), and it was assayed with pea epicotyl epidermis under the optimized conditions *in situ*. However, still no incorporation was observed (Fig. 56).

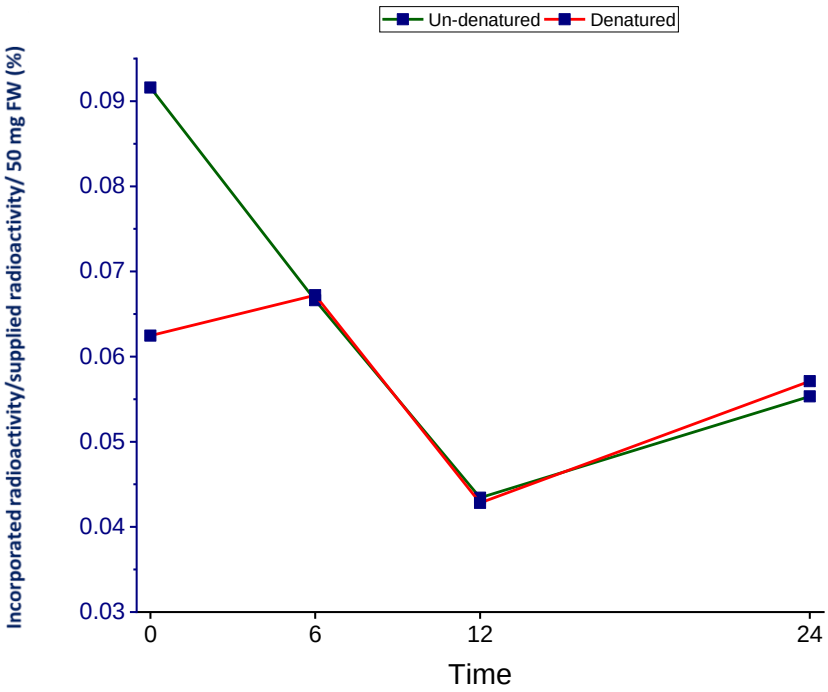

Figure 56. The putative methyl esterified [^{3}H]GalA$_8$-ol-to-cutin transacylase activity in pea epicotyl epidermis *in situ*. Experimental details were the same as figure 50, except that 0.42 kBq exogenous uniformly methyl esterified [^{3}H]GalA$_8$-ol (acyl acceptor) was used at pH 6.5. The incorporated radioactivity ratio (%) illustrates the endogenous cutin-to-methyl esterified [^{3}H]GalA$_8$-ol transacylase activity. Green line: un-denatured. Red lines: denatured (control). No bars (n=1).

A value of 0.1% total incorporated radioactivity/50 mg epidermis/supplied radioactivity corresponds to an absolute incorporation of 8 cpm/50 mg epidermis.

To test whether methyl esterified [^{3}H]GalA$_8$-ol can be an acyl donor in a different plant species, tomato fruit (cv. Ailsa Craig) epidermis at different developmental stages was assayed with it under the optimized conditions *in situ*. Nevertheless, the result was still similar (Fig. 57).

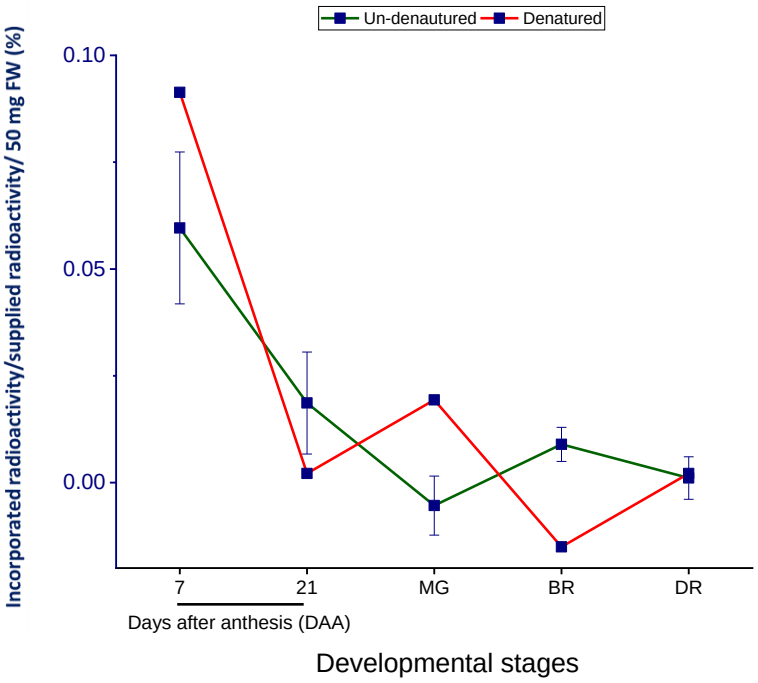

Figure 57. The putative methyl esterified [^{3}H]GalA$_8$-ol-to-cutin transacylase activity in rapid expanding tomato fruit epidermis *in situ*. Experimental details were the same as figure 52, except that 50 mg tomato fruit epidermis (acyl donor) was incubated with 0.26 kBq exogenous uniformly methyl esterified [^{3}H]GalA$_8$-ol (acyl acceptor). Green line: un-denatured. Red lines: denatured (control). Bars indicate standard errors (*n*=3). No bars for the 'denatured' group (*n*=1).

A value of 0.1% total incorporated radioactivity/50 mg epidermis/supplied radioactivity corresponds to an absolute incorporation of 5 cpm/50 mg epidermis.

Acetyl esterified homogalacturonan (reviewed by Scheller *et al*., 2007; Harholt *et al*., 2010) oligomer was not considered because the donor group would be acetyl, instead of galacturonoyl.

In summary, [^{3}H]GalA$_8$-ol and its methyl esterified version were neither a donor nor an acceptor of the proposed transacylases, clearly indicating that the no covalent link between cutin and the pectin backbone. The slight incorporation of [^{3}H]Ara$_8$-ol might point out that pectin sidechains may become linked with cutin.

4.2.2 Primary cell wall hemicellulosic oligosaccharides' acceptor abilities

Xyloglucan: further investigation of the cutin-to-[^{3}H]XXXGol transacylation under the optimized conditions

XXXG is the most abundant building block in dicotyledonous xyloglucan (reviewed by Takahisa and Rumi, 2011). The abbreviation and structure have been introduced above according to Fry *et al*. (1993) (Fig. 42).

#In the '***optimization***' section above, I have illustrated that [^{3}H]XXXGol can be incorporated via ester bonds into plant shoot epidermis enzymically *in situ*, and this conclusion was further confirmed by observing an increase of the radioactivity incorporation into un-denatured epidermis with time (Fig. 58).

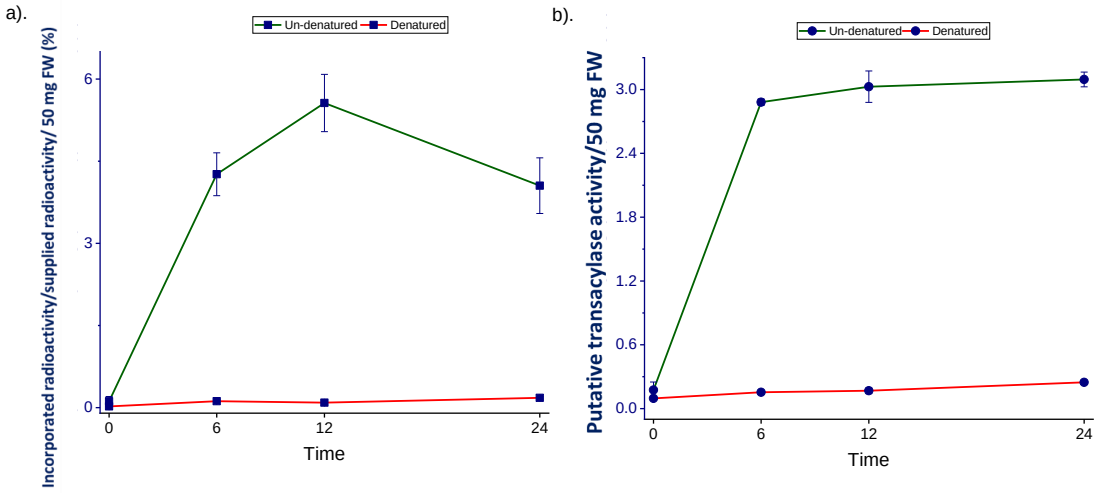

Figure 58. Effects of incubation time on the putative cutin-to-[^{3}H]XXXGol transcylase activity in pea epicotyl epidermis *in situ*. Experimental details were as in figure 43, except 0.4 kBq exogenous [^{3}H]XXXGol was supplied as the acyl acceptor at pH 6.5 only. (a). The total incorporated radioactivity ratio % and (b) CMNaOH-releasable radioactivity ratio (%) illustrate the endogenous cutin-to-[^{3}H]XXXGol transacylase activity. Green line: un-denatured. Red lines: denatured (control). Bars indicate standard errors (*n*=3).

A value of 1% incorporated radioactivity/50 mg epidermis/supplied radioactivity corresponds to an absolute incorporation of 75 cpm/50 mg epidermis.

The incorporation was proposed to consist of the proposed transacylase and transglucanase (e.g. XET) products (Lorences and Fry, 1993), which were distinguished roughly as above by CMNaOH hydrolysis (which should have no effect on XET products). The un-denatured group had incorporated much higher (35 times) total ^{3}H than the denatured control by our first time-point (6 h) ($P < 0.01$) (Fig. 58a), which was also the starting point of the incorporation plateau in this experiment; and 19-fold more CMNaOH-releasable ^{3}H by the same time (Fig. 58b). The total incorporation (Fig, 54a) consists of XET and the proposed transacylase activities, which together was ~5.6% at 12 h as an example, whereas the putative transacylase activity alone (Fig. 58b) was ~3% by the same time, indicating that the XET activity was ~2.6%, which is smaller than the transacylase one. This observation was different from our expectation (i.e. XET activity > the transacylase activity), one possible explanation is that the total radioactivity was measured by counting the MFW-insoluble residues (Fig. 58a), which were solid and caused a lower counting efficiency compared with the aqueous sample (CMNaOH hydrolysis supernatant) (Fig. 58b). Another possibility is that CMNaOH mixture also dissolved some XET products (will be explained in ***4.4.3***).

This plateau was not unique, since it was also observed in the pea epicotyl XET activity from 4 or 6 h onwards (Fry *et al*., 1992; my own un-shown data). The two most plausible reasons may be (1) the exogenous [^{3}H]XXXGol was used up and/or degraded, and (2) the proposed enzymes were denatured after some hours, but we also cannot exclude the possibilities that (3) the transacylase product was degraded by unspecified lipase(s).

To test the first possibility, the remaining incubation mixture, which was predicted to contain un-incorporated [^{3}H]XXXGol and/or its degraded products, was analysed by TLC, followed by fluorography (Fig. 59).

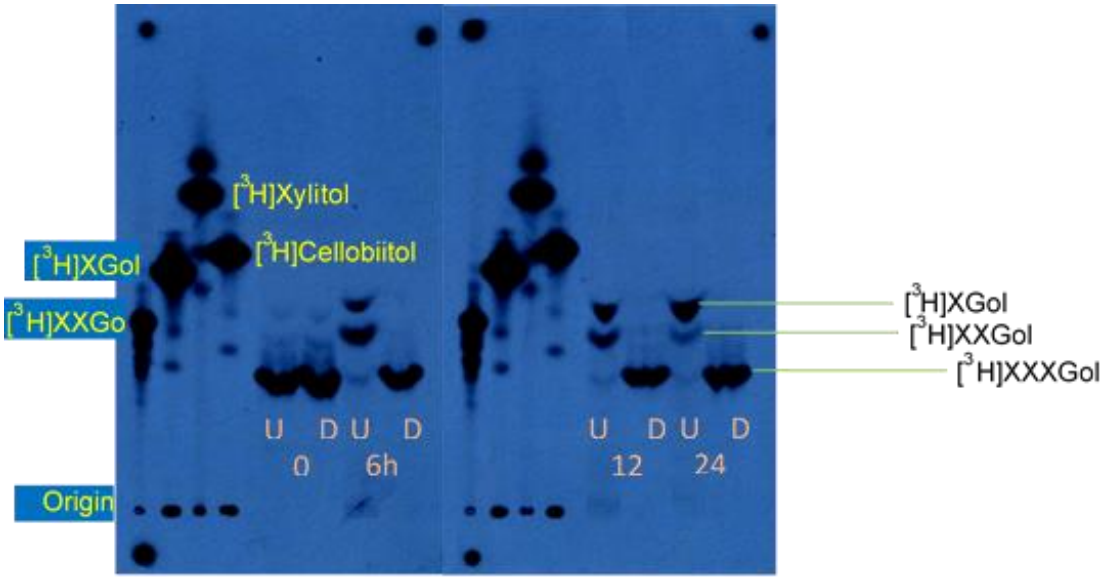

Figure 59. Chromatographic analysis of the un-incorporated ^{3}H in the *in-situ* cutin-to-[^{3}H]XXXGol transacylase assay. The pea epicotyl epidermis (50 mg; acyl donor) with or without active endogenous transacylases were incubated with ~0.4 kBq exogenous [^{3}H]XXXGol (acyl acceptor) under the standardised conditions for 0, 6, 12 and 24 h. The reaction mixture containing remaining soluble radioactivity was collected and subjected to TLC analysis [butan-1-ol/acetic acid/water (BAW), 2/1/1 v/v/v, 2 ascents)], together 4 external radio-labelled markers: [^{3}H]XXGol, [^{3}H]XGol, [^{3}H]cellobiitol and [^{3}H]xylitol (**yellow**), followed by fluorography analysis. The un-incorporated radioactive compounds were annotated besides the TLC plate (**black**). UD: un-denatured. D: denatured.

In un-denatured samples, majority of the un-incorporated [^{3}H]XXXGol was degraded to [^{3}H]XXGol and [^{3}H]XGol in 6 h, and almost completely into [^{3}H]XGol after 24 h, whereas no degradation was detected in the denatured control and also in the 0-h samples, indicating that it was an enzymic degradation (Fig. 59). The imperfect alignments between samples and markers were because some sugars are liberated into incubation mixture

from pea epidermis samples, and the salts from incubation buffer, resulting in retarding the [^{3}H]XXGol and [^{3}H]XGol migration (Fig. 59).

The most likely enzymes to have caused the degradation were α-D-xylosidase (Guillen *et al*., 1995) and β-D-glucosidase (Miyamoto *et al*., 1997) (reviewed by Fry, 1995; Franková and Fry, 2013), which hydrolyses the α-D-xylopyranosyl-(1→6)-D-glucose and β-D-glucopyranosyl-(1→4)-D-glucose bonds respectively. The xylose is removed first, making the remaining glucose of the former X unit labile to β-D-glucosidase, resulting in a complete erasure of an X (Koyama *et al*., 1993).

This fluorography partially answered the first hypothesis, that the degradation of exogenous [^{3}H]XXXGol caused no incorporation, but it needed to be fully solved by assaying acceptor abilities of the [^{3}H]XXXGol degradation products with pea epicotyl epidermis as above. Thus, [^{3}H]XXGol, [^{3}H]XGol, [^{3}H]cellobiiotol and [^{3}H]glucitol, together with [^{3}H]XXXGol itself were tested *in situ*.

The CMNaOH-releasable ^{3}H incorporation ratio clearly showed that the longest molecule, [^{3}H]XXXGol was the best acceptor substrate, exhibiting ~2% incorporation from 6-h incubated un-denatured epidermis samples, and this value was reduced sharply to ~0.2% when [^{3}H]XXGol was the substrate (Fig. 60a). These incorporations were enzymic because the un-denatured samples released significantly higher ^{3}H than the denatured control did ($P < 0.01$) (Fig. 60). [^{3}H]XGol and the other smaller molecules were not incorporated ($P_{(\text{un-denatured vs. control})} > 0.05$) (Fig. 60).

The fluorography (Fig. 59) and the *in-situ* assay results (Fig. 60) together fully confirmed that the enzymic degradations of exogenous [^{3}H]XXXGol caused the incorporation plateau. However, more data suggested that it is not the only reason (the next section).

In summary, [^{3}H]XXXGol was much preferred by the putative cutin-to-XXXGol transacylase than its smaller building blocks; and to prevent the degradation, a shorter incubation time and/or adding glycosidase inhibitors should be considered.

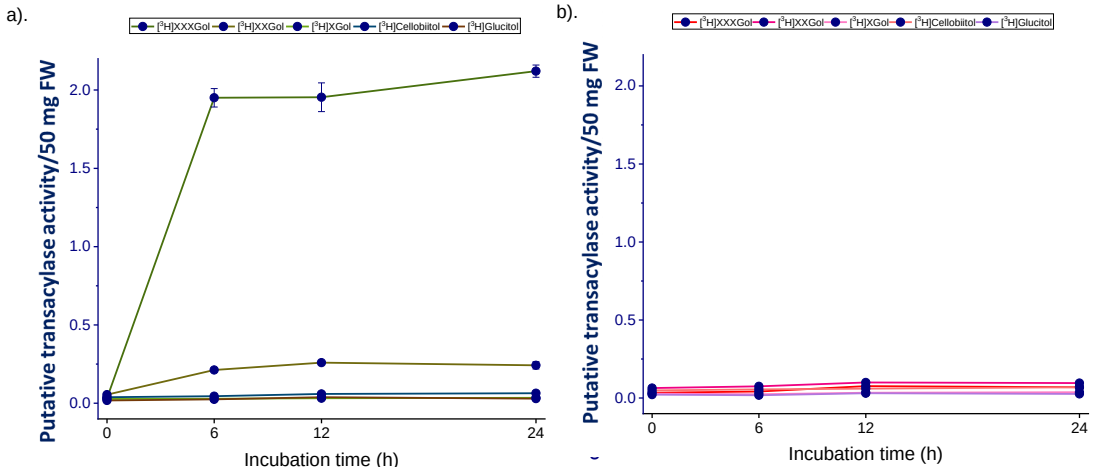

Figure 60. Acyl acceptor abilities of [^{3}H]XXXGol and its building blocks under the catalysis of the proposed cutin-to-[^{3}H]XXXGol transacylase in pea epicotyl epidermis *in situ*. Experimental details were as in figure 54, except 0.58 kBq of exogenous [^{3}H]XXXGol and its building blocks were supplied as the acyl acceptors. The CMNaOH-releasable radioactivity ratio (%) illustrate these compounds' acceptor abilities. (a). CMNaOH-releasable radioactivity ratio (%) from un-denatured epidermis samples. (b). Denatured epidermis samples (control). Bars indicate standard errors (n=3).

A value of 1% CMNaOH-releasable radioactivity/50 mg epidermis/supplied radioactivity corresponds to an absolute incorporation of 110 cpm/50 mg epidermis.

Strategies to prevent the [^{3}H]XXXGol degradations

To prevent the degradations and in turn, obtain more putative cutin-to-XXXGol transacylase products, potential α-D-xylosidase inhibitors (e.g. erythrosin B, riboflavin and nojirimycin-1-sulfonic acid) were added to the incubation buffer (Tajima *et al*., 2011; Chormova *et al*., 2015), and incubated under light (resource: bulb; intensity: ~9 µmol/m^2/s) at room temperature. However, a plateau was reached again from 4 h onwards, and they did not improve ^{3}H incorporation significantly compare with the inhibitor-free control ($P > 0.05$) (Fig. 61). The CMNaOH hydrolysis was not carried out because none of the inhibitors was effective.

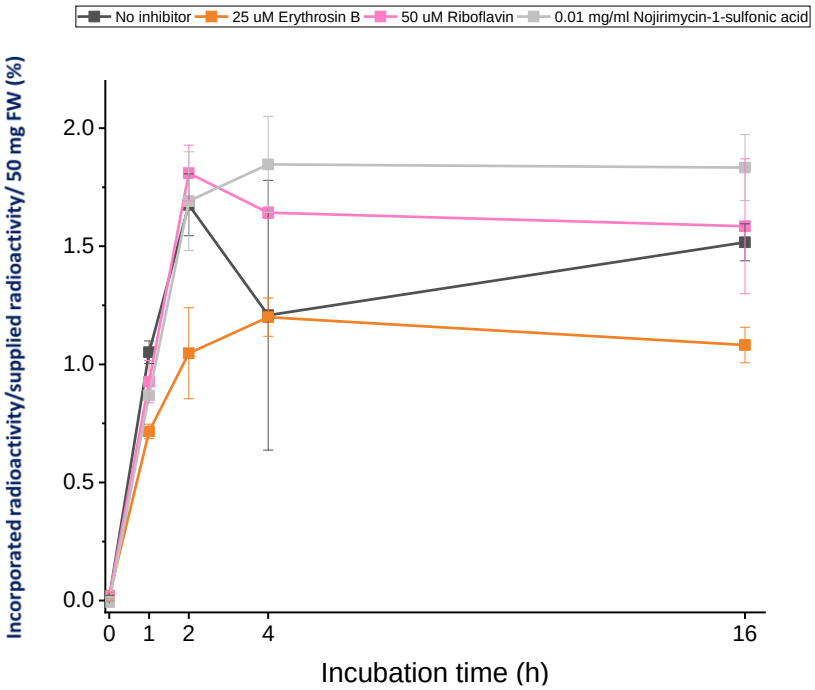

Figure 61. Screen of the inhibitors to antagonist α-D-xylosidase activity in pea epicotyl epidermis *in situ*. Experimental details were as in figure 54, except pea epicotyl epidermis was incubated with 0.26 kBq exogenous [^{3}H]XXXGol (acyl acceptor) together with or without 25 µM (final conc.) Erythrosin B, 50 µM riboflavin and 0.01 mg/ml nojirimycin-1-sulfonic acid. The total incorporated radioactivity ratio (%) illustrates the effects of these α-D-xylosidase inhibitors on the putative cutin-to-[^{3}H]XXXGol transacylase activity. Bars indicate standard errors (n=3).

A value of 1% total incorporated radioactivity/50 mg epidermis/supplied radioactivity corresponds to an absolute incorporation of 50 cpm/50 mg epidermis.

Thus, the incubation time did not need to be as long as 4 or 6 h, because the maximum incorporation may occur much before that. Thus, pea epicotyl epidermis was assayed with [^{3}H]XXXGol *in situ* again, but with a finer temporal resolution than experiments above (Fig. 62a). The CMNaOH-releasable ^{3}H ratio was linearly increased until 80 min (Fig. 62a). This result and a TLC analysis of the incubation mixture indicated again that the enzymic degradations caused the incorporation plateau, because 80 min was also the time point when [^{3}H]XXGol started appearing (Fig. 62b). The CMNaOH-releasable ^{3}H may have further increased till 320 min but with a much slower speed than the first 80 min (Fig. 62a), and [^{3}H]XXGol was the dominant exogenous substrate at 320 min, while [^{3}H]XGol also appeared (Fig. 62b).

a)

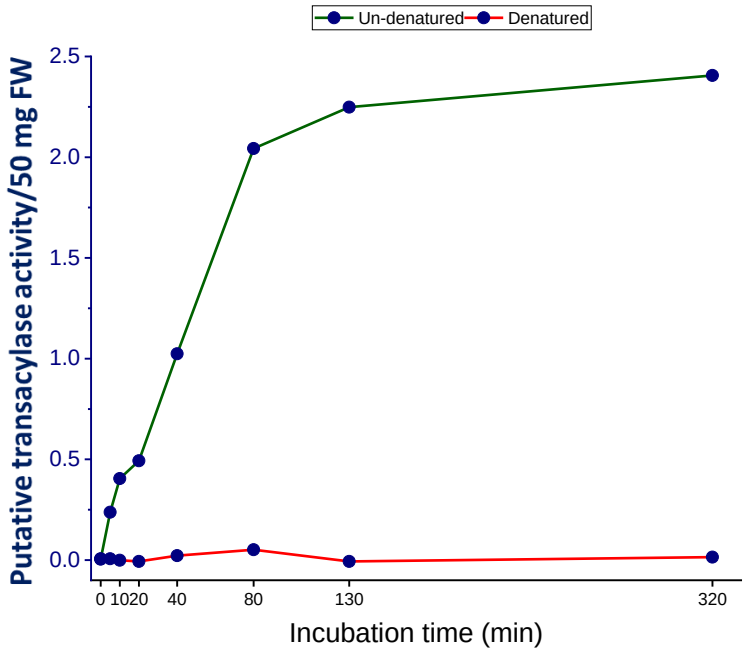

b).

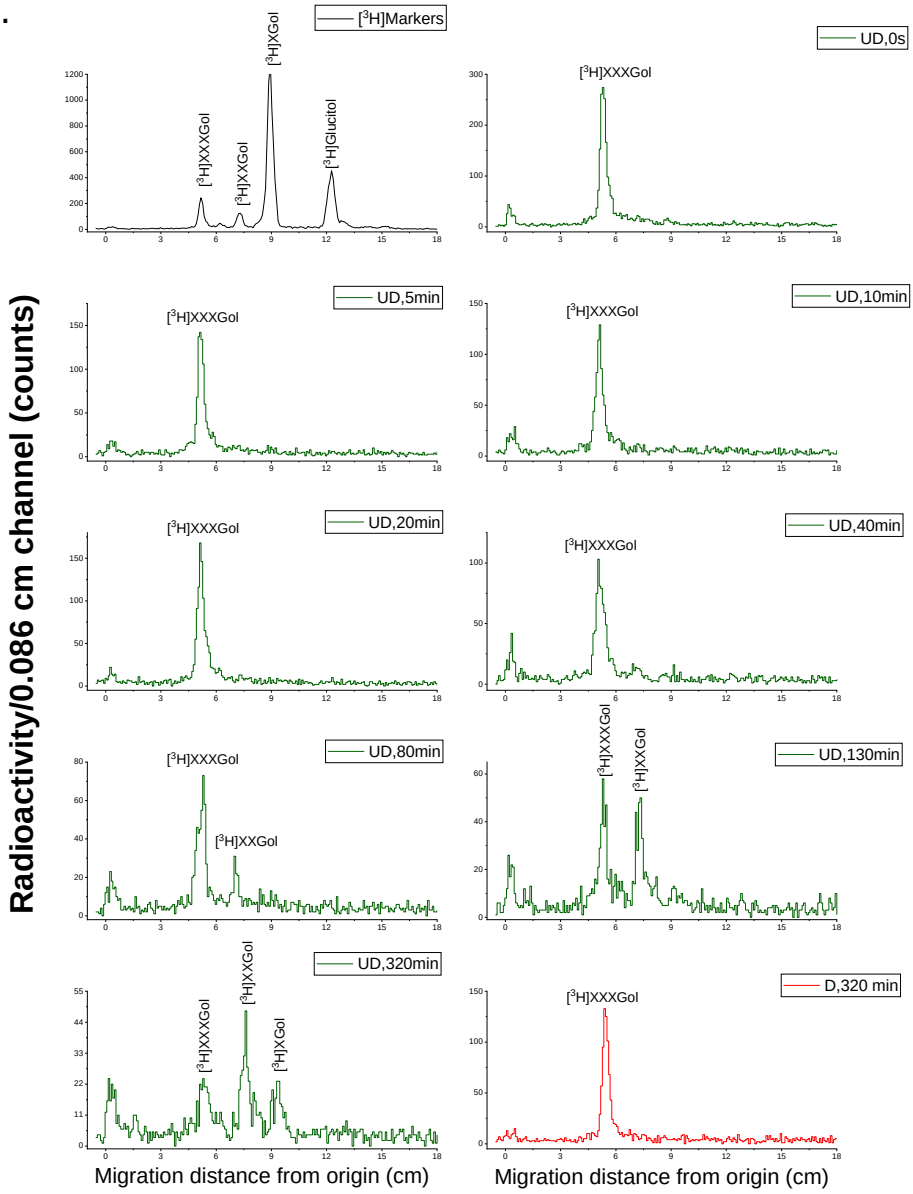

Figure 62. The correlation between the substrate degradation and the proposed cutin-to-[^{3}H]XXXGol transacylation reaction speed *in situ*. Experimental details were as in figure 54, except 0.79 kBq exogenous [^{3}H]XXXGol was supplied as the acyl acceptor.

(a) The CMNaOH-releasable radioactivity ratio (%) illustrates the endogenous cutin-to-[^{3}H]XXXGol transacylase activity (n=1). A value of 1% CMNaOH-releasable radioactivity/50 mg epidermis/supplied radioactivity corresponds to an absolute incorporation of 150 cpm/50 mg epidermis.

(b) The un-incorporated radioactivity was analysed by TLC (BAW, 2/1/1, v/v/v, 3 ascents), and then radio-scanned for 1 h per lane (unit: counts) to annotate the chemical compositions. Green lines: un-denatured epidermis samples (UD). Red lines: denatured epidermis samples (D).

Summarizing the results above (Fig. 62), we decided the incubation time of the cutin-to-[^{3}H]XXXGol *in-situ* assays should be 3 h, which allows the putative transacylase activity not to be underestimated and the best substrate, [^{3}H]XXXGol to be still available.

In this section, I concluded that no effective α-D-xylosidase inhibitors could be found to prevent the [^{3}H]XXXGol degradation reactions, and the 3-h incubation time is enough to obtain the same amount of CMNaOH-releasable ^{3}H as the 24-h one.

The remaining question was, as I have stated above, whether the [^{3}H]XXXGol degradation might not be the only reason to cause the plateau seen in Fig. 62a. The second possibility, the degradation of the possible cutin-to-XXXGol transacylase in the course of incubation, was examined by adding the putative acyl acceptor, [^{3}H]XXXGol to pea epicotyl epidermis at different timings (Fig. 63).

The CMNaOH-releasable ^{3}H ratio from the group that incubated with [^{3}H]XXXGol for the first (‘early’) 80 min was significantly higher (1.4-fold; $P < 0.05$) than from the group, which [^{3}H]XXXGol was added after the epidermis had been incubated in buffer alone for 80 min (‘late’: allowing the putative transacylase to be denatured prior to the transacylation reaction) (Fig, 59). This observation suggested that the possible cutin-to-XXXGol transacylase activity was significantly decreased after 80 min of incubation, agreeing with our hypothesis.

A similar trend as in Fig. 62a was also observed: samples incubated with [^{3}H]XXXGol for 80 and 160 min did not release significantly different amount of ^{3}H in CMNaOH (Fig. 63) even though the putative transacylase activity (Fig. 63) and exogenous [^{3}H]XXXGol are still available in the 'late' 80 min (Fig. 62b), suggesting another mechanism is involved in causing the plateau (see below).

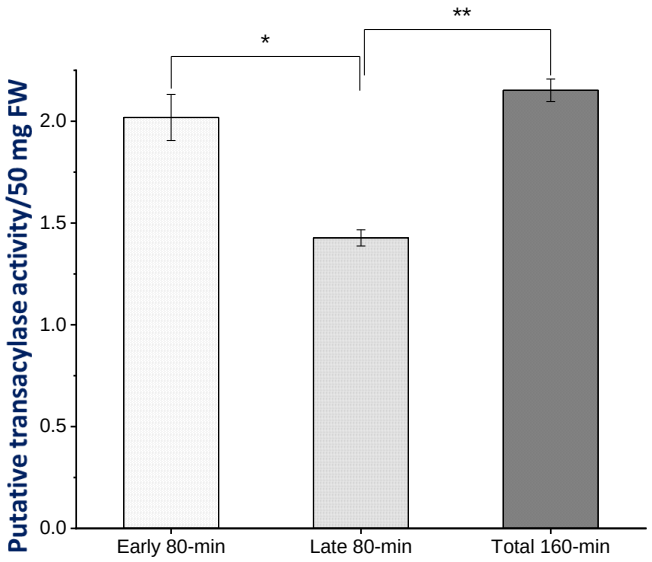

Fig. 63. An *in-situ* enzyme stability test for the putative cutin-to-[^{3}H]XXXGol transacylase in pea epicotyl epidermis. Experimental details were as in figure 58, except [^{3}H]XXXGol 80 mg blot-dried pea epicotyl epidermis (acyl donor) was added with 5.4 kBq [^{3}H]XXXGol (acyl acceptor) from the beginning for 80 min (early 80-min), or without [^{3}H]XXXGol for the first 80 min and then added with 6.9 [^{3}H]XXXGol (late 80-min), or 7 kBq [^{3}H]XXXGol from the beginning for 160 min (total 160-min). The CMNaOH-releasable radioactivity ratio (%) illustrate the effects of incubation time on the putative cutin-to-[^{3}H]XXXGol transacylase's stability. Bars indicate standard errors (*n*=3). *: P< 0.05; **: P < 0.01.

A value of 1% CMNaOH-releasable radioactivity/50 mg epidermis/supplied radioactivity corresponds to an absolute calculated incorporation of 1027–1317 cpm/50 mg epidermis.

The third possibility was that the ester bonds in the possible cutin–[^{3}H]XXXGol conjugates are broken by potential apoplastic lipase(s) when the

conjugate concentration reaches a threshold, resulting in an equilibrium between the proposed transacylation product (cutin–[^{3}H]XXXGol) and reactants (e.g. [^{3}H]XXXGol).

This hypothesized turnover was tested by supplying a general hydrolase (including lipases) inhibitor, phenylmethylsulfonyl fluoride (PMSF) (Kanwar *et al*., 2005; Appendix 1) to *in-situ* assays with [^{3}H]XXXGol as the acyl acceptor. The ^{3}H incorporation ratio is expected to be increased upon adding PMSF.

However, there was no significant difference ($P > 0.05$) between the samples with or without PMSF (Fig. 64), suggesting that no PMSF-inhibitable lipase hydrolysed the cutin–[^{3}H]XXXGol conjugates (the putative transacylase's product), but a more specific lipase (e.g. cutinase) inhibitor should be tested in future. The significant ($P < 0.01$) contrast between the two un-denatured groups with the denatured control again confirming that it was an enzymic incorporation (Fig. 64).

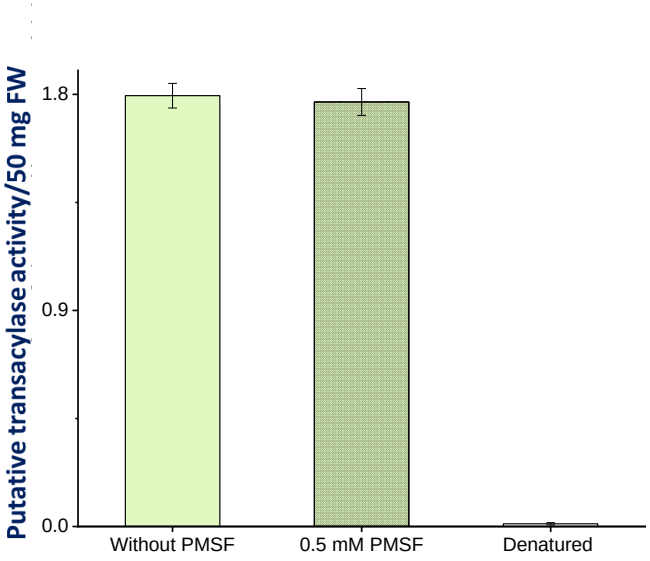

Fig. 64. The test of a possible lipase acting on the putative product of cutin-to-[^{3}H]XXXGol transacylase in pea epicotyl epidermis. Experimental details were as

in figure 43, except 0.68 kBq [^{3}H]XXXGol (acyl acceptor) together with 0.5 mM (final concentration) PMSF (dissolved in DMSO) or 0.77 kBq [^{3}H]XXXGol without PMSF were supplied to the pea epicotyl epidermis (acyl donor) for 3 h at room temperature. The CMNaOH-releasable radioactivity ratio (%) illustrate the effects of PMSF on the putative cutin-to-[^{3}H]XXXGol transacylase activity. Bars indicate standard errors (*n*=3).

A value of 1% CMNaOH-releasable radioactivity/50 mg epidermis/supplied radioactivity corresponds to an absolute calculated incorporation of 128 or 145 cpm/50 mg epidermis.

Taken together, the observed ^{3}H incorporation plateau at 80 min (Fig. 62a) is proposed to be because of multiple reasons, but it was difficult to characterise them *in situ*. Therefore, only two possible mechanisms were elucidated here: (1) the favourable substrate, [^{3}H]XXXGol started being degraded from 80 min; (2) the possible cutin-to-XXXGol transacylase was also degraded after the same time.

Xyloglucan-related acceptor substrates: cutin-to-[³H]XXFGol transacylation

Besides XXXG, XXFG is another abundant building block of xyloglucan (reviewed by Takahisa and Rumi, 2011). The X represents the α-D-xylopyranosyl-(1→6)-D-glucose as in XXXG, and the F has an additional α-L-fucopyranosyl-(1→2)-β-D-galactopyranosyl segment attach to xylose at C-2 (Fry *et al*., 1993) (Fig. 65).

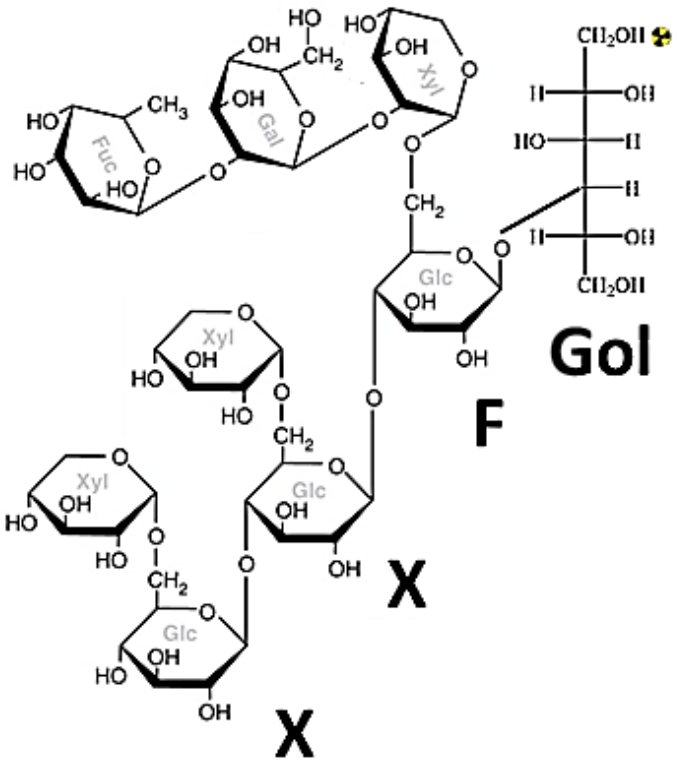

Figure 65. Structural formula of [^{3}H]XXFGol. XXFG and its radiolabelled version [^{3}H]XXFGol are structurally similar to XXXG in figure 42 except that an additional D-galactose (hexose) is glycosidically linked to the third X (from the left) via a β-1→2 bond. An L-fucose (deoxyhexose) is also glycosidically linked to the galactose via α-1→2 bond. As in figure 42, the fourth glucose (from the left, G) is the last unit in this xyloglucan building block, and in most cases, it is attached to the next building block *in muro* (no reducing end). In the laboratory, we mimicked this situation by reducing the G with NaB^3H_4 to glucitol (Gol), which does not have the oxo group at C-1 and is radiolabelled at position 1 to produce [^{3}H]XXFGol.

To test if XXFGol is also a substrate of the putative cutin transacylase, it was assayed *in situ* as above. Surprisingly, unlike ~2% of the supplied [^{3}H]XXXGol becoming incorporated via CMNaOH-labile bonds in un-denatured epidermis samples (Fig. 58b and 58a), only a trace, ~0.3% of supplied [^{3}H]XXXFol, was incorporated in this form (Fig. 66). In contrast, a much higher amount of radioactivity (~13%) was released by XEG from 1.5-h incubated un-denatured epidermis samples (Fig. 66). This XEG-releasable

radioactivity represented the XET product, which was quantitatively similar to that obtained in [^{3}H]XXXGol experiments (16%) (Fig. 74a), indicating that even though [^{3}H]XXFGol was not a preferred substrate of the putative transacylase, it was a good substrate of XET as reported before (Fry *et al*., 1993; Warneck *et al*., 1998).

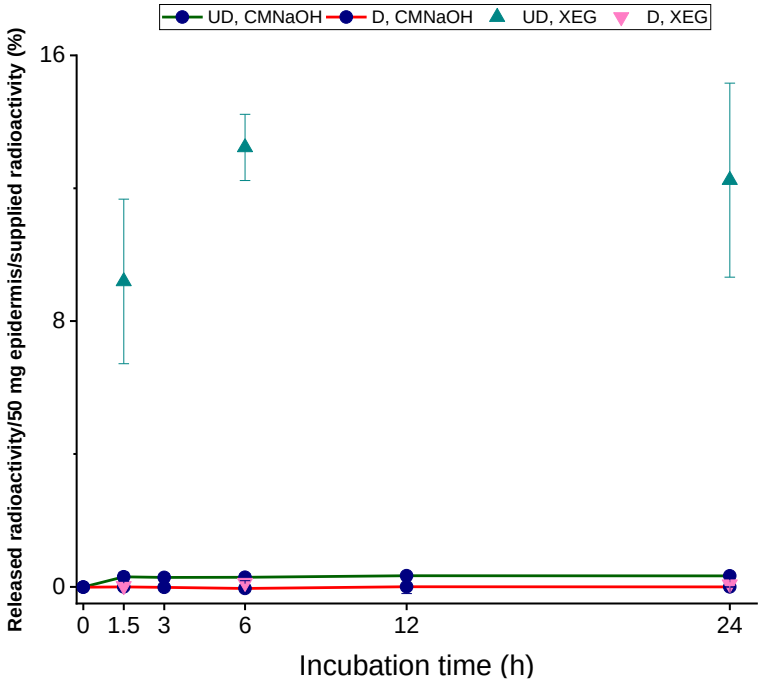

Figure 66. The putative cutin-to-[^{3}H]XXFGol transacylase activity in pea epicotyl epidermis *in situ*. Experimental details were as in figure 54, except 0.34 kBq exogenous [^{3}H]XXFGol was supplied as the acyl acceptor. The CMNaOH-releasable radioactivity ratio (%) (**navy circles**) illustrates the endogenous cutin-to-[^{3}H]XXFGol transacylase activity. The 0.1% (w/v) XEG-releasable radioactivity ratio (%) (**green** and **pink** triangle) shows the endogenous XET activity. UD: un-denatured epidermis samples. D: denatured epidermis samples (control). Bars indicate range (*n*=2).

A value of 0.1% CMNaOH- or 0.1 (w/v) XEG-releasable radioactivity/50 mg epidermis/supplied radioactivity corresponds to an absolute incorporation of 6.4 cpm/50 mg epidermis.

The big contrast of the putative cutin: [^{3}H]oligoxyloglucan transacylase activities when using [^{3}H]XXXGol and its longer side-chain version, [^{3}H]XXFGol, as substrates may gave a hint of where possibly cutin was

linked to. For example, cutin might be ester-bonded to the ‘X’ next to the ‘Gol’, and therefore the additional galactose and fucose (in ‘F’) imposed steric hinderance to the putative transacylase and the donor (cutin)’s approach, resulting in almost no product. However, a more precise suggestion as to the linking point, e.g. the glucose or xylose of the third ‘X’ and which –OH was involved can only be speculated in this thesis (more discussions later).

4.2.3 Secondary cell wall hemicellulosic oligosaccharides’ acceptor abilities

Cutin-to-[^{3}H]Man$_3$-ol transacylation

Although we hypothesized that cutin and polysaccharides are linked during rapid growth, we cannot exclude the possibility that cutin also covalently bonds to secondary cell wall components after cell expansion is ceased, especially as the pH optima of the cutin-to-oligosaccharide transacylase had suggested this (Fig. 46–46).

Homomannan (β-1→4-linked) is found in secondary cell wall hemicellulose, involved in supporting land plants mechanically and acting as a non-starch carbohydrate reservoir (reviewed by Moreira and Filho, 2008). Unlike [^{3}H]XXXGol and [^{3}H]XXFGol (Fig. 42 and 61), the –OH groups of 1→4-linked β-D-mannopyranosyl residues at C-6 point to the same direction, resulting in strong H bond formation with endogenous polysaccharide in the cuticle, and the non-covalently incorporated substrate is difficult to be removed by MFW, interfering with the covalently (e.g. ester bond) incorporated one. Thus, instead of a heptasaccharide as [^{3}H]XXXGol, a shorter mannan oligomer,

[^{3}H]Man$_3$-ol (a trisaccharide, with no reducing group) (Fig. 67) was assayed with pea epicotyl epidermis *in situ*.

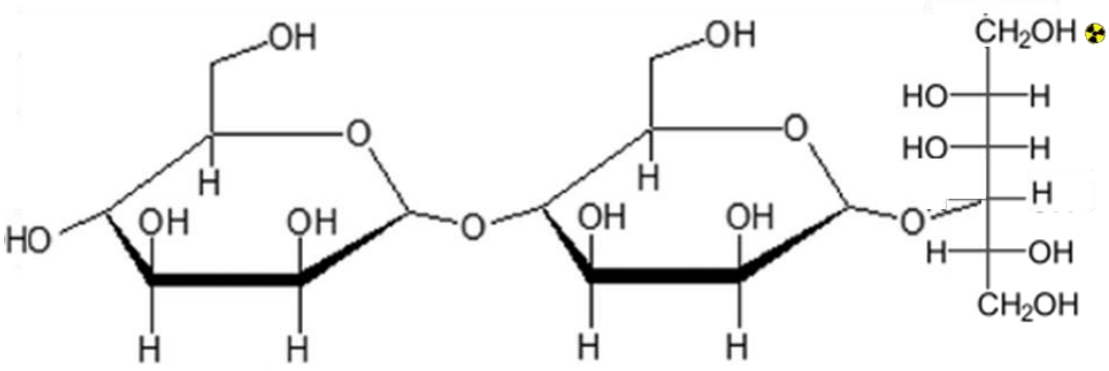

Figure 67. Structural formula of [^{3}H]Man$_3$-ol. Tritiated labelled Man$_3$-ol ([^{3}H]Man$_3$-ol) is composed of three 1→4-linked β-D-mannopyranosyl residues whilst the last one was reduced to mannitol and tritiated labelled at C-1.

After a 24-h incubation under the standardised conditions, no enzymic incorporation was seen on comparing the un-denatured group with the denatured control ($P > 0.05$) (Fig. 68), suggesting that cutin does not link to the secondary cell wall mannan.

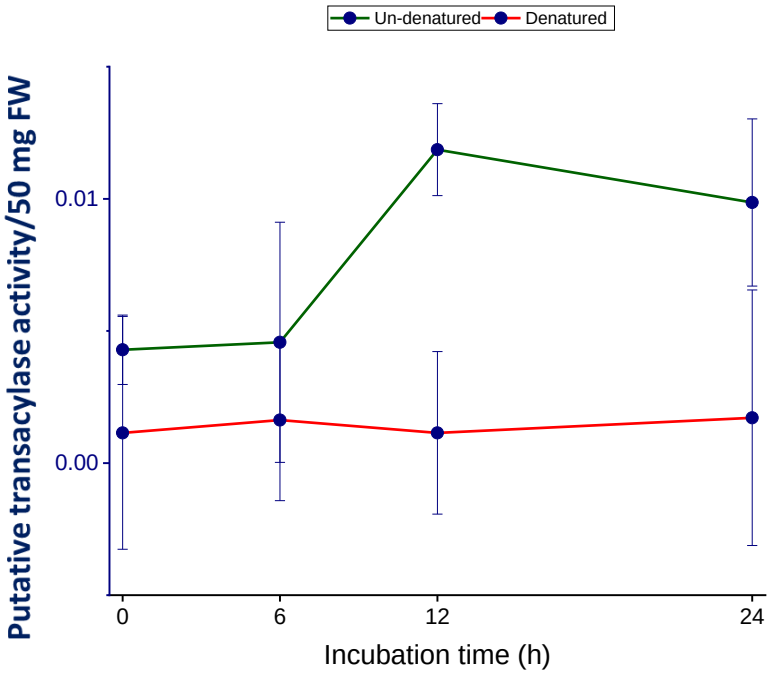

Figure 68. The proposed cutin-to-[^{3}H]Man$_3$-ol transacylase activity in pea epicotyl epidermis *in situ*. Experimental details were as in figure 54, except 0.26 kBq exogenous [^{3}H]Man$_3$-ol was supplied as the acyl acceptor. The CMNaOH-releasable radioactivity ratio (%) illustrates the endogenous cutin-to-[^{3}H]Mna$_3$-ol transacylase activity. Green lines: un-denatured epidermis samples (UD). Red lines: denatured epidermis samples (D). Bars indicate standard errors (*n*=3).

A value of 0.01% CMNaOH-releasable radioactivity/50 mg epidermis/supplied radioactivity corresponds to an absolute incorporation of 1 cpm/50 mg epidermis.

Cutin-to-[^{3}H]Xyl$_5$-ol transacylation

Homoxylan, composed of β-1→4-linked xylanopyranosyl residues, is another common secondary cell wall hemicellulose. It plays a role in strengthening plants mechanically as mannan does (reviewed by Zhong *et al*., 2019).

I assayed [^{3}H]Xyl$_5$-ol (a pentasaccharide with no reducing group) (Fig. 69) *in situ* as above. Similar result was obtained as [^{3}H]Man$_3$-ol: there was no incorporation into un-denatured epidermis samples (Fig. 70). The

incorporation was only higher in un-denatured epidermis samples than in the denatured control at 6 h, but further chemical and enzymic degradation results indicated that it was because of the un-through MFW wash (data not shown).

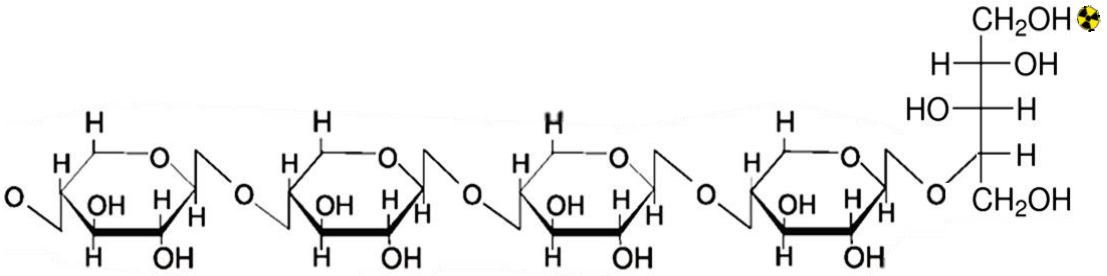

Figure 69. Structural formula of [^{3}H]Xyl$_5$-ol. Tritiated labelled Xyl$_5$-ol ([^{3}H]Xyl$_5$-ol) is composed of five 1→4-linked β-D-xylanopyranosyl residues whilst the last one was reduced to xylitol and tritiated labelled at C-1.

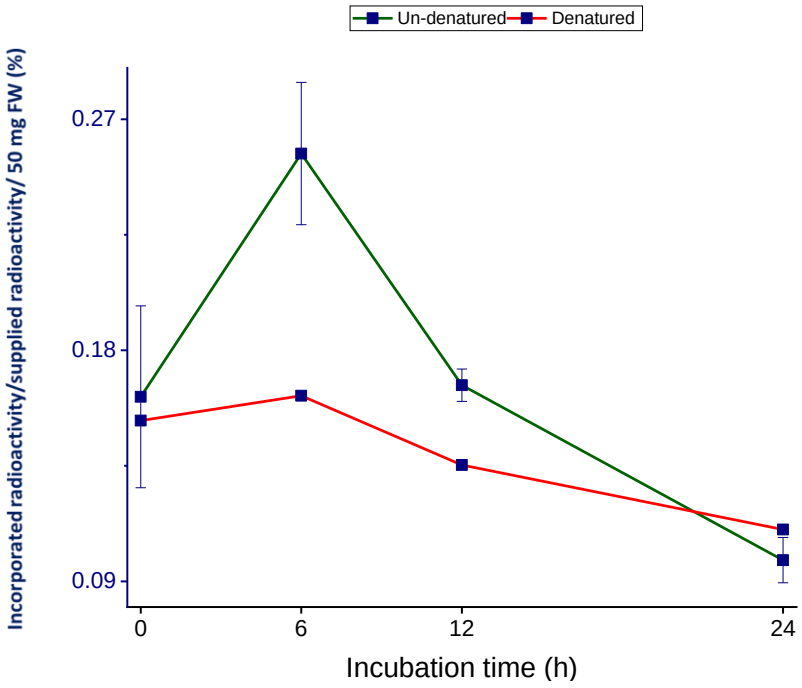

Figure 70. The proposed cutin-to-[^{3}H]Xyl$_5$-ol transacylase activity in pea epicotyl epidermis *in situ*. Experimental details were as in figure 54, except 0.85 kBq exogenous [^{3}H]Xyl$_5$-ol was supplied as the acyl acceptor. The CMNaOH-releasable radioactivity ratio (%) illustrates the endogenous cutin-to-[^{3}H]Xyl$_5$-ol transacylase activity. Green lines: un-denatured epidermis samples (UD). Red lines: denatured epidermis samples (D). Bars indicate standard errors (n=3). No bars for the 'denatured' group (n=1).

A value of 0.1% total incorporated radioactivity/50 mg epidermis/supplied radioactivity corresponds to an absolute incorporation of 16 cpm/50 mg epidermis.

In summary, these two negative results suggested that cutin is likely to only link with primary cell wall components, especially XXXG domains in xyloglucan.

4.3 Cutin-to-XGO transacylase *ex situ*

In the *in-situ* experiments above, the endogenous putative transacylase was believed to be nearby cutin, in a hydrophobic environment. To test whether the transacylase activity is still detectable when the environment is purely aqueous, I extracted apoplastic enzymes from frozen and thawed dark-grown pea epicotyl epidermis (Chapter 2), followed by incubating the extract with prepared pea epicotyl epidermis (no endogenous active enzymes, no wax; Chapter 2) and the best performing radio-labelled substrate, [^{3}H]XXXGol.

Like in *in-situ* assays (e.g. Fig. 58b), [^{3}H]XXXGol was incorporated into epidermis in a form capable of being released back to solution by CMNaOH hydrolysis (Fig. 71), indicating that the putative transacylase was still active after being extracted into aqueous buffer. The optimum pH (6.5) decided by *in-situ* assays was used, and high (350 mM) ionic strength buffer (succinate, Na^{+}) did not show any significant benefit compared with 10-fold diluted buffer (35 mM) ($P > 0.05$) (Fig. 71), suggesting that the putative transacylase may not be ionically bonded to epidermis (i.e. concentrated buffers can compete with enzymes in forming ionic bonds to epidermis).

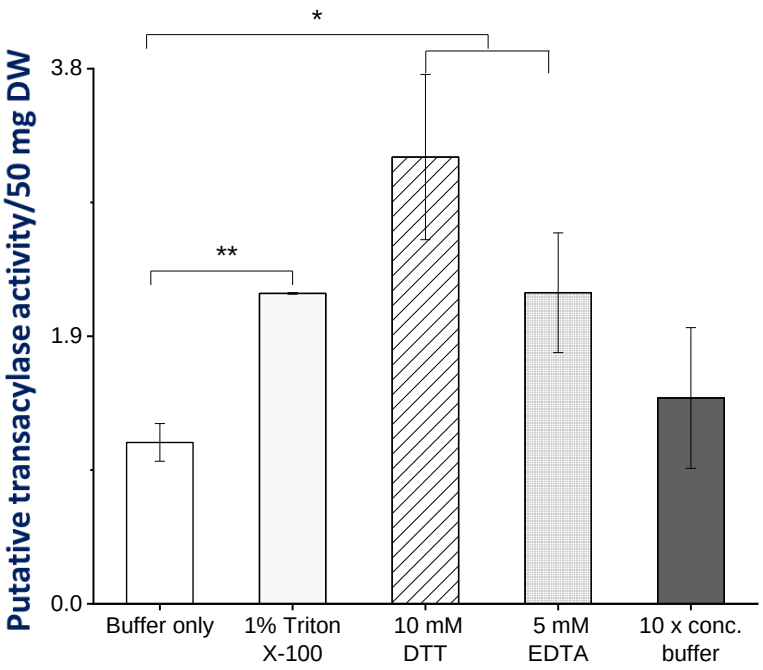

Figure 71. The optimization of the putative cutin-to-[^{3}H]XXXGol transacylase extraction buffer for *ex-situ* assays. Low (35 mM; the routine concentration for *in-situ* assays) and high (10 X) concentrations of succinate (Na^+) (pH 6.5) buffers were used to extract apoplastic enzymes of pea epicotyl epidermis with or without the addition of 1% (v/v) Triton X-100, 10 mM DTT and 5 mM EDTA. The prepared (dewaxed) pea epicotyl epidermis (50 mg dry weight; acyl donor) without active endogenous enzymes was incubated with 300 µl apoplastic enzyme extract and 0.37–0.53 kBq exogenous [^{3}H]XXXGol (acyl acceptor) at room temperature for 1 day. The CMNaOH-releasable radioactivity ratio (%) illustrates the effects of buffers on the cutin-to-[^{3}H]XXXGol transacylase activity. Bars indicate range (n=2). *: $P < 0.05$. **: $P < 0.01$.

A value of 1% CMNaOH-releasable radioactivity/50 mg epidermis/supplied radioactivity corresponds to an absolute incorporation of 70–100 cpm/50 mg epidermis.

Addition of Triton X-100 (a non-ionic detergent to destroy cell membranes), EDTA (a metal ion chelator) and DTT (a reducing agent) (Konigsberg, 1972) to the extraction buffer improved [^{3}H]XXXGol incorporation significantly ($P < 0.01$ or 0.05) (Fig. 71). These effects suggested that (1) the putative transacylase may be susceptible to existing Ca^{2+}-dependent proteases

(Ayache *et al*., 2006) because EDTA improved the proposed transacylase activity and/or extraction; (2) the putative transacylse does not require a metal ion co-factor, and some divalent ions in epidermis may even harm its activity also because EDTA was beneficial; (3) its 3-dimensional (3-D) structure may allow cysteine residues to form undesired disulphide bonds because DTT improved the activity.

In a repeat experiment, the high ionic strength buffer did not have impact on the putative transacylase extraction efficiency consistently; 10 mM DTT increased the putative transacylase products' quantity, but not as much as the 1% (v/v) Triton X-100 and 5 mM EDTA (Fig. 72) did. Combining Triton X-100 and EDTA together did not harm the transacylase activity and extraction, but also did not dramatically improve it compared with Triton X-100 alone added to the high-concentration buffer (Fig. 72). The addition of Triton X-100 to the low-concentration buffer also improved the transacylase activity and extraction, but the CMNaOH-releasable ^{3}H was only 67% of the more concentrated buffer group (Fig. 72). The rest of the combinations generated similar amount of CMNaOH-releasable radioactivity (Fig. 72).

Comparing all the samples together, the 350 mM succinate (Na^{+}) buffer, pH 6.5 with 1% (v/v) Triton X-100 was the best to extract and keep the putative cutin-to-XXXGol transacylase activity (Fig. 72), and therefore it was used for subsequent *ex-situ* assays. Moreover, the addition of EDTA benefited the proposed transacylase activity, and thus the effect of metal ions on the activity was not tested here as in Chapter 3.

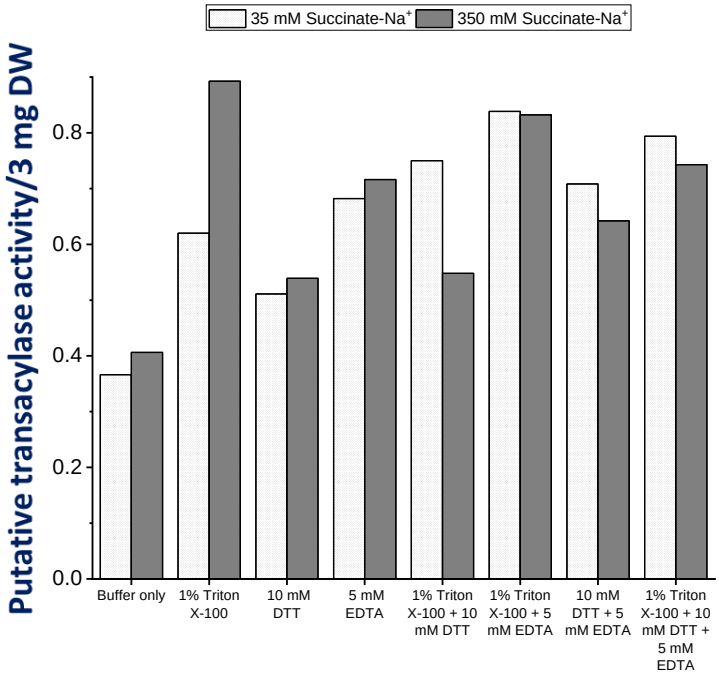

Figure 72. A repeat test of the optimizing putative cutin-to-[^{3}H]XXXGol transacylase extraction buffers for *ex-situ* assays. Experimental details were as in figure 63, except 3 mg prepared pea epicotyl epidermis was incubated with 0.69–0.74 kBq exogenous [^{3}H]XXXGol (acyl acceptor. And all the possible combinations of Triton X-100, DTT and EDTA were also tested. The CMNaOH-releasable radioactivity ratio (%) illustrates the buffers' effects on the cutin-to-[^{3}H]XXXGol transacylase activity. No bars (n=1).

A value of 1% CMNaOH-releasable radioactivity/3 mg epidermis/supplied radioactivity corresponds to an absolute incorporation of 130–140 cpm/3 mg epidermis.

4.4 Cutin-to-XXXGol transacylase products analysis

It has been reproducibly observed that [^{3}H]XXXGol can be enzymically incorporated into pea epicotyl epidermis *in-* and *ex-situ* (e.g. Fig. 58b and 66). The next question is which epidermal component was enzymically bonded with [^{3}H]XXXGol, and whether [^{3}H]XXXGol was modified during and/or after being incorporated. Thus, the enzymic product required to be identified.

4.4.1 Un-incorporated radioactivity and wax–[^{3}H]XXXGol conjugate in the enzymic products

I incubated frozen/thawed, cold-buffer-washed dark-grown pea epicotyl epidermis with [^{3}H]XXXGol for 3 h under the optimized conditions, and after being washed in MFW (5/1/5, v/v/v), the insoluble residue was again washed in toluene, CM (2/1, v/v) and CMW (10/10/3, v/v/v) sequentially as in Chapter 3, to thoroughly remove un-bonded radioactivity and possible hydrophobic interferences, such as wax oligoester–[^{3}H]XXXGol product. Oligoesters are proposed to be soluble in acidic and neutral organic solvents, whereas cutin (polyester) and its conjugate are insoluble.

The MFW wash was analysed by paper chromatography. Like the TLC analysis results (Fig. 62b), the majority of the supplied [^{3}H]XXXGol had been degraded to [^{3}H]XXGol and some [^{3}H]XGol (Fig. 73a). There was no detectable remaining [^{3}H]XXXGol, possibly because of the complete hydrolysis and/or technical reasons (i.e. the small quantity of [^{3}H]XXXGol was spread out into a 3–4-cm smear on the chromatography paper, and therefore not detectable in individual 1-cm strips) (Fig. 73a). [^{3}H]XXXGol was not hydrolysed in the denatured control as expected (Fig, 67b).

There was no peak migrating faster than [^{3}H]XGol did (Fig. 73a), indicating that there is no wax oligo-ester–[^{3}H]XXXGol conjugate dissolved in MFW because the more hydrophobic compounds are proposed to move faster in this system.

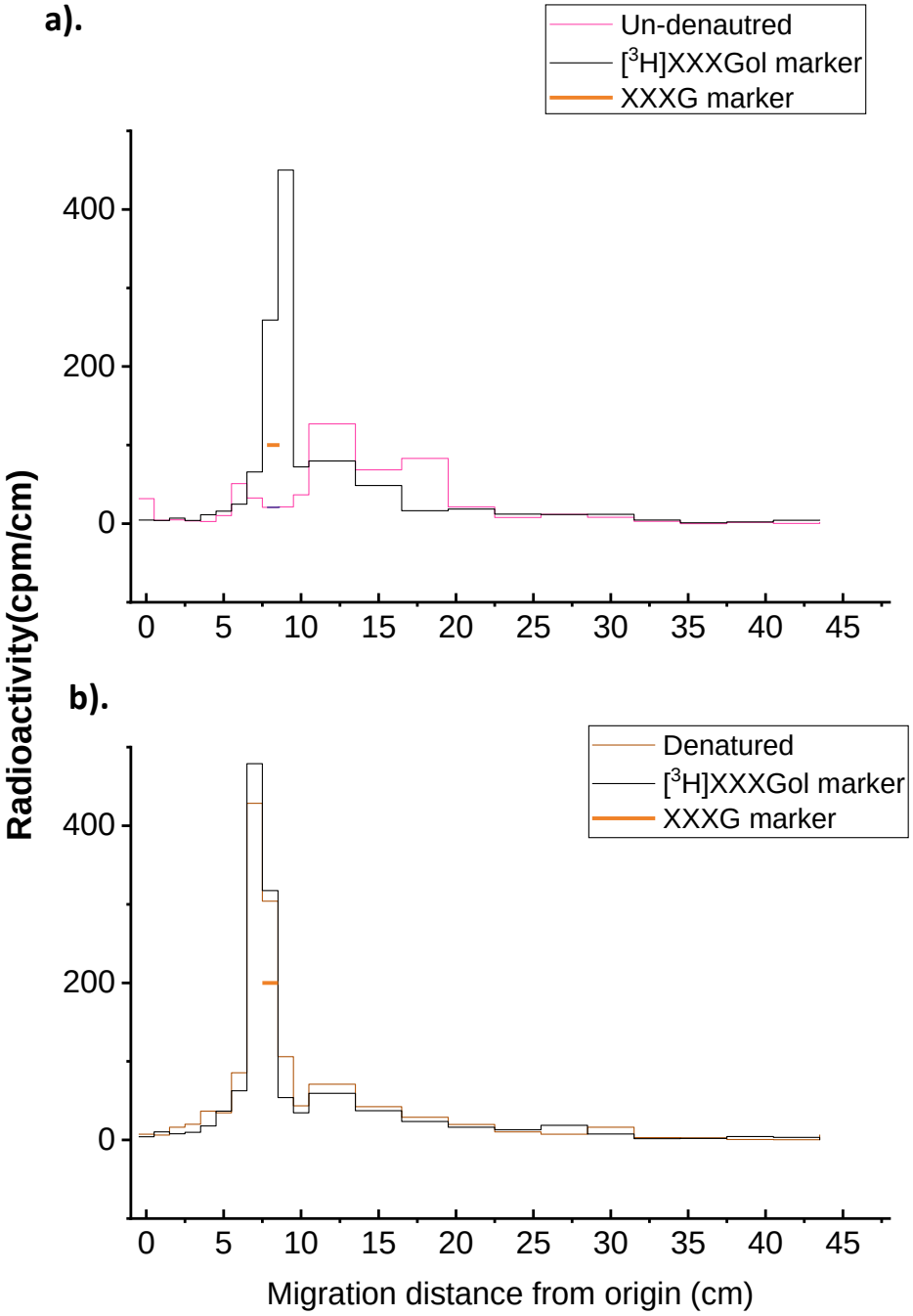

Figure 73. Chromatographic analysis of the acidified methanolic wash of [^{3}H]XXXGol-incubated epidermis samples. Blotted-dry pea epicotyl epidermis (100 mg fresh weight; acyl donor) with (a) or without (b) active endogenous transacylases was incubated with 13.7 kBq exogenous [^{3}H]XXXGol (acyl acceptor) in 600 µl pH 6.5 buffer at room temperature for 3 h. MFW (5/1/5) was used to stop reactions and remove un-incorporated ^{3}H-oligosaccharides. The supernatant was dried, and re-dissolved in a small volume of MFW, and loaded onto Whatman No. 1 chromatography paper [butan-1-ol/pyridine/water (BPW), 4/3/4, v/v/v, 48 h], together with external [^{3}H]XXXGol (**black**) and XXXG (**orange**) markers. The solubilised

substances were identified by scintillation counting the paper strips (spatial resolution: 1 cm) (unit: cpm).

Radioactivity removed by the next three hydrophobic solvents (toluene etc.) from un-denatured epidermis samples accounted for only trace proportions of the supplied radioactivity (~0.01%–0.06%) (Fig. 74a), and the value was even decreasing from toluene to CMW, suggesting that (1) the un-bonded radioactivity has been efficiently removed; and (2) the CMW would provide a good control for later CMNaOH. Moreover, the very low radioactivity solubilized in neutral hydrophobic solvents suggested that (3) no wax oligo-ester–[^{3}H]XXXGol conjugate had been formed (Fig. 72a) because otherwise it could have been dissolved in these neutral hydrophobic solvents.

The chemical analysis of these three extracts was not carried out because the negligible radioactivity may be under the detection limit of the employed chromatographic techniques.

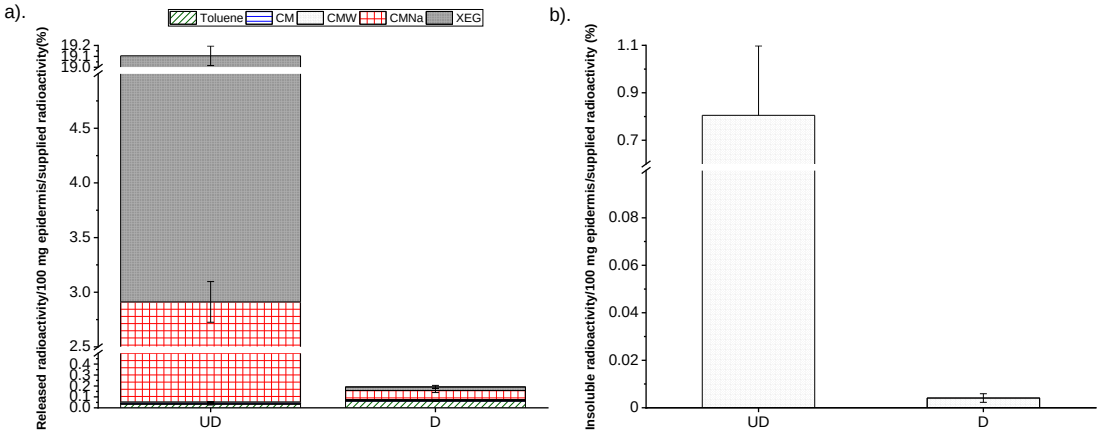

Figure 74. Quantification of all the chemical extractions and MFW-insoluble residues of [^{3}H]XXXGol-incubated pea epicotyl epidermis. (a) After an MFW wash, aliquots of the supernatants of the toluene, CM (2/1, v/v), CMW (10/10/3, v/v/v), CMNaOH (10/10/3, v/v/v) and 0.1% (w/v) XEG treatments of the [^{3}H]XXXGol (13.7

kBq)-incubated pea epicotyl epidermis (100 mg) were scintillation counted. (b) The insoluble residues after all the extraction and degradation treatments were scintillation counted. UD: un-denatured epidermis samples. D: denatured epidermis samples (control). Bars indicate range (*n*=2).

A value of 1% incorporated radioactivity/100 mg epidermis/supplied radioactivity corresponds to a calculated (for CMNaOH) or absolute (for XEG etc.) incorporation of 2600 cpm/100 mg epidermis.

4.4.2 Possible protein–[^{3}H]XXXGol conjugate in the enzymic products

Besides cutin and xyloglucan, another possible epidermal component to be covalently bonded with [^{3}H]XXXGol is cell wall protein. The amino acids, such as asparagine and glutamine, whose β- and γ-carboxy groups are activated by amide (–$CONH_2$), enabling them to potentially act as acyl donors (reviewed by Lamport, 1970). Thus, proteinase K was applied to the CMW-washed epidermis samples, to look for amino acid–[^{3}H]XXXGol conjugate, or even free [^{3}H]XXXGol if proteinase K also has esterase activity (reviewed by Hedstrom, 2002). Like Chapter 3 results, proteinase K did not release any ^{3}H back into solution (data not shown here), indicating that no [^{3}H]XXXGol is covalently bonded with cell wall proteins, and the proteinase K employed does not catalyse ester hydrolysis.

4.4.3 Probable cutin–[^{3}H]XXXGol conjugate in the enzymic products

After the proteinase K digestion, the epidermis samples were proposed to only contain two classes of enzyme products: (1) transacylase and (2) XET; and they should be carefully distinguished from each other.

Lipase hydrolyses aqueous-insoluble esters (Chahinian and Sarda, 2009). However, a commercial lipase from *Aspergillus niger* (activity shown in

Appendix 2) was not able to release ^{3}H from un-denatured epidermis samples, and it also has an XEG activity (preliminary data not shown), which interfered with the expected transacylase products. Thus, it was not used to identify the cutin–[^{3}H]XXXGol conjugate.

A cutinase (*AN7541.2*, activity was predicted by aligning nucleotide sequence with known cutinases from *A. fumigatus* and *A. oryzae*) (Liu *et al*., 2009; Baker *et al*., 2012; Ping *et al*., 2017), encoded by an *A. nidulans* gene, was heterologously produced in *P. pastoris* (strain: SB). The cutinase was harvested by isolating the culture medium because it was designed to be secretory (Bauer *et al*., 2006) (Appendix 1). Nevertheless, similar to the results in Chapter 3 with [^{3}H]HHA, this cutinase also did not release radioactivity from un-denatured epidermis samples fed [^{3}H]XXXGol (data not shown here), even though it catalysed *p*-NPP hydrolysis (Appendix 1).

So far, neither the general nor the specific lipase can hydrolyse the putative cutin–[^{3}H]XXXGol ester bonds, and thus we used a general chemical method, CMNaOH (~0.5 M NaOH) as above, to hydrolyse cutin. It released ~3% of the supplied radioactivity from the un-denatured epidermis samples, but only ~0.1% from the denatured control, indicating that the released radioactivity had been incorporated enzymically (Fig. 74a) as other *in-situ* results above. The remained unextracted ^{3}H was ~16% of the supplied radioactivity was putatively XET product (Fig. 74a), much higher than the CMNaOH-liable product as expected (i.e. the XET activity is proposed to be higher than the putative cutin-to-xyloglucan transacylase activity due to (1) cutin and xyloglucan are in two separate layers in epidermis, naturally less

physical interaction compared with xyloglucan component-to-another one; (2) a non-intact xyloglucan or cutin can be problematic, but the lack of cutin–xyloglucan conjugates may not cause dramatic changes.

To study this alkali-labile product more thoroughly, after being neutralized, the CMNaOH hydrolysis supernatant was analysed by Bio-Gel P-2 column, which resolve compounds based upon their molecular weights (size exclusion column, Chapter 2) (Fig. 75). This technique was validated by comparing the ratio of $K_{av(XXXG)}$ to $K_{av(XLLLG)}$ (~1.2) (Fig. 75) with the published data (McDougall and Fry, 1988).

The XET products, xyloglucan–[^{3}H]XXXGol conjugates, were proposed to be stable in alkali as stated above, only the ester-bonded, putative cutin–[^{3}H]XXXGol conjugates can release [^{3}H]XXXGol or its modified products in CMNaOH because of the ester bonds. In summary, even if the XET products were solubilised by CMNaOH, they would be eluted earlier than the proposed transacylase products because they should remain as oligomers and/or polymers.

A small portion of each eluent fraction was quantified by scintillation counting (Fig. 74a) and another aliquot was analysed by TLC (Fig. 75) to explore the eluted identities of the solubilised ^{3}H-labelled products. Unexpectedly, from the un-denatured epidermis samples, there was no radioactivity peak co-eluting with the internal marker XXXG (Fig. 75a), indicating that the incorporated [^{3}H]XXXGol was otherwise modified.

The first radioactive peak (fraction no. 12) was co-eluted with heavier oligosaccharides (e.g. XLLG, a nonasaccharide) than the initially supplied [^{3}H]XXXGol (a heptasaccharide, Fig. 75a). It is unlikely to represent oligo-xyloglucan–[^{3}H]XXXGol conjugates, even small ones, produced by XET activity since these would not be expected to be soluble in CMNaOH, having failed to dissolve in MFW and CMW (Fig. 74a). Unless the increase of OH^- ions compete with a xyloglucan polymer to form H-bonds with another one, resulting in solubilizing some short XET product.

The second peak (fraction no. 19) from the un-denatured epidermis samples was co-eluted with XG (trisaccharide) and glucose, smaller than the initially supplied [^{3}H]XXXGol (Fig. 75a). Since only the ester-bonded products can release compounds with the molecular sizes ≤ [^{3}H]XXXGol (i.e. glycosidically bonded products should remain in oligo- and/or poly-mers), the second peak was very likely to be the proposed transacylase product, whose initial [^{3}H]XXXGol moiety had also been degraded as well as the non-incorporated oligosaccharides (Fig. 73).

In contrast, the denatured epidermis sample released a small peak (fraction no. 11) that eluted before XXXG, which may represent a much smaller (~40 times) quantity of oligo-xyloglucan–[^{3}H]XXXGol conjugates than in the un-denatured epidermis samples (Fig. 75b). The majority of the radioactivity the second peak (fraction no. 14), which co-eluted with the XXXG internal marker (Fig. 75b), suggesting that the putative cutin-to-XXXGol transacylase may not be completely denatured, but the glycosidases were. Thus, I hypothesized that the boiling process denatured the enzymes localised in cell wall (XET,

glycosidases) more than the one in and/or close to cutin layer, such as the putative cutin-to-XXXGol transacylase.

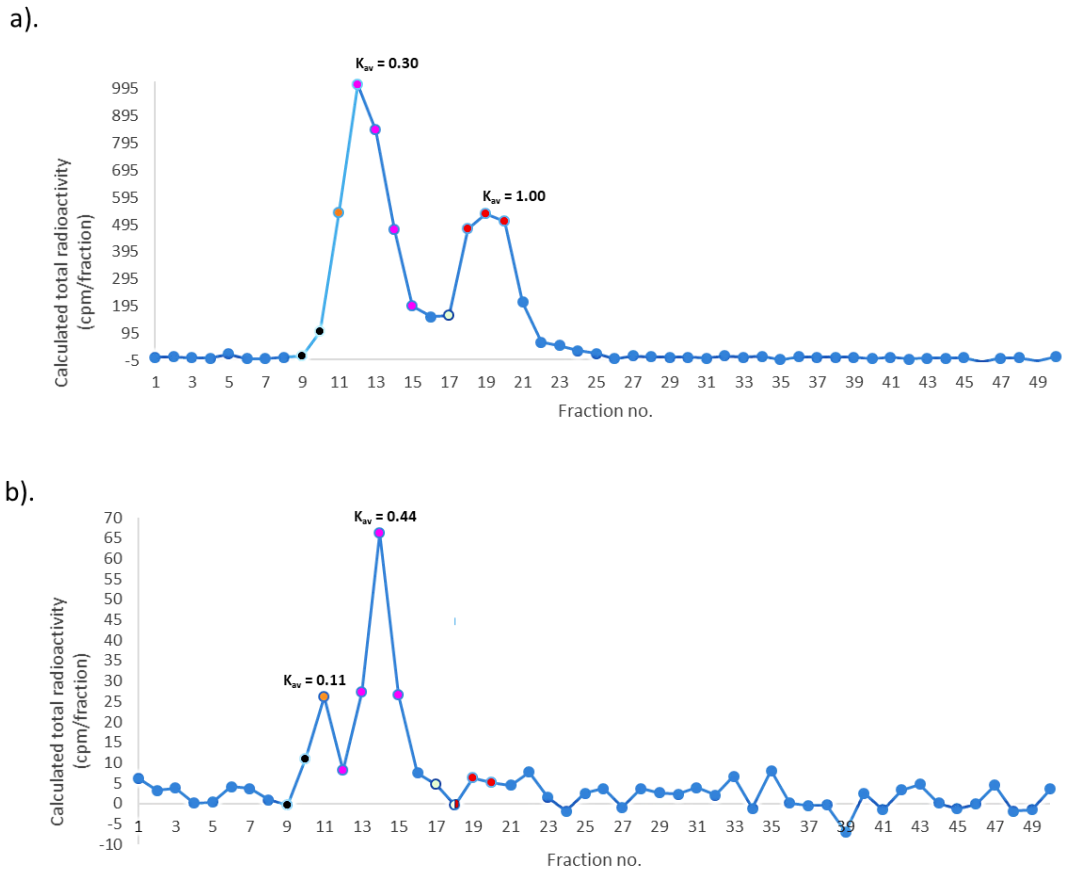

Figure 75. Chromatographic analysis of the CMNaOH-hydrolysed radioactive material from [^{3}H]XXXGol-incubated pea epicotyl epidermis. The neutralized CMNaOH (10/10/3, v/v/v) supernatant was dried in a SpeedVac and re-dissolved in 0.5% (w/v) chlorobutanol, together with five non-radio-labelled internal markers: dextran (polysaccharide), xyloglucan oligosaccharides (XLLG, XXLG and XXXG) and glucose. The compounds dissolved in CMNaOH were well resolved in Bio-Gel P-2 column (volume: 120 ml; flowrate: 0.5 ml/min) according to their molecular weight (3 ml x 50 fractions). An aliquot of each fraction was scintillation counted to quantify the dissolved radioactivity. And the eluted compounds were roughly identified by comparing their fraction numbers with the internal markers', which were visualized on TLC (BAW, 2/1/1, v/v/v, 3 ascents). **Black** dots: polysaccharide internal marker. **Orange** dots: big oligosaccharides. **Magenta** dots: short oligosaccharides (XLLG, XXLG, XXXG). **Green** dots: XG. **Red** dots: glucose. Un-denatured epidermis samples (a) and denatured (b) were compared.

K_{av} was annotated for each peak and calculated as follows: the fraction number as the centre elution of a certain compound – the fraction number as the centre elution of dextran (V_0) / the fraction number as the centre elution of glucose (V_i) – V_0.

To identify the second peak [K_{av} = 1.00, suggesting the degree of polymerisation (DP) ~ 3 because for the heptasaccharide, XXXG, the DP ≈ 0.44] (Fig. 75), the corresponding fractions (no. 18–20) were further analysed by paper chromatography, which suggested that the ^{3}H peak comprises [^{3}H]XXGol and [^{3}H]XGol, identified by comparing the scintillation counting data with the external radioactive and non-radioactive markers (Fig. 76).

However, this result was puzzling: the previous *in-situ* assays showed that [^{3}H]XXGol and [^{3}H]XGol's acceptor abilities were very poor (Fig. 60a) (0.2% and 0.03% of the supplied radioactivity was released by CMNaOH respectively), but the transacylase product was dominated by putative cutin–[^{3}H]XGol and cutin–[^{3}H]XXGol conjugates. Moreover, the ratio of [^{3}H]XGol/[^{3}H]XXGol increased in the products than in the substrate mixture (Fig. 73a and 70). Hence, I suspect that the cutin–[^{3}H]XXXGol or even cutin–[^{3}H]XXGol conjugates were formed first, and then the 'cutin-substituted' [^{3}H]XXXGol and [^{3}H]XXGol were better substrates for α-D-xylosidase than the free oligosaccharides (more discussion later).

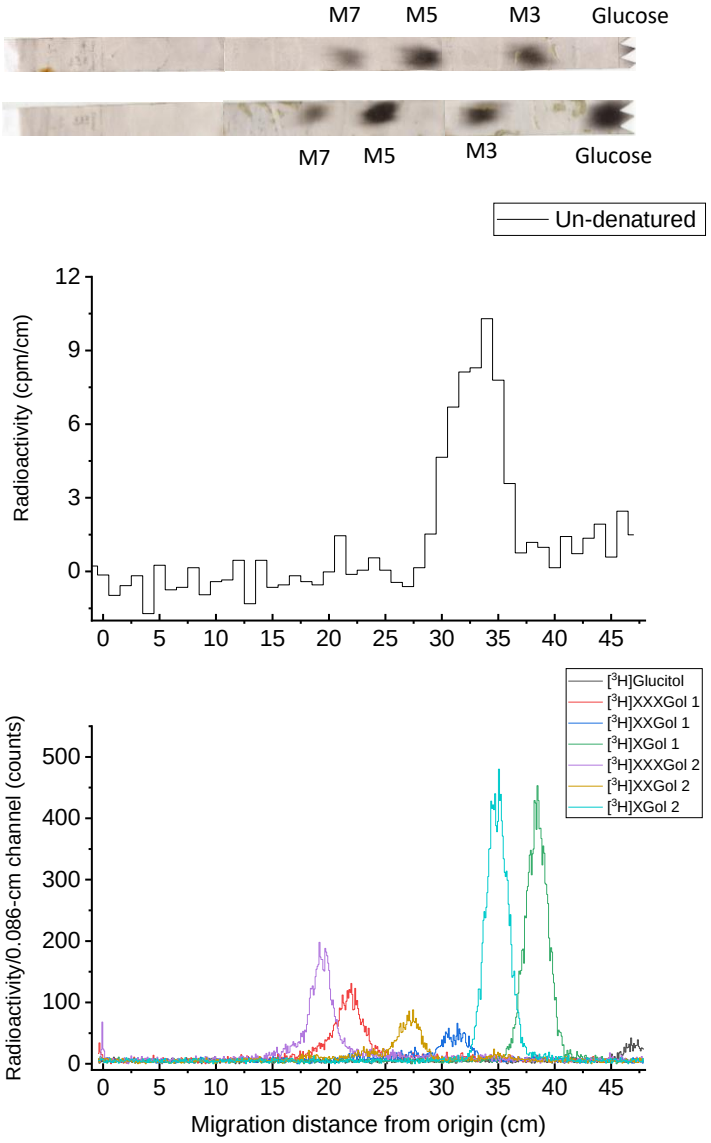

Figure 76. Paper-chromatography analysis of the Bio-Gel P-2 fractions containing the putative cutin-to-[^{3}H]XXXGol transacylase products. The fractions 18-20 were pooled and dried in a SpeedVac, and then re-dissolved in a small volume of 0.5% (w/v) chlorobutanol, which was then loaded onto Whatman No. 3 chromatography paper (BPW, 4/3/4, v/v/v, 46.5 h), together with four external non-radiolabelled markers: 40 µg glucose, 60 µg maltotriose (M3), maltopentaose (M5) and maltoheptaose (M7) (top); and four external radio-labelled markers: [^{3}H]glucose, [^{3}H]XGol, [^{3}H]XXGol and [^{3}H]XXXGol (bottom). All the markers were loaded at both sides (left and right) of the fractions 18–20 sample. The sample lane was then cut into 1-cm strips, to be scintillation counted (unit: cpm) (middle). The non-radiolabelled external markers were stained by silver nitrate. The radiolabelled external markers were radio-scanned for 1 h per lane (spatial resolution: 0.086 cm) (unit: counts).

In summary, a measurable trace of XET product was found to be dissolved in CMNaOH (~0.9% of the supplied radioactivity), and even contributed nearly half of the CMNaOH-releasable radioactivity (~42%) (calculated from Fig. 75a). Despite this interference, putative cutin-to-[^{3}H]XXXGol and -[^{3}H]XXGol transacylase products were also found (~0.6% of the supplied radioactivity; ~27% of the CMNaOH-releasable radioactivity) (calculated from Fig. 75a).

This tandem chromatographic analysis of CMNaOH-releasable ^{3}H was repeated in an independent experiment with the incubation time shortened to 80 min (minimising the time available for hydrolysis of the supplied acceptor substrate by α-D-xylosidase and β-D-glucosidase action), in order to test whether the initially formed ester-bonded ^{3}H could be mainly in the form of [^{3}H]XXXGol (Fig. 77).

The un-bonded ^{3}H (remaining methanol-soluble) was also analysed to give a comparison with the putative ester-bonded products. Consistent with Fig. 62b, the un-bonded [^{3}H]XXXGol was partly degraded to [^{3}H]XXGol ([^{3}H]XXGol / [^{3}H]XXXGol ≈ 0.25) after 80-min incubation; the imperfect alignment between samples and markers could be because of the liberation of epidermal sugars into the supernatant (Fig. 77a). Alternatively, the 'heptasaccharide' [^{3}H]XXXGol-annotated peaks in MFW washes may represent products of trans-α-xylosidase activity, such as the hexasaccharides [^{3}H]GXXGol and [^{3}H]VXGol and the octasaccharide [^{3}H]VXXGol (Franková and Fry, 2012). However, there was no hint of such products in other comparable experiments (Fig. 59, 58 and 67), and also GXXGol is not stable in the presence of β-D-glucosidase activity (Miyamato

et al., 1997), suggesting that the peaks may indeed be remaining intact [^{3}H]XXXGol (Fig. 77a), which was clearly observed in Fig. 62b.

I expected to capture the CMNaOH-releasable [^{3}H]XXXGol being co-eluted with XXXG from the Bio-Gel P-2 column this time because the short incubation time should not allow appreciable degradation, unlike in Fig. 73. However, a pattern was obtained similar to that in Fig. 75a: a higher peak of ^{3}H was co-eluted with large oligosaccharides (K_{av} = 0.11), which were putatively longer than the initially supplied [^{3}H]XXXGol; and the lower peak (K_{av} = 0.89) was co-eluted with a putative trisaccharide, XG, again even though there was no [^{3}H]XGol formed in the incubation mixture (Fig. 77a and 71b).

The fractions constituting the lower ^{3}H peak (fraction no. 17–19) were pooled as in the last experiment, and further analysed by paper chromatography (Fig. 77c). By comparing the Bio-Gel-eluted fractions with radioactive and non-radioactive markers, I found that [^{3}H]XXXGol (the peak shoulder) and [^{3}H]XXGol (the peak summit) comprise the 'trisaccharide'-co-eluted ^{3}H (Fig. 77c: they are not separated well by the paper chromatography, maybe because the ~3 mg internal markers interfered with running), which was not expected. This finding suggested that the Bio-Gel P-2 column may not separate compounds based on their molecular weights precisely, making it a facilitating tool rather than a sole one in this project. Based on the hypothesis that only ester-bonded products can release the compounds with molecular weight ≤ [^{3}H]XXXGol in alkali, I conclude that the putative transacylase products in this experiment were cutin–[^{3}H]XXXGol and cutin–[^{3}H]XXGol

(Fig. 77c). Noticeably, the [^{3}H]XXGol/[^{3}H]XXXGol ratio became higher in the putative transacylase products than in the substrates (Fig. 77a and c), consistent with the previous observation (Fig. 73 and 70) and agreeing with the hypothesis: the cutin-linked [^{3}H]XXXGol is a better substrate for glycosidases than the free oligosaccharides.

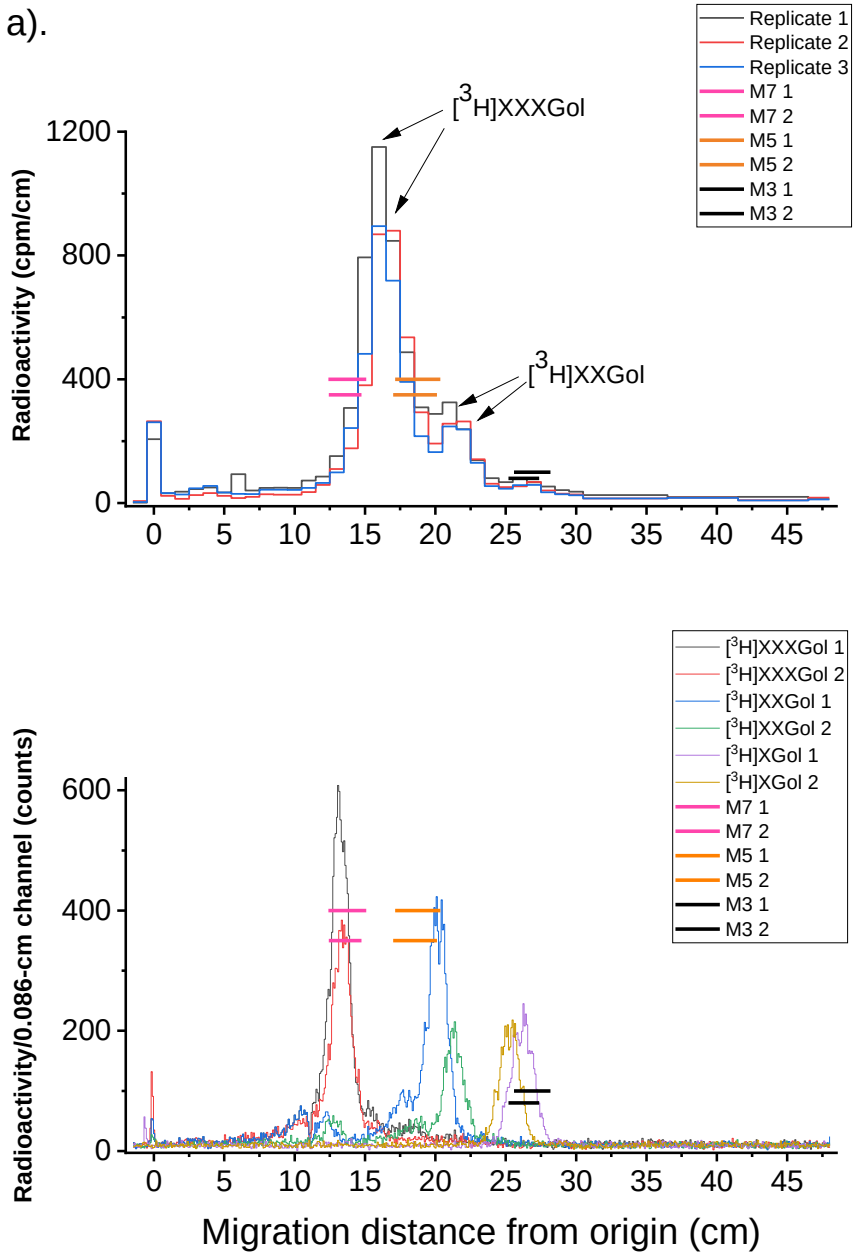

b).

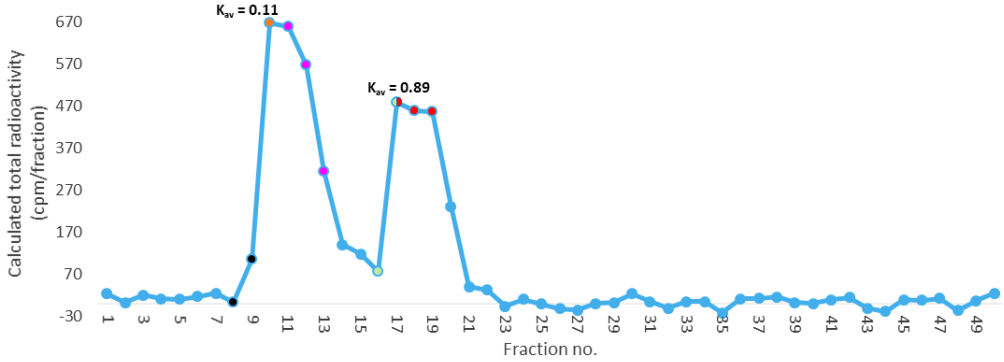

c).

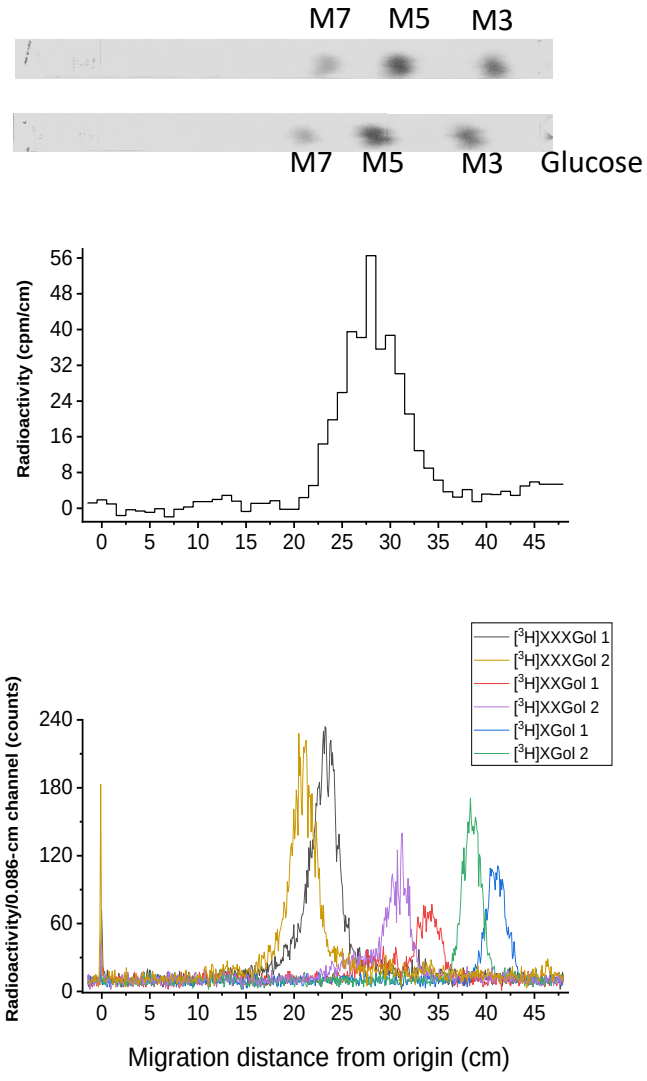

Figure 77. Chromatographic analysis of unincorporated [^{3}H]XGOs and cutin-esterified [^{3}H]XGOs in an 80-min incubated *in-situ* assay. Experimental details were as in figure 67–70, except 80 mg pea epicotyl epidermis (acyl donor) was

incubated with 5.4 kBq [^{3}H]XXXGol in 0.48 ml pH 6.5 buffer at room temperature for 80 min. (a) Paper chromatographic (BPW, 4/3/4, 46 h) analysis of MFW-soluble products; the positions of non-radioactive external markers are marked by coloured horizontal lines; profiles of radioactive markers are also shown (bottom) (radio-scanned: 40 min per lane). (b) Size-exclusion chromatographic (Bio-Gel P-2) analysis of CMNaOH-releasable radioactivity (3 ml x 50 fractions; flowrate = 0.5 ml/min). K_{av} values were calculated as in figure 69. **Black** dots: polysaccharide internal marker. **Orange** dots: big oligosaccharides. **Magenta** dots: short oligosaccharides (XLLG, XXLG, XXXG). **Green** dots: XG. **Red** dots: glucose. (c) Paper chromatographic (as in a) analysis of the radioactivity peak co-eluted with XG (trisaccharide) plus glucose in (b); silver-stained non-radioactive markers: 40 µg glucose, 80 µg each of maltotriose (M3), maltopentaose (M5) and maltoheptaose (M7) at top, radioactive markers at bottom (radio-scanned: 40 min per lane)

Taking these two independent experimental results together, we found that a small proportion of the XET product can be solubilized in CMNaOH (Fig. 75 and 71). Hence, to avoid any confusion between transacylase and XET products in the results below, the XET product was always quantified as a reference for the CMNaOH-releasable ^{3}H. Moreover, the apparent promoting effect of cutin-linkage on glycosidase activities was also consistently observed, suggesting that it is not an artefact, but the mechanism remains a question here.

Since the initial transacylase product was believed to be cutin-to-[^{3}H]XXXGol and -[^{3}H]XXGol, the newly discovered transacylase was named cutin-to-XGO transacylase in this chapter.

4.4.4 Xyloglucan–[^{3}H]XXXGol conjugate in the enzymic products

To have a quantitative comparison between the newly found cutin-to-XGO transacylase and the well-established XET activities, the CMNaOH-hydrolysed epidermis samples were digested XEG. About 25-fold more

radioactivity was released than by CMNaOH from un-denatured epidermis samples (Fig. 74a); and negligible realised ^{3}H from the denatured control (0.03% of the supplied radioactivity) (Fig. 74a). There was still some ^{3}H left after this XEG hydrolysis treatment, very likely remaining XET product (Fig. 74b) because putatively there was no cutan (non-alkali hydrolysable polyether made of *n*-alkane or alkene; Gupta *et al*., 2006) in pea epicotyl epidermis (Chapter 3), and therefore no cutan–[^{3}H]XXXGol conjugate; and the CMNaOH was evidenced to hydrolyse ester bonds thoroughly (Chapter 3).

These results indicated that the XET activity is much higher than the transacylase activity, but this observation was expected because the cutin–oligosaccharide hetero-polymer quantity is believed to be less than either of the homo-polymers (xyloglucan and cutin), due to the physical localisations (i.e. xyloglucan and cutin are in two separate layers) and also their physiological vitalities (i.e. the lack of xyloglucan or cutin can be dramatic for plants, but the cutin–xyloglucan conjugate may not be that vital).

In summary, I found the novel cutin-to-XGO transacylase activity by employing enzymic and chemical extraction, as well as degradation methods. The final product was identified as cutin–[^{3}H]XXGol and cutin–[^{3}H]XGol (~0.6% of the supplied radioactivity in total) after 3 h incubation, and cutin–[^{3}H]XXXGol and cutin–[^{3}H]XXGol after 80 min because the initial [^{3}H]XXXGol was hydrolysed by glycosidases. Under the comparable conditions, this product quantity (~0.6% of supplied radioactivity; Fig. 75a) was similar to that of cutin-to-HHA transacylase, which was ~0.7% of the supplied radioactivity

(Chapter 3), suggesting that these two cutin transacylases are active at a similar level *in planta*. Moreover, the newly discovered cutin remodelling transacylase, cutin-to-XGO transacylase activity was much smaller than the xyloglucan re-modelling, XET's activity, suggesting a very low abundance of cutin–xyloglucan links in nature. Another possible explanation of the low activity is that [^{3}H]XXXGol may not be a preferable acyl acceptor for the new cutin-to-XGO transacylase activity, polymeric xyloglucan molecules may be a better option. However, this hypothesis cannot be answered in this thesis due to technical limitations mentioned in introduction ([^{3}H]xyloglucan forms H-bonds with epidermal polysaccharides and interfere analysis of the transacylase product).

4.5 Attempts to identify the putative cutin-to-XGO transacylase

The sections above introduce the presence of cutin-to-XGO transacylase activity in pea epicotyl epidermis, very likely also in ice plant leaf and tomato fruit epidermis. Nevertheless, the identity of this novel transacylase was still unknown. The cutin-to-XGO transacylation was proposed to be catalysed by a GDSL enzyme as in Chapter 3 (Fig. 6). As the only well-characterised cutin-related GDSL transacylase, CD1 was the first candidate to be tested (Yeats *et al*., 2012).

4.5.1 CD1 activity on [^{3}H]XXXGol *in situ*

The first strategy was assaying *cd1*-knockout tomato fruit (cv. M82) epidermis versus the WT with [^{3}H]XXXGol as the acyl acceptor *in situ*. However, the amount of CMNaOH-releasable ^{3}H from un-denatured

epidermis of *cd1*-knockout tomato fruit was only slightly lower than the one from WT (P > 0.05) (Fig. 78a), suggesting that the observed transacylase activity was at least not solely from CD1. To test whether the XET product dissolved in CMNaOH contribute to this observation, the CMNaOH-insoluble residue was hydrolysed by TFA to quantify the majority of the XET product.

The XET activity was slightly higher in the *cd1*-knockout (Fig. 78b), suggesting that the *cd1* mutation did not affect XET activity. Thus, XET activity may not interfere with the observation that less ^{3}H incorporated into CMNaOH-releasable form, supporting the hint that CD1 has the novel transacylase activity. However, this speculation required to be answered by *in-vitro* assays without interferences.

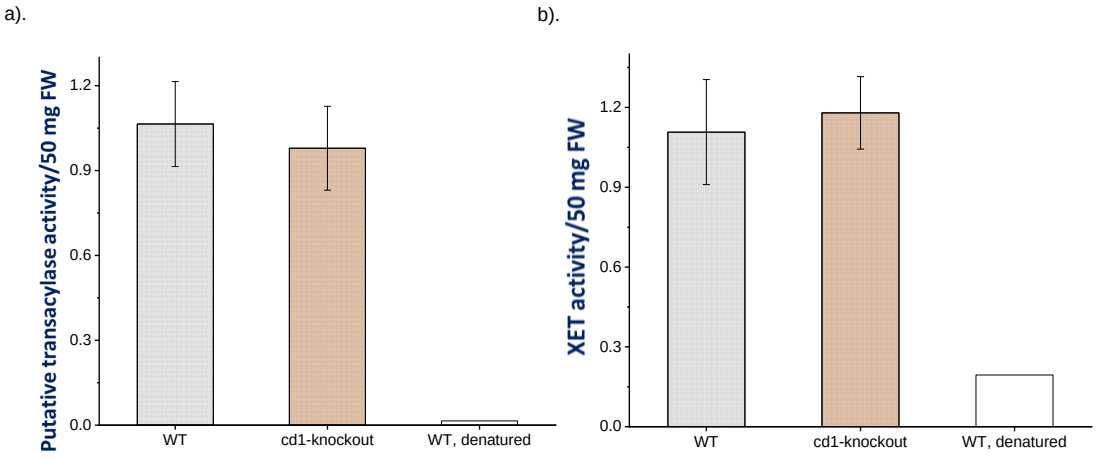

Figure 78. The comparison between the putative cutin-to-[^{3}H]XXXGol transacylase activity and the well-known XET activity in WT and *cd1*-knockout tomato fruit (cv. M82) epidermis *in situ*. The epidermis samples (50 mg; acyl donor) with or without active endogenous enzymes were incubated with 0.9 kBq exogenous [^{3}H]XXXGol (acyl acceptor) under the standardised conditions for 24 h. (a) The CMNaOH-releasable radioactivity ratio (%) illustrates the endogenous cutin-to-[^{3}H]XXXGol transacylase activity. (b) The 2 M TFA-releasable radioactivity ratio (%) shows the endogenous XET activity. Bars indicate standard errors (*n*=3). No bars for the 'WT, denatured' group (*n*=1).

A value of 1% releasable radioactivity/50 mg epidermis/supplied radioactivity corresponds to an absolute incorporation of 170 cpm/50 mg epidermis.

4.5.2 His_6-tagged CD1 activity on [^{3}H]XXXGol and XXXG *in vitro*

The preliminary conclusion above was not supported by assaying the heterologously produced (in *Nicotiana benthamiana*) and purified His_6-tagged CD1 *in vitro* radiochemically and spectrophotometrically.

Assaying His_6-tagged CD1 activity radiochemically

The purified His_6-tagged CD1 was incubated with prepared M82 tomato fruit (the source of the CD1-encoding gene) epidermis and [^{3}H]XXXGol. However, the addition of CD1 did not affect the ^{3}H incorporation ($P > 0.05$), indicating that CD1 does not catalyse the cutin-to-XXXGol transacylation (Fig. 79).

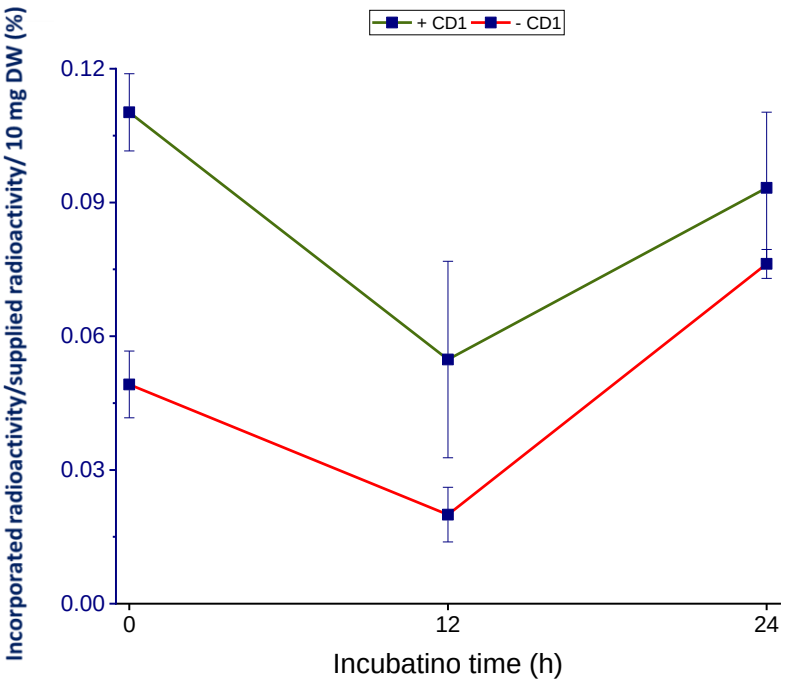

Figure 79. CD1 shows negligible cutin-to-[^{3}H]XXXGol transacylase activity *in vitro*. The prepared [wax and pectin were removed by boiling in chloroform for 90 s and in 0.2 M ammonium oxalate (pH 4.3) overnight respectively] tomato (cv. M82) fruit epidermis (10 mg; acyl donor) without active endogenous enzymes was incubated with 0.53 kBq exogenous [^{3}H]XXXGol (acyl acceptor) with or without tobacco-produced CD1 (1 µg) in 300 µl pH 6.5 buffer at 25°C for 3 days. The incorporated radioactivity ratio (%) illustrates the CD1's cutin-to-[^{3}H]XXXGol transacylase activity. Green line: un-denatured. Red lines: denatured (control). Bars indicate standard errors (*n*=3).

A value of 0.1% total incorporated radioactivity/10 mg epidermis/supplied radioactivity corresponds to an absolute incorporation of 10 cpm/10 mg epidermis.

Assaying His$_6$-tagged CD1 activity spectrophotometrically

As stated in Chapter 3, the artificial palmitate ester, *p*-nitrophenyl palmitate (*p*NPP) was used as an acyl donor, and a range of natural plant cell wall mono-, oligo- and polysaccharides were tested as the acyl acceptors of CD1 (Fig. 80). However, none of them (including XXXG as a representative xyloglucan oligomer, XGO) had detectable acyl acceptor ability; indeed, CD1

activity was even decreased in the presence of them compared with water alone ($P < 0.01$ or 0.05) (Fig. 80).

A comparable result was also observed in Chapter 3, with HHA as the potential acceptor substrate, and was hypothesized to be because the mobility of CD1 was impeded by the crowded carbohydrate molecules in the incubation mixture. Ester hydrolysis activity ($P_{(+ \text{ CD1 vs. } - \text{ CD1})} < 0.01$) (Fig. 79) of CD1 was demonstrated by comparing with proteins from WT tobacco (Chapter 3).

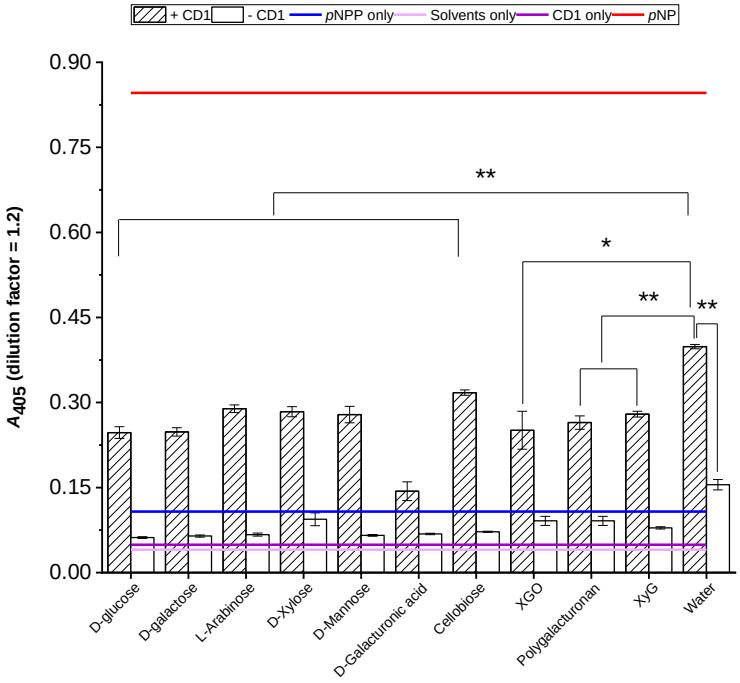

Figure 80. Possible CD1 *in-vitro* activity on *p*NPP with various acyl acceptors (primary cell wall components). The artificial ester, *p*NPP (acyl donor) (final conc. = 0.5 mM) was incubated 0.1% (w/v) (final conc.) natural cell wall polysaccharide components with or without the purified His_6-tagged CD1 (1 µg/100 µl) at pH 6.0 at 25°C for 3 days. The CD1 activity was illustrated by quantifying one of the products, *p*NP by A_{405} at pH 7.15±0.02 (dilution factor relative to reaction mixture = 1.2). The actual CD1 activity was calculated as follows: reaction mixture A_{405} – Σ (*p*NPP-only A_{405} + CD1-only A_{405}). The solvents-only A_{405} provided a blank, and the *p*NP A_{405} provided a reference. *p*NPP: 0.5 mM *p*-nitrophenyl palmitate; *p*NP: 0.5 mM *p*-nitrophenol. Bars indicate standard errors (n=3). *: $P < 0.05$. **: $P < 0.01$.

In summary, all the *in-vitro* results pointed to a clear conclusion that CD1 does not catalyse the observed cutin-to-XXXGol transacylation reaction, only a hydrolysis activity.

4.6 Age effects on cutin-to-XGO transacylase

We had hypothesized that cutin-to-XGO transacylation occurs during rapid growth, which occurs at early developmental stages. However, the experiments demonstrated that the pH optimum (6.5–7.5) is slightly out of the range for early development (reviewed by Cosgrove, 2005), hinting that this transacylase may be more required in the stages post growth. Thus, screening the whole developmental process may give more information about its physiological function.

4.6.1 Cutin-to-XGO transacylase activity through tomato fruit development

I screened the whole developmental process of cv. M82 and Ailsa Craig tomato fruit *in situ*, their dramatic expansion (i.e. from 0.5 cm diameter to 5 cm in 4 weeks) was predicted to provide a clear correlation between the cutin-to-XGO transacylase activity and cell expansion.

Unexpectedly, even though these two varieties were from the same species and have the same size of mature tomato fruit, [^{3}H]XXXGol incorporation into CMNaOH-releasable material peaked at 21 DAA of Ailsa Craig fruit epidermis (Fig. 81a), whereas for M82 it was at 30 DAA (Fig. 82a). Transcriptionally, this inconsistency of the cutin-to-XGO transacylase activity patterns during development within the species might be because the promoter was located at different alleles and/or different 5’ untranslated

region. Translationally, different inhibitors may present in these two tomato varieties at the same developmental stage.

Since CMNaOH also dissolves a small proportion of the XET product (Fig. 75 and 71b), and to test whether the results (Fig. 81a and 76a) were heavily affected by interfering XET activity, the polysaccharide in the CMNaOH-insoluble residue was hydrolysed by TFA and quantified, to be compared with the CMNaOH-releasable ^{3}H. Consistent with Fig. 74a, the XET activity was higher than the transacylase (Fig. 81 and 76), especially in Ailsa Craig samples (~10-fold). Even though the XET activity was also highest at 21 DPA (Fig. 81b) and 30 DAA (Fig. 82b) as the putatively novel transacylase activity (revealed by CMNaOH-releasable ^{3}H), the general patterns were slightly different. For Ailsa Craig samples, XET activity dropped steeply at 28 DPA (Fig. 81b), instead of at the MG stage as the transacylase did (Fig. 81a), whereas in M82 samples, the complete ripening (dark red tomato fruit) affected the transacylase activity more than XET (Fig. 82).

Thus, the results above provide a hint that the transacylase activity was highest at the stage when both cultivars were approaching the end of expansion, especially in the M82 fruit epidermis (Fig. 82a). This observation may be because the cutin-to-XGO transacylase activity is more required after cells have dramatically expanded than before. Essentially, once the expansion was ceased, the cutin-to-XGO transacylase activity started dropping down, suggesting that the cutin-to-XGO transacylase activity may be only required during expanding, and definitely not during ripening, consistent with our hypothesis (Fig. 81a and Fig. 82a).

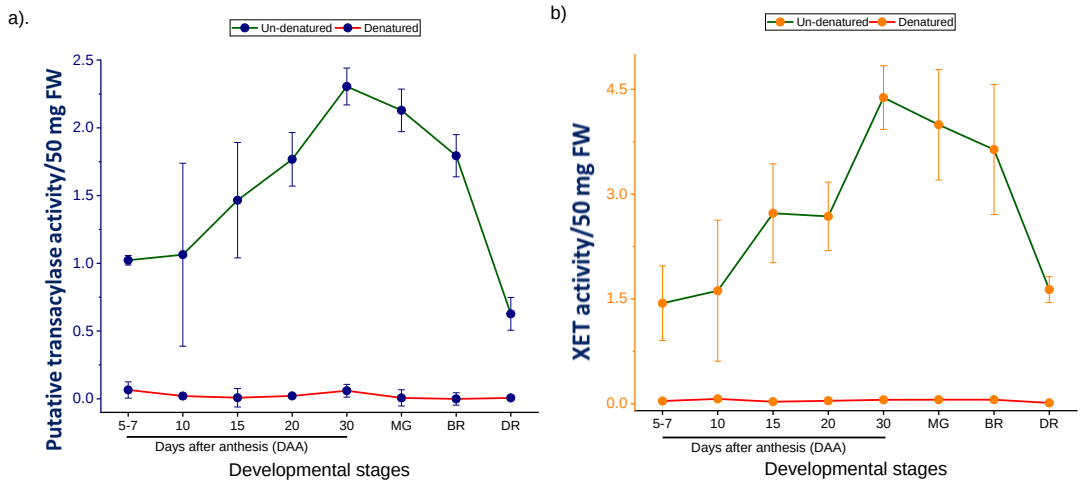

Figure 81. Effects of tomato fruit (cv. Ailsa Craig) development on the putative cutin-to-[^{3}H]XXXGol transacylase activity and the well-known XET activity *in situ*. The tomato fruit (cv. Ailsa Craig) epidermis samples (50 mg; acyl donor) with or without active endogenous enzymes were incubated with ~0.7 kBq exogenous [^{3}H]XXXGol (acyl acceptor) under the standardised conditions. (a) The CMNaOH-releasable radioactivity ratio (%) was used to illustrate the effects of development on the endogenous cutin-to-[^{3}H]XXXGol transacylase activity. (b) 2 M TFA, instead of XEG, was used to hydrolyse XET product. The 2 M TFA-releasable radioactivity ratio (%) shows the effects of development on the endogenous XET activity. MG: mature green. BR: breaker (~10% colour change). TR: turner (~30% colour change). OR: orange. LR: light red. DR: dark red. Green lines: un-denatured. Red lines: denatured (control). Bars indicate range (*n*=2) in (a); range (*n*=2) in (b).

A value of 1% releasable radioactivity/50 mg epidermis/supplied radioactivity corresponds to an absolute incorporation of 120 cpm/50 mg epidermis.

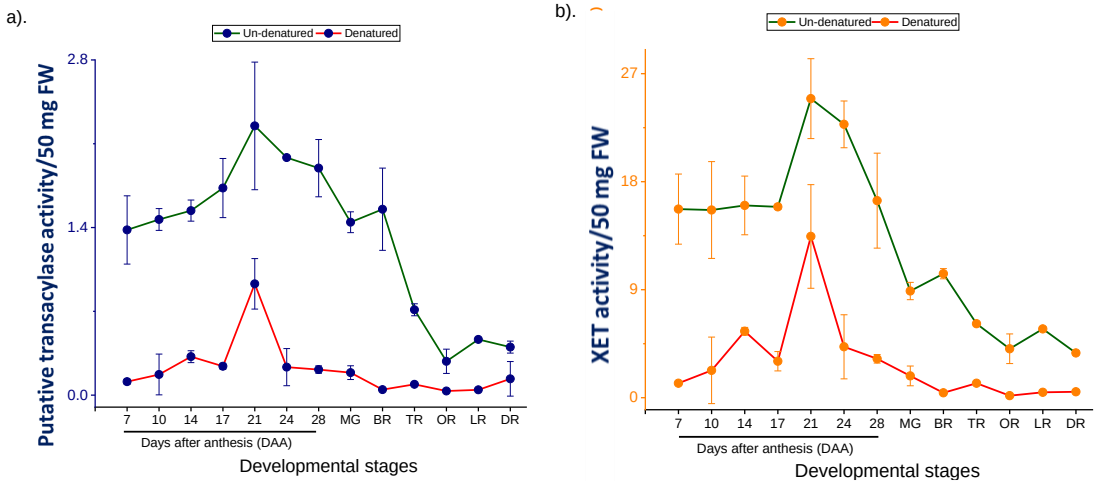

Figure 82. Effects of tomato fruit (cv. M82) development on the putative cutin-to-[^{3}H]XXXGol transacylase activity and the well-known XET activity *in situ*. Experimental details were as in figure 72, except the tomato fruit (cv. M82) epidermis

samples were incubated with 0.42 kBq exogenous [^{3}H]XXXGol (acyl acceptor) under the standardised conditions. (a) The CMNaOH-releasable radioactivity ratio (%). (b) The 2 M TFA-releasable radioactivity ratio (%). MG: mature green. BR: breaker (~10% colour change). DR: dark red. Green line: un-denatured. Red lines: denatured (control). Bars indicate range (n=2).

A value of 1% releasable radioactivity/50 mg epidermis/supplied radioactivity corresponds to an absolute incorporation of 80 cpm/50 mg epidermis.

4.6.2 Cutin-to-XGO transacylase activity during ice plant leaf expansion

Small (3–5 cm lamina length) and big (8–12 cm) ice plant leaf adaxial epidermis was also compared, and consistently showed that the big, but still growing leaf epidermis samples incorporated more [^{3}H]XXXGol per 50 mg fresh epidermis within certain time than the samples from small leaf (e.g. 1.5-fold at 12 h, $P < 0.05$; 2-fold at 24 h) (Fig. 83a). The incorporating rate slowed down from 12-h possibly because of the degraded transacylase ('***4.2.2***'). The significant difference between the un-denatured epidermis samples and the denatured control indicated that it was an enzymic incorporation again ($P < 0.01$ or 0.05) (Fig. 83a). To have a comparison, XET activity was quantified by scintillation counting the CMNaOH-insoluble residues and it was also higher in the bigger leaf than in the smaller ones, but the difference between them (i.e. 1.2-fold at 12 h; 1.3-fold at 24 h) was slightly smaller than of transacylase activity, and not significant ($P > 0.05$) (Fig. 83b). These results suggested that the XET activity in ice plant leaf epidermis was less affected by expansion than the transacylase activity was.

Thus, we can conclude that the results in Fig. 83a provided a hint of the newly discovered cutin-to-XGO transacylase's response to development,

which is consistent with the results obtained from tomato fruits: higher cutin-to-XGO transacylase activity in the more expanded organs' epidermis (Fig. 81 and 76).

I did not test fully expanded ice plant leaf epidermis (lamina length: ~16 cm), due to material availability.

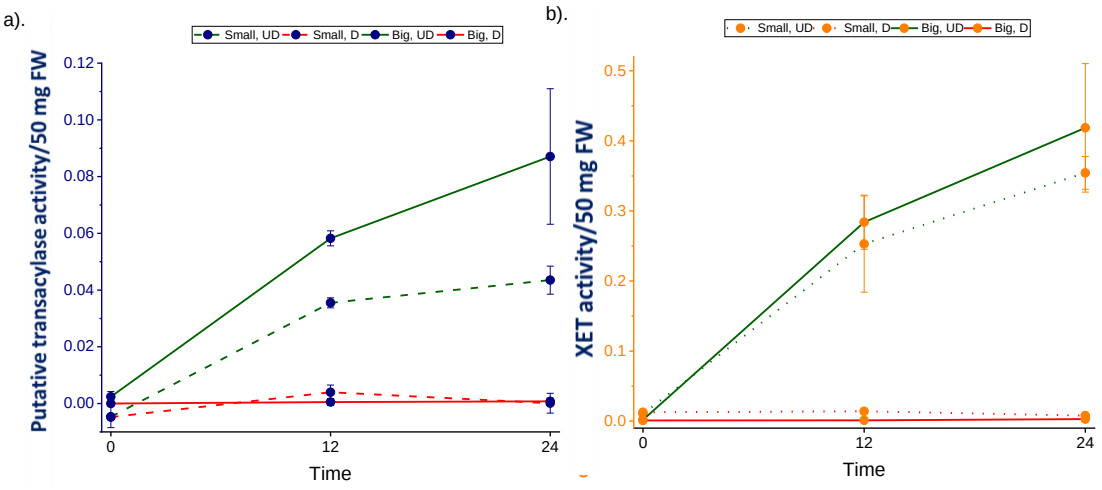

Figure 83. Effects of ice plant leaf expansion on the putative cutin-to-[^{3}H]XXXGol transacylase activity and the well-known XET activity *in situ*. Experimental details were as in figure 73, except that epidermis from different sizes of expanding ice plant leaf was compared by using 1.1 kBq exogenous [^{3}H]XXXGol as the acyl acceptor. Green line: un-denatured. Red lines: denatured (control). Bars indicate standard errors (*n*=3). Small: 3-5 cm lamina length; big: 12 cm lamina length. UD: un-denatured. D: denatured.

(a) The CMNaOH-releasable radioactivity (%) illustrates the effects of development on the endogenous cutin-to-XGO transacylase activity.

(b) The CMNaOH-insoluble residue radioactivity ratio (%) shows the effects of development on the endogenous XET activity.

A value of 0.1% CMNaOH-releasable or -insoluble radioactivity/50 mg epidermis/supplied radioactivity corresponds to an absolute incorporation of 20 cpm/50 mg epidermis.

4.6.3 Cutin-to-XGO transacylase activity during pea epicotyl elongation

As in Chapter 3, dark-grown pea epicotyls were harvested at different days after sowing (DAS), and the epidermis was assayed for cutin-to-XGO transacylase activity with [^{3}H]XXXGol *in situ*. Epicotyl length increased ~4-fold between 4 and 7 DAS (i.e. 16 cm vs. 4 cm), but only increased ~0.06-fold between 7 and 10 DAS (i.e. 17 cm vs. 16 cm).

Based on the results above, I expected the putative cutin-to-XGO transacylase activity to be higher at 7 and 10 DAS than the younger one, since pea epicotyl had been more elongated. However, there was no significant difference of the amount of CMNaOH-releasable ^{3}H between the three age groups, only a slight decrease at 7 DAS ($P > 0.05$) (Fig. 84a). Similar results were observed in Chapter 3, and the reason was speculated to be that the pea epicotyl at these three ages were the beginning of rapidly elongating stage, resulting in no big contrast as had been observed in tomato fruit (Fig. 81 and 76) and ice plant leaf (Fig. 83).

Different from the transacylase activity, the XET activity, revealed by TFA hydrolysis, was dramatically affected by age: it was decreased linearly by age increase ($P < 0.05$) (Fig. 84b).

The different patterns observed by quantifying CMNaOH- and TFA-releasable radioactivity, led us conclude that the newly discovered cutin-to-XGO transacylase activity does not vary during pea epicotyl elongation up to 10 DAS.

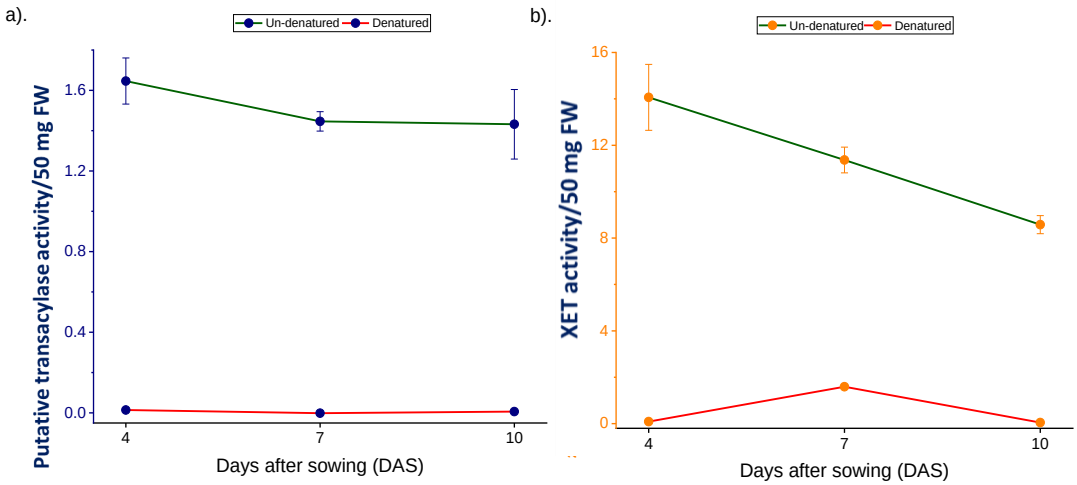

Figure 84. Effects of pea epicotyl elongation on the putative cutin-to-[^{3}H]XXXGol transacylase activity and the well-known XET activity *in situ*. Experimental details were as in figure 74, except epidermis from different lengths (4, 7 and 10 DAS) of the expanding pea epicotyl was compared by incubating with 0.74 kBq exogenous [^{3}H]XXXGol as the acyl acceptor. (a) The CMNaOH-releasable radioactivity ratio (%). (b) The 2 M TFA-releasable radioactivity ratio (%). Green line: un-denatured. Red lines: denatured (control). Bars indicate standard errors (*n*=3).

A value of 1% releasable radioactivity/50 mg epidermis/supplied radioactivity corresponds to an absolute incorporation of 140 cpm/50 mg epidermis.

Overall, screening the amount of CMNaOH-releasable ^{3}H formed in different plant organs at different developmental stages showed that the cutin-to-XGO transacylase activity tends to be higher at later stages of cell expansion, and allowed us to speculate on its physiological function, that it may reinforce epidermis mechanically for large, and expanding cells to prevent epidermis rupture.

4.7 Effects of environmental stresses on cutin-to-XGO transacylase activity

4.7.1 Effects of light on the cutin-to-XGO transacylase activity

As an apoplastic enzyme, the cutin-to-XGO transacylase activity is proposed to face environmental stresses directly. By testing the effects of stresses, we can obtain more information of the cutin-to-XGO transacylase's physiological functions.

Peas were routinely grown in the dark routinely to boost their growth rate as I stated above. However, land plants are usually exposed to light. To investigate if the laboratory growth conditions impose artefacts on the cutin-to-XGO transacylase activity, epidermis from continuous dark- and light (resource: bulb)-grown pea epicotyls was separately assayed with [^{3}H]XXXGol *in situ*.

Even though the darkness produced ~4 times taller pea epicotyls than light (i.e. 4 cm vs 16 cm), the quantity of CMNaOH-releasable ^{3}H incorporated (per 50 mg epidermis per 12 h) was only ~1.2 times higher in the 'dark' samples than in the 'light' one as an example, but the difference was significant ($P < 0.05$) (Fig. 85a). It also applies to the 24-h incubated samples ($P < 0.01$) (Fig. 85a).

The effect of light exposure on incorporation of ^{3}H into CMNaOH-insoluble material (putative XET products) was slightly higher than that on the CMNaOH-releasable ^{3}H (putative transacylase products): the insoluble ^{3}H in 'dark' samples was 1.5-fold higher than in 'light' ones at 12 h ($P > 0.05$) (Fig.

85b). This correlation between growth rate and XET activity has been noted in numerous plant species and organs (Potter and Fry, 1994; Palmer and Davies, 1996).

Due to the similar patterns of CMNaOH-releasable and -insoluble ^{3}H (Fig. 85), the results only suggested a trend that the newly discovered cutin transacylation reaction was mildly boosted by the default, dark growth condition. This phenomenon was observed by quantifying the final product (CMNaOH-releasable ^{3}H), but whether it is caused by higher transacylase activity or more cutin available in faster growing plants than the slower one remains a question here, which could be answered preliminarily by *ex-situ* experiments (‘***4.7.2*** ’).

Nevertheless, the CMNaOH-releasable radioactivity from un-denatured epidermis of light-grown pea epicotyls was 20–30 times higher than from the denatured control (Fig. 85a), clearly indicating that the cutin-to-XGO transacylase also exists in the light grown pea epicotyls. Thus, in summary, the default pea growing condition (darkness) may lead to a slight promotion on the transacylation reaction *in situ*, but not dramatically.

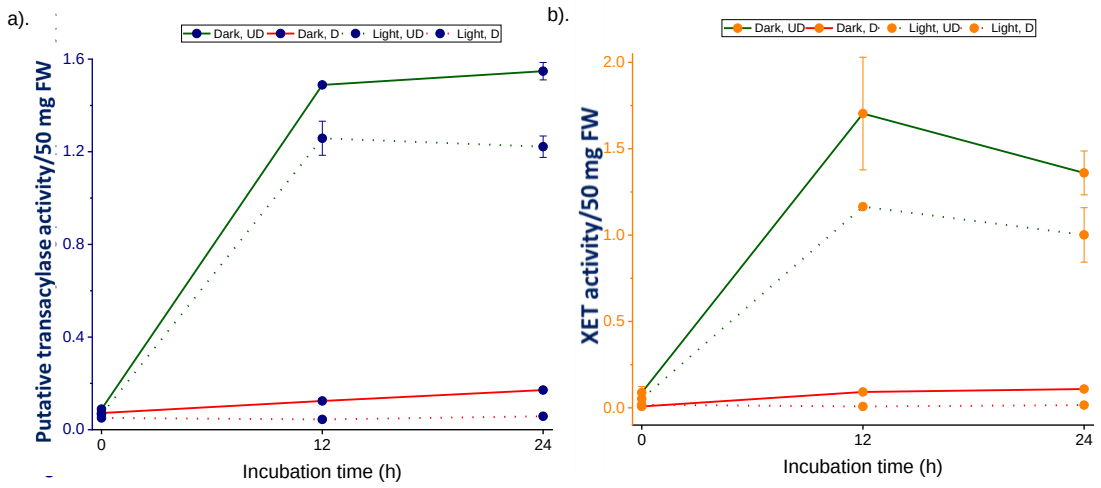

Figure 85. Effects of light on the putative cutin-to-[^{3}H]XXXGol transacylase activity and the well-known XET activity *in situ*. The epidermis samples (50 mg; acyl donor) with or without active endogenous enzymes was incubated with 0.79 kBq exogenous [^{3}H]XXXGol (acyl acceptor) under the standardised conditions. Dark: grew in complete dark for 7 days at 25°C; light: grew in bulb-light (light intensity: ~2 µmol/m^2/s) for 7 days at 25°C. Green lines: un-denatured epidermis samples. Red lines: denatured epidermis samples (control). Bars indicate standard errors (*n*=3). No bars for the 'denatured' group (*n*=1).

(a) The CMNaOH-releasable radioactivity ratio (%) illustrates the effects of light on the endogenous cutin-to-[^{3}H]XXXGol transacylase activity.

(b) The CMNaOH-insoluble residue radioactivity ratio (%) shows the effects of light on the endogenous XET activity.

A value of 1% CMNaOH-releasable or -insoluble radioactivity/50 mg epidermis/supplied radioactivity corresponds to an absolute incorporation of 150 cpm/50 mg epidermis.

4.7.2 Effects of humidity on the cutin-to-XGO transacylase activity

Another important environmental factor is humidity. Cell wall re-modelling enzymes, such as pectate lyase activity, has been reported to be enhanced by high humidity in banana fruit peel (Saengpook *et al*., 2007). However, as far as we were aware, cutin was suggested not playing an important role in controlling water loss, which is a usual response of plants to humidity change

(Schönherr and Riederer, 1989; Isaacson *et al*., 2009). Here, I looked for the effects of humidity on the cutin re-modelling enzyme activity, cutin-to-XGO transacylase, instead of cutin.

Testing the effects of humidity on cutin-to-XGO transacylase activity in situ

A tray of pea seeds was germinated, and the seedlings were grown in natural Edinburgh humidity (40–45%), whereas the other tray was wrapped in a polythene bag to increase the internal humidity to 80–90%. Both were grown in continuous light (type of light: bulb; intensity: ~2 µmol/m^2/s).

Pea epidermis was incubated with [^{3}H]XXXGol under the optimized conditions as above. CMNaOH released 1.1-fold less ^{3}H from high-humidity samples than from the normal-humidity' control ($P > 0.05$) (Fig. 86a), whereas TFA released 1.3-fold more ^{3}H from the former than the latter ($P > 0.05$) (Fig. 86b).

These two opposite effects of high humidity on CMNaOH- and TFA-releasable (putative XET product) ^{3}H suggested that the cutin-to-XGO transacylase activity was not affected by high humidity *in situ*. To obtain more information, an *ex-situ* assay was carried out because the effects of humidity on the cutin-to-XGO transacylase activity may be masked by minor changes of cutin (e.g. quantity and components).

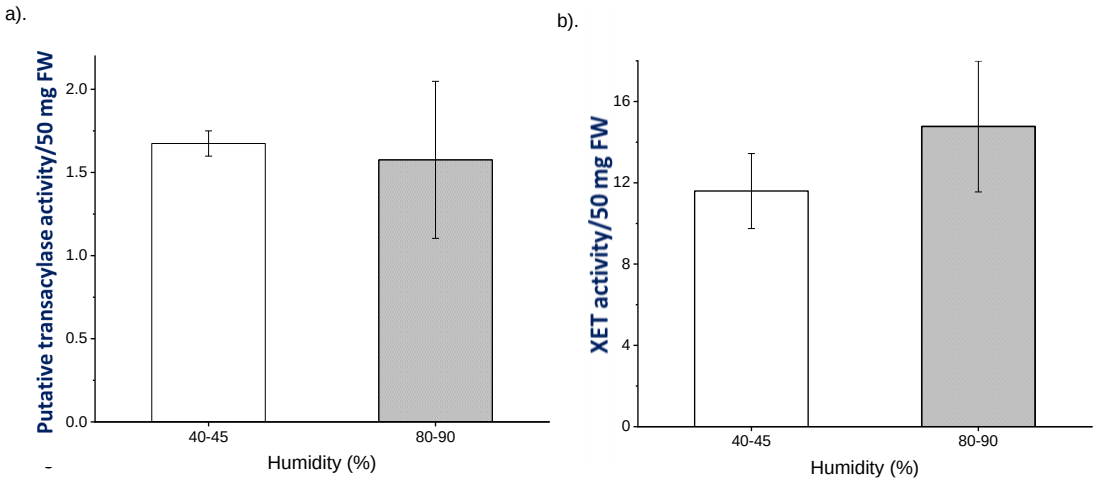

Figure 86. Effects of humidity on the putative cutin-to-[^{3}H]XXXGol transacylase activity and the well-known XET activity *in situ*. The epidermis samples (50 mg; acyl donor) with active endogenous enzymes were incubated with 0.53 kBq exogenous [^{3}H]XXXGol (acyl acceptor) under the standardised conditions. (a) The CMNaOH-releasable radioactivity ratio (%) illustrates the effects of humidity on the endogenous cutin-to-[^{3}H]XXXGol transacylase activity. (b) The 2 M TFA-releasable radioactivity ratio (%) shows the effects of humidity on the extracted XET activity. Bars indicate standard errors (*n*=3).

A value of 1% releasable radioactivity/50 mg epidermis/supplied radioactivity corresponds to an absolute incorporation of 100 cpm/50 mg epidermis.

Test the effects of humidity on cutin-to-XGO transacylase activity ex situ

Denatured epidermis, and endogenous enzymes extracted from un-denatured epidermis, were obtained from three groups: light-grown pea epicotyls in 90–95% humidity, light-grown pea epicotyls in 40–45% humidity and standard dark-grown pea epicotyls in 80% humidity (the standard humidity in the default dark condition). All combinations of prepared epidermis and enzyme extract samples were tested for the effects of humidity on the cutin-to-XGO transacylase activity and cutin separately. Consistently, there was little effects imposed by different humidity conditions (Fig. 87a):

only a slight trend of high humidity decreasing the extracted transacylase activity and cutin (Fig. 87a) was noted, because all the three epidermis species incorporated less ^{3}H under the catalysis of the enzyme extract from high-humidity samples than from the ‘normal’ one, and the prepared epidermis from high-humidity samples incorporated less CMNaOH-releasable ^{3}H than the ‘normal-humidity’ control under the catalysis of the same enzyme extract. I did not have replicates in this experiment due to material availability, but it still provided an indication that humidity does not impose dramatic effects on the cutin-to-XGO transacylase activity or the cutin.

Interestingly, I also observed that CMNaOH released ~2-fold higher ^{3}H from dark-grown pea epicotyl epidermis than from the light-grown ones, independent of the humidity (Fig. 87a). However, the cutin availability may be even slightly lower than the light-grown samples (Fig. 87a). This result may contribute to explain the significant, but small difference of the CMNaOH-releasable ^{3}H between the two groups with different light exposure (Fig. 85a): more cutin-to-XGO transacylase product in the dark-grown samples was because of higher transacylase activity during the faster growth, but the possible reduced cutin availability may have countered the increased transacylase activity.

The XET activity was also slightly decreased by high humidity, but the xyloglucan availability was not decreased by high humidity (Fig. 87b) as cutin was (Fig. 87a). Consistently, dark-grown pea epicotyl provided higher XET

activity because of the faster growth rate than the light-grown samples (e.g. Potter and Fry, 1994) (Fig. 87b).

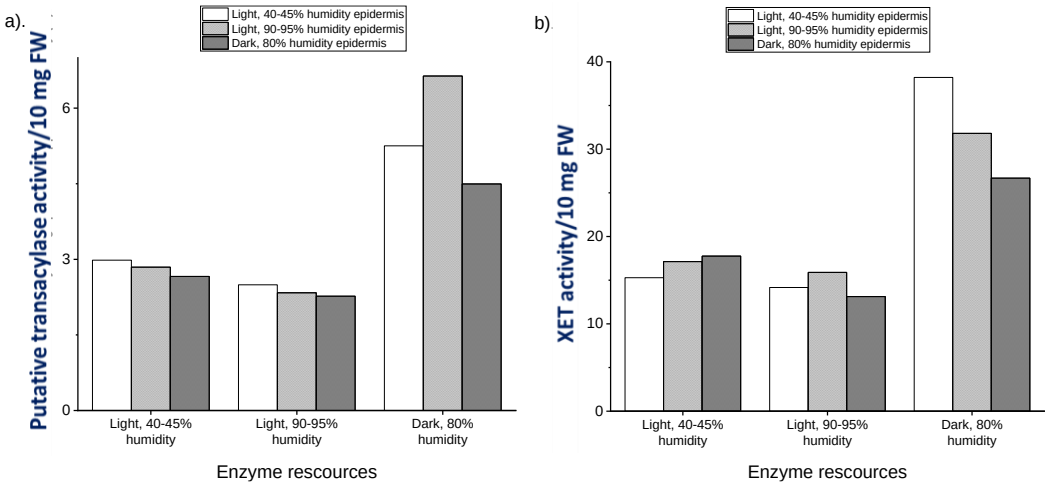

Figure 87. Effects of humidity on the putative cutin-to-[^{3}H]XXXGol transacylase activity and the well-known XET activity *ex situ*. Experimental details were as in figure 70, except that the enzyme extract and prepared epidermis without active enzyme were from pea epicotyl, which were incubated together with 0.32 kBq exogenous [^{3}H]XXXGol (acyl acceptor) under the standardised conditions. (a) The CMNaOH-releasable radioactivity ratio (%). (b) The 2 M TFA-releasable radioactivity ratio (%). No standard errors (n=1).

A value of 1% releasable radioactivity/10 mg epidermis/supplied radioactivity corresponds to an absolute incorporation of 60 cpm/10 mg epidermis.

Combining the *in-* and *ex-situ* results together, we can conclude that reducing effect of high humidity on the newly discovered cutin-to-XGO transacylase activity was very slight. Thus, cutin and its metabolism reactions may not be essential during humidity change, consistent with literatures (e.g. Schönherr and Mérida, 1981).

4.7.3 Effects of pre-growth temperature on the cutin-to-XGO transacylase activity

Dramatic change of temperature is another common stress that plants usually face to; and cell wall is response to it. For instance, pectin in pea stipules was reported to be more methyl esterified under colder temperature than under warmer one (Baldwin *et al*., 2014). There was no study about how cutin re-modelling mechanisms respond to temperature, only literatures about the cutin load. For example, the cutin load increased in respond to low temperature in tree tobacco (*Nicotiana glauca*) leaf (Skoss, 1955), and it decreased in response to high temperature in field pea (*P. sativum* L.) leaf (Liu *et al.*, 2019).

To investigate how cold affect the newly discovered cutin-to-XGO transacylase activity, I assayed epidermis of pea epicotyls, which were grown in continuous dark for different days at 4°C as in Chapter 3, but with [^{3}H]XXXGol as the acyl acceptor. The CMNaOH hydrolysis showed that the transacylase activity was mildly increased in the first 4 days at 4°C ($P_{(0\text{-day vs. }4\text{-day})} < 0.05$), and then slightly decreased at 8 day ($P > 0.05$) (Fig. 88a).

The XET activity was also mildly increased in the first 4 days (1.2-fold) ($P > 0.05$), and then in-significantly decreased at 8 day ($P > 0.05$) (Fig. 88b).

Since the patterns of CMNaOH- and TFA-releasable ^{3}H were very similar, and for the awareness that XET activity may interfere the novel cutin transacylase results, we can only suggest that the cutin–[^{3}H]XXXGol link may

be required during a short-period of cold shock, but it is not important for a long-term low temperature (e.g. winter).

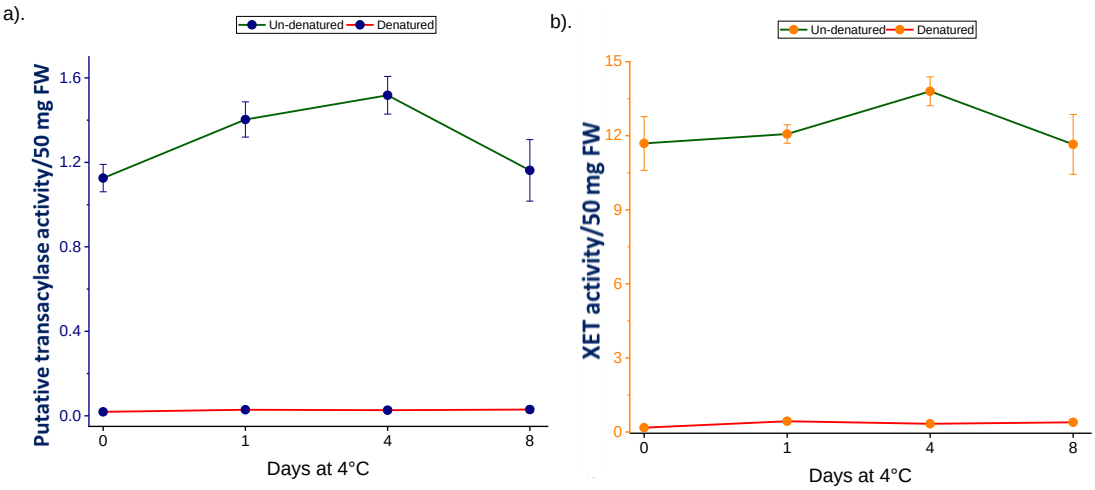

Figure 88. Effects of pre-growth temperature on the putative cutin-to-[^{3}H]XXXGol transacylase activity and the well-known XET activity *in situ*. Epidermis samples (50 mg; acyl donor) with or without active enzymes were isolated from pea epicotyls exposed to 4°C for different days. They were incubated with 0.85 kBq exogenous [^{3}H]XXXGol (acyl acceptor) under the standardised conditions. (a) The CMNaOH-releasable radioactivity ratio (%) illustrates the effects of temperature on the endogenous cutin-to-[^{3}H]XXXGol transacylase activity. (b) The 2 M TFA-releasable radioactivity ratio (%) shows the effects of temperature on the endogenous XET activity. Green lines: un-denatured epidermis samples. Red lines: denatured epidermis samples (control). Bars indicate standard errors (n=3).

A value of 1% releasable radioactivity/50 mg epidermis/supplied radioactivity corresponds to an absolute incorporation of 160 cpm/50 mg epidermis.

Taken together, the environmental stress studies enabled us to obtain more hints about the newly discovered putative cutin-to-XGO transacylase's physiological function(s), which will be discussed later in this chapter.

Discussion

4.8. The discovery of novel cutin-to-XGO transacylase activity

Based on the reported observations (e.g. Jeffree 2006; Tian *et al*., 2008), a model of cutin–cell wall polysaccharide bonding had been proposed, but its mechanism was unknown (Chapter 1, Fig. 5). The discovery of CD1 enabled us to hypothesise that besides being loosened (Chapter 3), cutin can also be mechanically reinforced during cell expansion via transfer of a transiently-cut cutin chain (acyl donor) to a nearby cell wall polysaccharide molecule (acyl acceptor) by a GDSL transacylase.

One of the most abundant dicot xyloglucan oligomers, XXXG is also found in pea epicotyl epidermis (reviewed by Hayashi 1989), which was the specimen I used to find the proposed transacylase activity. XXXG was radio-labelled: the reducing end was reduced by sodium borohydride (NaB^3H_4) to a non-reducing product ([^{3}H]XXXGol), to mimic most of the XXXG motifs in a xyloglucan molecule, whose reducing ends are usually not available (i.e. involved in glycosidic bonds). The same principle was applied to all other mono- and oligosaccharides which were used in this thesis.

The putative cutin-to-XGO transacylase activity was reproducibly observed in different organs of different land plants *in* and *ex situ* (~1–3.5%, usually ~2.5% of the supplied radioactivity became ester-bonded — i.e. releasable by the hydrophobic alkali mixture, CMNaOH) (e.g. Fig. 46, 44, 75 and 76), and therefore a further product identification was carried out.

As in Chapter 3, enzymic and chemical extraction, as well as degradation strategies, were applied to pea epicotyl epidermis samples. However, differently from the cutin-to-[^{3}H]HHA *in-situ* experiment results, toluene and the chloroform mixtures only extracted negligible amounts of radioactivity (Fig. 74a), which was expected because un-bonded [^{3}H]XXXGol is hydrophilic. Furthermore, the very low neutral hydrophobic-extractable [^{3}H] also indicated that no wax oligo-ester–[^{3}H]XXXGol conjugate formed, which could have been otherwise dissolved in e.g. toluene. The chemical analysis of MFW (5/1/5, v/v/v)-soluble radioactivity demonstrated that the majority of exogenous [^{3}H]XXXGol was degraded to [^{3}H]XXGol and [^{3}H]XGol by glycosidases within 3 h (Fig. 62b, 67 and 71a).

The lipase and cutinase did not hydrolyse the ester bonds of proposed cutin–[^{3}H]XXXGol conjugate as also being reported in Chapter 3. Therefore, the basic hydrophobic extractant, CMNaOH (~0.5 M NaOH) was employed as in all other experiments to release the putatively ester-bonded radioactivity. Size-exclusion chromatography and paper chromatography of the CMNaOH-releasable products of the 3-h incubated epidermis samples showed that the majority of the putative transacylase product behaved as [^{3}H]XGol and [^{3}H]XXGol (Fig. 75 and 70), suggesting that ester-bonded [^{3}H]XXXGol is degraded by the same glycosidases as free [^{3}H]XXXGol. [^{3}H]XGol and [^{3}H]XXGol showed their very low acyl acceptor abilities, especially the former one (Fig. 60), and therefore the observed CMNaOH-releasable [^{3}H]XGol can only be produced by hydrolysis of [^{3}H]XXXGol. This observation is very surprising because we hypothesized that the addition of cutin dramatically

changes the structure of [^{3}H]XXXGol, making it not a substrate of glycosidases anymore.

This glyosidic hydrolysis of the ester-bonded [^{3}H]XXXGol was reproducibly observed in the independent experiment, whose incubation time was only 80-min but [^{3}H]XXGol was found in both CMNaOH and MFW (Fig. 77a and c). Based on the reported β-D-glucosidase activity (e.g. Hrmova *et al*., 1996), this putative hydrolysis of cutin–[^{3}H]XXXGol conjugate may point out that cutin is not linked to the first X (from left) unit, the non-reducing terminus, but other units.

[^{3}H]XXXGol, [^{3}H]XXGol and [^{3}H]XGol cannot be released from the XET products (xyloglucan→[^{3}H]XGOs, where → represents a glycosidic bond) because first, glycosidic bonds are stable in alkali (reviewed by Glaus and Van Loon, 2008), and second, numerous studies have reported that the glycosidases in different plants are not efficient in hydrolysing molecules that are much longer than [^{3}H]XXXGol (Koyama *et al*., 1983; O'Neill *et al*., 1989; Fanutti *et al*., 1991; Hrmova *et al*., 1996; Crombie *et al*., 2002), while the XET product here is xyloglucan–[^{3}H]XXXGol and xyloglucan–[^{3}H]XXGol (Fry *et al*., 2008). Furthermore, even though [^{3}H]XGol and [^{3}H]XXGol were produced from both xyloglucan-incorporated and free [^{3}H]XXXGol by glycosidases, the MFW wash should have removed them before CMNaOH hydrolysis. Thus, the compounds with molecular weight ≤ [^{3}H]XXXGol detected in the 18–20 fractions (Fig. 75) and 17–19 (Fig. 77b) are very likely to be transacylase products, which were not extracted by neutral solvents but in alkali (Fig. 73a).

The ratio of [^{3}H]XXXGol/[^{3}H]XXGol/[^{3}H]XGol was different between the un-incorporated (Fig. 73) and the putatively ester-bonded fractions (Fig. 76), maybe because the linkage between cutin and [^{3}H]XXXGol (more discussions in '***4.9***') promoted the α-D-xylosidase activity. It was suggested not to be a coincidence because another independent experiment (80-min incubation) also showed a higher [^{3}H]XXGol/[^{3}H]XXXGol ratio in the putative product than in the substrate mixture (Fig, 71c).

The relatively low transacylase activity compare with XET activity (e.g. Fig. 74) might have been predicted. Unlike the known XyG–XGO homo-transglycosylation products (Fry *et al*., 1992), the cutin and xyloglucan are from two separate layers in high land plants, and thus naturally have less chance to interact with each other than two components from the same epidermis compartment.

In summary, this work was the first to provide biochemical evidence showing that cutin's acyl groups can be linked to xyloglucan's (XGO's) hydroxy groups, fitting with model 1 (Chapter 1, Fig. 5a). It had been proposed that xyloglucan tethers cellulose microfibrils via H bonds to strengthen cell wall (Fry, 1989; reviewed by Cosgrove, 2005); in this project we discovered that xyloglucan may also strengthen cutin, but via ester bonds.

4.9 Other cutin-to-carbohydrate transacylase activities

By screening the acyl acceptor abilities of progressively smaller XGOs, we found that only [^{3}H]XXXGol and [^{3}H]XXGol can be the acyl acceptor of the novel cutin transacylase, with the latter exhibiting only 1/10 the ability of the

former (Fig. 60), suggesting a substrate specificity based on the substrates' molecular weight.

Like XXXG, XXFG is another abundant xyloglucan building block in dicot plants, also found in pea epicotyl epidermis (reviewed by Hayashi, 1989), and with a fucose and a galactose added to the X next to the G, turning it into an F (Fig. 65) (Fry *et al*., 1993). [^{3}H]XXFGol was used as with [^{3}H]XXXGol *in situ*. Surprisingly, even though their structures are very similar, the CMNaOH-releasable ^{3}H ratio of [^{3}H]XXFGol was only ~0.3% of the supplied substrate (Fig. 62) [cf. ~2.5% in the case of [^{3}H]XXXGol], indicating that it has little acyl acceptor ability in cutin transacylase reactions.

The addition of two monosaccharide residues onto X almost prevented transacylation. This is possibly because the linkage point accessed by cutin is one of the free hydroxy groups (C-3 or C-4) of the third xylose residue in XXXGol, the additional groups impose steric hindrance to prevent the approach of the transacylase. The free hydroxy group at C-2 is less likely compared with the two above because it is completely hindered in XXFGol, and therefore may would have resulted in complete no incorporation, instead of ~0.3% (Fig. 62). I propose that cutin is more likely to ester bond with the hydroxy group at C-4 of the α-D-xylose, because it is stereo-structurally close to the additional monosaccharides at C-2 (Fry *et al*., 1993; Xue and Fry, 2012) (Fig. 89). Furthermore, as stated above, even though it has not yet been reported, this cutin ester bond could conceivably promote the α-D-xylosidase or β-D-glucosidase activities by unidentified mechanisms, resulting in the majority transacylase product being cutin–[^{3}H]XGol (Fig. 90).

This hypothesis was not tested in this project but could be studied in future ('***future perspectives***').

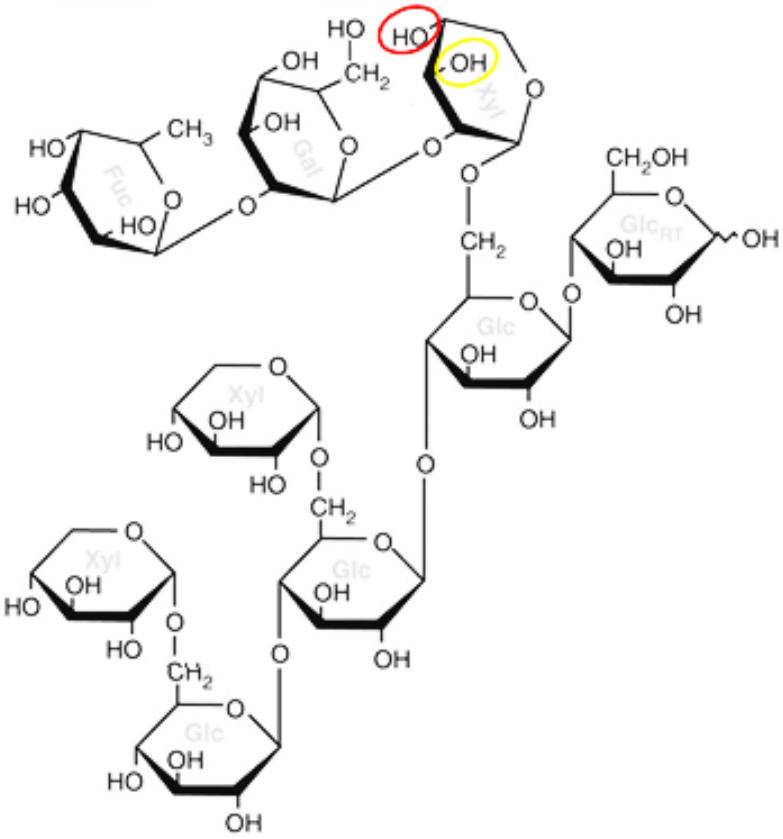

Figure 89. A simplified diagram of XXFG's stereo-structure. As in figure 65, the first unit (from left), X, is composed of α-D-xylopyranosyl-(1→6)-β-D-glucose. The third X is converted into F with the addition of a D-galactose (β-1→2) and an L-fucose (α -1→2). The two free hydroxy groups on the xylose in the F unit are circled out: the hydroxy group at C-4 (red circle) is closer to the D-galactose than the one at C-3 (yellow circle), which points to the opposite direction of D-galactose and L-fucose (adapted from Xue and Fry, 2012).

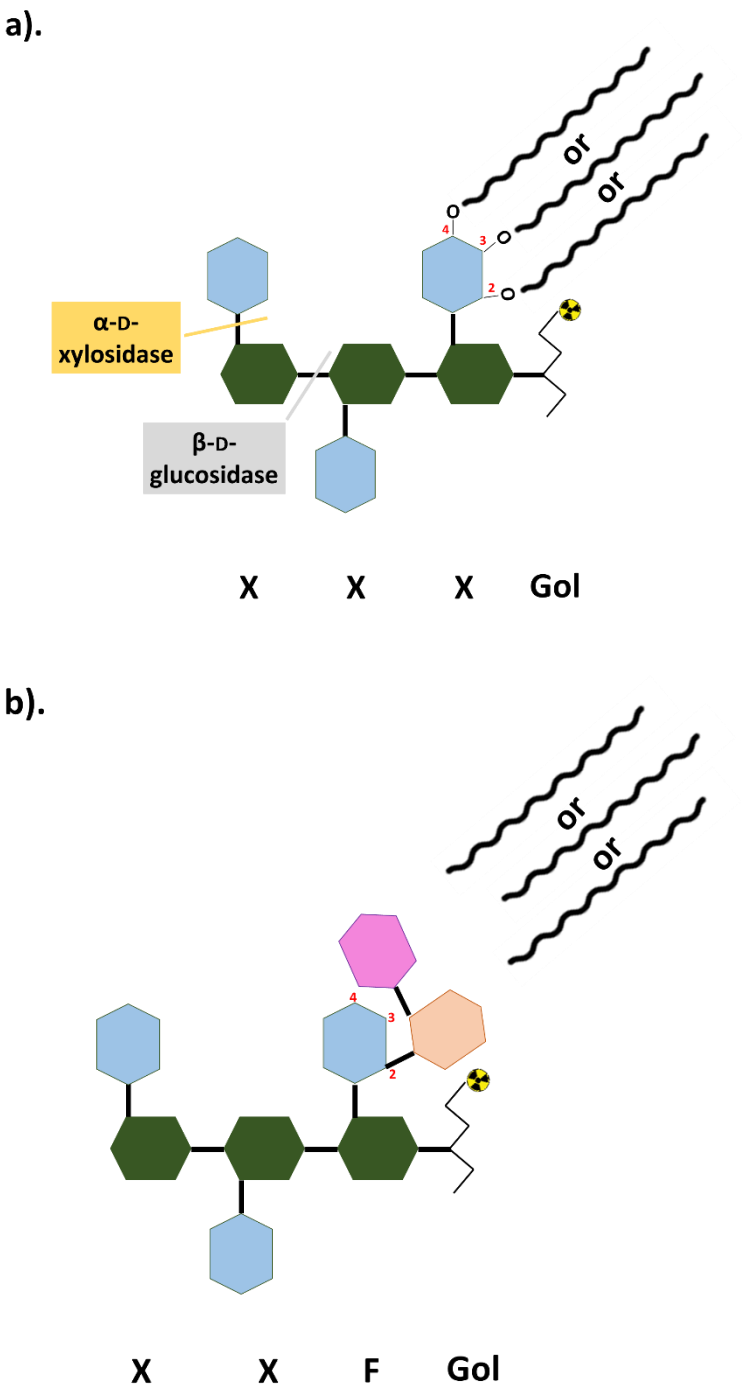

Figure 90. A simplified diagram of the cutin–[^{3}H]XGO conjugate structure. Details of [^{3}H]XXXGol and [^{3}H]XXFGol are as in figure 42 and 61. (a). Cutin (**black wiggle line**) is proposed to ester bond with three free hydroxy groups at C-2, C-3 and C-4 (numbered in red) of the xylose next to the Gol unit in [^{3}H]XXXGol. The α-D-xylosidase (in yellow) and β-D-glucosidase (in grey) release xylosyl and glucosyl residues from the non-reducing terminus respectively, eventually producing cutin–[^{3}H]XGol from the original cutin–[^{3}H]XXXGol conjugates. (b). The addition of D-galactose and L-fucose in [^{3}H]XXFGol at C-2 (in red) is predicted to impose

steric hindrance on the hydroxy groups at C-3 and C-4 (in red) as well, resulting in no linkage with cutin (**black wiggle line**).

Some polysaccharides contain acyl groups, such as homogalacturonan, which has –COOH at C-6, and sometimes being methyl esterified to –$COOCH_3$. The latter with an activated acyl group can potentially be an acyl donor, but they both can be acyl acceptors. However, neither of the oligogalacturonides was incorporated into pea epicotyl or tomato fruit epidermis (Fig. 55–53), these consistent results clearly indicated that the newly discovered transacylase only uses certain oligosaccharides as the acyl acceptor. The methyl esterified oligogalacturonan also cannot be the acyl donor, under the catalysis of neither the transacylase we proposed nor pectin methylesterases (PMEs) (reviewed by Brummell and Harpster, 2001), which can potentially act as a transacylase (i.e. transferring the acyl group of methyl esterified [^{3}H]$GalA_8$-ol to cutin hydroxyl groups). Thus, we can conclude that model 2 (Chapter 1, Fig. 5b), which proposed that a polysaccharide's acyl group is linked to a hydroxy group of cutin is invalidated, at least under our experimental conditions.

Besides the pectic backbone, an oligomer related to a side chain in the RG-I domain, arabinan, was also assayed *in situ*. The arabinan length in nature varies depends upon species (e.g. tetrasaccharide in *Arabidopsis* leaf, but longer than pentasaccharide in sugar beet cell wall) (reviewed by Willats *et al*., 1998; Harholt *et al*., 2010). The arabinan length in pea epicotyl RG-I is not reported as we were aware, so the octasaccharide, [^{3}H]Ara_8-ol was used due to availability. Only a very small portion (~0.12%) of supplied

radioactivity was incorporated into a product releasable by CMNaOH in both ice plant and pea epidermis samples (Fig. 48 and 46), suggesting that Ara_8-ol has a very low acceptor ability. However, comparing with the zero incorporation of oligogalacturonides, the slight formation of ester-bonded RG-I side chain oligomer may suggest that if cutin does become ester-linked to pectin, it is probably only to the side chains.

The secondary cell wall component oligomers, [^{3}H]Man_3-ol and [^{3}H]Xyl_5-ol were not incorporated into pea epicotyl epidermis *in situ* (Fig. 63 and 64), suggesting that cutin can ester-link only to primary cell wall components.

In summary, these results show that cutin is only ester-linked to specific xyloglucan domains at a specific hydroxy group to form hetero-conjugates, the other tested oligosaccharide and the monosaccharide, glucose, have little or no acceptor ability.

4.10 Preliminary knowledge of the protein responsible for cutin-to-XGO transacylase activity

The *in-situ* and *in-vitro* assays (Fig. 78–74) together strongly indicated that cutin synthase (CD1; Yeats *et al*., 2012) is not the transacylase we observed *in-* and *ex-situ* (e.g. Fig. 62a, 65 and 66), because the CMNaOH-releasable ^{3}H was not reduced in *cd1*-knockout tomato fruit epidermis significantly, and the purified His_6-tagged CD1 did not catalyse the ester bond formation of XXXGol with tomato fruit epidermis or the acyl group in *p*-NPP. Moreover, the developmental stages with the highest transacylase activity in tomato fruit (cv. M82 and Ailsa Craig) were later than the stage with the highest quantity

of CD1 (cv. M82) (Yeats *et al*., 2012) (i.e. 21–30 DAA for the transacylase vs. 15 DAA for CD1) (Fig. 81 and 76).

Comparing with the cutin-to-HHA transacylase, whose highest activity co-occurred with the highest amount of CD1 (Fig. 34, Chapter 3), suggesting that (a) the cutin-to-XGO transacylase is a different enzyme from the cutin-to-HHA transacylase, and (b) the cutin-to-XGO transacylase is less related to CD1 than the cutin-to-HHA transacylase is because of its lagged peak time during development.

A pre-incubation cold-buffer wash tended to decrease the cutin-to-XGO transacylase activity (Fig. 52 and 50), which was not expected because the transacylase was predicted to be stably embedded within the epidermis based on its substrates (cutin and xyloglucan). This result may indicate the *in-muro* localisation of the cutin-to-XGO transacylase: it is within the hydrophilic, polysaccharide-rich cell wall (thus aqueous extractants can penetrate easily and solubilise the enzyme), unlike the cutin-to-HHA transacylase, which may be associated with the more hydrophobic cutin-rich layers (Fig. 11 and 12, Chapter 3).

Ex-situ assays results showed that the reducing agent DTT and the metal chelator EDTA slightly increased the cutin-to-XGO transacylase activity and/or extraction (Fig. 71 and 66), suggesting that (a) this transacylase does not require a metal-ion co-factor, and (b) its 3-D structure may allow undesired disulphide bond formation, which changed the conformation and resulted in decreasing activity. The potential XET activity interferences did

not invalidate this conclusion because XET activity from pea epicotyl has been reported to be decreased by EDTA (Fry *et al*., 1992).

An *Arabidopsis* rosette cell wall proteome study demonstrated that the addition of CDTA, which is also a metal chelator sometimes used in parallel with EDTA (Carver *et al*., 1984; Sousa and Silva, 2005), helps in solubilising cell wall proteins involved in defence (Boudart *et al*., 2005). This report might suggest that some structural traits (e.g. spatial distribution of charged amino acids) are shared between the cutin-to-XGO transacylase and known defence proteins.

In summary, even though the cutin-to-XGO transacylase was not identified in this project, the results above provide useful hints for future identification.

4.11 Speculation as to cutin-to-XGO transacylase's physiological function

In both ice plant and pea epidermis samples, the highest cutin-to-XGO transacylase activity occurred at pH 6.5 and 7.5 (Fig. 46 and 44), which were slightly out of the physiological apoplastic pH range for expanding cells, suggesting that this reaction may be only required after cell expansion ceased. This observation may not be obtained from the XET interferences, because the optimum pH for XET activity in pea epicotyl has been reported to be pH 5.5 (Fry *et al*., 1992).

Physiological functions of the cutin-to-XGO transacylase can be predicted by comparing its activity characters with a known enzyme. For instance, TCH4 (AtXTH), an XET-active XTH of *Arabidopsis*, has highest activity at pH values

(6.0–6.5; Purugganan *et al.*, 1997) slightly out of the physiological range (reviewed by Cosgrove, 2005); and it is expected to increase cell wall strength (Purugganan *et al.*, 1997), providing a hint of that the newly discovered transacylase also reinforces epidermis.

The preference for a slightly basic pH was consistent with the results of screening developmental stages, because more [^{3}H]XXXGol became ester bonded in the epidermis of the organs at late expanding stages (tomato fruit and ice plant leaf) (Fig. 81–77). However, different from the earlier speculation, this novel transacylase activity was shown to be decreased after the cessation of tomato fruit's expansion (Fig. 81 and 76), which is consistent with our hypothesis that cutin-to-XGO transacylase activity is required during growth. Taken together, these results suggested that the transacylation reaction is actually required during cell expansion, but not from the beginning when cells were too small to need epidermal mechanical reinforcement.

The effects of environmental factors on the transacylase activity can also be used to speculate on its physiological functions. For example, light exposure was found to diminish the novel transacylase activity because when the growth rate of pea epicotyl was 4 times slower, the transacylase activity was reduced to half in the *ex-situ* assay (Fig. 87), and ~23% lower in the *in-situ* assay (Fig.79). This observation supported our hypothesis that the cutin-to-XGO transacylase is required during cell expansion and suggested a positive correlation between cell expansion rate and the novel transacylase activity. A possible explanation of the correlation is that rapidly expanding epidermal cells require more epidermal reinforcement.

The effects of humidity were tested *in*- and *ex-situ*, but high humidity only reduced the cutin availability and the cutin-to-XGO transacylase activity slightly (Fig. 86 and 81), suggesting that the transacylase does not play a role in e.g. controlling water permeation. If it does, then it might be via tightening cell wall pore sizes.

The effects of cold temperature were tested *in situ*. The significant increase of the novel transacylase activity in the first 4 days at 4°C followed by a decrease (Fig. 88) is interesting because it hinted that the cutin-to-[^{3}H]XXXGol transacylation reaction may be involved in resisting a short period of cold. Again, the XET activity of TCH4, which putatively strengthens the cell wall as mentioned above, is also higher at 12–18°C than at warmer temperatures (Purugganan *et al*., 1997), providing another piece of possible evidence as to the transacylase's physiological function. A possible explanation of the increase of cutin-to-XGO transacylase activity at the beginning of the cold stress is similar to the last paragraph: the cutin–[^{3}H]XXXGol link changed the cell wall porosity size to reduce the risk of ice formation in the apoplast (Beck *et al*., 2007).

Taken together, the data may suggest that the cutin-to-XGO transacylase is involved in mechanically strengthening cuticle; other physiological functions (e.g. cell wall pore size regulation) are more speculative and would require more evidence.

Conclusions

In this project, I reproducibly observed the novel cutin-to-[^{3}H]XXXGol (thus potentially cutin-to-xyloglucan) hetero-transacylase activity in different organs of different plants and demonstrated the activity by identifying the low-abundance transacylase product via chemical degradation coupled with chromatographic strategies. By comparing various cell wall oligosaccharides, I solved the long-standing question by proving that the only acyl donor for the cutin–polysaccharide conjugate is cutin (model 1), instead of methyl esterified homogalacturonan (model 2). Based on the results so far, I propose that cutin is ester bonded with a hydroxy group of the xylose of the X unit next to Gol, because the linkage with cutin was prevented when the xylose is hindered (XXFGol). The precise linking site is predicted to be the free hydroxy group at C-4 of the xylose in XXXGol, because it can be largely affected by the additional residues in XXFGol (stereo-structurally close), but not completely shielded as the C-2. CD1 as the only well-studied GDSL enzyme was tested and did not catalyse the cutin-to-[^{3}H]XXXGol transacylation reaction; therefore, we cannot conclude whether the protein responsible for the novel transacylase activity belongs to the GDSL family. The pH optimum and the effects of DTT and EDTA on the transacylase's activity provided hints for its future identification. The new transacylase's physiological functions are proposed to be mechanical reinforcing the epidermis based on changes in its activity during development. More potential functions (e.g. regulating cell wall pore size during a short cold period) are also speculated but lack of evidence here.

Future perspectives

The chemical degradation, alkali-hydrolysis (CMNaOH) strategy, which was employed to elucidate the XGO-incorporation mechanism should be replaced by a functional cutinase, hydrolysing cutin specifically to avoid contaminations from XET products. Unfortunately, to detect isotopes, special types of mass spectrometry (MS) are required (e.g. isotope-ratio mass spectrometry which used to determine the relative abundance of isotopes in given samples) and the technology must be highly sensitive to detect a small amount of product. Thus, radiochemistry is the best technology to pioneer this study so far.

The newly discovered hetero-transacylase product, cutin–XXXG/XXG/XG is valuable to be characterised via e.g. partial hydrolysis coupled with mass spectrum, to explore the precise linking position and how the linkage promotes glycosidase activities.

The hetero-transacylase will be identified by starting from recombinant expressing and assaying CD1 homologues (e.g. *Solyc04g050570.2.1*, coding a polypeptide with 74% similarity to CD1). Other methods such as screening genes with enhanced expression (transcriptomic study) at the tomato fruit developmental stage with the highest cutin-to-[^{3}H]XXXGol transacylase activity should be considered. Or more directly, proteomic studies (i.e. using active site probes which can specifically bind to the serine residue covalently and contain e.g. biotin groups for pulling-down by binding to streptavidin resins non-covalently) is another option. In addition, the hetero-transacylase

will be heterologously produced and purified, and its substrate specificity (e.g. polymeric xyloglucan and newly synthesized xyloglucan oligomer will be compared), kinetics and other characteristics will be studied *in vitro* by adapting the optimised assaying methods.

The hetero-transacylase's physiological functions will be investigated *in planta* by generating mutated plants (e.g. tomato fruit) followed by e.g. mechanical tests and microscopic studies. It is hypothesized that the plants lack of the hetero-transacylase will show a different cutin-to-cell wall interface pattern from WT and less resistant to external forces.

Chapter 5. Cutin-to-glycerol transacylation

Introduction

Glycerol, as a natural component in cutin, is proposed to be important for plant growth due to the following reasons. First, as a by-product from the cutin synthesis reaction (Chapter 1, *Eq*. 1), additional glycerol can theoretically reverse the polymerisation process, and therefore loosen the existing cutin matrix to allow faster plant growth (hypothesis: cutin restrains cell expansion). Second, Yang *et al*. (2016) found that glycerol quantity increased with dicarboxylic acid in cutin, suggesting that glycerol may be required for cross-linking cutin molecules. Graça *et al*. (2002) also proposed that glycerol might act as a scaffold for cuticle fatty acids to form ester bonds with its three hydroxy groups, and H-bonds between adjacent hydroxyl-fatty acids, which may contain free hydroxy groups can strengthen cutin. In this project, we focused on the effect of exogenous glycerol on cutin metabolism (based on *Eq.* 1), which had not been reported yet as far as we were aware.

We hypothesized that glycerol can act as an acyl acceptor because of it contains hydroxy groups, under catalysis of (1) a novel cutin-to-glycerol transacylase, (2) the cutin-to-HHA transacylase we observed in Chapter 3, with the assumption that this enzyme is not strict with the acceptor species, or (3) CD1 (*Eq*. 1) (Yeats *et al*., 2012), or all of them (1) to (3).

Five experimental strategies (Table 10) were employed to investigate the hypotheses above: cutin-to-[U-^{14}C]glycerol transacylation (*in situ*); the effects of exogenous glycerol on [^{3}H]HHA incorporation (*in situ*); exogenous glycerol

was supplied to observe its predicted effect on cutin degradation (*in situ*), and glycerol's acceptor ability under the catalysis of CD1 was also assayed *in vitro*. Any exogenous glycerol effects on cutin were also observed from a physiological aspect: seed germination and seedling elongation were measured (*in planta*).

Overview of the 5 experimental strategies

The 5 strategies used to test exogenous glycerol effects on cutin are listed in Table 10.

Assay name	Assay set up	Details	Assay type	Detection method
Cutin-to-[U-^{14}C]glycerol transacylation		Epidermis was incubated with [U-^{14}C]glycerol at pH 5.5	*In situ*	Scintillation counting methanol-insoluble residues
Exogenous glycerol effect on [^{3}H]HHA incorporation		Epidermis was incubated with [^{3}H]HHA together with glycerol		
Exogenous glycerol effect on previously cutin-incorporated [^{3}H]HHA		Cutin was incubated with [^{3}H]HHA first to be radio-labelled, and then incubated with glycerol		Scintillation counting glycerol
p -Nitrophenyl palmitate-to-glycerol transacylation assay		*p* -Nitrophenyl palmitate was incubated with glycerol and CD1	*In vitro*	A_{405}
Exogenous glycerol effects on seeds		Exogenous glycerol was added to seeds	*In planta*	No. of germinated seeds and seedling lengths were

Table 10. Summary of the 5 strategies: testing exogenous glycerol effects on cutin.

*Green circles: cutin fatty acid residues; **black lines**: ester bonds; **blue circles** with or without radio-labels: [U-^{14}C]glycerol or glycerol; **pale red circles** with radio-labels: [^{3}H]HHA; **yellow circles**: *p*-nitrophenyl or *p*-nitrophenol; **purple circles**: palmitate.

Results

5.1 Testing a novel cutin-to-glycerol transacylase activity *in situ*

Based on *Eq*.1 (Chapter 1) we hypothesized that cutin can also be transacylated onto glycerol molecules, under catalysis of an unspecified GDSL transacylase (Fig. 91). The assay conditions were the same as for cutin-to-[^{3}H]HHA (Chapter 3), and the transacylase product, cutin-[U-^{14}C]glycerol conjugate, was looked for by scintillation counting of the methanol-insoluble residues.

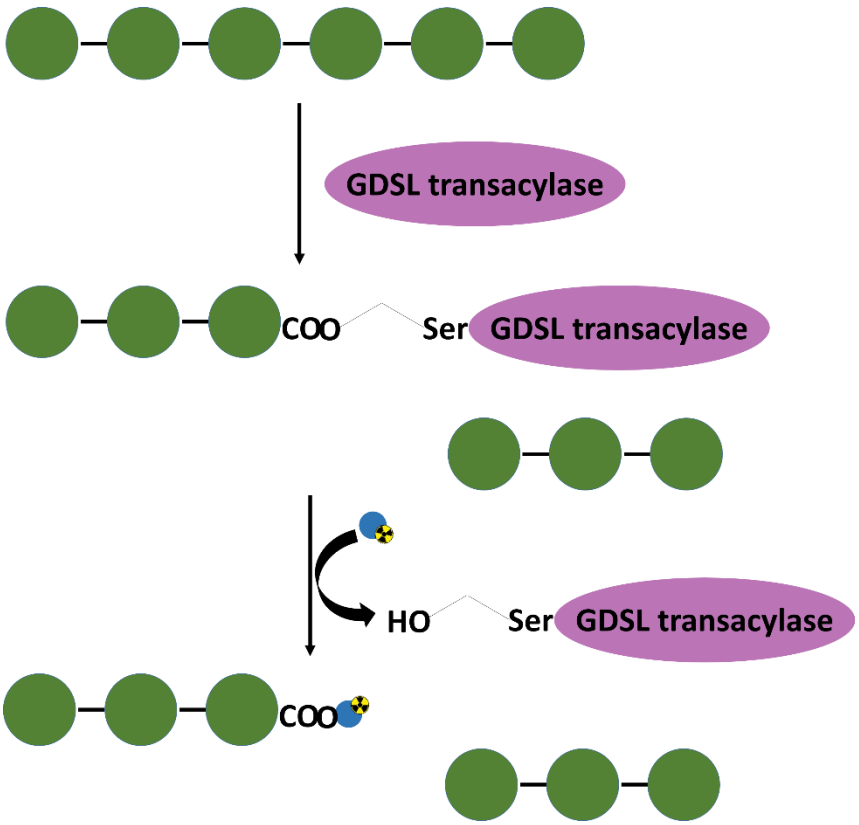

Figure 91. Proposed cutin-to-glycerol transacylation reaction. An intact cutin polymer (**green circles**: cutin fatty acid residues; **black lines**: ester bonds) is proposed to be attacked by an unspecified GDSL transacylase (**pale purple oval**), followed by formation of a cutin-transacylase intermediate via cross-linking a carboxy group of cutin to the hydroxy group of serine (Ser) in the catalytic triad. The carboxy group of cutin (acyl donor) is then transferred to hydroxy groups of [U-^{14}C]glycerol (acyl

acceptor, **blue circles** with radiolabels). The final products are a cutin-[U-^{14}C]glycerol conjugate, and the released cutin fragment.

After 24 h incubation of ice plant-leaf adaxial epidermis with [U-^{14}C]glycerol, the incorporation by frozen/thawed/pre-incubation washed and un-denatured epidermis was negligible (Fig. 92a).

To reduce any potential physical barrier for the endogenous enzyme to access exogenous glycerol, Triton X-100, which partially destroys cell membranes to render the cuticle enzymes more accessible to exogenous substrate, was added to incubation buffer in a repeat experiment. Nevertheless, there was still no enzymic incorporation because no significant differences between un-denatured epidermis samples and the controls were observed ($P > 0.05$) (Fig. 92b). In presence of Triton X-100, the effect of a pre-incubation wash of the epidermis was also investigated as in Chapters 3 and 4, but the un-washed epidermis also did not incorporate ^{3}H enzymically (Fig. 92c), agreeing with the samples that had been pre-washed (Fig. 92b).

In conclusion, these results indicate that the novel cutin-to-[U-^{14}C]glycerol transacylase may not exist.

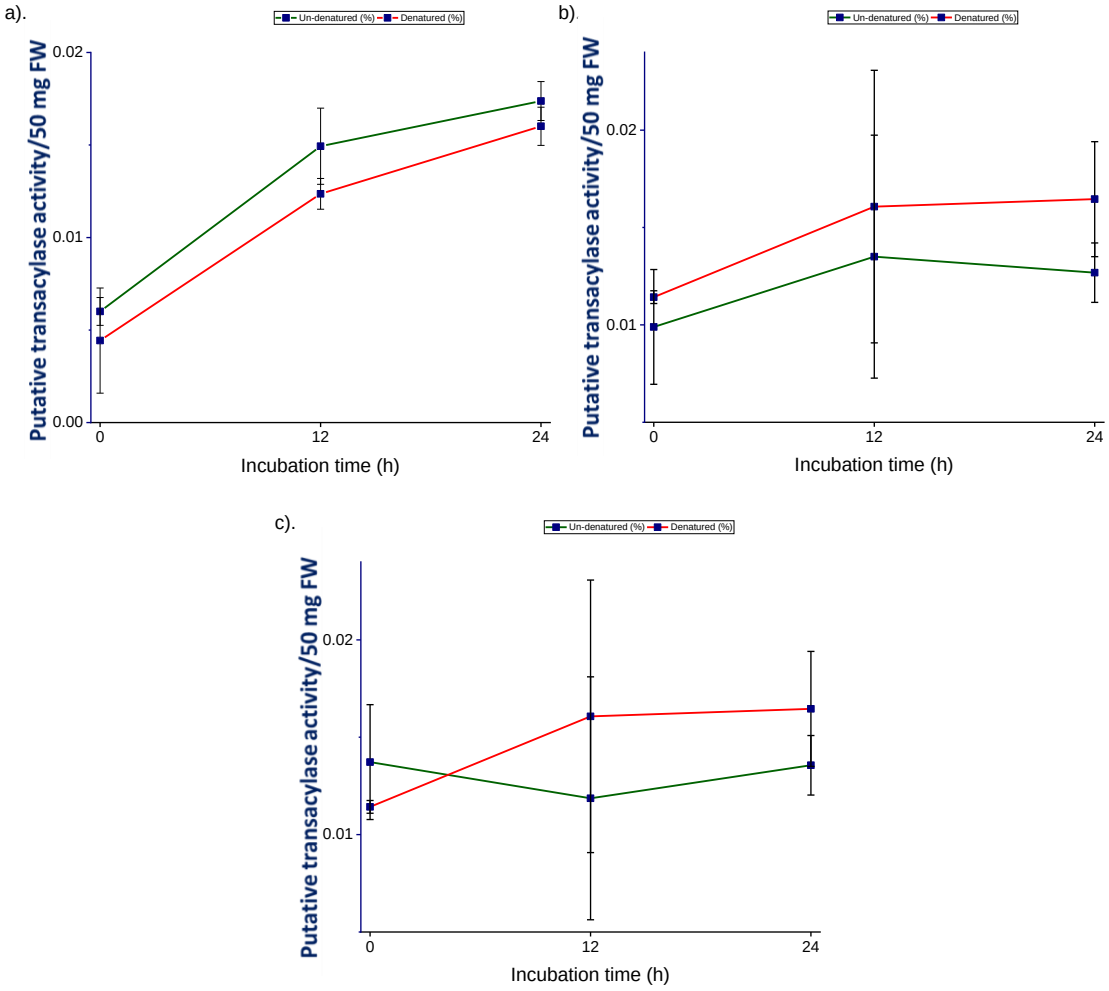

Figure 92. Cutin-to-[U-^{14}C]glycerol transacylation *in situ*. Blot-dried ice plant leaf epidermis (50 mg; acyl donor) with or without active endogenous enzymes was incubated with 2.1 kBq exogenous [U-^{14}C]glycerol (acyl acceptor) under the standardised conditions (Chapter 3). The MFW (9/1/1)-insoluble residues were scintillation counted to look for the cutin–[U-^{14}C]glycerol conjugates.

(a) Cutin-to-[U-^{14}C]glycerol reaction was incubated with buffer only;

(b) 0.1% Triton X-100 (v/v) was added to both the pre-wash and incubation buffer;

(c) un-prewashed epidermis was incubated with buffer containing 0.1% Triton X-100.

The total incorporated radioactivity ratio (%) was used to illustrate the endogenous cutin-to-[U-^{14}C]glycerol transacylase activity, it was calculated as follows: the detected radioactivity (cpm/50 mg epidermis) / supplied radioactivity (cpm) × 100%. Green line: um-denatured epidermis samples. Red line: denatured samples (control). Bars indicate standard errors in (a) (n=3); and range in (b) and (c) (n=2).

A value of 0.01% incorporated radioactivity/50 mg epidermis/supplied radioactivity corresponds to an absolute incorporation of 4 cpm/50 mg epidermis.

5.2 Testing a new activity of the cutin-to-HHA transacylase *in situ*

As a cutin component, glycerol may also be a competing substrate (acyl acceptor) of a cutin-to-cutin transacylase. Since we found such an enzyme activity by monitoring cutin-to-[^{3}H]HHA transacylation reactions (Chapter 3), I incubated pea epicotyl epidermis with [^{3}H]HHA together with non-radioactive glycerol solution up to 1 M, to test if the exogenous glycerol can compete with [^{3}H]HHA incorporation.

Un-denatured epidermis samples incorporated ~40 times more ^{3}H from [^{3}H]HHA than the control, indicating that it is an enzymic incorporation (observed repeatedly in Chapter 3) (Fig. 93). Thus, any decreased radioactivity incorporation in un-denatured epidermis samples may indicate that glycerol is also a substrate of the same transacylase. However, even 1 M glycerol solution, which is probably much higher than the physiological concentration, did not have any impact on ^{3}H incorporation ($P > 0.05$) (Fig. 82). This result indicates that the observed cutin-to-[^{3}H]HHA transacylase does not catalyse the proposed cutin-to-glycerol transacylation. Together with the *in-situ* results above (Fig. 92), we may conclude that glycerol is not a substrate of the cutin re-modelling transacylases, at least not detectable by the techniques we used.

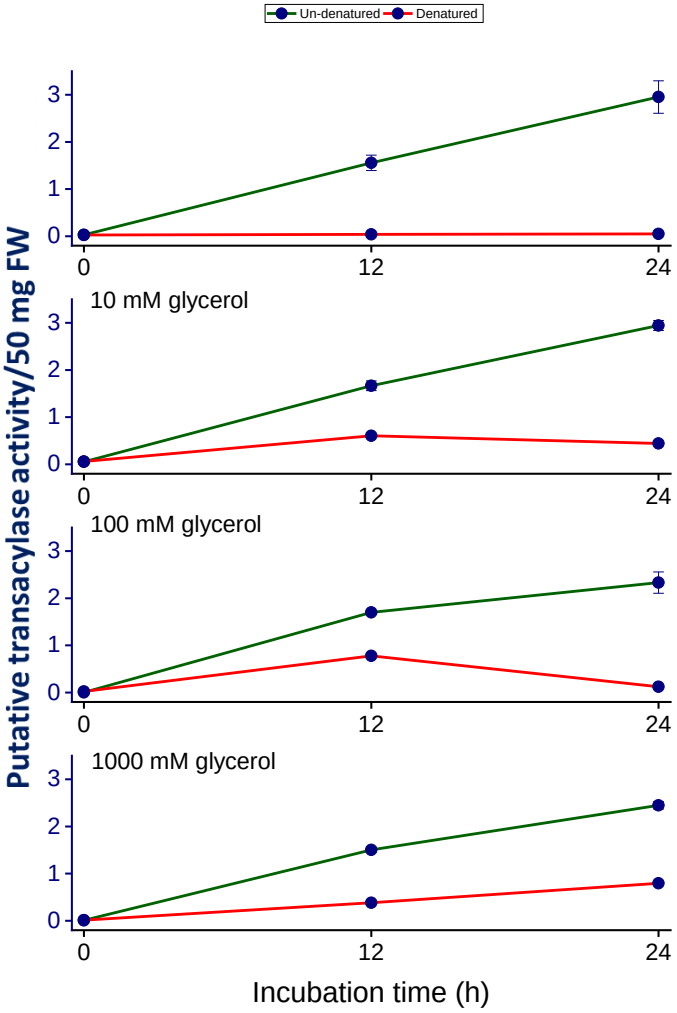

Figure 93. Exogenous glycerol effects on [^{3}H]HHA transacylation *in situ*. Pea epicotyl epidermis (50 mg; acyl donor) with or without endogenous active enzymes was incubated with 0.14 kBq exogenous [^{3}H]HHA (acyl acceptor) at pH 5.5 with or without non-radiolabelled glycerol (0–1000 mM) simultaneously at room temperature for 1 day. The CMNaOH-releasable radioactivity ratio (%) was used to illustrate the effects of exogenous glycerol on the endogenous cutin-to-[^{3}H]HHA transacylase activity. Green line: um-denatured epidermis samples. Red line: denatured samples (control). Bars indicate standard errors for the 'un-denatured' group (n=3). No bars for the 'denatured' group (n=1).

A value of 1% CMNaOH-releasable radioactivity/50 mg epidermis/supplied radioactivity corresponds to an absolute incorporation of 26 cpm/50 mg epidermis.

5.3 Testing a novel activity of CD1 *in vitro*

Based on the *Eq. 1* (catalysed by CD1), its reverse reaction by using glycerol as the acyl acceptor might possibly degrade pre-formed cutin (acyl donor). Thus, based on the assumption that CD1 equivalent exists in pea epicotyl epidermis, I radio-labelled cutin by [^{3}H]HHA under the optimized condition (Chapter 3), and then glycerol solution was added to putatively break cutin. Any broken down cutin fragments, such as [^{3}H]HHA–glycerol, would be released into supernatant and can be detected by scintillation counting.

Scintillation counting of aqueous solutions is highly sensitive; however, there was no significant difference ($P > 0.05$) between the amount of radioactivity released in 0 and 1 M glycerol solutions (Fig. 94a). The same procedure was repeated but with gently washing epidermis samples in the incubation buffer instead of water to keep the endogenous enzyme activity, but the result was consistent (Fig. 94b).

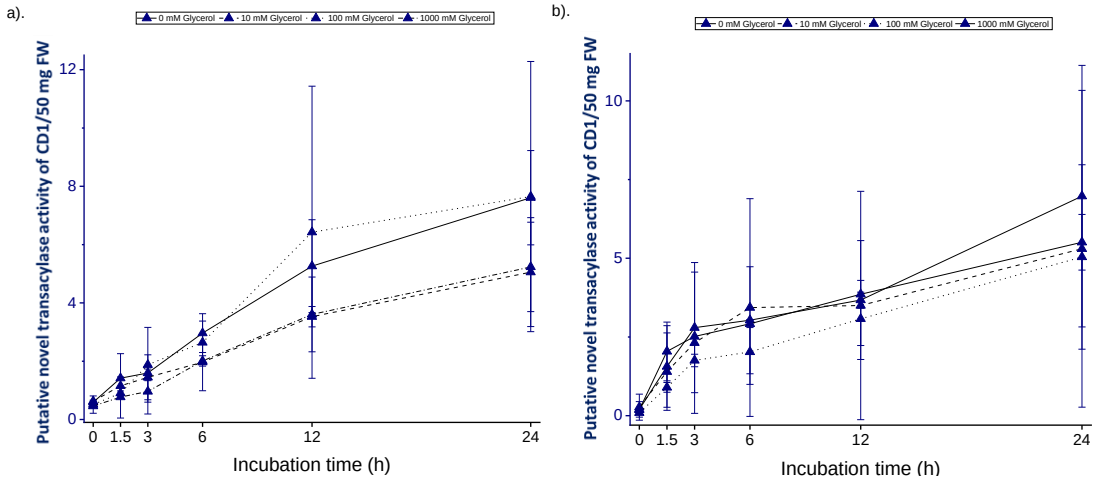

Figure 94. Exogenous glycerol effects on previously incorporated [^{3}H]HHA *in situ*. Pea epicotyl epidermis (50 mg; acyl donor) containing active endogenous enzymes was incubated with 0.42 kBq exogenous [^{3}H]HHA (acyl acceptor) under the standardised conditions, followed a gentle wash in water (a) or a pH 5.5 buffer (b) to

remove un-incorporated [^{3}H]HHA, but still keep the activity of endogenous enzymes (including the proposed transacylase), and then incubated in glycerol solutions (0–1 M) to look for the release of ^{3}H–glycerol conjugates. The releasable radioactivity ratio (%) was used to illustrate the proposed degradation effects of exogenous glycerol. Bars indicate range (n=2).

A value of 1% releasable radioactivity/50 mg epidermis/supplied radioactivity corresponds to an absolute incorporation of 80 cpm/50 mg epidermis.

The negative result might be because of the following possibilities: (1) the water or buffer wash of un-incorporated [^{3}H]HHA was not enough, and therefore the small quantity of released cutin-incorporated [^{3}H]HHA–exogenous glycerol conjugates was masked; (2) CD1 equivalent did not catalyse the reverse reaction of cutin synthesis; (3) a CD1 equivalent does not exist in pea epicotyl epidermis. The first possibility was difficult to overcome because the aqueous wash was never completely efficient at removing [^{3}H]HHA, whereas organic solvents (e.g. 80% methanol) harm endogenous enzymes. The third possibility was also difficult to test in this project. However, the possibility (2) can be partially answered by testing the purified CD1 activity on glycerol *in vitro*.

Therefore, I incubated the purified His_6-tagged CD1 with *p*-nitrophenyl palmitate (*p*-NPP, acyl donor) and glycerol (acyl acceptor) to look for the palmitoyl–glycerol product by measuring the release of *p*-nitrophenol spectrophotometrically (Fig. 95a).

However, in the presence of CD1, the amount of released *p*-NP was not significantly increased with 11 mM glycerol addition ($P > 0.05$) (Fig. 95b), suggesting that CD1 did not catalyse this transacylation reaction (Fig. 95a).

Taken together, glycerol may not be the substrate of CD1, in turn indicating that the cutin biosynthesis reaction catalysed by CD1 cannot be reversed.

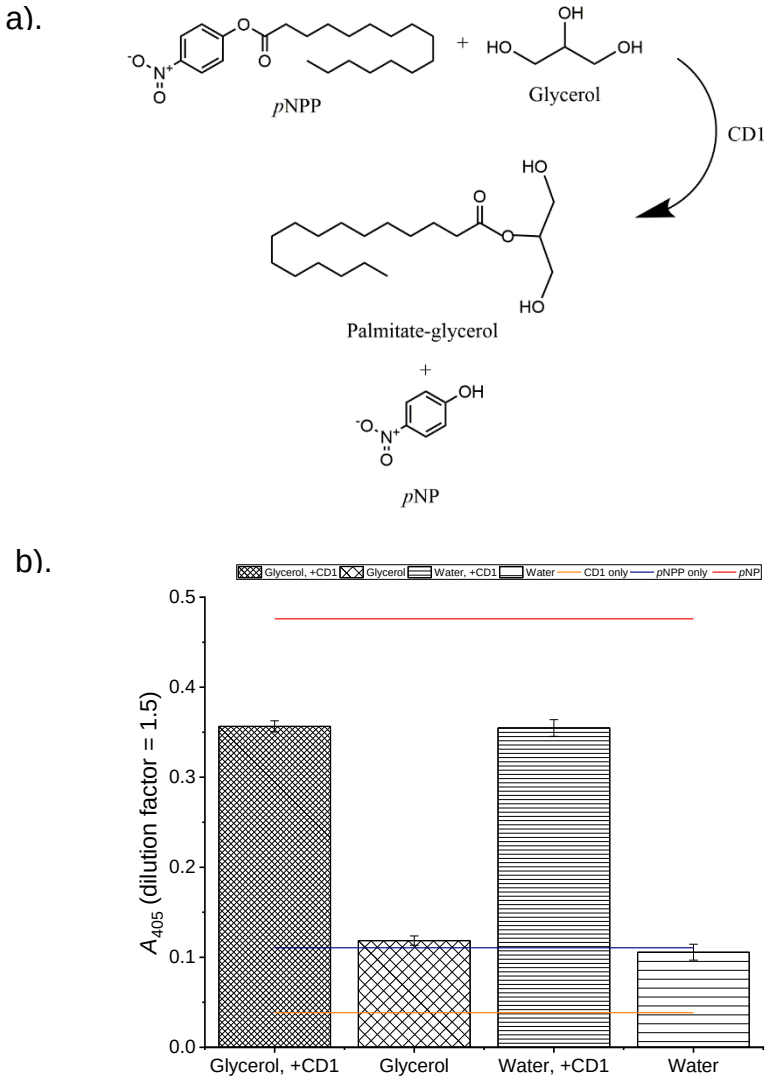

Figure 95. Proposed glycerol transacylation mechanism and *in-vitro* assay. (a) CD1 transfers the acyl group, palmitate, from *p*-nitrophenyl palmitate (*p*NPP) to any hydroxy group of a glycerol molecule, resulting in a palmitoyl–glycerol ester bonded conjugate and a free *p*-nitrophenol (*p*NP) molecule, which can be detected by spectrophotometer (A_{405}) at pH 7.15±0.02. (b) *p*-Nitrophenyl palmitate (final conc. = 0.5 mM) was incubated with or without 11 mM (final conc.) glycerol, in the presence of His_6-tagged CD1 (1 µg/100 µl 25 mM succinate-Na^+ buffer, pH 5.5) at 25°C for 3 days. The released *p*-nitrophenol was detected at 405 nm (dilution factor = 1.5). *p*NPP only: 0.5 mM *p*-nitrophenyl palmitate, a control; CD1 only: a blank; *p*NP: 0.5 mM *p*-nitrophenol, a standard if the *p*NPP was completely hydrolysed. Bars indicate standard errors in (b).

5.4 Testing how exogenous glycerol affect physiology *in planta*

Some plant seeds (e.g. soybean, *Arabidopsis thaliana* and *Brassica napus*) have been reported to contain cutin in the seed coat (Molina *et al*., 2008; Ranathunge *et al*., 2010). Exogenous glycerol was supplied to seeds on the assumption that it might loosen cutin and thus allow faster germination and seedling elongation by the reverse reaction of cutin biosynthesis (Chapter 1, *Eq*. 1).

Parsnips seeds were chosen because of their slow germination rate, allowing the effect of exogenous glycerol to be well monitored. However, there was no significant difference ($P > 0.05$) in germination ratio between seeds with or without glycerol (Fig. 96a). Even though 5 mM glycerol led to a slightly higher number of germinated seeds than 0 and 50 mM did from 10 days after sowing (DAS) in this experiment, it was not reproducible in other comparable ones (data not shown). As for the seedling lengths, there was also no significant difference ($P > 0.05$) among the samples with different glycerol concentrations (Fig. 96b). Similar results were also observed in comparable experiments with carrot seed (Fig. 96c).

In summary, the un-affected germination and shoot elongation processes indicated that exogenous glycerol does not help in loosening either cutin in seed coat or in seedlings.

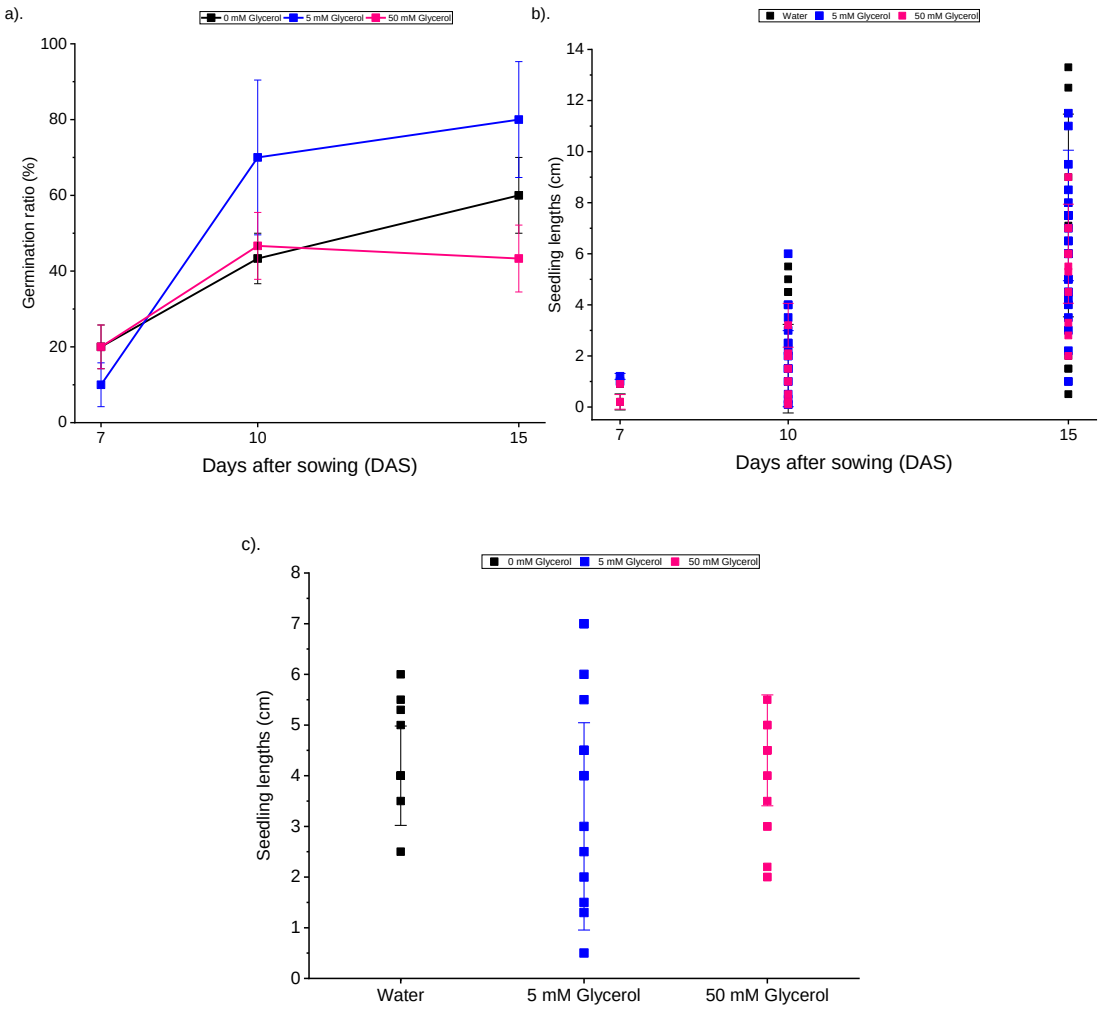

Figure 96. Exogenous glycerol effects on seed germination and seedling elongation. Parsnip and carrot seeds were placed on papers soaked with 0, 5 mM or 50 mM glycerol solution and grown in dark at 25°C. Parsnip: germination ratio was calculated as the No. of germinated seeds/No. of total seeds (a, *n*=3 Petri dishes); seedling (root and epicotyl) lengths were measured manually to ± 1 mm (b, 7-DAP: *n*>3 seedlings; 10-DAP: *n*>10). Carrot seed (c) was germinated under the same condition for 7 days, and the seedling length was measure as in (b) (*n*>10). Bars indicate standard errors in (a). For (b) and (c), bars indicate standard deviations.

Discussion

We expected that glycerol can serve as the acyl acceptor as [^{3}H]HHA and [^{3}H]XXXGol did, under the catalysis of CD1 or other transacylases. However, there was no radio-labelled glycerol incorporated into epidermis comparable with [^{3}H]HHA and [^{3}H]XXXGol incorporation (Fig. 92), and even 1 M exogenous glycerol did not compete with [^{3}H]HHA incorporation (Fig. 93), suggesting that glycerol was not the substrate of any novel transacylase, including the one catalysing the observed cutin-to-[^{3}H]HHA transacylation in ice plant leaf and pea epicotyl epidermis (Chapter 3). It might be because glycerol is not a cutin transacylase substrate, at least not the preferable one naturally. For example, there might be only a few free glycerol molecules or incorporated glycerol residues in pea epicotyl cutin, so the cutin re-modelling transacylases do not transfer a broken cutin chain to glycerol-containing molecules efficiently due to environmental selections. Another possibility is that the quantity of glycerol residues in cutin is not the reason, but their available –OH groups may not be favourable for the cutin re-modelling transacylases: e.g. the *sn*-2 –OH groups is involved in ester bonds, exemplified by the cutin precursor, 2-MHG, and the free *sn*-1,3 –OH groups may be barely used as the acyl acceptor sites. There was no published data to be compared with, since this is the first study of exogenous glycerol effects on cutin.

We also hypothesized that exogenous glycerol can reverse the cutin polymerisation reaction (*Eq*.1) in pea epicotyl epidermis catalysed by CD1 equivalent enzyme, resulting in releasing cutin residues, which in turn

loosens cutin to allow faster germination and seedling growth. However, neither phenomenon was observed (Fig. 96). Comparable experiments have reported that 1 mM exogenous glycerol in growth media can be converted to glycerol-3-phosphate (G3P), which substitutes for glucose 6-phosphate as an energy source (Aubert *et al*., 1994), resulting in increase of *Arabidopsis* shoot length (Hu *et al*., 2014). Spraying ~40 mM glycerol solutions to carrot seedlings also increased shoot length (Tisserat and Stuff, 2011). The inconsistency between those and our own observations suggested that the effects of exogenous glycerol on plant growth requires more independent studies.

However, from a molecular aspect, my results showed that glycerol was not involved in cutin loosening because there was no released cutin residues could be detected by the very sensitive technique, scintillation counting (Fig. 94). Moreover, the purified CD1 did not catalyse *p*-NPP-to-glycerol transacylation (Fig. 95b). Thus, we preliminarily conclude that the cutin polymerisation reaction catalysed by CD1 cannot be reversed, because glycerol is not CD1's substrate, and CD1 may can only use 2-MAGs as the donor, excluding the existing cutin. Yeats *et al*. (2012) have revealed that CD1 transcript and protein amount peak during the rapid growing stages of tomato fruit, so it is possible that the absence of a detectable cutin de-polymerisation reaction is a self-protective strategy, to guarantee that cutin synthesis keeps pace with cell expansion.

Conclusion

Glycerol cannot serve as the substrate of cutin re-modelling transacylases (putatively GDSL enzymes) or the cutin biosynthesis transacylase, CD1 (a GDSL enzyme), maybe because it is naturally a non-preferred substrate in the tested epidermis samples due to the availability and the free hydroxy group species, and/or because the cutin polymerisation reaction is naturally irreversible.

Future perspectives

A plant model with a glycerol-rich cutin matrix should be considered, and the real CD1 substrate, 2-MHG should be chemically synthesized or purified from plants, to test if its acyl group can be transferred from the 2-MHG to glycerol in the presence of CD1.

Chapter 6. Outlook and summary

6.1 Frontier knowledge of plant cutin

6.1.1 Reported characterisations of plant cutin

Plant cutin is widely believed to be an acquired trait for plants to adapt to the terrestrial environment (reviewed by Edwards, 1993; Nawrath, 2006); one of the arguments is that no indication of cutin exists in the land plants' closest living relatives, charophytic green algae, which live in water (Cook and Graham, 1998; reviewed by Wellman *et al*., 2003). Cutin is very widespread among land plants: it can be detected in the epidermis of bryophytes (e.g. in the phylloid of *Physcomitrella patens* and in the thallus of *Marchantia paleacea*) (Schönherr and Ziegler, 1975; Buda *et al*., 2013) up to angiosperms (e.g. tomato fruit and *Arabidopsis* shoot) (Franke *et al*., 2005; Girard *et al*., 2012). Cutin was originally believed to be restricted to the plant shoot (reviewed by Fich *et al*., 2016); however, it was reported very recently that it is also in *Arabidopsis* roots (Berhin *et al*., 2019).

The main roles of cutin in land plants are proposed to be fairly diverse ('***cutin function***', Chapter 1). For instance, it defines organ boundaries (Sieber *et al.*, 2000; Weng *et al.*, 2010). Another important function is cutin's role, together with wax, in preventing water loss (Schreiber *et al.*, 2005; Isaacson *et al.*, 2009). The most interesting biological role of cutin to us is its proposed restricting effect on epidermal cell expansion (epidermal-growth-control theory), and thus on organ growth (Hoffmann-Benning and Kende, 1994; Kutschera and Niklas, 2007). Based on this hypothesis, we proposed that

cutin required to be loosened to allow rapid growth. The effects of plant development on the new cutin-to-fatty acid transacylase activity (summarization in ***6.1.3***) were compatible with our hypothesis.

Cutin has been characterised as a polyester whose building blocks are hydroxy fatty acids (e.g. 10,16-dihydroxyhexadecanoic acid, di-HHA, and 16-hydroxyhexadecanoic acid, HHA) and a minority of other lipophilic compounds, such as aldehydes and alcohols (reviewed by Fich *et al*., 2016). Cutin is putatively a continuous lipid layer as it has been observed under microscope via being stained by lipid staining reagents (Jeffree, 2006; Yeats *et al*., 2012); and the insolubility of cutin in neutral organic solvents, but the capability of being alkali-hydrolysable (Kolattukudy, 1977) provides chemical evidence for its polyester nature. Nevertheless, an overview of cutin architecture still remains hypothetical because of contradicting results ('***cutin structure***', Chapter 1). For example, by marking the free hydroxy groups, Deas and Holloway (1976) and Kolattukudy (1977) found that mainly primary hydroxy groups are involved in polymerisation, whereas the partial hydrolysis of cutin suggests that mainly secondary hydroxy groups contribute to polymerisation (Fang *et al*., 2001; Graça and Lamosa, 2010).

A very recent study of cutin architecture is that conducted by Bhunia *et al*. (2018), who coupled partial hydrolysis of cutin by cutinase, chemical marking of the free hydroxy groups and high-resolution mass spectrometry to study apple fruit cutin's structure. However, by using the cutinase hydrolysis strategy, Bhunia *et al*. (2018) only found oligoesters with primary hydroxy groups involved, whereas the chemical marking strategies showed that

secondary hydroxy groups are more involved in polymerisation than the primary ones. These contradicting results again suggest that the current investigating strategies can produce biased results. For example, ester bonds made via secondary hydroxy groups are more resistant to alkali hydrolysis than those via primary hydroxy groups (Deshmukh *et al*., 2003). Thus, a strategy of investigating the intact cutin layer is required to obtain more *in-vivo* information on the cutin architecture.

Atomic force microscopy could be a powerful tool to obtain nanostructural details of the cutin surface (reviewed by Vahabi *et al*., 2013). However, the resolution of atomic force microscopy does not allow an elucidation of cutin architecture details (e.g. Isaacson *et al.*, 2009; Fig. 4), such as how separate cutin molecules cross-link to each other.

Nevertheless, a general putative cutin molecular architecture has been illustrated in Chapter 1 (Fig. 3).

Covalent links between cutin and cell wall polysaccharides have been proposed for a long time, but only general hints supporting this idea have been obtained, for example from analysing partially digested lime fruit cuticle: oligomers made of cutin fatty acids and cell wall oligosaccharides were found by NMR, and the linkage type was proposed to be ether (Fang *et al.*, 2001; Tian *et al*., 2008; reviewed by Fich *et al*., 2016). However, no evidence of the responsible enzyme activity was shown (Tian *et al*., 2008). Physiologically, polysaccharides in the cell wall are proposed to be involved in reinforcing the cuticle (López-Casado *et al*., 2007; Takahashi *et al*., 2012; España *et al.*,

2014). My findings of a cutin re-modelling (cutin-to-XGO) transacylase activity are the first to indicate a cutin–polysaccharide linking mechanism based on biochemical studies (summarization in ***6.1.3***).

6.1.2 The only well-studied apoplastic cutin transacylase, CD1

The only well-studied apoplastic cutin-related transacylase is cutin synthase (CD1); it has been characterised by *in-vitro* assays and *in-planta* studies (Yeats *et al*., 2012). The polypeptide sequence of CD1 indicates that it belongs to the GDSL family, which is characterised as containing a relatively conserved Gly-Asp-Ser-Leu consensus near the N-terminus (Akoh *et al*., 2004). Proteins belong to this family have a broad substrate specificity due to their induced-fit catalytic mechanism: as an example, the TEP-I protein from *E. coli* is multi-functional as protease and thioesterase etc. (Akoh *et al*., 2004). For plants, more than a hundred of genes are assigned to code GDSL enzymes in e.g. *Arabidopsis* (Lai *et al*., 2017), and the encoded proteins are widely accepted to have diverse physiological functions. For instance, a CD1 homologue in *Arabidopsis*, AtCUS2 (encoded by *At5g33370*), was suggested to maintain cuticular ridges on sepals (Hong *et al*., 2017). Differently, another *Arabidopsis* GDSL esterase, cuticle destructing factor 1 (CDEF 1, encoded by *At4g30140*), an extracellular enzyme as CD1, was demonstrated to have a cutinase activity, which hydrolyses the cuticle on stigma and helps the penetration of pollen tubes (Takahashi *et al*., 2010). Another type of function of GDSL enzymes is mediating xenobiotic metabolism: e.g. AmGDSH1 in black-grass (*Alopecurus myosuroides*) was identified to hydrolyse aryloxyphenoxypropionate (AOPP) graminicides, and in turn activates it

(Cummins and Edwards, 2004). In summary, GDSL proteins in plants are involved in diverse mechanisms, such as morphogenesis, reproduction and herbicide metabolism.

Like the AmGDSH1 (Cummins and Edwards, 2004), CD1 is also a 40 kDa protein (Yeats *et al*., 2012) with *N*-glycosylations that are predicted based on its polypeptide sequence (comp.chem.nottingham.ac.uk/glyco/) and the fact it can only be heterlogously produced in plants (tobacco) rather than *E. coli* or even *Pichia pastoris* (personal communication with Prof. JKC Rose). CD1 is predicted (UniProt) to be hydrophilic (Grand average of hydropathicity = -0.035), agreeing with the fact that it is not a membrane protein. Moreover, CD1 is proposed to contain disulphide bonds made by nearby cysteine residues (DIANA; Bakan and Marion, 2017) based on its polypeptide sequences. As an apopastic protein, it has an N-terminal signal peptide for guiding it to be secreted from cytoplasm (Yeats *et al.,* 2012). In the whole tomato plant, CD1 is mapped to be mainly expressed in young, rapidly growing leaves and fruits, with a relatively low abundance in stem and floral buds, but not detectable in roots (Yeats *et al.,* 2012). CD1's physiological significance was studied by knocking it out in tomato plants and found that cutin load is decreased, and the harvested tomato fruits loses water faster than the wild-type one (Yeats *et al.,* 2012).

CD1 (SlCUS1) homologues are found in moss (*Physcomitrella patens*) and vascular plants (*Arabidopsis thaliana*) (Yeats *et al*., 2014). They all use 2-mono(10,16-dihydroxyhexadecanoyl)glycerol (2-MHG), a precursor of cutin, as the substrates (both acyl donor and acceptor), to produce cutin polymer

by their transacylase activity (Yeats *et al*., 2014). This transacylase activity is highest at pH 5.0 *in vitro* (Yeats *et al*., 2014), which is within the physiological range of expanding cells' apoplast (reviewed by Cosgorve, 2005) and fitting into the *in-planta* characteristics: CD1's transcript and protein are most abundant in young, rapidly expanding tomato fruits and leaves (Yeats *et al*., 2012; Yeats *et al*., 2014). A hydrolysis activity of CD1 on 2-MHG was also reported, but very low compared with the 2-MHG-to-2-MHG transacylase activity (Yeats *et al*., 2014). Nevertheless, CD1 is not strictly restricted to 2-MHG; it can also use the isomer, 1-MHG to produce oligoesters, but with a weaker activity (Yeats *et al*., 2014). *In-vitro* studies showed that CD1 can only transfer acyl groups to the terminal hydroxy group of di-HHA (Yeats *et al*., 2014). However, *in-planta* evidence showed that CD1 can also use the secondary hydroxy group as the acyl acceptor site (Philippe *et al*., 2016) ('***Cutin polymer biosynthesis***', Chapter 1).

A very recent unpublished study reported that a CD1 (SlCUS1)'s orthologue, SlCUS2 (another GDSL transacylase), catalyses the cutin polymerisation reaction with the same mechanism as CD1 *in vitro* (Segerson, 2018).

Based on the findings above, we proposed that unspecified GDSL transacylase(s) can also re-model cutin for different physiological purposes (see below) besides cutin hydrolysis (e.g. CDEF1; Takahashi *et al*., 2010) and cutin synthase (CD1; Yeats *et al*., 2012).

6.1.3 Two novel apoplastic cutin transacylase activities discovered in this thesis

i. Background

We proposed that cutin, as a polyester layer in epidermis, requires to be re-modelled by a transacylase(s) during rapid growth of plant shoots as the cell wall is (e.g. xyloglucan; Fry *et al*., 1992). In this thesis, I devised and built up a portfolio of *in*- and *ex-situ* radio-chemical assays involving cutin as the transacylation acyl donor, and various cutin and cell wall polysaccharide components as the acyl acceptors.

I chose three angiosperm plants with thick epidermis as the study models: pea (epicotyl), ice plant (leaf) and tomato (fruit). Moss and the most commonly used angiosperm model plant, *Arabidopsis*, were not selected here because of the technical difficulty in isolating epidermis (Franke *et al*., 2005). I found two novel cutin transacylase activities in all the three model plants via radio-chemical assays (very sensitive to monitor low abundant enzymic products) coupled with chromatographic analysis, indicating that the putative re-modelling mechanisms exist in a wide range of angiosperm plants.

One re-modelling mechanism is conferred by an endo-homo-transacylase activity (acyl donor: cutin, acceptor: cutin or cutin fatty acids; [^{3}H]HHA being the model in this thesis), which is proposed to be involved in loosening cutin during cell expansion (i.e. transiently cutting a cutin molecule, to allow cutin to be loosened, and then transfer the broken cutin to a nearby one to form an

ester bond again after incremental expansion, re-forming an intact cutin matrix); the other one is conferred by an endo-hetero-transacylase activity (donor: cutin, acceptor: cell wall xyloglucan; [^{3}H]XXXGol here), which is proposed to reinforce cutin mechanically during growth. Their mechanisms were elucidated by identifying the products via chemical degradation coupled with chromatographic analysis.

ii. Novel cutin endo-homo-transacylase activity

The putative cutin endo-homo-transacylase activity, cutin:cutin transacylase (CCT) was detected by monitoring the incorporation of a radio-labelled fatty acid, [^{3}H]HHA, whose non-radio-labelled version is a common cutin fatty acid in nature (e.g. (Kosma *et al.*, 2010). The CCT product is proposed to be a cutin–[^{3}H]HHA ester-bonded conjugate, which is labile in alkali. After a series of thorough washes in acidic and neutral organic solvents to remove interferences, [^{3}H]HHA was released into solution from insoluble epidermis under alkaline condition (e.g. Fig. 29, Chapter 3), indicating that [^{3}H]HHA was indeed ester-bonded. [^{3}H]HHA's primary hydroxy group was demonstrated to be the acyl acceptor site by comparing its incorporation with that of [^{14}C]hexadecanoic acid (HA), which is the same as [^{3}H]HHA except for lacking the hydroxy group (Fig. 17, Chapter 3). Other possible acyl donors besides cutin, such as wax oligoesters and methyl esterified homogalacturonan, were demonstrated to be unlikely because there was no evidence of the wax oligoesters exist in the serial neutral organic solvent washes (Yeats *et al*., 2010; Yeats *et al*., 2012) (Fig 24 and 26, Chapter 3; Fig. 67 and 71, Chapter 4), and the methyl esterified homogalacturonan

oligomer does not have the acyl donor ability (Fig. 54, Chapter 4), and thus cutin was the only feasible acyl donor in this transacylation reaction. This work provided the first evidence for the existence of the putative CCT activity. Its *in-muro* localisation was not studied in this thesis, but it is proposed to be in both electron-dense and -lucent regions under microscopes (i.e. the whole cutin region) (Jeffree, 2006) because the CCT was not seem to be washed away by buffers when it is embedded in epidermis (Fig. 13 and 14, Chapter 3), suggesting that it may associates with the hydrophobic cutin-rich layer.

The substrate specificity of CCT was not studied due to the failure of purifying di-HHA (Appendix 6). Moreover, the cutinase (from *Aspergillus nidulans*, AN7541.2) I employed to hydrolyse cutin specifically for finding the possible ester-bonded [^{3}H]HHA, which may have been incorporated by the putative CCT activity, did not have the predicted activity (Fig. 28b, Chapter 3). Instead, I used the chemical (CMNaOH) degradation strategy, which is less specific than the enzymic one. Therefore, in summary, more substrates and a functional cutinase should be added in future experimental portfolios.

This putative CCT activity's physiological function is believed to be consistent with our hypothesis, loosening cutin. Two main arguments support this statement: (1) CCT activity has been suggested to operate during rapid growth: young and rapidly expanding tomato fruit and ice plant leaf showed the highest CCT activity, which steeply dropped once cells stopped expanding (Fig. 36 and 37, Chapter 3). (2) CCT activity is highest at pH 4.5–6.5 *in situ* (Fig. 9 and 10, Chapter 3), further suggesting that CCT operates during cell expansion (reviewed by Cosgrove, 2005). These characteristics

and the putative 'cut-and-paste' mechanism of CCT activity together are compatible with the idea that cutin may indeed restrain cell expansion ('***6.1.1'***). More direct evidence needs to be obtained in future work by identifying the gene (and protein) responsible for CCT activity, and then investigating phenotypes of mutants (*in-planta* studies).

Another question is that whether CCT is only required during growth for loosening cutin (epidermal-growth-control theory) or also plays other roles, such as healing wounds in the cuticle after the cessation of expansion. This hypothesis is raised because the CCT activity is not decreased dramatically at pH 7.5, a pH value out of the physiological range of rapidly expanding cells' apoplast (reviewed by Cosgrove, 2005) (Fig. 9 and 10, Chapter 3). As a comparison, CD1, a transacylase only required during fast growth, was degraded once the expansion stopped (Yeats *et al*., 2012).

The protein corresponding to the transacylase activity was not identified in this thesis, and therefore we cannot conclude whether it is also a GDSL enzyme as CD1 (Yeats *et al*., 2012). However, the only solid evidence is that CD1 does not have the observed CCT activity *in situ* and *in vitro*: [^{3}H]HHA incorporation was not significantly reduced in the *cd1*-null tomato fruits; and the purified His_6-tagged CD1 protein did not use HHA as an acyl acceptor (Fig. 33 and 35, Table 9, Chapter 3). The pH optima of CCT and CD1 are also different based on my own *in-situ* assays (Fig. 9 and 10, Chapter 3) and the published *in-vitro* assays (Yeats *et al*., 2014). Nevertheless, we cannot exclude the possibility that CCT and CD1 are co-regulated, because tomato fruit at 14-days after anthesis (DAA) has the highest CCT activity (Fig. 36,

Chapter 3), similar to CD1 (Yeats *et al*., 2012). For the metal co-factor requirement, there is no published study for CD1 (June, 2019), so I cannot compare the beneficial effect of Ca^{2+} on CCT activity with any effect on CD1 (Fig. 22, Chapter 3). Another different enzymological difference is that CD1 is predicted to contain disulphide bonds based on its polypeptide sequence as stated above (Bakan and Marion, 2017), but my biochemical results suggested the opposite of CCT: the addition of the reducing agent, DTT, to prevent undesirable disulphide bonds did not affect the CCT activity, enabling us to propose that the 3-D structure of CCT does not allow the disulphide bonds formation (Fig. 19 and 20, Chapter 3).

Environmental stresses were also applied to plants to obtain more information of the CCT activity's physiological significance. High humidity decreased the putative CCT activity insignificantly (Fig. 40, Chapter 3), providing a hint that this new cutin transacylase activity may not play an important role in response to humidity change. Low temperature decreased the CCT activity significantly after 8 days at 4°C (Fig. 41, Chapter 3), which may hint that the CCT activity is not important in resisting cold temperature. Continuous light exposure also did not affect CCT activity significantly (Fig. 39, Chapter 3), even though the light produced 4-fold shorter pea epicotyls than the samples gown in the dark. Noticeably, the data here was obtained from *in-situ* assays, which demonstrate the synergic results (cutin-to-[^{3}H]HHA transacylation product) of substrate (cutin) and enzyme (CCT activity). Therefore, to focus on the effects of environmental factors on the CCT activity, more approaches (e.g. *in-vitro* assays involving the purified CCT and

in-vivo assays with the CCT protein being immuno-labelled) should be recruited once the CCT transacylase has been identified.

Taken together, I added new aspects (metabolism) to the understanding of plant cutin by discovering a novel putatively cutin-loosening transacylase activity, CCT, in vascular land plant shoots. It is the only reported apoplastic cutin transacylase activity besides the cutin synthase activity of CD1 (Yeats *et al*., 2012) and SlCUS2 (Segerson, 2018). Whether bryophytes also contain the CCT activity remains a question here, but it is valuable to be studied in future to investigate CCT activity's physiological significance from an evolutionary perspective. Moreover, CCT activity's pH optimum and the effects imposed by growth enable us to propose that it may loosen cutin during cell expansion, supporting the 'epidermal-growth-control theory' of cutin from a side angle.

Another cutin loosening mechanism was also proposed by us: cutin can be loosened by degrading via the reverse reaction of cutin synthesis catalysed by CD1 (*Eq.1*, Chapter 1) (Yeats *et al*., 2012). In this reverse reaction, cutin polymer is the acyl donor and glycerol is the acyl acceptor (in the forward reaction, acyl groups from 2-MHG molecules are transferred onto cutin, producing elongated cutin and glycerol molecules) (*Eq.1*, Chapter 1) (Yeats *et al*., 2012). However, this reverse reaction was not detectable *in situ*, *in vitro* and *in planta* under our conditions (Chapter 5). Thus, we propose that the CD1 does not catalyse the reverse reaction of the cutin biosynthesis ('***discussion***', Chapter 5).

iii. Novel cutin endo-hetero-transacylase activity

The other novel activity is cutin endo-hetero-transacylase activity, conferred by the cutin:XGO transacylase (CXT). As in the last section, epidermis was isolated from pea epicotyl, ice plant leaf and tomato fruit as the acyl donor because it contains cutin, but the acyl acceptor was [^{3}H]XXXGol here to be a model of cell wall xyloglucan, which is a very abundant cell wall polysaccharide (reviewed by Cosgrove, 1997). [^{3}H]Xyloglucan was not used because it may form H-bonds with endogenous cell wall polysaccharides, resulting in interfering the covalently bonded ^{3}H, which may contain the proposed CXT product.

The CXT activity was also reproducibly observed in independent experiments of one plant model, and repeatedly in all three models. CXT's product is modelled as ester-bonded cutin–[^{3}H]XXXGol/[^{3}H]XXGol/[^{3}H]XGol conjugates because [^{3}H]XXXGol, [^{3}H]XXGol and [^{3}H]XGol were incorporated into alkali-labile products (Fig. 75, 76 and 77, Chapter 4); and cutin is the most feasible acyl donor because no evidence (e.g. no ^{3}H dissolved in neutral organic solvents; Yeats *et al.*, 2010) for any oligoester to form ester bonds with [^{3}H]XGO (Fig. 73 and 77a, Chapter 4), and the methyl esterified galacturonan does not have the acyl donor ability (see below). The cutin–[^{3}H]XXGol/[^{3}H]XGol conjugates are proposed to be mainly produced from the initially formed cutin–[^{3}H]XXXGol, whose XGO motif was then hydrolysed by glycosidases (α-D-xylosidase and β-D-glucosidase) (Guillen *et al.*, 1995; Miyamoto *et al.*, 1997). However, this hydrolysis was unexpected because the cutin linkage was thought to prevent the [^{3}H]XXXGol from being the

substrate of the glycosidases. Moreover, the ratio of the shorter [^{3}H]XGO/longer [^{3}H]XGO increased in the putative CXT products than in the substrate (Fig. 75, 76 and 77, Chapter 4), hinting that the glycosidase activities were even promoted by the cutin linkage. However, the corresponding mechanism remains a mystery here.

Beyond XXXGol, different oligomers from hemicellulose and pectin were screened, but [^{3}H]XXXGol is the only one has the acyl acceptor ability followed by [^{3}H]XXGol (Fig. 62, Chapter 4). [^{3}H]XXFGol only has trace of acceptor ability (Fig. 66, Chapter 4), implying that the putative cutin transacylation reaction was hindered by adding two monosaccharide residues onto the third X unit (from left; Fig. 67). Thus, I propose that cutin is ester bonded to a free hydroxy group of the xylose in the third X unit of an XXXGol molecule, because as the closest residue to the additional monosaccharides in XXFGol, the xylose has a higher potential to be sterically hindered than others, e.g. the glucose residue in the third X unit (Fig. 84, Chapter 4). In addition, the stereo-structure of XXFGol indicates that the hydroxy group at C-4 is closest to the additional D-galactose and L-fucose residues, but not completely hindered by them as at C-2 (Fig. 89, Chapter 4), leading to the hypothesis that it is the actual cutin-linking site in XXXGol. The hydroxy group at C-3 is also a candidate, even though it protrudes to the opposite direction to the additional residues (Fig. 89, Chapter 4).

Strikingly, as the nearby polysaccharide to cutin, pectin components (Fang *et al.*, 2001; reviewed by Fich *et al*., 2016) do not have acyl acceptor ability (Fig. 57–59, Chapter 4), except that the arabinan oligomer, [^{3}H]Ara$_8$-ol, related to

a RG-I side chain showed a very low one (Fig. 47 and 48, Chapter 4). These results not only indicate that covalent bonds between cutin and pectin is very rare in spite they are physically close (Jeffree, 2006), but also as the first evidence to point out that only cutin is the acyl donor in the hetero-linking reaction, instead of methyl esterified galacturonan (reviewed by Fich *et al*., 2016; Fig. 5a, Chapter 1). The complete lack of acyl acceptor ability of secondary cell wall hemicellulosic components indicates the putative CXT's substrate specificity, and also suggests that the CXT may only operates during cell expansion (i.e. secondary cell wall appears after cell stops expansion; reviewed by Cosgrove, 2005).

CXT activity with [^{3}H]XXXGol as the acyl acceptor is much lower than the xyloglucan endotransglucosylase (XET) activity, which also uses [^{3}H]XXXGol as a substrate (Fry *et al*., 1992; reproducibly observed throughout Chapter 4). This difference was expected because cutin and xyloglucan are physically separated in two layers of epidermis, relatively low chance to interact; and the cutin–XGO hetero-polymer may not as vital as cutin–cutin and XGO–XGO homo-polymers (i.e. xyloglucan- or cutin-deprivation can be lethal for plants).

Since the new CXT activity and XET activity share the same substrate, an interaction-network of CXT and XET activities *in planta* may be hinted. For instance, one possible scenario is that CXT activity competes with XET activity for the newly synthesized xyloglucan oligomers (XXXG) as the substrates (Simmons *et al*., 2015); another possibility is that CXT also links cutin to the XET products, xyloglucan oligo- and/or poly-mer (Fry *et al*., 1992;

Simmons *et al*., 2015). The second scenario could be partially answered by looking for the cutin-to-xyloglucan transacylase activity to be compared with the new CXT activity (XGO as the acyl acceptor). However, it could not be studied in this thesis due to the technical limitation as stated above. In the future, investigating the interactions between epidermal re-modelling mechanisms may deepen the understanding of plant physiological changes during growth.

Like CCT above, CXT was also not identified in this thesis, and again CD1 clearly does not catalyse the cutin-to-[^{3}H]XXXGol transacylation reaction (Fig. 75, 76 and 77, Chapter 4) due to similar reasons as in the last section: (1) the putative CXT activity was not decreased in the *cd1*-knockout tomato fruit mutant's epidermis significantly; (2) the purified His_6-tagged CD1 did not catalyse the cutin-to-XGO or *p*NPP-to-XGO transacylation (Fig. 78–80, Chapter 4). Moreover, my results indicate that CXT is a separate enzyme from CCT, because of their different pH optima, responses to development and cold temperature (see below). In addition, different from the CCT activity (last section), the CXT activity is benefited by the additions of a metal chelator, EDTA, and the reducing agent, DTT (Fig. 71 and 72, Chapter 4), suggesting that CXT activity can be inhibited by adding metal ions, and its 3-D structure may allow undesired disulphide bonds to be formed. Preliminary evidence also suggests that CXT may locate more in the electron-dense region (closer to cell wall) under microscope (Jeffree, 2006) compared with CCT, because its activity was suggested to be decreased after the epidermis specimen being washed in buffer based on my preliminary data, possibly

because the CXT associates with the cell wall (hydrophilic layer) more than the CCT does ('***3.1.3***', Chapter 3; '***4.1.3***', Chapter 4).

The hypothesized CXT's physiological function is supported by CXT's pH optimum, which is 6.5–7.5 (Fig. 45 and 46, Chapter 4), similar to a xyloglucan re-modelling transglucosylase, TCH4 (AtXTH) in *Arabidopsis*, whose physiological function is characterised to be reinforcing cell wall mechanically (Purugganan *et al*., 1997). Furthermore, CXT activity in tomato fruit and ice plant leaf is highest towards the end of cell expansion (Fig. 81–83, Chapter 4). This observation might be explained as that the CXT activity increases in expanded organs to prevent ruptures, whereas the smaller and rapidly growing organs do not demand this reinforcement.

Like in the last section, environmental stresses were also applied to our model plants besides the healthy growing condition, to study the physiological functions of CXT activity. I found that the CXT activity was increased by a short period of cold temperature *in situ* (Fig. 82), suggesting that the CXT activity might be involved in resisting short-term cold, possibly by regulating cell wall pore sizes to prevent ice formation in the apoplast (Beck *et al*., 2007). Again, this putative characteristic is shared with the TCH4, which is also reported to have a higher activity at lower temperature (Purugganan *et al*., 1997), supporting the proposed CXT function (reinforcing epidermis mechanically) further. As another environmental stress, high humidity did not affect CXT activity significantly *in situ* (Fig. 86, Chapter 4). The *ex-situ* assay also only showed a slight trend of that high humidity decreases CXT activity (Fig. 87, Chapter 4).

Continuous light also did not decrease CXT activity as for CCT *in situ*, but the effect was more significant for CXT (Fig. 85, Chapter 4). Furthermore, the *ex-situ assay* revealed that the CXT activity is much higher in the dark-grown samples than the in 'light' ones (Fig. 87, Chapter 4), suggesting a positive correlation between growth rate and the CXT activity. This correlation was not observed *in situ* may be because the cutin availability (substrate) was slightly decreased by the dark condition, countering the improved CXT activity (enzyme), resulting in increasing the product (alkali-releasable ^{3}H) quantity slightly (Fig. 85 and 87, Chapter 4).

Taken together, I obtained the first biochemical evidence of the covalent bonds putatively between cutin and xyloglucan oligomer and solved the historical mystery of the linking mechanism (reviewed by Fich *et al*., 2016) by providing a model of cutin–xyloglucan conjugate structure. To avoid the contamination from XET product (i.e. xyloglucan oligomer–[^{3}H]XGO was found to be dissolved in the hydrophobic alkali solution, CMNaOH) and increase the specificity, cutinase hydrolysis should replace the current chemical hydrolysis to support our current mechanism elucidation.

iv. Summary

Both new transacylases putatively use cutin as the only acyl donor, and their activities were quantitatively similar when the conditions were very comparable ('***3.7***', Chapter 3; '***4.4.4***', Chapter 4). These findings enable us to propose a dynamic epidermis model: in parallel with cell wall loosening, cutin is also loosened to allow cell expansion at the young, rapidly growing stage,

but soon after, cutin is cross-linked to neighbouring xyloglucan to strengthen the epidermis of the highly expanded, but still growing cells. These discoveries answered long-standing questions and opened new possibilities for future cutin re-modelling studies (see below).

6.2. Prospects of understanding cutin re-modelling mechanisms

6.2.1 Exploring more cutin re-modelling and biosynthesis mechanisms

There is only very limited understanding that how other cutin components are incorporated. For examples, phenolic compounds are suggested to be incorporated into cutin by forming cutin fatty acid–phenolic conjugates before being exported to apolast (Rautengarten *et al*., 2012). However, the mechanism of cutin alcohols and aldehydes incorporation is completely unknown. It is also unknown whether other cell wall components, such as arabinoxylans and glucuronoxylan (reviewed by Ebringerová *et al*., 2005) in hemicellulose, as well as other pectin sidechains, such as arabinogalactan and xylogalacturonan (reviewed by Voragen *et al*., 2009) can be incorporated into cutin. Besides the cell wall, wax is also nearby cutin (Jeffree, 2006; reviewed by Beisson and Ohlrogge 2012), and therefore a link between them can be possible. The developed experimental strategies involving highly sensitive radio-chemical assays in this thesis can be easily adapted to explore other hetero-conjugates of cutin and broaden the understanding of cutin biosynthesis.

6.2.2 Dissecting the regulatory mechanisms of cutin metabolism

It is still unclear of that how these two transacylase activities are regulated (i.e. cell expansion stimulates them or the opposite). The similar issue has been solved for the xyloglucan re-modelling enzyme, XET activity: cell expansion stimulates the expression of *TCH4*, a gene encoding an enzyme with XET activity in *Arabidopsis* (Xu *et al*., 1996). At the translational level, the XET activity in barley leaves increases with the increase of growth rate (Palmer and Davis, 1995).

This question regarding cutin can be studied by different strategies. For example, to study the first possibility that whether growth stimulates re-modelling enzyme activities, CCT and CXT should be identified first, and the effects of growth rates on their transcripts can be quantified by e.g. RNA-seq (reviewed by Garber *et al*., 2011). For the effects on the translational level, CCT and CXT protein quantity, as well as activities *in vivo* can be quantified by e.g. western blotting (i.e. quantifying the protein abundance in samples with different growth rate) (reviewed by Kurien and Scofield, 2006) and immunocytochemistry (i.e. monitoring substrate incorporation *in vivo*) (reviewed by Knox *et al*., 1980) respectively. Moreover, auxin is well known for inducing rapid growth *in planta* (reviewed by Cosgrove, 2005), but whether it can directly affect the two new transacylase activities alone without changing their transcripts level through signal transductions would be interesting, exemplified by the fast response of the transport inhibitor response 1 (TIR1) to auxin within seconds (reviewed by Badescu and Napier,

2006). This hypothesis could be investigated by supplying auxin to the purified CCT and CXT in *in-vitro* assays.

For the second possibility, the CCT and CXT coding genes can be knockout to observe the effects on cell expansion *in planta*.

6.2.3 Significances of current knowledge in synthetic biology

CCT and CXT activities putatively can loosen cutin and reinforce cutin respectively. Thus, the understanding of them can be applied to improve plants' adaptions in response to changing environment via genetic engineering (reviewed by Mittler and Blumwald, 2010). For instance, more phenolic components can be introduced into cutin to resist stronger UV (Auyong *et al*., 2015); and more links between cutin and cell wall can be useful in resisting wind.

After being identified, CCT and CXT can also be engineered via e.g. directed evolution strategy (reviewed by Arnold and Volkov, 1999) to improve their promiscuity and broaden the stereoselectivity, that can be applied in generating novel biocatalyst for synthesizing novel bio-degradable plastics *in vitro*.

Appendix 1. Cutinase (*Aspergillus nidulans*) extraction and *in-vitro* assay

P. pastoris cultivation and induction

The received *P. pastoris* (strain SB) (FGSC), which heterologously produced an annotated cutinase (AN7541.2, ~28 kDa), was replicated onto fresh YPDS plates (with 100 µg/ml zeocin) and incubated at 30°C for 1 day. The following *P. pastoris* cultivation protocol and media recipe was obtained from Bauer *et al*. (2005): the individual colonies were inoculated into 100 ml BMGY medium (buffered complex glycerol medium) in 500 ml flasks, which were shaken (200 rpm) at 30°C till OD_{600} = 3.0–6.0. Cells were sediment down by centrifuging at 2000 rpm with brake 3 for 30 minutes. Supernatant was discarded and cell pellets were re-suspended in ~50 ml BMMY (buffered complex methanol medium; the best induction medium, comparison results not shown) to wash the last trace of BMGY. The cell suspension was then centrifuged as before, and the supernatant was discarded again. Cells were then transferred into 500 ml flasks containing 100 ml BMMY to achieve the final concentration as OD_{600} = 1.0 and shaken under the same conditions as above for 1 day.

Cutinase (AN7541.2) extraction

PpICZα vector was used to express *AN7541.2*, and therefore the cutinase was secretory. Culture medium containing the cutinase was obtained by centrifuging the cell culture at full speed for 30 min, and then dialyzed (cut-off: 12–14 kDa) against water for 2 days, followed by freeze-drying at –60°C.

In-vitro assay

The dried medium was weighed and re-dissolved in pH 8.0 buffer (50 mM collidine-acetate) to achieve desired concentration. A stock solution (5 mM) of *p*NPP was prepared by emulsifying it in 1% (v/v) Triton X-100, followed by adding 1% (v/v) isopropanol to completely dissolve it (Muralidharan *et al*., 2013). For assays the *p*-NPP stock solution was diluted 10 times (final conc.= 0.5 mM), which was then incubated with 0.15% (w/v) cutinase-containing culture medium solution at 37°C for 3 days. The cutinase activity was quantified by quantifying the produced *p*-NP via measuring light absorption at 410 nm.

After 3 days incubation, all the *p*NPP was hydrolysed (Fig. 97a). Phenylmethylsulfonyl fluoride (PMSF) was found to inhibit the cutinase activity for 3.3 times (Fig. 97b)

a).

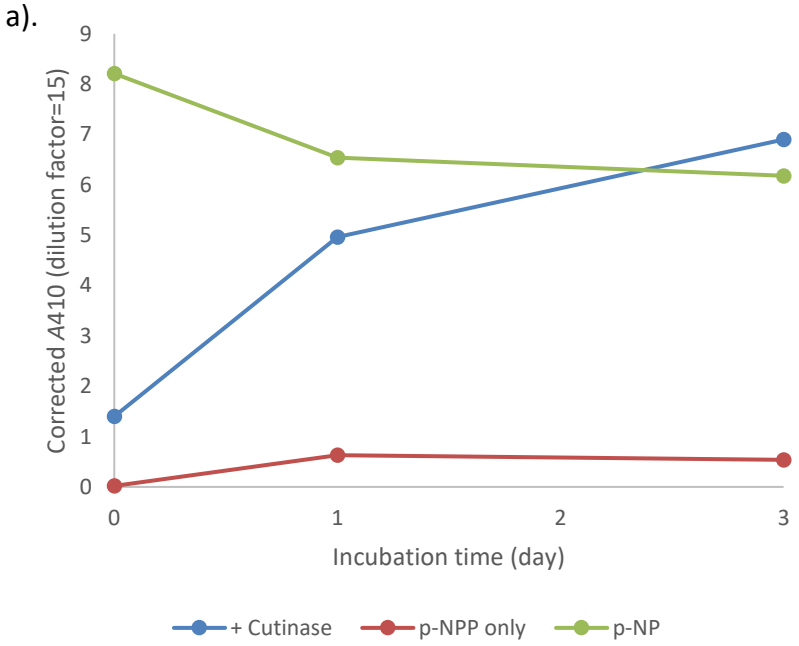

b).

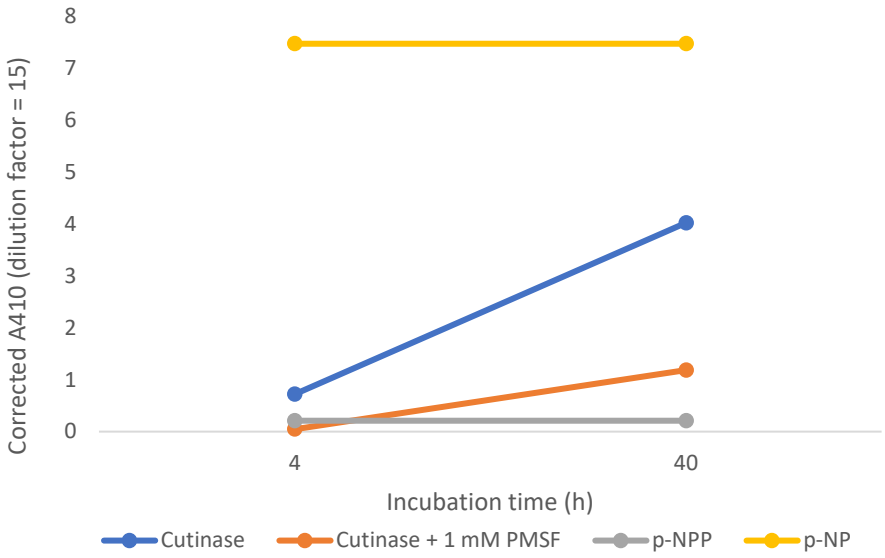

Figure 97. Cutin estarase (AN7541.2) activity on *p*NPP *in vitro*. (a). Heterologously produced cutinase (*AN7541.2*) with culture medium (0.15% w (dry weight)/v) was incubated with 0.5 mM *p*-NPP in 1 ml pH 8.0 buffer (50 mM collidine-acetate) at 37°C for 3 days. The A_{410} reading of '+ cutinase' samples was obtained by using 'cutinase only' samples as the blank (A_{410} = 0, not shown), because the culture medium colour was very dark. '*p*-NPP only' provided a control; '*p*-NP' with the same concentration of *p*-NPP (0.5 mM) provided a standard for complete hydrolysis of *p*-NPP. (b). Experimental strategies were as in (a), except 0.075% w/v cutinase-containing medium was incubated with *p*-NPP with or without 1 mM PMSF (dissolved in DMSO).

p-NPP hydrolysis percent (%): A_{410} of '+ cutinase' samples - A_{410} of '*p*-NPP-only' samples/ A_{410} of '*p*-NP' × 100%. No standard errors (n=1).

Appendix 2. Lipase (*Aspergillus niger*) *in-vitro* assay

The stock solution of *p*NPP was made as in Appendix 1. For assays, it was diluted to 33 µM and incubated with 0.02 U/ml *A. niger* lipase in pH 7.5 buffer (80 mM collidine-acetate) at 25°C for 3 days, , and the activity was quantified as in Appendix 1.

After 3 days incubation, ~30% *p*NPP was hydrolysed (Fig. 98).

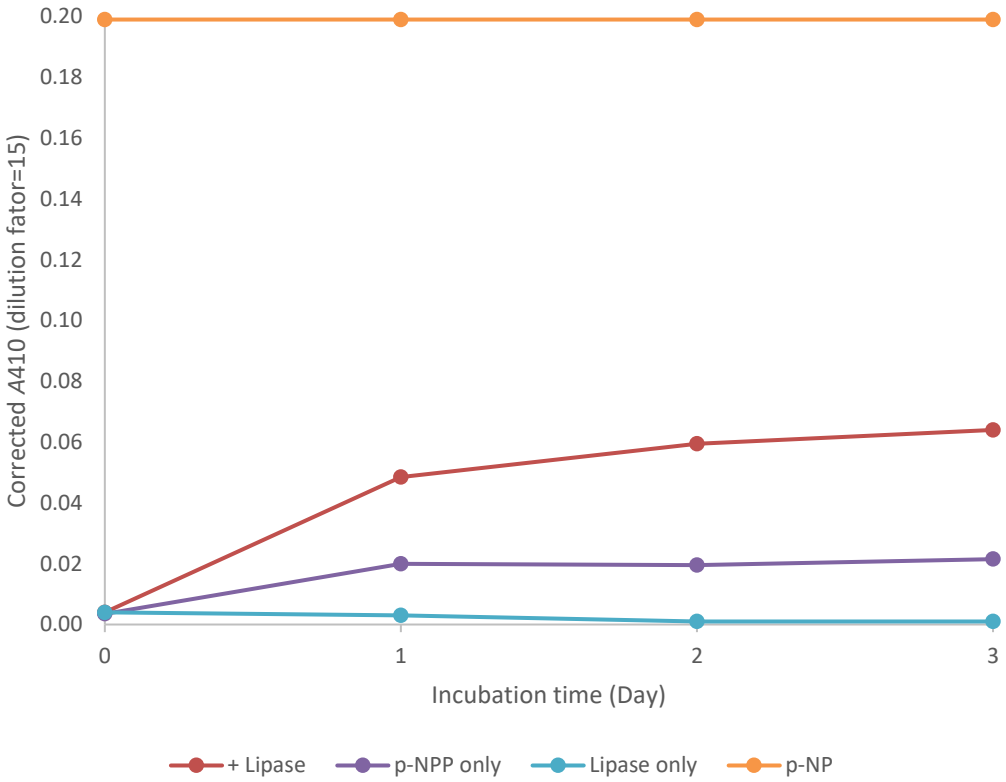

Figure 98. Lipase (*A. niger*) activity on *p*NPP *in vitro*. Commercial lipase (0.02 U/ml) was incubated with 0.33 mM *p*-NPP in 1 ml pH 7.5 buffer (80 mM collidine-acetate) at 25°C for 3 days. The product was quantified by measuring A_{410}. The reading of 'lipase only' sample provided a blank; the '*p*-NPP only' sample provided a control for auto-hydrolysis; the '*p*-NP' sample with the same concentration of *p*-NPP (0.33 mM) provided a standard for complete hydrolysis of *p*-NPP. The percent (%) of hydrolysed *p*-NPP in '+ Lipase' samples was calculated as in figure 91. No standard errors (n=1).

Appendix 3. The quantitative comparison of cutin in adaxial and abaxial *Sedum* leaf epidermis

Adaxial and abaxial epidermis was stripped from fresh *Sedum* leaves with mixed sizes, and immediately frozen at –80°C. It was thawed before use, and the intracellular interferences and cuticle wax were removed by washing in water, acetone and boiled in chloroform for 90 s as in Chapter 2. The dried prepared epidermis was incubated with C/M/0–4 M NaOH (10/10/3, v/v/v) mixture to hydrolyse cutin at room temperature for 1 day. The reaction was terminated by adding excessive amount of acetic acid (5 moles/mole of NaOH), and the supernatant was collected and phase partitioned as in Chapter 2, followed by drying in SpeedVac. The residues were re-dissolved in a small volume of CMW (10/10/3, v/v/v), which was then loaded onto a TLC plate (silica gel 60) and developed in toluene/acetic acid (9/1, v/v, 1 ascent). Hydrolysed fatty acids were visualised by staining the TLC plate in iodine atmosphere (Fig. 99 left) and 0.06% (w/v) rhodamine 6G dissolved in 96% ethanol (Fig. 99 right).

Both staining methods showed that, always more residues released from adaxial epidermis than from abaxial at all NaOH concentrations (Fig. 99). Moreover, the rhodamine 6G staining showed that *Sedum* leaf cutin may contain HHA and HA (Fig. 99 right).

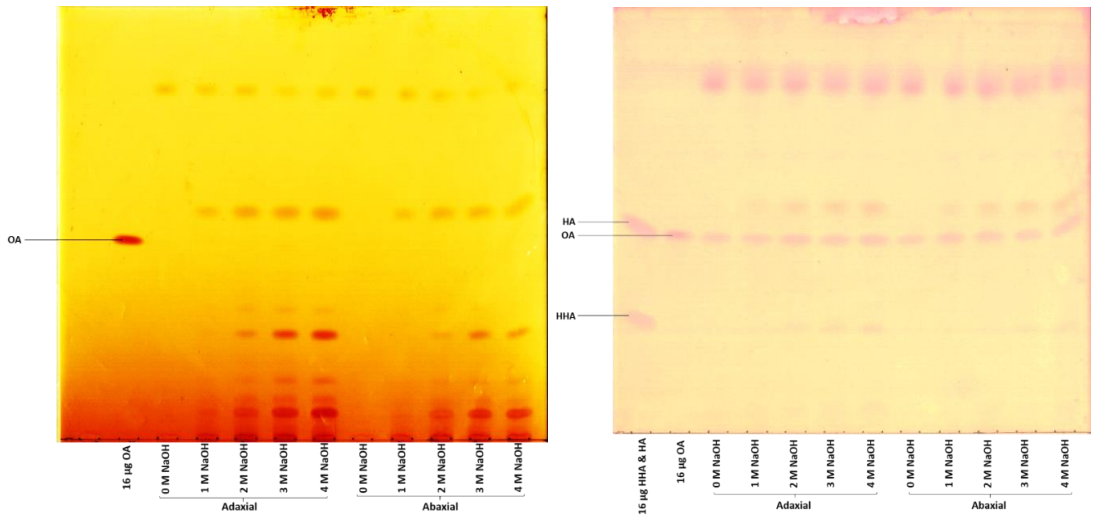

Figure 99. Quantitative comparison of CMNaOH-releasable residues between adaxial and abaxial *Sedum* leaves cutin. *Sedum* leaves epidermis was harvested and prepared to roughly remove interferences. The remained cutin was alkaline hydrolysed by CM, mixed with 0–4 M NaOH (10/10/3, v/v/v). The TLC plate was developed in toluene/acetic acid (9/1, v/v) for 1 ascent, followed by staining in iodine atmosphere first to visualize un-saturated fatty acids. And after the iodine was completely evaporated, the TLC plate was stained in 0.06% (w/v) rhodamine 6G to visualize saturated fatty acids. External markers were 25 µg HHA, HA and OA. HHA: 16-hydroxyhexadecanoic acid. HA: hexadecanoic acid. OA: oleic acid.

Appendix 4. [^{3}H]HHA–[^{3}H]HHA ester chemical synthesis

Desired amount of [^{3}H]HHA (dissolved in ethyl acetate) was dried, and re-dissolved in a small volume of tetrahydrofuran/water (5/1, v/v) to make a stock. The stock solution of NHS (0.23% w/v) and EDC (1.5% w/v) were prepared by dissolving them together in tetrahydrofuran/water (5/1, v/v). For assays, the NHS-EDC stock solution were diluted to 10 times and mixed with an aliquot of [^{3}H]HHA solution. The concentration was adjusted by adding tetrahydrofuran/water (5/1, v/v) to ~100 µl. The reaction was incubated at room temperature for up to 28 h, and being stopped by adding equal volume of freshly prepared methanol/acetic acid (1/1, v/v), followed by drying in SpeedVac. The residues containing putative [^{3}H]HHA–[^{3}H]HHA ester was re-dissolved in toluene, followed by CM (2/1, v/v) to mimic the chemical degradation procedure of cutin transacylase product (Chapter 3 and 4). TLCs were developed in the same solvents as above, but 3 ascends.

A new peak emerged after 100s incubation, and the [^{3}H]HHA peak (R_F = 0.32–0.34) was completely converted to the new peak (R_F = 0.25–0.26) after 28h incubation (Fig. 100). This new peak was annotated to be [^{3}H]HHA–[^{3}H]HHA, which was solubilized in toluene very well.

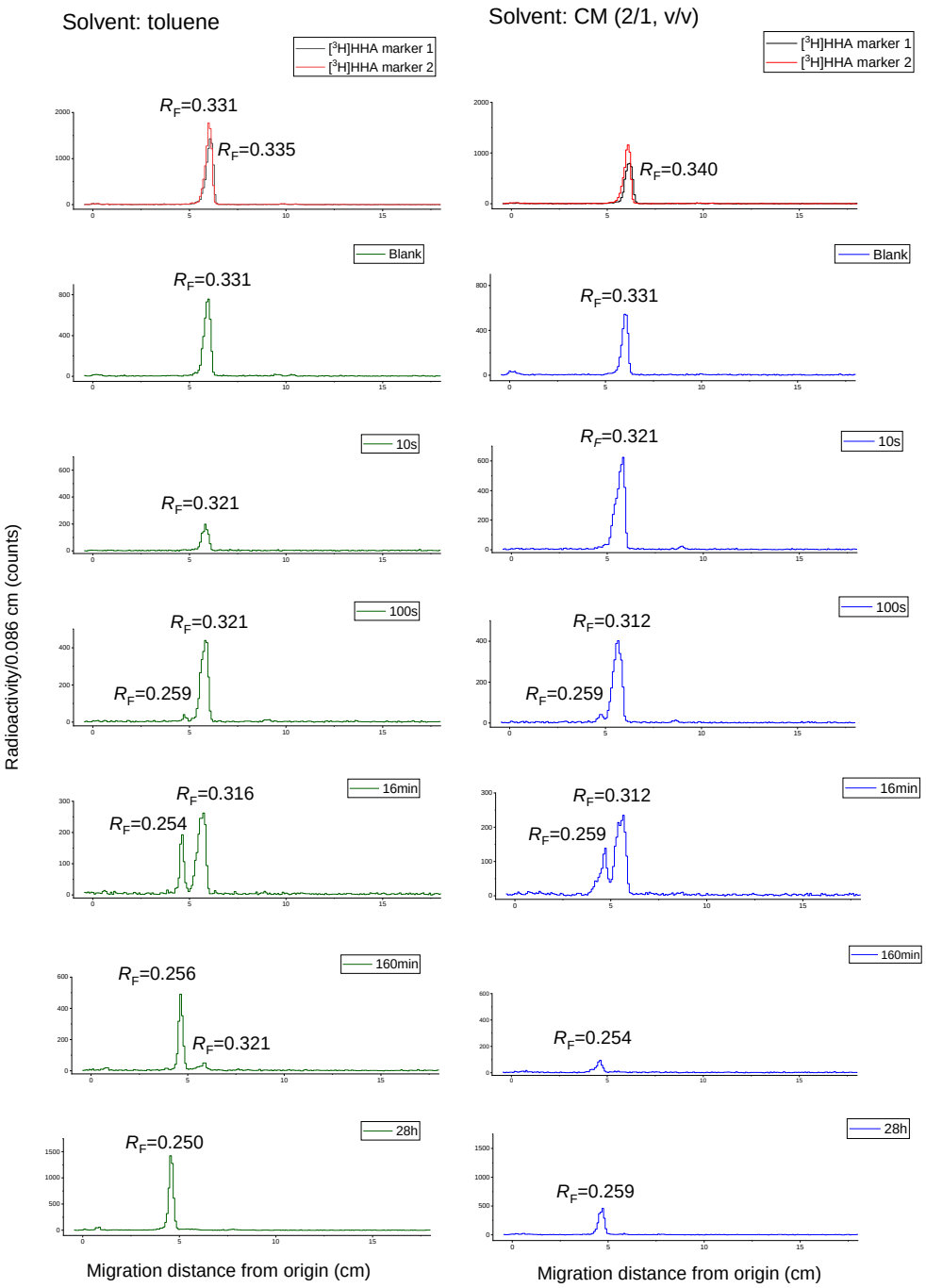

Figure 100. The R_F of the putative ester, [^{3}H]HHA–[^{3}H]HHA on TLC. [^{3}H]HHA was incubated with or without (blank) EDC (0.15% w/v) and NHS (0.023% w/v) solution in 100 µl tetrahydrofuran/water (5/1, v/v) at room temperature for up to 28 h. The mixture was dried and re-dissolved in toluene and CM (2/1, v/v) sequentially, which were loaded onto TLC plates as separate streaks. The TLCs were developed in toluene/acetic acid (9/1, v/v) for 3 ascents, and were radio-scanned by AR2000 for 1 h per sample (spatial resolution = 0.086 cm) (unit: counts). R_F values were annotated.

Appendix 5. Annotation of the unknown compound (R_F ≈ 0.66) in MFW (9/1/1)

The unknown compound (R_F ≈ 0.66) in the MFW (91/1, v/v/v) wash (Fig. 22, Chapter 3) was proposed to be a chemical product of [^{3}H]HHA and other ingredients in the assay incubation mixture. Thus, these ingredients were screened as below.

Desired amount of [^{3}H]HHA (dissolved in ethyl acetate) was divided into two aliquots before drying. The first aliquot was re-dissolved in a few µl of DMSO and adjust to ~10 kBq/ml by adding 25 mM succinate (Na^+), pH 5.5 buffer. The other dried aliquot was directly added with the same buffer to achieve the same concentration as the first aliquot.

To mimic the cutin-to-[^{3}H]HHA *in-situ* assays, the mixtures above were incubated at room temperature for 1 day. The DMSO-involved aliquot was further divided into 4 aliquots, and then 1 ml of each freshly prepared MFWs were added to one of the aliquots: 9/1/1, 0/1/10. 9/0/2, 0/0/0 (v/v/v). The aliquot without DMSO was only added with 1 ml of MFW (9/1/1, v/v/v). These 5 newly made mixtures were incubated further at room temperature overnight.

They were then dried in SpeedVac, and re-dissolved in ethyl acetate to be analysed by TLC (toluene/acetic acid, 9/1, v/v, 3 ascents).

The unknown peak (R_F = 0.65–0.69) emerged in all the samples, and thus indicating that none of the ingredients caused it (Fig. 101a).

However, the [^{3}H]HHA marker from the same stock as the samples did not show the unknown peak, the difference was that it was not dried in SpeedVac. Moreover, the ratio of the R_F of the unknown compound peak to [^{3}H]HHA was the same as the one of OHA to HHA (Fig. 101b). Thus, we concluded that this unknown peak is very likely to represent OHA, which was produced by heat generated by the overnight SpeedVac drying process.

a).

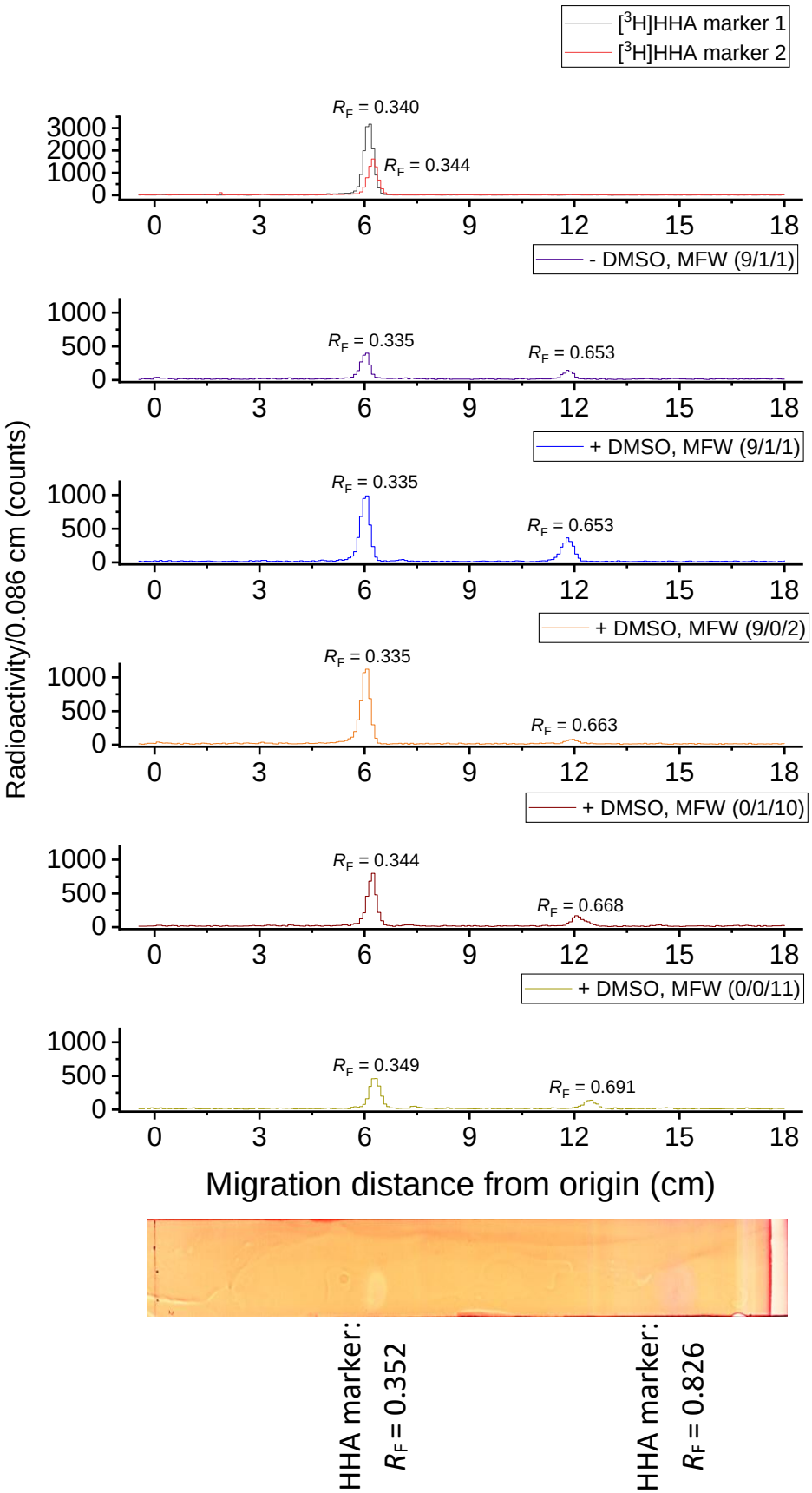

HHA marker: $R_F = 0.352$

HHA marker: $R_F = 0.826$

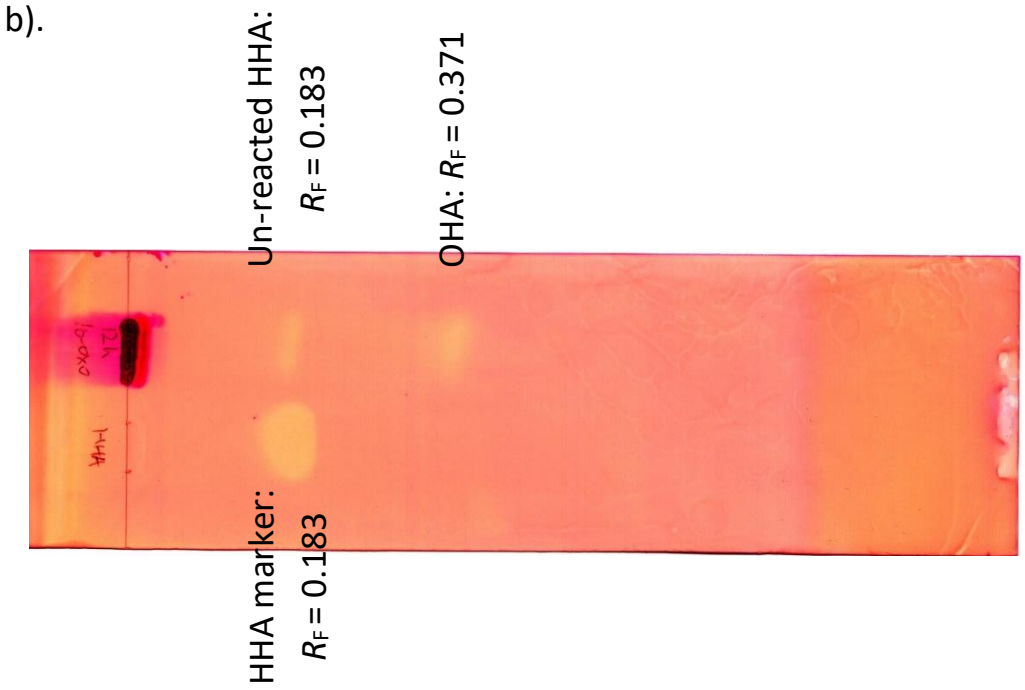

Figure 101. Identification of the unknown product ($R_F \approx 0.66$) in MFW wash of the *in-situ* cutin-to-[^{3}H]HHA assay in Chapter 3.

(a) [^{3}H]HHA was incubated in 110–117 µl 25 mM succinate (Na^+) buffer, pH 5.5 with or without 7 µl DMSO at room temperature for 1 day. MFWs (9/1/1, 9/0/2, 0/1/10, 0/0/11, v/v/v) were added and incubated at room temperature overnight to screen which ingredient interacted with [^{3}H]HHA. The mixtures were dried in SpeedVac overnight and re-dissolved in ethyl acetate, which was then loaded on to a TLC plate, together with 1 kBq [^{3}H]HHA, 50 µg HHA and HA as external markers (toluene/acetic acid, 9/1, v/v, 3 ascents). The radio-samples were scanned by AR-2000 for 1 h per sample (spatial resolution: 0.086 cm; unit: counts), whereas the non-radioactive markers were stained by 0.06% (w/v) rhodamine 6G.

(b) 10 mg HHA was incubated with 32 mg pyridinium chlorochromate (oxidising agent) in 1 ml chloroform at room temperature for 12 h, and the reaction was stopped by adding 1 ml methanol. A portion of the incubation mixture was directly subjected to TLC analysis (toluene/acetic acid, 9/1, v/v, 1 ascent), together with HHA and HA external markers. Chemical names and R_F values were annotated.

Appendix 6. Isolation and purification of 10,16-dihydroxyhexadecanoic acid

Extraction from tomato fruit

Fully ripened tomato fruit (cv. Ailsa Craig) epidermis was isolated manually and frozen at –80°C before use. The frozen epidermis was then thawed and washed in water, acetone, chloroform/methanol (2/1, v/v) for three times in each solvent or mixture to remove intracellular molecules (e.g. pigments) and cuticle wax. The washed epidermis was subsequently boiled in chloroform for 90 s to remove wax more thoroughly.

The completely dried epidermis was hydrolysed in chloroform/methanol/6 M NaOH (10/10/3, v/v/v) at room temperature for 1 day to release cutin fatty acid residues. This alkaline hydrolysis reaction was stopped by adding adequate acetic acid (5 moles to 1 mole of NaOH). The supernatant was then phase partitioned as described in chapter 2 to remove aqueous-soluble compouned (e.g. sodium acetate).

TLC analysis

The hydrophobic layer was loaded to TLC plates to analyse the composition (Fig. 96). The TLC plate was then stained with iodine vapour, and the visible bands (Fig. 96) were carefully cut down and eluted in ethyl acetate after the iodine vapour was completely evaporated. The lowest band ($R_F \approx 0.222$)'s eluent colour was yellow, and the colour intensity decreased with the R_F value increases. Markers were stained by iodine vapour first, followed by rhodamine 6G after evaporation (Fig. 102).

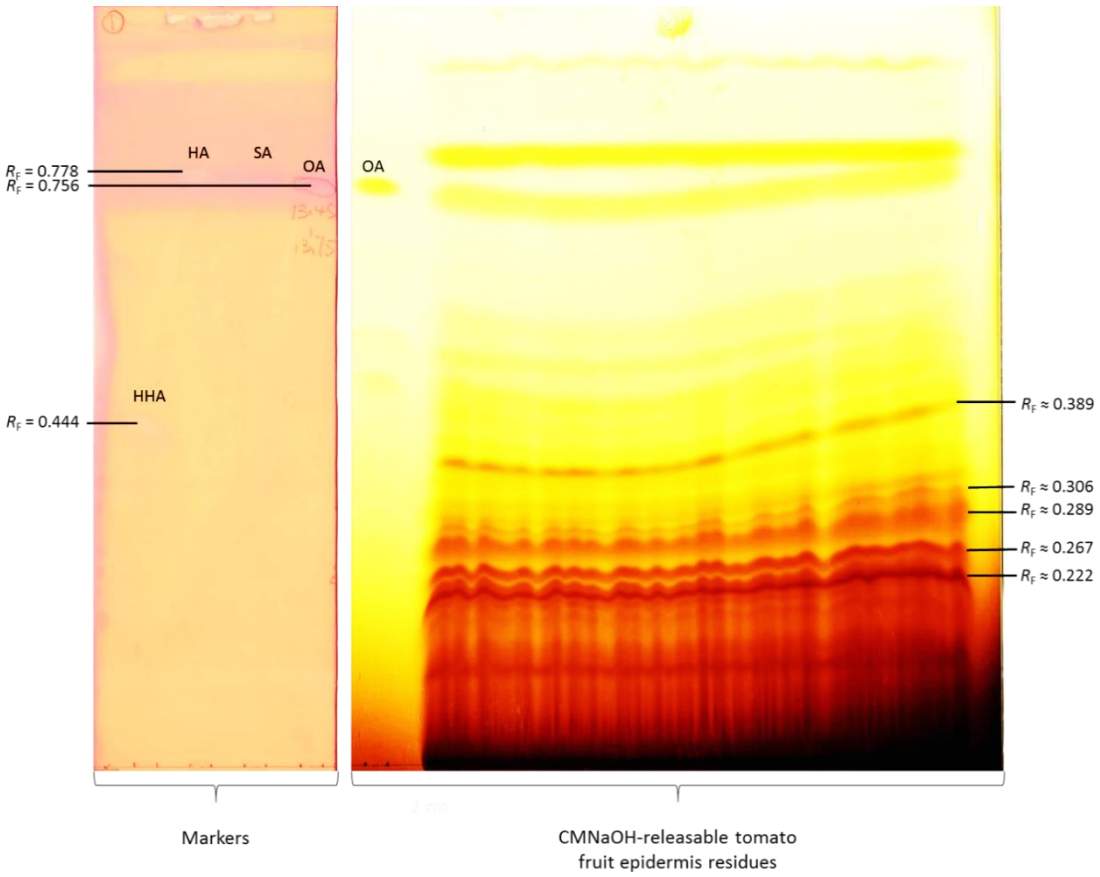

Figure 102. TLC analysis of the CMNaOH-releasable residues from tomato fruit (cv. Ails Craig) epidermis. Prepared (i.e. dewaxed etc.) tomato fruit epidermis (20 mg dry weight) was incubated with 1 ml chloroform/methanol/6 M NaOH (10/10/3, v/v/v) at room temperature for 1 day. Acetic acid (5 moles of NaOH) was used to stop the hydrolysis reaction. Phase partitioning was carried out as stated in Chapter 2. The hydrophobic layer in supernatant was loaded onto a TLC plate as a 12-cm streak, and developed in toluene/acetic acid (9/1, v/v) for 3 ascents (prolonged running time for ~40 min in the last ascent). The residues released from tomato fruit epidermis was only visualized by iodine vapour to prevent contaminations for subsequent analysis. The external markers (40 µg HHA, HA, SA and OA) were visualized by iodine vapour first, and then by 0.006% (w/v) rhodamine 6G dissolved in 96% ethanol. R_F values of the bands which were used for further analysis are annotated. HHA: 16-hydroxyhexadecanoic acid. HA: hexadecanoic acid. SA: stearic acid. OA: oleic acid.

LC-MS analysis

An aliquot from each eluent was analysed by LC-ESI-QTOF-mass spectrometer (collaborated with Dr. Hannah Fluorance, University of Edinburgh) by following the protocol below:

● Buffer A: 0.1% (v/v) formic acid in water

● Buffer B: 5% (v/v) Buffer A and 0.1% (v/v) formic acid in acetonitrile

* Samples were ran in positive mode first, followed by the negative one with 10 mM ammonium formate added to buffer A

● Column: Agilent 1.7u x 50mm x 2.1mm

● Program: 0.3 ml/min flow rate; injection volume: markers were 10 ul

● Markers: 0.2 mg/ml HHA, HA, stearic acid and oleic acid dissolved in 75% (v/v) acetonitrile

● Sample: 500 µl of each eluent was dried in SpeedVac and then re-dissolved in 250 µl 75% (v/v) acetonitrile.

● Gradient:

Elution time (min)	**% Buffer A**	**% Buffer B**
0	95	5
1	95	5
10	0	100
11	0	100
15	95	5

Data was analysed in both positive and negative modes, a peak of *m/z* 287.2228 was annotated to be the 10,16-dihydroxyhexadecanoic acid ($C_{16}H_{32}O_4$) with a proton loss ($[M - H]^-$ adduct, $C_{16}H_{31}O_4$), resulting in the formation of [di-HHA^-] adduct (Fig. 104). And the quantity is highest in the lowest band on TLC ($R_F \approx 0.222$) (Fig. 102) and decreasing with the R_F values increase (Fig. 104). All the four markers were also only detected in the

negative mode, but with very different elution times compare with di-HHA

(Fig. 103 and 104).

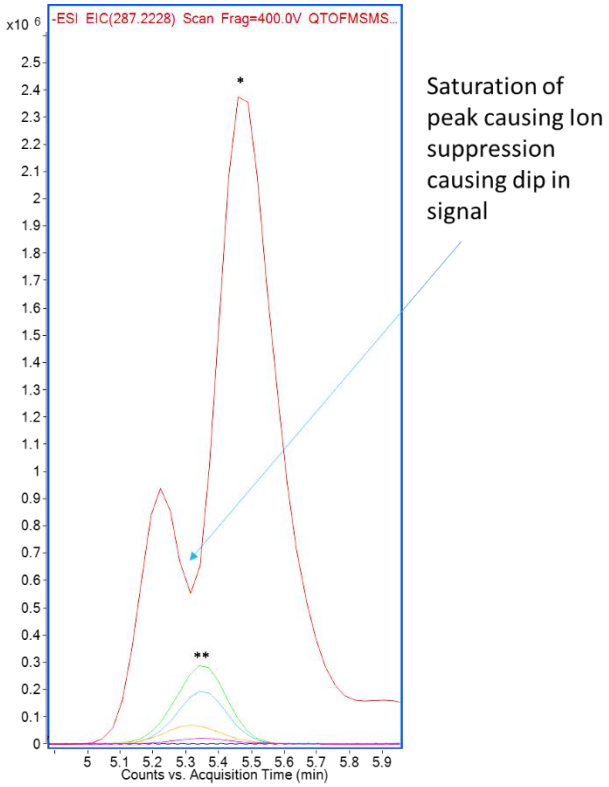

Figure 103. LC-ESI-QTOF-MS analysis of the CMNaOH-releasable residues from tomato fruit epidermis. An aliquot of each TLC eluent (re-dissolved in 75% acetonitrile), which putatively contained di-HHA was subjected to LC-MS, and the dissolved compounes were chemically ionized by 0.1% (v/v) formic acid and 10 mM ammonium formate. Data was analysed in both positive and negative modes, but di-HHA was only found in negative mode.

*. The highest amount of [di-HHA$^-$] adduct is from the lowest band on TLC ($R_F \approx$ 0.222) in figure 96.

**. The amount of [di-HHA$^-$] decreases with the order of R_F values in figure 96.

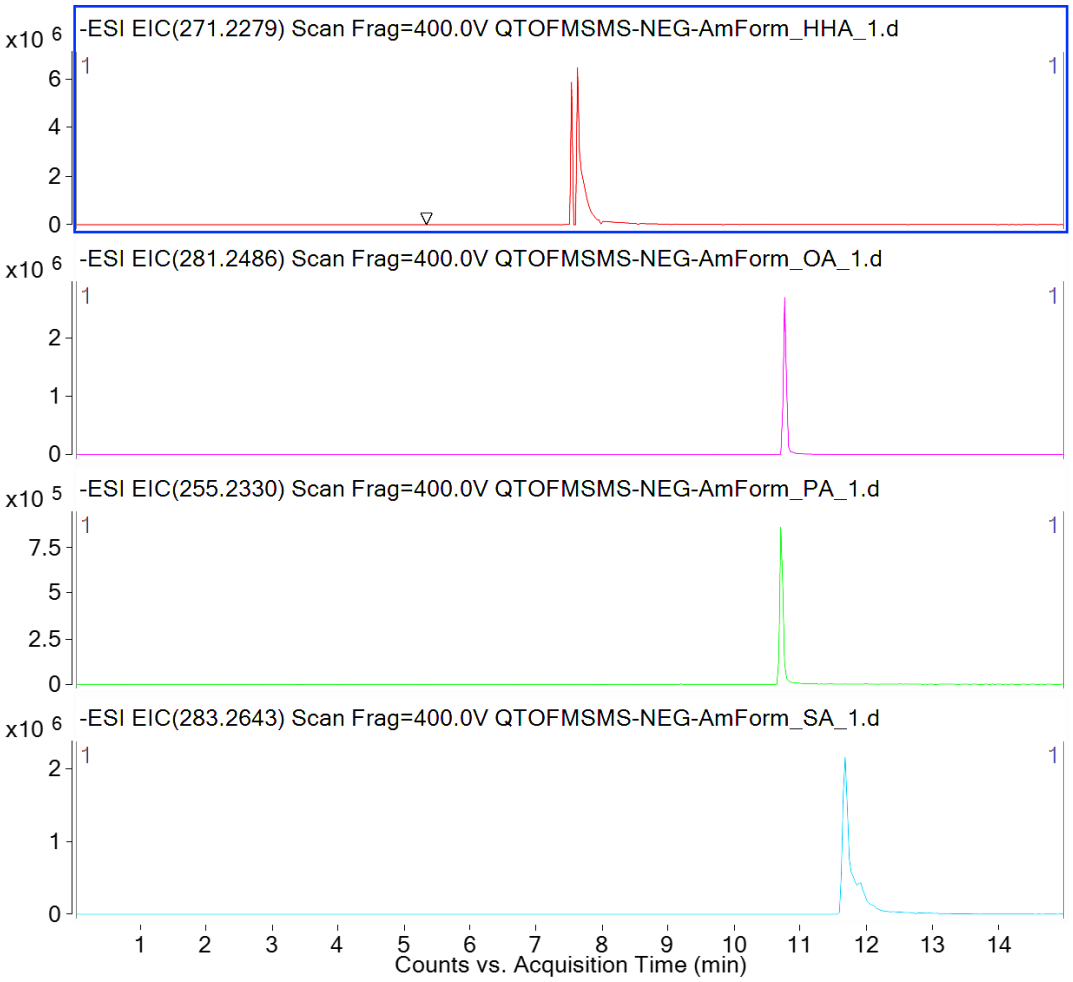

Figure 104. Validation of LC-ESI-QTOF-MS methods for analysing fatty acids in CMNaOH-releasable residues from tomato fruit epidermis. Experimental details as in figure 97 were also applied to external markers HHA, OA, PA and SA (top to bottom) (2 µg), which were ran together the TLC eluent from figure 96. $[M - H]^-$ adducts of all the markers were found in the negative mode. HHA: 16-hydroxyhexadecanoic acid; OA: oleic acid; PA: palmitic acid (hexadecanoic acid); SA: stearic acid.

Purification by HPLC

After being confirmed that the di-HHA was extracted and present in eluents, I attempted to purify it by following the reverse-phase HPLC protocol below.

The detective facility conjugated with HPLC (VWR, US) is evaporative light

scattering detector (ELSD) (Shimadzu, Japan), because the di-HHA does not absorb UV.

HPLC was operated by following the protocol below:

● Buffer A: 0.1% formic acid and 1% ammonium formate in water

● Buffer B: 5% water and 0.1% formic acid in acetonitrile

● Column: ACE Excel 1.7 C18 AR, 100 x 2.1 mm

● Program: 0.1 ml/min flow rate; injection volume: markers were 5–20 ul; the least abundant sample was 20 ul

● Wavelength: 200 nm

● Markers: 0.1 mg/ml HHA dissolved in 90% MeOH, 0.5 mg/ml HA dissolved in MeOH

● Sample: 100 µl of each eluent was dried in SpeedVac and then re-dissolved in 50 µl 75% (v/v) acetonitrile

● ELSD temperature: 70 °C

● Oven temperature: 25 °C

● Gradient:

Elution time (min)	**% Buffer A**	**% Buffer B**
0	95	5
1	95	5
10	0	100
11	0	100
12	95	5
15	95	5

A peak from the eluent sample had a similar elution time with 16-Hydroxyhexadecanoic acid (HHA) and hydroxyhexadecanoic acid (HA) markers, only a trend that the elution time decreases with the increase of

hydroxylation degree (Fig. 105). Thus, this HPLC protocol did not successfully separate the fatty acids with the same length but different hydroxylation degrees.

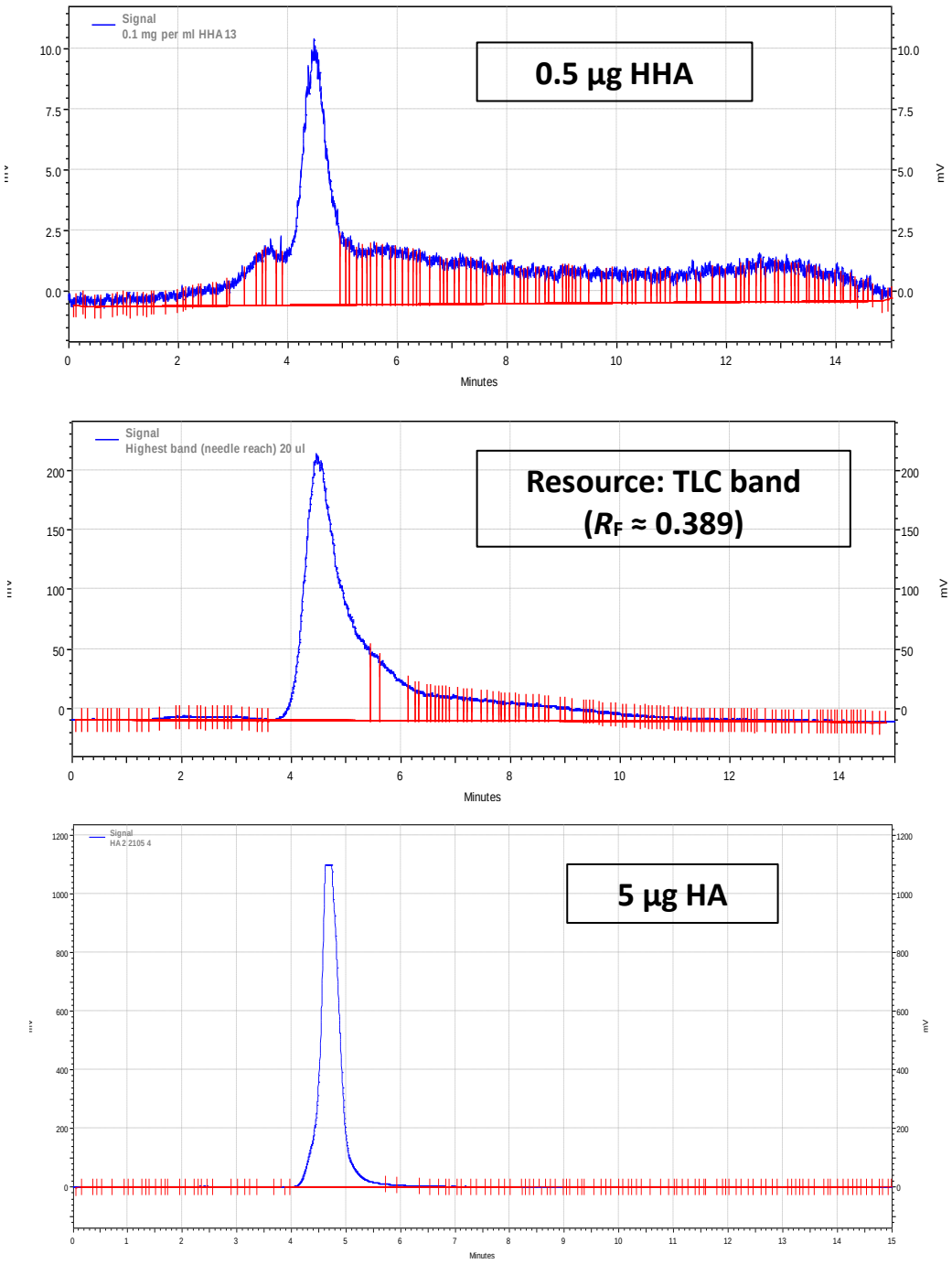

Figure 105. Reverse-phase HPLC-ELSD analysis of the CMNaOH-releasable residues from tomato fruit epidermis. By following the protocol of the reverse-

phase HPLC-ELSD above, 0.5 µg HHA (top) (elution time: 4.48789 min) and 5 µg HA (bottom) (elution time: 4.68388 min) showed neat peaks. The peak in the middle panel (elution time: 4.46757 min) was proposed to be di-HHA; it was obtained by injecting 20 µl of the eluent residues from the highest band on TLC in figure 96 (R_F ≈ 0.389). HHA: 16-hydroxyhexadecanoic acid. HA: hexadecanoic acid.

LC-MS validation

To confirm that the peak appeared in the eluent samples was di-HHA, I collected six fractions from the HPLC facility according to elution time: 0–3 min, 3–4 min, 4–4.5 min, 4.5–5 min, 5–10 min and 10–15 min. These factions were then analysed via LC-MS to validate the compound identity. Experimental details were the same as above, except that only HHA was used as a marker and samples were only ran in negative mode:

● Buffer A: 10 mM ammonium formate in water

● Buffer B: 5% Buffer A in acetonitrile

* 0.1% (v/v) formic acid was added to both buffers for a second run.

However, di-HHA was not found in any fraction (Fig. 106). The LC-MS method was validated by detectable markers (Fig. 107).

a).

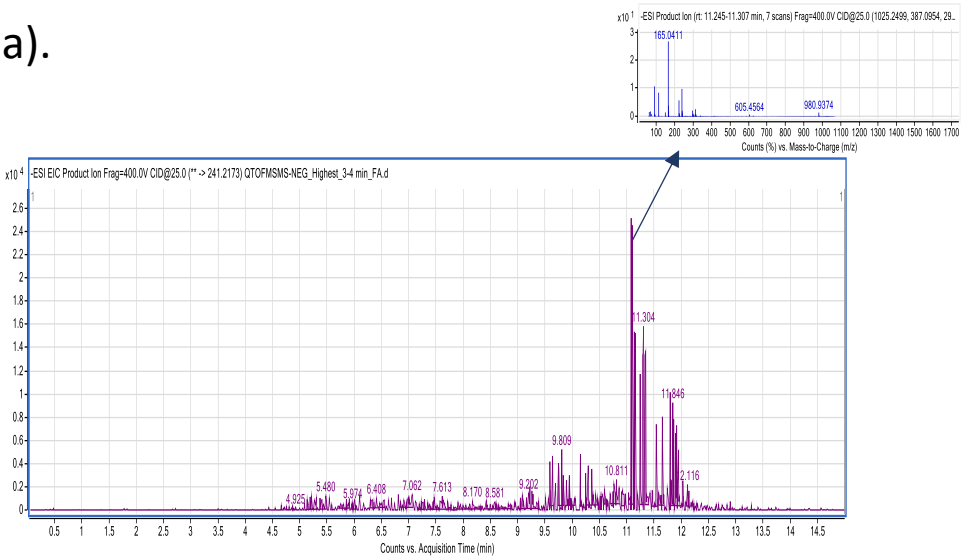
-ESI Product Ion (rt: 11.245-11.307 min, 7 scans) Frag=400.0V CID@25.0 (1025.2499, 387.0954, 29..
165.0411
605.4564
980.9374
Counts (%) vs. Mass-to-Charge (m/z)
-ESI EIC Product Ion Frag=400.0V CID@25.0 (** > 241.2173) QTOFMSMS-NEG_Highest_3-4 min_FA.d
11.304
11.846
9.809
10.811
2.116
4.925
5.480
5.927
6.408
7.062
7.613
8.170
8.581
9.202
Counts vs. Acquisition Time (min)

b).

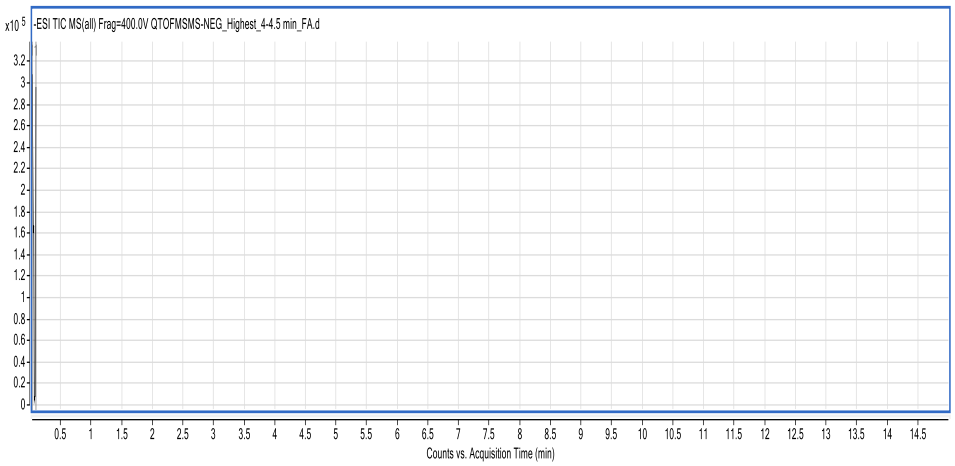
-ESI TIC MS(all) Frag=400.0V QTOFMSMS-NEG_Highest_4-4.5 min_FA.d
Counts vs. Acquisition Time (min)

c).

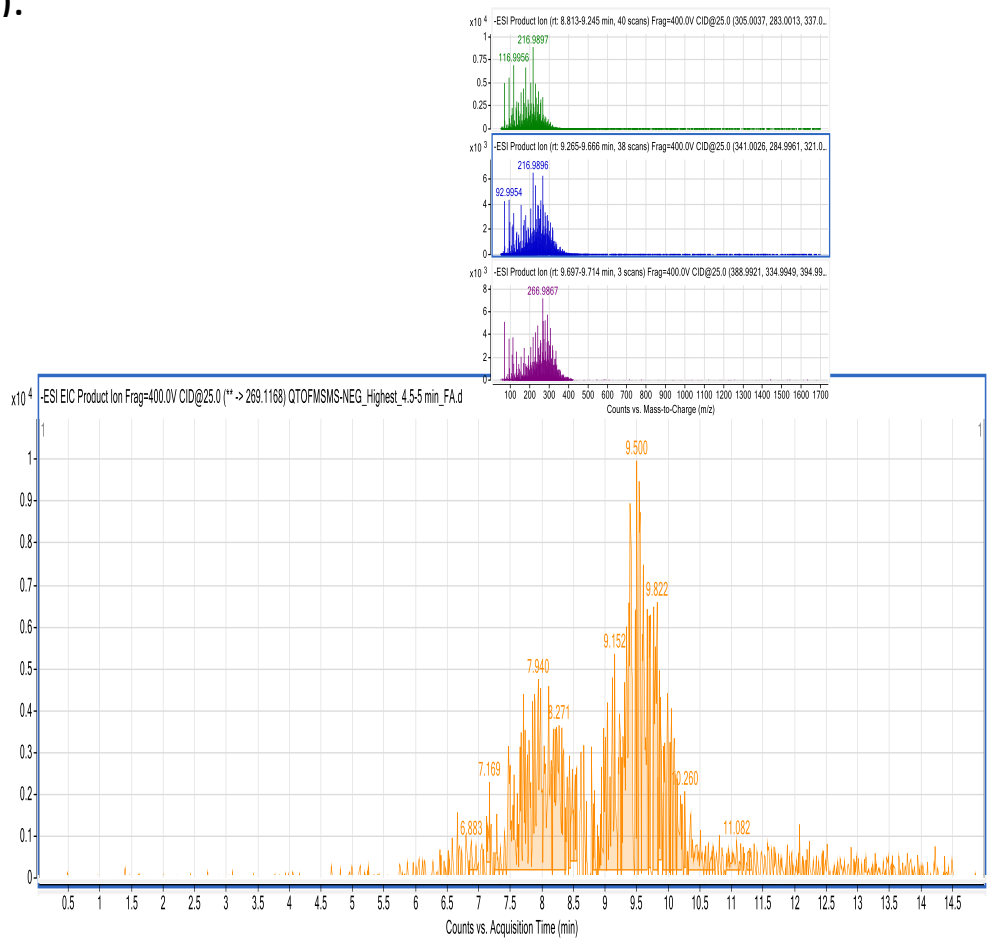

Figure 106. LC-ESI-QTOF-MS analysis of the HPLC fractions putatively containing di-HHA. An aliquot of each HPLC fraction (resource: 0–3, 3–4, 4–4.5, 4.5–5, 5–10 and 10–15 min) were dried and re-dissolved in 75% acetonitrile, followed by being subjected to LC-MS (negative mode) and any fatty acid was chemically ionized by 0.1% (v/v) formic acid and 10 mM ammonium formate. Data was analysed in negative mode. Here are results of three putatively important fractions from HPLC (Fig. 100): (a) 3–4 minute; (b) 4–4.5 minute; (c) 4.5–5 minute. $[M - H]^-$ and $[M - COOH]^-$ adducts were looked for in all the fraction samples, and the more promising one was extracted (the bigger chromatograms in all the graphs). A further analysis (the smaller spectra in all the graphs) was carried out to confirm the presence of corresponding adducts in observed peaks (the bigger chromatograms), if any.

a)

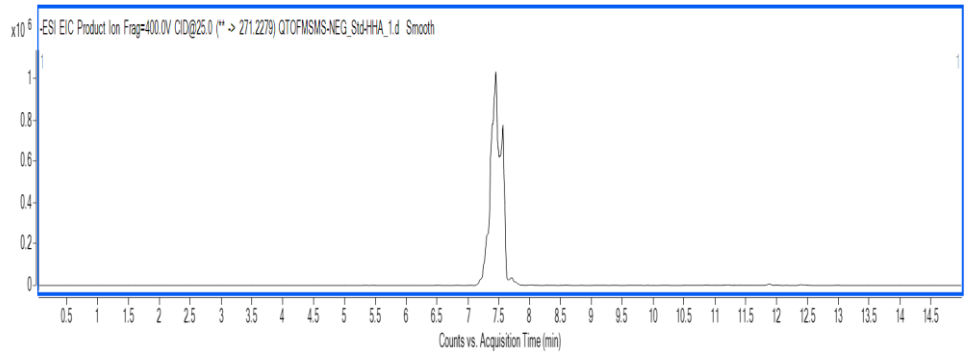

b).

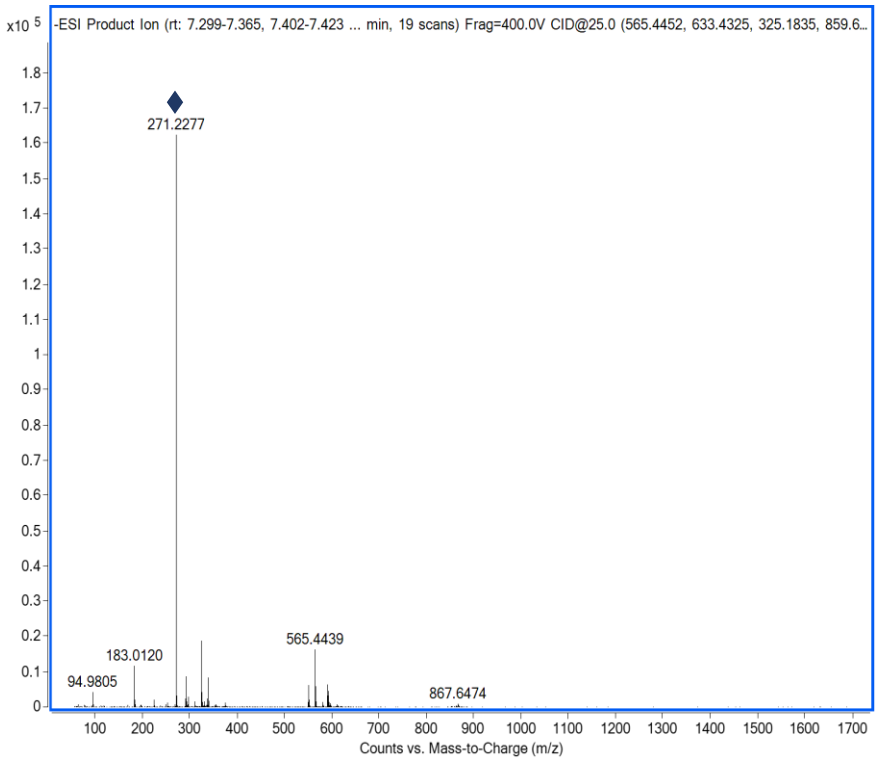

Figure 107. Validation of LC-ESI-QTOF-MS methods for analysing fatty acids from HPLC fractions. Experimental details as in figure 100 were also applied to the external marker, HHA (2 µg). Data was analysed in negative mode, and only $[M - H]^-$ adduct was found (*m/z* 271.2277) in the chromatogram (a). A further analysis (b) of the peak (a) was carried out. The $[M - H]^-$ adduct with its *m/z* was indicated by (⧫) in the spectra (b).

Appendix 7. Expression of pEAQ-GFP in *Nicotiana benthamiana*

To check if pEAQ-HT-CD1 (the plasmid with *CD1* insert) was infiltrated into tobacco and expressed successfully, in parallel with it, the same plasmid but with a GFP insert, pEAQ-HT-GFP was also agroinfiltrated into independent tobacco leaves. After 5 days post infiltration, the plants containing GFP proteins were observed under UV (498 nm) (Fig. 108).

The fluorescent green in tobacco leaves indicated that the pEAQ-HT plasmid was functional, and therefore the CD1 should have been expressed heterologously.

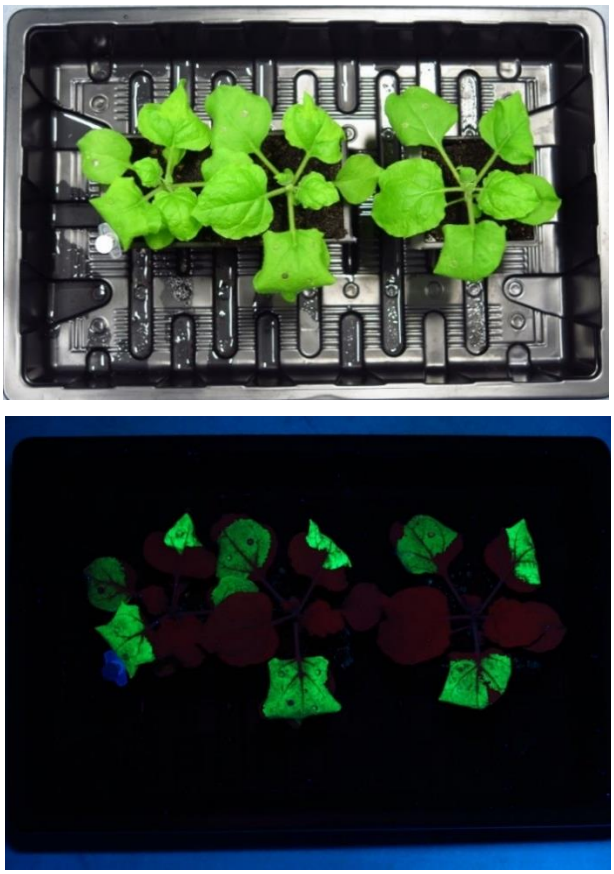

Figure 108. Observation of the heterologously expressed pEAQ-HT-GFP in tobacco leaves. The tobacco plants agroinfiltrated with pEAQ-HT-GFP constructs were grown under than standard conditions for 5 days before the photos were taken. Both photos showed the same set of plants, but the lower one was taken under UV_{498}, whereas the upper one was taken under the normal day light.

References

Akoh CC, Lee GC, Liaw YC, Huang TH & Shaw JF (2004). GDSL family of serine esterases/lipases*. Progress in Lipid Research* **43**, 534–552.

Arnold FH & Volkov AA (1999). Directed evolution of biocatalysts. *Current Opinion in Chemical Biology* **3**, 54–59.

Aubert S, Gout E, Blignyl R and Douce R (1994). Multiple effects of glycerol on plant cell metabolism. *The Journal of Biological Chemistry* **269**, 21420–21427.

Auyong ASM, Ford R & Taylor PWJ (2015). The role of cutinase and its impact on pathogenicity of *Colletotrichum truncatum*. *Journal of Plant Pathology & Microbology* **6**, 259–269.

Ayache S, Panelli M, Marincola FM & Stroncek DF (2006). Effects of storage Time and exogenous protease inhibitors on plasma protein levels. *American Journal of Clinical Pathology* **126**, 174–184.

Badescu GO & Napier RM (2006). Receptors for auxin: will it all end in TIRs? *Trends in Plant Science* **11**, 217–223.

Bakan B & Marion D (2017). Assembly of the cutin polyester: from cells to extracellular cell walls. *Plants* **6**, 57–68.

Baker EA & Holloway PJ (1970). The constituent acids of angiosperm cutins. *Phytochemistry* **9**, 1557–1562.

Baker EA (1974). The Influence of environment on leaf wax development in *Brassica oleracea* var. gemmifera. *New Phytologist* **73**, 955–966.

Baker EA, Bukovac MJ & Hunt GM (1982). Composition of tomato fruit cuticle as related to fruit growth and development. In: *The Plant Cuticle* (Cutler DF, Alvin KL and Price CE, eds.), Academic Press, New York, US. pp. 33–44.

Baker PJ, Poultney C, Liu Z, Gross R & Montclare JK (2012). Identification and comparison of cutinases for synthetic polyester degradation. *Applied Microbiology and Biotechnology* **93**, 229–240.

Baldwin L, Domon JM, Klimek JF, Fournet F, Sellier H, Gillet F, Pelloux J, Lejeune-Hénaut I, Carpita NC & Rayon C (2014). Structural alteration of cell wall pectins accompanies pea development in response to cold. *Phytochemistry* **104**, 37–47.

Batteas JD, Stark RE, Jenks MA & Rose JKC (2009). Cutin deficiency in the tomato fruit cuticle consistently affects resistance to microbial infection and biomechanical properties, but not transpirational water loss. *The Plant Journal* **60**, 363–377.

Bauer S, Vasu P, Mort AJ & Somerville CR (2005). Cloning, expression, and characterization of an oligoxyloglucan reducing end-specific xyloglucanobiohydrolase from *Aspergillus nidulans*. *Carbohydrate Research* **340**, 2590–2597.

Bauer S, Vasu P, Persson S, Mort AJ & Somerville CR (2006). Development and application of a suite of polysaccharide-degrading enzymes for analyzing plant cell walls. *Proceedings of the National Academy of Sciences* **103**, 11417–11422.

Beck EH, Fettig S, Knake, C, Hartig K & Bhattarai T (2007). Specific and unspecific responses of plants to cold and drought stress. *Journal of Biosciences* **32**, 501–510.

Belge B, Llovera M, Comabella E, Gatius F, Guillen P, Graell J & Lara I (2014). Characterization of cuticle composition after cold storage of “Celeste” and “Somerset” Sweet Cherry Fruit. *Journal of Agricultural and Food Chemistry* **62**, 8722−8729.

Berhin A, de Bellis D, Franke RB, Buono RA, Nowack MK & Nawrath C (2019). The root cap cuticle: a cell wall structure for seedling establishment and lateral root formation. *Cell* **176**, 1367–1378.

Beisson F, Li-Beisson Y & Pollard M (2012). Solving the puzzles of cutin and suberin polymer biosynthesis. *Current Opinion of Plant Biology* **15**, 329–337.

Bhalekar M, Sonawane S & Shimpi S (2013). Synthesis and characterization of a cysteine xyloglucan conjugate as mucoadhesive polymer. *Brazilian Journal of Pharmaceutical Sciences* **49**, 285–292.

Bhunia RK, Showman LJ, Jose A & Nikolau BJ (2018). Combined use of cutinase and high‐resolution mass‐spectrometry to query the molecular architecture of cutin. *Plant Methods* **14**, 117–134.

Bird D, Beisson F, Brigham A, Shin J, Greer S, Jetter R, Kunst L, Wu X, Yephremov A & Samuels L (2007). Characterization of *Arabidopsis* ABCG11/WBC11, an ATP binding cassette (ABC) transporter that is required for cuticular lipid secretion. *The Plant Journal* **52**, 485–498.

Boudart G, Jamet E, Rossignol M, Lafitte C, Borderies G, Jauneau A, Esquerré-Tugayé M & Pont-Lezica R (2005). Cell wall proteins in apoplastic fluids of *Arabidopsis thaliana* rosettes: Identification by mass spectrometry and bioinformatics. *Proteomics* **5**, 212–221.

Brummell DA & Harpster MH (2001). Cell wall metabolism in fruit softening and quality and its manipulation in transgenic plants. *Plant Molecular Biology* **47**, 311–340.

Buda GJ, Barnes WJ, Fich EA, Park S, Yeats TH, Zhao L, Domozych DS, Rose JKC (2013). An ATP binding cassette transporter is required for

cuticular wax deposition and desiccation tolerance in the moss *Physcomitrella patens*. *The Plant Cell* **25**, 4000–4013.

Burstin J (2000). Differential expression of two barley XET-related genes during coleoptile growth. *Journal of Experimental Botany* **51**, 847–852.

Caldicott AB & Eglinton G (1976). Cutin acids from bryophytes: an ω-hydroxy alkanoic acid in two liverwort species. *Phytochemistry* **15**, 1139–1143.

Carver MA, Humphery KM, Patchett RA & Jones CW (1984). The effect of EDTA and related chelating agents on the oxidation of methanol by the methylotrophic bacterium, *Methylophilus methylotrophus*. *European Journal of Biochemistry* **138**, 611–615.

Casado CG & Heredia A (2001). Ultrastructure of the cuticle during growth of the grape berry (*Vitis vinifera*). *Physiologia Plantarum* **111**, 220–224.

Chahinian H & Sarda L (2009). Distinction between esterases and lipases: comparative biochemical properties of sequence-related carboxylesterases. *Protein & Peptide Letters* **16**, 1149–61.

Chen X, Snyder CL, Truksa M, Shah S & Weselake RJ (2011). sn-Glycerol-3-phosphate acyltransferases in plants. *Plant Signaling & Behavior* **6**, 1695–1699.

Chormova D, Franková L, Defries A, Cutler SR & Fry SC (2015). Discovery of small molecule inhibitors of xyloglucan endotransglucosylase (XET) activity by high-throughput screening. *Phytochemistry* **117**, 220–236.

Cook ME & Graham LE (1998). Structural similarities between surface layers of selected charophycean algae and bryophytes and the cuticles of vascular plants. *International Journal of Plant Sciences* **159**, 780–787.

Cosgrove DJ (1997). Assembly and enlargement of the primary cell wall in plants. *Annual Review of Cell and Developmental Biology* **13**, 171–201.

Cosgrove DJ (2005). Growth of the plant cell wall. *Nature Reviews Molecular Cell Biology* **6**, 850–861.

Crombie HJ, Chengappa S, Jarman C, Sidebottom C, Reid JG (2002). Molecular characterisation of a xyloglucan oligosaccharide-acting α-D-xylosidase from nasturtium (*Tropaeolum majus* L.) cotyledons that resembles plant 'apoplastic' α-D-glucosidases. *Planta* **214**, 406–413.

Cummins I & Edwards R (2004). Purification and cloning of an esterase from the weed black-grass (*Alopecurus myosuroides*), which bioactivates aryloxyphenoxypropionate herbicides. *The Plant Journal* **39**, 894–904.

Deas AH & Holloway PJ (1977). The intermolecular structure of some plant cutins. In: *Lipids and Lipid Polymers in Higher Plants* (Tevini M, Lichtanthaler HK, Eds.). Springer-Verlag: Berlin, Germany. pp 293−299.

Deshmukh AP, Simpson AJ & Hatcher PG (2003). Evidence for cross-linking in tomato cutin using HR-MAS NMR spectroscopy. *Phytochemistry* **64**, 1163–1170.

Desjardins P & Conklin D (2010). NanoDrop microvolume quantitation of nucleic acids. *Journal of Visualized Experiments* **45**, e2565.

Doi Y, Steinbüchel A, Kolattukudy PE, Doi Y & Steinbüchel A (2005). Cutin from Plants. In: *Biopolymers Online* (Steinbüchel A eds.). Wiley-VCH: Münster, Germany. pp 1–35.

Dominguez E (2014). Biomechanical properties of the tomato (*Solanum lycopersicum*) fruit cuticle during development are modulated by changes in the relative amounts of its components. *New Phytologist* **202**, 790–802.

Domínguez E, López-Casado G, Cuartero J & Heredia A (2008). Development of fruit cuticle in cherry tomato (*Solanum lycopersicum*). *Functional Plant Biology* **35**, 403–411.

Ebringerová A, Hromádková Z & Heinze T (2005). Hemicellulose. In: *Polysaccharides I. Advances in Polymer Science volume 186* (Heinze T, eds). Springer: Berlin & Heidelberg, Germany. pp 1–67

Edwards D (1993). Cells and tissues in the vegetative sporophytes of early land plants. *New Phytologist* **125**, 225–247.

Edwards D, Edwards DS & Rayner R (1982). The cuticle of early vascular plants and its evolutionary significance. In: *The Plant Cuticle (Linnean Society Symposium Series)* (Cutler DF, Alvin KL & Price CE, eds). Academic Press: London, UK. pp. 341–361.

España L, Heredia-Guerrero JA, Segado P, Benitez JJ, Heredia A & F. Beisson & J. Ohlrogge (2012). Plants: Knitting a polyester skin. *Nature Chemical Biology* **8**, 603–604.

España L, Heredia-Guerrero JA, Segado P, Benítez JJ, Heredia A & Domínguez E (2014), Biomechanical properties of the tomato (*Solanum lycopersicum*) fruit cuticle during development are modulated by changes in the relative amounts of its components. *New Phytologist* **202**: 790–802.

Fang X, Qiu F, Yan B, Wang H, Mort AJ & Stark RE (2001). NMR studies of molecular structure in fruit cuticle polyesters. *Phytochemistry* **57**, 1035–1042.

Fanutti C, Gidley MJ & Reid JSG (1991). A xyloglucan-oligosaccharide-specific α-D-xylosidase or exo-oligoxyloglucan-α-xylohydrolase from germinated nasturtium (*Tropaeolum majus* L.) seeds. *Planta* **184**, 137–147.

Fernández V, Guzmán-Delgado P, Graça J, Santos S & Gil L (2016). Cuticle structure in relation to chemical composition: re-assessing the prevailing model. *Frontiers in Plant Science* **7**, 427–441.

Fich EA, Segerson NA & Rose JKC (2016). The plant polyester cutin: biosynthesis, structure, and biological roles. *Annual Review of Plant Biology* **67**, 207–233.

Folch J, Lees M & Stanley GHS (1957). A simple method for the isolation and purification of total lipids from animal tissues. *The Journal of Biological Chemistry* **226**, 497–509.

Franke R, Briesen I, Wojciechowski T, Faust A, Yephremov A, Nawrath C & Schreiber L (2005). Apoplastic polyesters in *Arabidopsis* surface tissues--a typical suberin and a particular cutin. *Phytochemistry* **66**, 2643–2658.

Franková L & Fry SC (2012). Trans-α-xylosidase, a widespread enzyme activity in plants, introduces (1→4)-α-D-xylobiose side-chains into xyloglucan structures. *Phytochemistry* **78**, 29–43.

Franková L & Fry SC (2013). Biochemistry and physiological roles of enzymes that 'cut and paste' plant cell-wall polysaccharides. *Journal of Experimental Botany* **64**, 3519–3550.

Fry SC (1989). Cellulases, hemicelluloses and auxin-stimulated growth: A possible relationship. *Physiologia Plantarum* **75**, 532–536.

Fry SC (1995). Polysaccharide-modifying enzymes in the plant cell wall. *Annual Review of Plant Physiology and Plant Molecular Biology* **46**, 497–520.

Fry SC, Aldington S, Hetherington PR, & Aitken J (1993). Oligosaccharides as signals and substrates in the plant cell wall. *Plant Physiology* **103**, 1–5.

Fry SC, Mohler KE, Nesselrode BH & Franková, L (2008). Mixed-linkage β-glucan : xyloglucan endotransglucosylase, a novel wall-remodelling enzyme from *Equisetum* (horsetails) and charophytic algae. *The Plant Journal* **55**, 240–252.

Fry SC, Smith RC, Renwick KF, Martin DJ, Hodge SK & Matthews KJ (1992). Xyloglucan endotransglycosylase, a new wall-loosening enzyme activity from plants. *Biochemical Journal* **282**, 821–828.

Fry SC, York WS, Albersheim P, Darvill A, Hayashi T, Joseleau J, Kato Y, Lorences EP, Maclachlan GA, McNeil M, Mort AJ, Grant Reid JS, Seitz HU, Selvendran RR, Voragen AG & White AR (1993). An unambiguous nomenclature for xyloglucan–derived oligosaccharides. *Physiologia Plantarum* **89**, 1–3.

Fry, S. C. (2004), Primary cell wall metabolism: tracking the careers of wall polymers in living plant cells. *New Phytologist* **161**, 641–675.

Garber M, Grabherr MG, Guttman M & Trapnell C (2011). Computational methods for transcriptome annotation and quantification using RNA-seq. *Nature Methods volume* **8**, 469–477.

Gershater M, Sharples K & Robert Edwards (2006). Carboxylesterase activities toward pesticide esters in crops and weeds. *Phytochemistry* **67**, 2561–2567.

Giller K (1996). Origin of land plants: L. E. Graham. J. Wiley and Sons. In: *Agricultural Systems volume 51* (Hansen JW, Thornton PK & Berentsen PBM, eds.). Elsevier: New York, US. pp. 125–126.

Girard AL, Mounet F, Lemaire-Chamley M, Gaillard C, Elmorjani K, Vivancos J, Runavot JL, Quemener B, Petit J, Germain V, Rothan C, Marion D & Bakan B (2012). Tomato GDSL1 is required for cutin deposition in the fruit cuticle. *The Plant Cell* **24**, 3119–3134.

Glaus MA & Van Loon LR (2008). Degradation of cellulose under alkaline conditions: new insights from a 12 years degradation study. *Environmental Science & Technology* **42**, 2906–2911.

Goetz S, Rejzek M, Nepogodiev SA & Field RA (2016). The impact of aminopyrene trisulfonate (APTS) label in acceptor glycan substrates for profiling plant pectin b-galactosyltransferase activities. *Carbohydrate Research* **433**, 97–105.

Goñi MA & Hedges JI (1990). Potential applications of cutin-derived CuO reaction products for discriminating vascular plant sources in natural environments. *Geochimica et Cosmochimica Acta* **54**, 3073–3081.

Graça J and Lamosa P (2010). Linear and branched poly(ω-hydroxyacid) esters in plant cutins. *Journal of Agricultural and Food Chemistry* **58**, 9666–9674.

Graça J, Schreiber L, Rodrigues J & Pereira H (2002). Glycerol and glyceryl esters of ω-hydroxyacids in cutins. *Phytochemistry* **61**, 205–215.

Greer S, Wen M, Bird D, Wu X, Samuels L, Kunst L & Reinhard Jetter (2007). The cytochrome P450 enzyme CYP96A15 is the midchain alkane hydroxylase responsible for formation of secondary alcohols and ketones in stem cuticular wax of *Arabidopsis*. *Plant Physiology* **145**, 653–667.

Guillen R, York WS, Pauly M, An JH, Impallomeni G, Albersheim P & Darvill AG (1995). Metabolism of xyloglucan generates xylose-deficient oligosaccharide subunits of this polysaccharide in etiolated peas. *Carbohydrate Research* **277**, 291–311.

Gupta NS, Collinson ME, Briggs DEG, Evershed RP & Pancost RD (2006). Reinvestigation of the occurrence of cutan in plants: implications for the leaf fossil record. *Paleobiology* **32**, 432–449.

Guzmán P, Fernández V, García ML, Khayet M, Fernández A & Gil L (2014). Localization of polysaccharides in isolated and intact cuticles of eucalypt, poplar and pear leaf by enzyme-gold labelling. *Plant Physiology and Biochemistry* **76**, 1–6.

Guzmán P, Fernández V, Graça J, Cabral V, Kayali N, Khayet M and Gil L (2014) Chemical and structural analysis of *Eucalyptus globulus* and *E. camaldulensis* leaf cuticles: a lipidized cell wall region. *Frontiers in Plant Science* **5**, 481–493.

Harholt J, Suttangkakul A & Scheller HB (2010). Biosynthesis of Pectin. *Plant Physiology* **153**, 384–395.

Hayashi T & Rumi K (2011). Functions of xyloglucan in plant cells. *Molecular Plant* **4**, 17–24.

Hayashi T (1989). Xyloglucans in the primary cell wall. *Annual Review of Plant Physiology and Plant Molecular Biology* **40**, 139–168.

Hedrich R (1989). The physiology of ion channels and electrogenic pumps in higher plants. *Annual Review of Plant Biology* **40**, 539–569.

Hedstrom L (2002). Serine protease mechanism and specificity. *Chemical Reviews* **102**, 4501–4524.

Hetherington PR & Fry SC (1993). Xyloglucan Endotransglycosylase activity in carrot cell suspensions during cell elongation and somatic embryogenesis. *Plant Physiology* **103**, 987–992.

Hoffmann-Benning S & Kende H (1994). Cuticle biosynthesis in rapidly growing internodes of deepwater rice. *Plant Physiology* **104**, 719–723.

Holloway PJ (1982). The chemical constitution of plant cutins. In: *The Plant Cuticle (Linnean Society Symposium Series)* (Cutler DF, Alvin KL & Price CE, eds). Academic Press: London. pp. 45–85.

Hong L, Brown J, Segerson NA, Rose JKC & Roeder AHK (2017). Cutin synthase 2 maintains progressively developing cuticular ridges in *Arabidopsis* sepals. *Molecular Plant* **10**, 560–574.

Hrmova M, Harvey AJ, Wang J, Shirley NJ, Jones GP, Stone BA, Høj PB & Fincher GB (1996). Barley beta-D-glucan exohydrolases with beta-D-glucosidase activity. Purification, characterization, and determination of primary structure from a cDNA clone. *The Journal of Biological Chemistry* **271**, 5277–5286.

Hu J, Zhang Y, Wang J and Zhou Y (2014). Glycerol affects root development through regulation of multiple pathways in *Arabidopsis*. *PLoS ONE* **9**, e86269.

Hunneman DH & Eglinton G (1972). The constituent acids of gymnosperm cutins. *Phytochemistry* **11**, 1989–2001.

Hunt GM & Baker EA (1980). Phenolics constituents of tomato fruit cuticles. *Phytochemistry* **19**, 1415–1419.

Isaacson T, Kosma DK, Matas AJ, Buda GJ, He Y, Yu B, Pravitasari A, Batteas JD, Stark RE, Jenks MA & Rose JKC (2009). Cutin deficiency in the tomato fruit cuticle consistently affects resistance to microbial infection and biomechanical properties, but not transpirational water loss. *The Plant Journal* **60**, 363–377.

Ishii T, Matsuoka K, Ono H, Kameyama MO, Yaoi K, Nakano Y, Ohtani M, Demura T, Iwai H & Satoh S (2017). Characterization of xylan in the early stages of secondary cell wall formation in tobacco bright yellow-2 cells. *Carbohydrate Polymers* **176**, 381–391.

Jeffree CE (2006). The Fine Structure of the Plant Cuticle. In: *Annual Plant Reviews Volume 23: Biology of the Plant Cuticle* (Riederer M & Müller C, eds.). Blackwell: New Jersey, US.

Jenks MA, Tuttle HA, Eigenbrode SD & Feldmann KA (1995). Leaf epicuticular waxes of the Eceriferum mutants in *Arabidopsis*. *Plant Physiology* **108**, 369–377.

Jork H, Funk W, Fischer W & Wimmer H (1994). *Thin layer chromatography: reagents and detection methods*. Volume 1b, *Physical and chemical detection methods; activation reactions, reagent sequences, reagents II.* Weinheim, VCH.

Kanwar SS, Kausha RK, Jawed A, Gupta R & Chimni SS (2005). Methods for inhibition of residual lipase activity in colorimetric assay: A comparative study. *Indian Journal of Biochemistry and Biophysics* **42**, 233–237.

Kim H, Lee SB, Kim HJ, Min MK, Hwang I & Suh MC (2012). Characterization of Glycosylphosphatidylinositol-Anchored Lipid Transfer Protein 2 (LTPG2) and overlapping function between LTPG/LTPG1 and LTPG2 in cuticular wax export or accumulation in *Arabidopsis thaliana*. *Plant and Cell Physiology* **53**, 1391–1403.

Kim S, Bae SY, Kim SJ, Ngo TD, Kim KK & Kim TD (2012). Characterization, amyloid formation, and immobilization of a novel SGNH hydrolase from *Listeria innocua* 11262. *International Journal of Biological Macromolecules* **50**, 103–111.

Kirkwood RC (1999). Recent developments in our understanding of the plant cuticle as a barrier to the foliar uptake of pesticides. *Pesticide Science* **55**, 69–77.

Knox RB, Vithanage HIMV & Howlett BJ (1980). Botanical immunocytochemistry: a review with special reference to pollen antigens and allergens. *The Histochemical Journal* **12**, 247–272.

Kolattukudy PE (1977). Lipid polymers and associated phenols, their chemistry, biosynthesis, and role in pathogenesis. *Recent Advances in Phytochemistry* **77**, 185–246.

Konigsberg W (1972). Reduction of disulfide bonds in proteins with dithiothreitol. *Methods in Enzymology* **25**, 185–188.

Kosma DK, Parsons EP, Isaacson T, Lu S, Rose JKC & Jenks MA (2010). Fruit cuticle lipid composition during development in tomato ripening mutants. *Physiologia Plantarum* **139**, 107–117.

Koyama T, Hayashi T, Kato Y & Matsuda K (1983). Degradation of xyloglucan by wall-bound enzymes from soybean tissue II: degradation of the fragment heptasaccharide from xyloglucan and the characteristic action pattern of the α-D-xylosidase in the enzyme system. *Plant and Cell Physiology* **24**,155–162.

Kunst L & Samuels AL (2003). Biosynthesis and secretion of plant cuticular wax. *Progress in Lipid Research* **42**, 51–80.

Kunst L & Samuels AL (2009). Plant cuticles shine: advances in wax biosynthesis and export. *Current Opinion in Plant Biology* **12**, 721–727.

Kurien BT & Scofield RH (2006). Western blotting. *Methods* **38**, 283–293.

Kutschera U & Niklas KJ (2007). The epidermal-growth-control theory of stem elongation: an old and a new perspective. *Journal of Plant Physiology* **164**, 1395–1409.

Lai C, Kunst L & R Jetter (2007). Composition of alkyl esters in the cuticular wax on inflorescence stems of *Arabidopsis thaliana* cer mutants. *The Plant Journal* **50**, 189–196.

Lai CP, Huang LM, Chen LO, Chan MT & Shaw JF (2017). Genome-wide analysis of GDSL-type esterases/lipases in *Arabidopsis*. *Plant Molecular Biology* **95**, 181–197.

Lamport DTA (1970). Cell wall metabolism. *Annual Review of Plant Physiology* **21**, 235–270.

Lee SB1, Go YS, Bae HJ, Park JH, Cho SH, Cho HJ, Lee DS, Park OK, Hwang I & Suh MC (2009). Disruption of glycosylphosphatidylinositol-anchored lipid transfer protein gene altered cuticular lipid composition, increased plastoglobules, and enhanced susceptibility to infection by the fungal pathogen *Alternaria brassicicola*. *Plant Physiology* **150**, 42–54.

Li F, Wu X, Lam P, Bird D, Zheng H, Samuels L, Jetter R & Kunst L (2008). Identification of the wax ester synthase/acyl-Coenzyme A: diacylglycerol acyltransferase WSD1 required for stem wax ester biosynthesis in *Arabidopsis*. *Plant Physiology* **148**, 97–107.

Li LO, Klett EL & Coleman RA (2010). Acyl-CoA synthesis, lipid metabolism and lipotoxicity. *Biochimica et Biophysica Acta (BBA) - Molecular and Cell Biology of Lipids* **1801**, 246–251.

Li N, Xu C, Li-Beisson Y & Philippar K (2016). Fatty acid and lipid transport in plant cells. *Trends in Plant Science* **21**, 145–158.

Li-Beisson Y, Shorrosh B, Beisson F, Andersson MX, Arondel V, Bates PD, Baud S, Bird D, DeBono A, Durrett TP, Franke RB, Graham IA, Katayama K, Kelly AA, Larson T, Markham JE, Miquel M, Molina I, Nishida I, Rowland O, Samuels L, Schmid KM, Wada H, Welti R, Xu C, Zallot R & Ohlrogge J (2010). Acyl-lipid metabolism. *Arabidopsis Book* **8**, e0133.

Liu N, Karunakaran C, Lahlali R, Warkentin T, Bueckert RA (2019). Genotypic and heat stress effects on leaf cuticles of field pea using ATR-FTIR spectroscopy. *Planta* **249**, 601–613.

Liu Z, Gosser Y, Baker PJ, Ravee Y, Lu Z, Alemu G, Li H, Butterfoss GL, Kong XP, Gross R & Montclare JK (2009). Structural and functional studies of *Aspergillus oryzae* Cutinase: enhanced thermostability and hydrolytic activity of synthetic ester and polyester degradation. *Journal of the American Chemical Society* **131**, 15711–15716.

López-Casado G, Matas AJ, Domínguez E, Cuartero J & Heredia A (2007). Biomechanics of isolated tomato (*Solanum lycopersicum* L.) fruit cuticles: the role of the cutin matrix and polysaccharides. *Journal of Experimental Botany* **58**, 3875–3883.

Lorences EP & Fry SC (1993), Xyloglucan oligosaccharides with at least two α-D-xylose residues act as acceptor substrates for xyloglucan endotransglycosylase and promote the depolymerisation of xyloglucan. *Physiologia Plantarum* **88**, 105–112.

Lü, S, Song T, Kosma DK, Parsons EP, Rowland O & Jenks MA (2009). *Arabidopsis* CER8 encodes long-chain acyl-CoA synthase 1 (LACS1) that has overlapping functions with LACS2 in plant wax and cutin synthesis. *The Plant Journal* **59**, 553–564.

Lukesh JC, Palte MJ & Raines RT (2012). A Potent, versatile disulfide-reducing agent from aspartic Acid. *Journal of the American Chemical Society* **134**, 4057–4059.

Luque P, Bruque S & Heredia A (1995). Water permeability of isolated cuticular membranes: a structural analysis. *Archives of Biochemistry and Biophysics* **317**, 417–422.

Maris A, Kaewthai N, Eklöf JN, Miller JG, Brumer H, Fry SC, Verbelen JP & Vissenberg K (2011). Differences in enzymic properties of five recombinant xyloglucan endotransglucosylase/hydrolase (XTH) proteins of *Arabidopsis thaliana*. *Journal of Experimental Botany* **62**, 261–271.

Maris A, Suslov D, Fry SC, Verbelen JP & Vissenberg K (2009). Enzymic characterization of two recombinant xyloglucan endotransglucosylase/hydrolase (XTH) proteins of *Arabidopsis* and their

effect on root growth and cell wall extension. *Journal of Experimental Botany* **60**, 3959–3972.

Martin JT (1964). Role of cuticle in the defense against plant disease. *Annual review of Phytopathology* **2**, 81–100.

Matas AJ, Yeats TH, Buda GJ, Zheng Y, Chatterjee S, Tohge T, Ponnala L, Adato A, Aharoni A, Stark R, Fernie AR, Fei Z, Giovannoni JJ & Rose JKC (2011). Tissue- and cell-type specific transcriptome profiling of expanding tomato fruit provides insights into metabolic and regulatory specialization and cuticle formation. *The Plant Cell* **23**, 3893–3910.

Matsunaga T, Ishii T & Watanabe-Oda H (1997). HPLC/ICP-MS study of metals bound to borate-rhamnogalacturonan-II from plant cell walls. In: *Plant Nutrition for Sustainable Food Production and Environment* (Ando T, Fujita K, Mae T, Matsumoto H, Mori S, Sekiya J, eds.), Kluwer Academic Publishers, Dordrecht, The Netherlands, pp 81–82.

Mazurek S, Garroum I, Daraspe J, De Bellis D, Olsson V, Mucciolo A, Butenko MA, Humbel BM & Nawrath C (2017). Connecting the molecular structure of cutin to ultrastructure and physical properties of the cuticle in petals of *Arabidopsis*. *Plant Physiology* **173**, 1146–1163.

McDougall GJ & Fry SC (1988). Inhibition of auxin-stimulated growth of pea stem segments by a specific nonasaccharide of xyloglucan. *Planta* **175**, 412–416.

McFeeters RF & Fleming HP (1989). Inhibition of cucumber tissue softening in acid brines by multivalent cations: inadequacy of the pectin “egg box” model to explain textural effects. *Journal of Agricultural and Food Chemistry* **37**, 1053−1059.

Mittler & Blumwald E (2010). Genetic engineering for modern agriculture: challenges and perspectives. *Annual Review of Plant Biology* **61**, 443–462.

Miyamoto K & Schopfer P (1997). Sugar release from maize coleoptiles during auxin-, fusicoccin- and acid-mediated elongation growth. *Journal of Plant Physiology* **150**, 309–316.

Mohler KE, Simmons TJ & Fry SC (2013). Mixed-linkage glucan:xyloglucan endotransglucosylase (MXE) re-models hemicelluloses in *Equisetum* shoots but not in barley shoots or *Equisetum* callus. *New Phytologist* **197**, 111–122.

Molina I, Ohlrogge JB & Pollard M (2008). Deposition and localization of lipid polyester in developing seeds of *Brassica napus* and *Arabidopsis thaliana*. *The Plant Journal* **53**, 437–449.

Moreira LRS & Filho EXF (2008). An overview of mannan structure and mannan-degrading enzyme systems. *Applied Microbiology Biotechnology* **79**, 165–178.

Muralidharan M, Buss K, Larrimore KE, Segerson NA, Kannan L & Mo TS (2013). The *Arabidopsis thaliana* ortholog of a purported maize cholinesterase gene encodes a GDSL-lipase*. Plant Molecular Biology* **81**, 565–576.

Nadakuduti SS, Pollard M, Kosma DK, Allen CJ, Ohlrogge JB & Barry CS (2012). Pleiotropic phenotypes of the sticky peel mutant provide new insight into the role of CUTIN DEFICIENT2 in epidermal cell function in tomato. *Plant Physiology* **159**, 945–960.

Nawrath C (2006). Unraveling the complex network of cuticular structure and function. *Current Opinion in Plant Biology* **9**, 281–287.

Nawrath, C. (2002). The Biopolymers Cutin and Suberin. *The Arabidopsis Book / American Society of Plant Biologists* **1**, e0021.

O'Neill MA, Warrenfeltz D, Kates K, Pellerin P, Doco T, Darvill AG & Albersheim P (1996). Rhamnogalacturonan-II, a pectic polysaccharide in the walls of growing plant cell, forms a dimer that is covalently cross-linked by a borate ester. *In vitro* conditions for the formation and hydrolysis of the dimer. *Journal of Biological Chemistry* **271**, 22923–22930.

Øbro J, Harholt J, Scheller HB & Orfila C (2004). Rhamnogalacturonan I in *Solanum tuberosum* tubers contains complex arabinogalactan structures. *Phytochemistry* **65**, 1429–1438.

O'Neill RA, Albersheim P & Darvill AG (1989). Purification and characterization of a xyloglucan oligosaccharide-specific xylosidase from pea seedlings. *The Journal of Biological Chemistry* **264**, 20430–20437.

Palmer SJ & Davies WJ (1996). An analysis of relative elemental growth rate, epidermal cell size and xyloglucan endotransglycosylase activity through the growing zone of ageing maize leaves, *Journal of Experimental Botany* **47**, 339–347.

Panikashvili D, Shi JX, Bocobza S, Franke RB, Schreiber L & Aharoni A (2010). The *Arabidopsis* DSO/ABCG11 transporter affects cutin metabolism in reproductive organs and suberin in roots. *Molecular Plant* **3**, 563–575.

Panikashvili D, Shi JX, Schreiber L, Aharoni A (2011). The *Arabidopsis* ABCG13 transporter is required for flower cuticle secretion and patterning of the petal epidermis. *New Phytologist* **190**, 113–24.

Parodi S, Kendall F & Nicolini C (1975). A clarification of the complex spectrum observed with the ultraviolet circular dichroism of ethidium bromide bound to DNA. *Nucleic Acids Research* **2**, 477–486.

Parsons EP, Popopvsky S, Lohrey GT, Lu S, Alkalai-Tuvia S, Perzelan Y, Paran I, Fallik I & Jenks MA (2012). Fruit cuticle lipid composition and fruit post-harvest water loss in an advanced backcross generation of pepper (*Capsicum sp*.). *Physiologia Plantarum* **146**, 15–25.

Partridge SM (1946). Application of the paper partition chromatogram to the qualitative analysis of reducing sugars. *Nature* **158**, 270–271.

Pauly M, Andersen LN, Kauppinen S, Kofod LV, York WS, Albersheim P & Darvill A (1999). A xyloglucan-specific endo-β-1,4-glucanase from *Aspergillus aculeatus*: expression cloning in yeast, purification and characterization of the recombinant enzyme. *Glycobiology* **9**, 93–100.

Perzelan Y, Paran I, Fallik I & Jenks MA (2012). Fruit cuticle lipid composition and fruit post-harvest water loss in an advanced backcross generation of pepper (*Capsicum sp*.). *Physiologia Plantarum* **146**, 15–25.

Peschel S, Franke R, Schreiber L & Knoche M (2007). Composition of the cuticle of developing sweet cherry fruit. *Phytochemistry* **68**, 1017–1025

Petit J, Bres C, Philippe Mauxion J, Tai FWJ, Martin LBB, Fich EA, Joubès J, Rose JKC, Domergue F & Rothan C (2016). The glycerol-3-phosphate acyltransferase GPAT6 from tomato plays a central role in fruit cutin biosynthesis. *Plant Physiology* **171**, 894–913.

Philippe G, Gaillard C, Petit J, Geneix N, Dalgalarrondo M, Bres C, Mauxion JP, Franke R, Rothan C, Schreiber L, Marion D & Bakan B (2016). Ester cross-link profiling of the cutin polymer of wild-type and cutin synthase tomato mutants highlights different mechanisms of polymerization. *Plant Physiology* **170**, 807–20.

Ping LF, Chen XY, Yuan XL, Zhang M, Chai YJ & Shan SD (2017). Application and comparison in biosynthesis and biodegradation by *Fusarium solani* and *Aspergillus fumigatus* cutinases. *International Journal of Biological Macromolecules* **104**, 1238–1245.

Potter I & Fry SC (1994). Changes in xyloglucan endotransglycosylase (XET) activity during hormone-induced growth in lettuce and cucumber hypocotyls and spinach cell suspension cultures. *Journal of Experimental Botany* **45**, 1703–1710.

Pratt CW & Cornely K (2013). Chapter 11. Carbohydrate. In: *Essential Biochemistry* (Third ed.). New Jersey, US: Wiley.

Purugganan MM, Braam J & Fry SC (1997). The *Arabidopsis* TCH4 xyloglucan endotransglycosylase (substrate specificity, pH optimum, and cold tolerance). *Plant Physiology* **115**, 181–190.

Ranathunge K, Shao S, Qutob D, Gijzen M, Peterson CA and Bernards MA (2010). Properties of the soybean seed coat cuticle change during development. *Planta* **231**, 1171–1188.

Renault H, Alber A, Horst NA, Lopes AB, Fich EA, Kriegshauser L, Wiedemann G, Ullmann P, Herrgott L, Erhardt M, Pineau E, Ehlting J, Schmitt M, Rose JKC, Reski R & Werck-Reichhart D (2017). A phenol-

enriched cuticle is ancestral to lignin evolution in land plants. *Nature Communications* **8**. Article number: 14713.

Rautengarten C, Ebert B, Ouellet M, Nafisi M, Baidoo EE, Benke P, Stranne M, Mukhopadhyay A, Keasling JD, Sakuragi Y & Scheller HV (2012). *Arabidopsis* deficient in cutin ferulate encodes a transferase required for feruloylation of ω-hydroxy fatty acids in cutin polyester. *Plant Physiology* **158**, 654–665.

Reese ET, Maguire AH & Parrish FW (1968). Glucosidases and exo-glucanases. *Canadian Journal of Biochemistry* **46**, 25–34.

Riley RG & Kolattukudy PE (1975). Evidence for covalently attached *p*-coumaric acid and ferulic acid in cutins and suberins. *Plant Physiology* **56**, 650–654.

Rogers LM, Flaishman MA & Kolattukudy PE (1994). Cutinase gene disruption in *Fusarium solani f sp pisi* decreases its virulence on pea*. The Plant Cell* **6**, 935–945.

Rowland O, Zheng H, Hepworth SR, Lam P, Jetter R & Kunst L (2006). CER4 encodes an alcohol-forming fatty acyl-coenzyme A reductase involved in cuticular wax production in *Arabidopsis*. *Plant Physiology* **142**, 866–77.

Rozema J, Blokker P, Mayoral Fuertes MA & Broekman R (2009). UV-B absorbing compounds in present-day and fossil pollen, spores, cuticles, seed coats and wood: evaluation of a proxy for solar UV radiation. *Photochemical & Photobiological Sciences* **8**, 1233–1243.

Saengpook C, Ketsa S & van Doorn WG (2007). Effects of relative humidity on banana fruit drop. *Postharvest Biology and Technology* **45**, 151–154.

Saladié M, Rose JK, Cosgrove DJ & Catalá C (2006). Characterization of a new xyloglucan endotransglucosylase/hydrolase (XTH) from ripening tomato fruit and implications for the diverse modes of enzymic action. *The Plant Journal* **47**, 282–295.

Sam S, Touahir L, Salvador Andresa J, Allongue P, Chazalviel JN, Gouget-Laemmel AC, Henry de Villeneuve C, Moraillon A, Ozanam F, Gabouze N & Djebbar S (2010). Semi-quantitative study of the EDC/NHS activation of acid terminal groups at modified porous silicon surfaces. *Langmuir* **26**, 809–814.

Sauveplane V, Kandel S, Kastner PE, Ehlting J, Compagnon V, Werck-Reichhart D, and Pinot F (2009). *Arabidopsis thaliana* CYP77A4 is the first cytochrome P450 able to catalyse the epoxidation of free fatty acids in plants. *The FEBS Journal* **276**, 719–35

Scheller HV, Jensen JK, Sorensen SO, Harholt J & Geshi N (2007) Biosynthesis of pectin. *Plant Physiology* **129**, 283–295.

Schnurr J, Shockey J & Browse J (2004). The acyl-CoA synthetase encoded by LACS2 is essential for normal cuticle development in *Arabidopsis*. *The Plant Cell* **16**, 629–642.

Schönherr J & Baur P (1994). Modelling penetration of plant cuticles by crop protecting agents (CPA) and effects of adjuvants on rates of penetration. *Pesticide Science* **42**, 185–208.

Schönherr J & Mérida T (1981). Water permeability of plant cuticular membranes: the effects of humidity and temperature on the permeability of non-isolated cuticles of onion bulb scales. *Plant, Cell & Environment* **4**, 349–354.

Schönherr J & Riederer M (1989). Foliar penetration and accumulation of organic chemicals in plant cuticles. In: *Reviews of Environmental Contamination and Toxicology. Reviews of Environmental Contamination and Toxicology*, vol 108 (Ware GW, ed.). Springer, New York, NY.

Schönherr J & Ziegler H (1975). Hydrophobic cuticular ledges prevent water entering the air pores of liverwort thalli. *Planta* **124**, 51–60.

Schreiber L (2005). Polar paths of diffusion across plant cuticles: new evidence for an old hypothesis. *Annuals of Botany* **95**, 1069–1073.

Segado P, Domínguez E & Heredia A (2016). Ultrastructure of the epidermal cell wall and cuticle of tomato fruit (*Solanum lycopersicum* L.) during development. *Plant Physiology* **170**, 935–946.

Segerson NA (2018). Biochemical and functional characterization of cutin synthase 2 from tomato (*Solanum Lycopersicum*). Cornell University, New York, US.

Shayk M & Kolattukudy PE (1977). Production of a novel extracellular cutinase by the pollen and the chemical composition and ultrastructure of the stigma cuticle of Nasturtium (*Tropaeolum majus*). *Plant Physiology* **60**, 907–915.

Shi JX, Adato A, Alkan N, He Y, Lashbrooke J, Matas AJ, Meir S, Malitsky S, Isaacson T, Prusky D, Leshkowitz D, Schreiber L, Granell AR, Widemann E, Grausem B, Pinot F, Rose JK, Rogachev I, Rothan C & Aharoni A (2013). The tomato SlSHINE3 transcription factor regulates fruit cuticle formation and epidermal patterning. *New Phytologist* **197**, 468–480.

Shi JX, Malitsky S, Oliveira SD, Branigan C, Franke RB, Schreiber L & Aharoni A (2011). SHINE transcription factors act redundantly to pattern the archetypal surface of *Arabidopsis* flower organs. *PLoS Genetics* **7**, e1001388.

Sieber P, Schorderet M, Ryser U, Buchala A, Kolattukudy P, Métraux JP & Nawrath C (2000). Transgenic *Arabidopsis* plants expressing a fungal cutinase show alterations in the structure and properties of the cuticle and postgenital organ fusions. *The Plant Cell* **12**, 721–737.

Simmons TJ, Mohler KE, Holland C, Goubet F, Franková L, Houston DR, Hudson AD, Meulewaeter F & Fry SC (2015). Hetero-trans-?-glucanase, an enzyme unique to Equisetum plants, functionalises cellulose. *The Plant Journal* **83**, 753–769.

Simón L & Goodman JM (2010). Enzyme catalysis by hydrogen bonds: the balance between transition state binding and substrate binding in oxyanion holes. *The Journal of Organic Chemistry* **75**, 1831–1840.

Skoss JD (1955). Structure and composition of plant cuticle in relation to environmental factors and permeability. *Botanical Gazette* **117**, 55–72.

Sousa SM & Silva TL (2005). Demineralization effect of EDTA, EGTA, CDTA and citric acid on root dentin: a comparative study. *Brazilian Oral Research* **19**, 188–192.

Suh MC, Samuels AL, Jetter R, Kunst L, Pollard M, Ohlrogge J, & Beisson F (2005). Cuticular lipid composition, surface structure, and gene expression in *Arabidopsis* stem epidermis. *Plant Physiology* **139**, 1649–1665.

Szafranek B, Tomaszewski D, Pokrzywinska K & Golebiowski M (2008). Microstructure and chemical composition of leaf cuticular wax in two *Salix* species and their hybrid. *Acta Biologica Cracoviensia series Botanica* **50**, 49–54.

Tajima Y, Saito S, Ohno K, Tsukimura T, Tsujino S & Sakuraba H (2011). Biochemical and structural study on a S529V mutant acid α-glucosidase responsive to pharmacological chaperones. *Journal of Human Genetics* **56**, 440–446.

Takahashi K, Shimada T, Kondo M, Tamai A, Mori M, Nishimura M & Hara-Nishimura I (2010). Ectopic expression of an esterase, which is a candidate for the unidentified plant cutinase, causes cuticular defects in *Arabidopsis thaliana*. *Plant and Cell Physiology* **51**, 123–131.

Takahashi Y, Tsubaki S, Sakamoto M, Watanabe S & Azuma J (2012). Growth-dependent chemical and mechanical properties of cuticular membranes from leaves of *Sonneratia alba*. *Plant, Cell and Environment* **35**, 1201–1210.

Thompson JE and Fry SC (2001). Restructuring of wall-bound xyloglucan by transglycosylation in living plant cells. *The Plant Journal* **26**, 23–34.

Tian S, Fang X, Wang W, Yu B, Cheng X, Qiu F, Mort AJ & Stark RE (2008). Isolation and identification of oligomers from partial degradation of lime fruit cutin. *Journal of Agricultural and Food Chemistry* **56**, 10318–10325.

Tisserat B and Stuff A (2011). Stimulation of short-term plant growth by glycerol applied as foliar sprays and drenches under greenhouse conditions. *HortScience* **46**, 1650–1654.

Vahabi S, Salman BN & Javanmard A (2013). Atomic force microscopy application in biological research: a review study. *Iranian Journal of Medical Sciences* **38**, 76–83.

Voragen AGJ, Coenen GJ, Verhoef RP & Schols HA (2009). Pectin, a versatile polysaccharide present in plant cell walls. *Structural Chemistry* **20**, 263–275.

Wang G, Wang Q, Lin X, Ng TB, Yan R, Lin J & Ye X (2016). A novel cold-adapted and highly salt-tolerant esterase from *Alkalibacterium sp*. SL3 from the sediment of a soda lake. *Scientific Reports* **6**, 19494.

Warneck H, Fulton DC, Seitz HU & Fry SC (1998). Transport, degradation and cell wall-integration of XXFGol, a growth-regulating nonasaccharide of xyloglucan, in pea stems. *Planta* **204**, 78–85.

Wechtersbach L and Cigić J (2007). Reduction of dehydroascorbic acid at low pH. *Journal of Biochemical and Biophysical Methods* **70**, 767–772.

Wellman CH, Osterloff PL & Mohiuddin U (2003). Fragments of the earliest land plants. *Nature* **425**, 282–285.

Weng H, Molina I, Shockey J & Browse J (2010). Organ fusion and defective cuticle function in a *lacs1 lacs2* double mutant of *Arabidopsis*. *Planta* **231**, 1089–100.

Willats WGT, Marcus SE & Knox JP (1998). Generation of a monoclonal antibody specific to (1→5)-α-L-arabinan, *Carbohydrate Research* **308**, 149–152.

Wolf S, Mouille G & Pelloux J (2009), Homogalacturonan methyl-esterification and plant development. *Molecular Plant* **2**, 851–860.

Wu SC, Blumer JM, Darvill AG & Albersheim P (1996). Characterization of an endo-[beta]-1,4-glucanase gene induced by auxin in elongating pea epicotyls. *Plant Physiology* **110**, 163–170.

Xiao FM, Goodwin SM, Xiao YM, Sun ZY, Baker D, Tang X, Jenks MA & Zhou JM (2004). *Arabidopsis* CYP86A2 represses *Pseudomonas syringae* type III genes and is required for cuticle development. *The EMBO Journal* **23**, 2903–2913.

Xu W, Campbell P, Vargheese AK & Braam J (1996). The *Arabidopsis XET*-related gene family: environmental and hormonal regulation of expression. *The Plant Journal* **9**, 879–889.

Xue X & Fry SC (2012). Evolution of mixed-linkage (1→3, 1→4)-b-D-glucan (MLG) and xyloglucan in *Equisetum* (horsetails) and other monilophytes. *Annals of Botany* **109**, 873–86.

Yang W, Pollard M, Li-Beisson Y and Ohlrogge J (2016). Quantitative analysis of glycerol in dicarboxylic acid-rich cutins provides insights into *Arabidopsis* cutin structure. *Phytochemistry* **130**, 159–169.

Yang W, Pollard M, Li-Beisson Y, Beisson F, Feig M & Ohlrogge JB (2010). A distinct type of glycerol-3-phosphate acyltransferase with *sn*-2 preference and phosphatase activity producing 2-monoacylglycerol. *PNAS* **107**, 12040–12045.

Yang W, Simpson JP, Li-Beisson Y, Beisson F, Pollard M, & Ohlrogge JB (2012). A land-plant-specific glycerol-3-phosphate acyltransferase family in *Arabidopsis*: substrate specificity, *sn*-2 preference, and evolution. *Plant Physiology* **160**, 638-–652.

Yeats TH, Huang W, Chatterjee S, Viart HM, Clausen MH, Stark RE & Rose JKC (2014). Tomato cutin deficient 1 (CD1) and putative orthologs comprise an ancient family of cutin synthase-like (CUS) proteins that are conserved among land plants. *The Plant Journal* **77**, 667–675.

Yeats TH, Martin LB, Viart HM, Isaacson T, He Y, Zhao L, Matas AJ, Buda DJ, Domozych DS, Clausen MH & Rose JKC (2012). The identification of cutin synthase: formation of the plant polyester cutin. *Nature Chemical Biology* **8**, 609–611.

Zhong R, Cui D & Ye Z (2019). Secondary cell wall biosynthesis. *New Phytologist* **221**, 1703–1723.